Development of different microtechnology-based approaches for point-of-care testing

Dissertation

submitted to the Faculty of Sciences of the University of Neuchâtel,

to obtain the degree of Doctor of Science

by

Laura Ceriotti

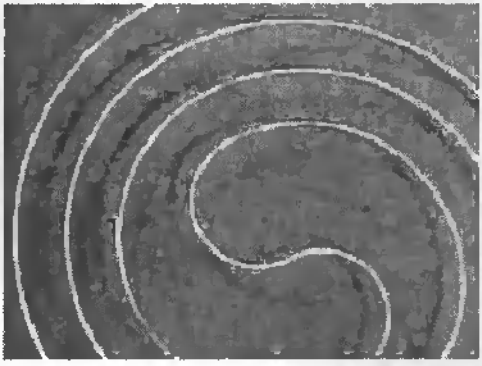

Institute of Microtechnology

University of Neuchâtel

Rue Jaquet-Droz 1, CH-2007 Neuchâtel

Switzerland

2002

UFO Dissertation Band 417

Die Deutsche Bibliothek – CIP-Einheitsaufnahme
Ein Titeldatensatz für diese Publikation ist bei
Der Deutschen Bibliothek erhältlich.

Dissertation der Universität Neuchâtel
Datum der mündlichen Prüfung: 05.09.2002
Referenten: Prof. Dr. N. de Rooij
Dr. E. Verpoorte
Prof. Dr. R. Tabacchi
Prof. Dr. J. Landers

UFO Atelier für Gestaltung & Verlag GbR · D-78476 Allensbach
Internet: www.ufo-verlag.de
Erste Auflage 2002 · Alle Rechte beim Autor
ISBN 3-935511-18-3

◄ The photo on the cover is a close-up of a spiral PDMS channel packed with 3-µm-sized, octadecylsilane-modified silica particles. The channel is 70 µm wide, 50 µm deep and 8 cm long. A tapered geometry integrated at the beginning of the separation channel (not shown in the photo) is used to retain the beads in the bed and create a stationary phase for on-chip chromatography. The fabrication and use of the packed microcolumn are described in Chapter 4 and Appendix 3.

The photo on the cover is a close-up of a spiral PDMS channel packed with 3-μm-sized, octadecylsilane-modified silica particles. The channel is 70 μm wide, 50 μm deep and 8 cm long. A tapered geometry integrated at the beginning of the separation channel (not shown in the photo) is used to retain the beads in the bed and create a stationary phase for on-chip chromatography. The fabrication and use of the packed microcolumn are described in Chapter 4 and Appendix 3.

Ai miei cari genitori

IMPRIMATUR POUR LA THESE

Development of different microtechnology-based approaches for point-of-care testing

de Mme Laura Ceriotti

UNIVERSITE DE NEUCHATEL

FACULTE DES SCIENCES

La Faculté des sciences de l'Université de Neuchâtel sur le rapport des membres du jury,

Mme S. Verpoorte,
MM. N. de Rooij (directeur de thèse),
R. Tabacchi et J. Landers (Uni. of Virginia USA)

autorise l'impression de la présente thèse.

Neuchâtel, le 10 septembre 2002

Le doyen:

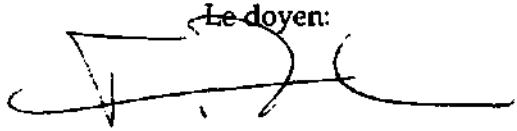

F. Zwahlen

Abstract

In the course of the present thesis, different microtechnology-based approaches have been investigated to develop chip-based methods of diagnostic interest.

A new assay for lipoprotein (LP) obtained from fresh serum was developed in a glass microchip format. Separation of high-density lipoprotein (HDL) and low-density lipoprotein (LDL) was achieved by microchip capillary electrophoresis (CE) in 30 seconds. Moreover, it was found that detection of LDL was possible in an untreated microchannel without use of a dynamic coating, in great contrast to conventional CE analysis. Results of the LDL analysis study in fact suggest that rapid analysis on chip of different low-density-lipoprotein (LDL) forms of clinical relevance is possible. The use of polymer substrates as an alternative to glass for microanalytical applications has also been of interest, with efforts focused on the development of poly(dimethylsiloxane) (PDMS) devices. This elastomer is cheap, UV transparent, and lends itself well to fast replica molding of microchannel devices using micromachined masters. Its good optical properties and the possibility to fabricate high-aspect-ratio channel profiles were exploited for transverse UV/visible absorbance detection. Tapered separation channels in PDMS were successfully packed with 3-μm, octadecylsilanized (ODS) silica beads by exploiting the "keystone effect". This approach is fritless, as beads agglomerate in the taper to form a stationary plug behind which beads are retained. The packed bed was used for capillary electrochromatography (CEC) and the separation of two neutral compounds was achieved in less than 15

seconds. A different approach based on 3-D PDMS microstructures was employed to create silica-bead packed beds suitable for nucleic acid extraction from purified lambda samples and human cell lysates. Taken together, these various studies represent a number of significant advances in the use of microfluidic devices for clinical diagnostics. Importantly, chips have been used for the analysis of complex matrices and samples of physiological origin, a barrier that many researchers have as yet not crossed.

Abbreviations

AFM:	atomic force microscope
BGE:	background electrolyte
BHF:	buffered hydrofluoric acid
CE:	capillary electrophoresis
CEC:	capillary electrochromatography
DI:	deionised (water)
DMSO:	dimethyl sulfoxide
DRIE:	deep reactive-ion etching
EDTA:	ethylenediaminetetraacetic acid
EDF:	electroosmotic flow
ESEM:	environmental scanning electron microscope
FITC:	fluorescein isothiocyanate
HDL:	high-density lipoprotein
HF:	hydrofluoric acid
HPLC:	high pressure liquid chromatography
HPV:	Human Papilloma Virus
IEOP:	indirect electroosmotic pumping
ICP-RIE:	inductively coupled plasma-reactive-ion etching
ITP:	isotachophoresis
LDL:	low-density lipoprotein
LIF:	laser-induced fluorescence
LLS:	laser light scattering

LOD:	limit of detection
LP:	lipoproteins
MB:	methylene blue
NASBA:	nucleic acid sequence-based amplification
NBD-ceramide:	7-nitrobenz-2-oxa-1,3-diazole-ceramide
O-CEC:	open channel CEC
ODS:	octadecylsilane
PCR:	polymerase-chain reaction
PDMS:	poly(dimethylsiloxane)
PMT:	photomultiplier tube
POC:	point-of-care
SDS:	sodium dodecyl sulfate
SNR:	signal-to-noise ratio
Tris:	tris(hydroxymethyl)aminomethane

Table of contents

1 Introduction

1.1 Microsystems for point-of-care testing

The increasing necessity for the human species to know and understand the surrounding world is pushing towards the creation of tools able to give real-time answers. Miniaturized systems have the potential to deal with this issue. They can, in fact, be used to perform analysis and reactions in short times and with high efficiency. The original idea to integrate all the analytical processes onto a microdevice and use it for the analysis of complex samples outside a central lab, at the point-of-care, is becoming a reality.

1.1.1 Miniaturized total chemical analysis system concept

In 1989, the concept of the miniaturized total chemical analysis system, or μTAS, was presented for the first time [1, 2]. The idea was to incorporate all the components required to accomplish a complete chemical measurement into a single, small and compact device. In other words, all the possible functions found in an analytical method, such as chemical mixing and reactions, chromatographic and electrophoretic separations, valves and pumps, detectors and electronics, should be miniaturized onto a device of a few square centimeters or less. Since then, miniaturization of analytical techniques has become a dominant trend in research. This trend encompasses various environments, from academia, where laboratories are interested in the fabrication of new microstructures and in new

solutions for their particular applications, to commercial companies, which realized the potential underlying the emerging "miniaturization" sector early on.

There are several arguments in favour of the miniaturization of analytical devices. They include better performance in terms of increased separation speed and higher sample throughput, reduced costs (particularly in the case of disposable devices), and high structure reproducibility because of fabrication in batch.

1.1.2 From microelectronic circuits to microfluidic networks

The technology for the miniaturization of analytical systems came directly from the microelectronic industries [3, 4]. If photolithography can create paths and control elements for electronic integrated circuits, it could also produce, combined with chemical etching and wafer bonding, components for the control and mobilization of fluids [5, 6]. Thus, the first liquid-based microfluidic system was realized on a silicon wafer, and electroosmosis was used as transport mechanism [7]. The device was fabricated using an electrically insulating layer of silicon dioxide or nitride on top of the silicon wafer, so that potentials could be applied to the solution to move the sample in the channel network. However, electric field strengths were limited to between 100 and 180 V/cm, since the insulating layers were highly susceptible to dielectric breakdown. To achieve the higher field strengths typically used in conventional fused-silica capillary electrophoresis (CE) systems (up to 500 V/cm), glass-based substrates were successfully introduced [5, 8, 9]. Glass can be photolithographically patterned, and exhibits electroosmotic flow and linear, Ohm's Law current-voltage curves comparable to the ones achieved for fused-silica capillaries. The numerous papers published on CE separations in etched glass channels proved that picoliter-volume samples and reagents can be manipulated with high precision simply by proper selection of applied potentials. Separations can be completed in a few

seconds due to the reduced distance between sample injection and detection point. Moreover, microchannels exhibit high surface-to-volume ratios, which improve Joule heat dissipation during the separation. Thus, higher electric fields can be applied along the microchannel compared to conventional capillary electrophoresis instrumentation, and faster separations can be achieved [10]. Photolithography allows the fabrication of multiple channels of the same geometry on the same substrate, allowing parallel analysis on small working areas. This feature makes microfabricated devices extremely attractive when high sample throughput is needed, such as in genomics [11-18] and proteomics [19-21].

Despite the advantages mentioned above, sometimes miniaturization introduces technical challenges that are not present in the macroworld. For example, the polyacrylamide gel used in slab gel electrophoresis for DNA sizing was used in the microchannel format only in the early years [22]. It has since been replaced with new polymer formulations based on non-cross-linked cellulose, which are less viscous. These matrices are more suited to the microcolumn format since microchannels are more easily reversibly filled with them and suffer less bubble formation [23, 24]. In microfluidic systems, surface effects such as analyte adsorption are also more significant because of the high surface-to-volume ratio. Evaporation can also be another significant problem when only a few microliters or less of reagent or sample are used.

In the course of the present thesis, a number of approaches were developed to overcome technical challenges related to the integration of new analysis methods onto chips. For instance, a new fritless approach for packing channels with particles was introduced to circumvent the fabrication of the types of frits typically employed in conventional capillary electrochromatography (CEC). The methods employed for making frits, such as silica particle sintering [25], are difficult in conventional capillaries, and are not easily transferable to chips. The use of tapered microchannels results not only in effective bead retention in a chip,

but is also easier to achieve and reproduce than in fused-silica columns [26]. Another challenge for microsystems is absorbance detection, since the scaling process reduces the optical path length and therefore the detection sensitivity. The fabrication of sharp and narrow channels for transverse UV absorbance detection was also investigated as a solution to this issue [27].

1.1.3 Towards point-of-care (POC) systems

Today, blood testing is predominantly performed in clinical laboratories. Samples are sent to a central facility to be analyzed. Depending on the test, results are obtained within a few hours to a few days. A centralized clinical laboratory generally contains a suite of instruments. Samples are usually analysed after some manual manipulations have been performed, during which the quality of the sample may be affected by the introduction of contamination, and human error in sample preparation. Though laboratory automation can bring considerable speed and efficiency to testing, new sensor technologies are pulling testing out of the laboratory and to the point-of-care (POC). Since multiple functions can be integrated into a single, sealed device, risk of contamination is reduced and sample consumption and cost are limited because of the small dimensions. Moreover, since the system can be portable and easy to use, testing can be performed directly by the clinicians at the POC, for instance at the patient bedside. Real-time answers at the POC can provide immediate information about the state of the patient, allowing quick diagnosis and treatment monitoring. As a consequence, this type of decentralized system would reduce health care costs, improve test reliability and increase patient-testing confidence.

A high degree of integration and automation is necessary to realize a portable and reliable instrument operable at the POC, as demonstrated for the analysis of nanoliter-size DNA samples [28], for multiple-step genetic assays [29] and pathogen detection [30]. Moreover, these systems have to be compatible with

unprocessed biological fluids such as blood, urine, and saliva. Handling such samples in a μTAS system is not easy, but the first encouraging results can be found in the literature [31-41]. Micronics, for instance, is currently developing POC hematology instruments based on plastic disposable microdevices for hemoglobin quantification and blood cell characterization [31]. Serum samples have been introduced into microchips for electrophoretic immunoassay of serum cortisol [32], theophilline [33, 34] and for bead-based immunoassay of carcinoembryonic antigen (CEA) [35]. Lactate concentration in serum has also been determined in miniaturized systems with very reproducible results, in good agreement with spectrophotometric reference methods [36]. Urine samples have been recently analyzed in microdevices to measure uric acid [37], ascorbic acid [38], carnitine [39], amino acids [40], and oxalate concentrations [41]. These examples demonstrate clearly the potential of microsystems for rapid analysis of physiological samples at the POC [42]. On-chip cell lysis and cell component analysis have also been recently reported, providing a route to fully automated and integrated analysis systems [30, 43].

Of course, the advantages mentioned above for rapid medical diagnostics are useful also for environmental testing [44-46] and defensive biological warfare agent detection [47-50]. A particular interest is also food quality, which influences the daily life of the whole world population. Detection of bovine spongiform encephalopathy (BSE) in meat and antibiotics in Chinese chickens are current problems to which microfluidics could be applied.

1.2 Chip technologies

Wolffenbuttel suggested that micromachining can be defined as "the sculpturing of silicon and silicon compatible materials" to produce three-dimensional structures with no direct electrical function [51]. Different materials

can be used for micromachining, ranging from glass, fused silica and quartz to metal and plastic. In this section, two classes of technological methods are described. The first class includes the "classical" methods, such as standard photolithography and wet etching, which were developed in microelectronics and then used to produce microfluidic systems on a planar substrate [2]. The second class includes "alternative" fabrication methods, which were developed to create microchannels in substrates other then silicon or glass [52].

1.2.1 Classical methods

Micromachining is the combination of four different classical methods used to create three-dimensional structures in a planar silicon based substrate: film deposition, photolithography, etching and bonding techniques.

Film deposition processes include spin coating, thermal oxidation, physical vapor deposition (PVD), chemical vapor deposition (CVD) and sputtering. A large variety of metals, inorganic oxides and polymers can be deposited on the wafer using these techniques, with film thickness from a few nanometers to a few micrometers, depending on the material and the deposition method.

Photolithography is the technique by which a pattern of geometric shapes is transferred to a layer of light-sensitive material, called photoresist. The patrern consists of dark and transparent surface regions defining the design on a quartz mask. To transfer a pattern from a mask to the photoresist, the mask is irradiated with UV. The light is stopped by the dark regions and passes through the transparent areas to reach the photoresist. Photoresists can be classified as positive and negative, depending on how they respond to irradiation [53]. Positive photoresists consist of three components: a photosensitive compound, a base resin, and an organic solvent. During exposure the photosensitive compound absorbs radiation in the exposed areas, changes its chemical structure, and

becomes soluble in the developer solution. Thus, the exposed areas are removed upon development. The negative photoresists are polymers. During exposure, the polymer absorbs the optical energy and converts it to chemical energy to initiate a reaction which crosslinks the polymer molecules. The crosslinked polymer has a higher molecular weight and becomes insoluble in the developer solution. Thus, upon development, the unexposed areas are removed.

Etching processes transfer two-dimensional patterns defined on the wafer surface to underlying films and substrates. These processes can be "wet" when the etchant species are in solution, or "dry" when the etching is carried out using plasma in the form of low-pressure discharge.

Wet etching In chemical wet etching, the patterned wafer is immersed in a liquid etching solution chosen specifically to selectively etch the desired material and not others exposed to the solution. The basic mechanisms for the wet etching involve three steps: 1) the reactants are transported (e.g. by diffusion) to the reacting surface, 2) chemical reactions occur at the surface, 3) the products are transported away from the surface (e.g. by diffusion). Silicon, for example, can be etched in basic solutions like potassium hydroxide (KOH). This kind of etching is orientation-dependent, since the etching rate is different for the different Si crystal planes, and produces channels with sidewalls inclined by 54.7° with respect to the horizontal plane. An example of anisotropic etching of a ⟨100⟩ silicon wafer in KOH is presented in Figure 1-1A. The resulting structure is quite different from the mask design (Figure 1-1B) due to underetching of convex corners (undercutting). This is due to the fact that these corners are composed of a variety of crystal planes that are more rapidly attacked by the etchant than those defining the walls of the vertically and horizontally laid-out channels. The etching continues until a more stable <111> surface is reached. As this behaviour is predictable, proper mask design can compensate for the undercut to achieve the desired structure after etching. Another example of wet etching is standard glass etching in 50 % hydrofluoric acid (HF), as will be described below. In this case,

the process is orientation-independent, resulting in a rounded channel profile, where the channel is at least two times wider than deep (Figure 1-2). Undercutting of the layer underneath the mask represents the major disadvantage of wet chemical etching, since it is responsible for the loss in resolution in the etched pattern.

Dry or plasma-assisted etching processes include those carried out in partially or fully ionized gases (plasmas) [3, 53]. The plasma is produced when an electric field of sufficient intensity is applied to a gas, causing the gas to break down and become ionised. Briefly, the process begins with the generation of etchant species (ions) in the gas phase. The reactive species are then transported by diffusion to the solid where they are adsorbed and react with the surface to form volatile compounds. These species are desorbed from the surface and diffuse into the bulk gas, to be pumped out of the system. Silicon wafers can be structured using a relatively new dry etching process, called Deep Reactive-Ion Etching (DRIE). This technology employs a time-multiplexed etching scheme with alternating etching and sidewall passivation steps to avoid lateral underetch. As a result, the mask design is faithfully transferred to the substrate, and nearly vertical sidewalls at extremely high-aspect ratios are produced (Figure 1-1B). In the case of Si, SF_6 with 10% O_2 added is used as gas for the etching and C_4F_8 is used for the side-wall passivation. SF_6 and C_4F_8 are alternatively pumped into the chamber and removed from the chamber by a pump. The time required to switch from one gas to the other is in the order of a few seconds. Dry etching processes for Si and fused-silica wafer machining will be presented in Chapter 2.

Bonding is the process by which structures are assembled and sealed together. Bonding can be realized between silicon-silicon, silicon-oxide, silicon-glass, metal-glass, glass-glass, glass-polydimethylsiloxane and other combinations of materials. The anodic bonding technique is a standard process widely used for Si-glass bonding. It is based on the migration of oxygen ions present in the glass into the silicon wafer under an applied electric field (500-

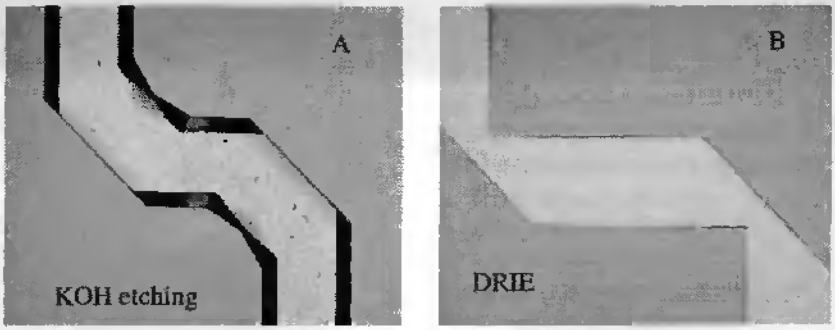

Figure 1-1 *A) Si anisotropic etching in KOH. The structures are 30 μm deep and 80 μm wide. B) Channel structure layout transferred into a Si substrate by DRIE. In B) the channel outline is exactly the same as on the mask. In A), the same pattern was transferred into the resist. However, undercutting of the convex corners for the wet-etched wafer has occurred. (Photos courtesy of J. Lichtenberg, IMT, Neuchâtel).*

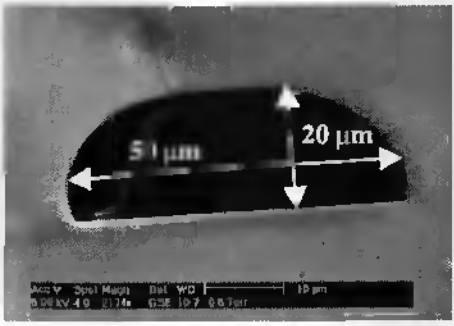

Figure 1-2 *ESEM image of a glass channel cross-section. The rounded channel profile is the result of isotropic etching in 50 % HF. (Photo courtesy of B. Weiller, IMT, Neuchâtel).*

1000 V) at temperatures between 250-450°C. The oxygen ions chemically react with the silicon, forming a strong bond between the wafers [54, 55]. Fusion bonding is used instead for glass-glass sealing. In this case, the SiOH groups at the surface are responsible for the formation of a strong bond (siloxane bonds)

during annealing at temperatures below the substrate softening temperatures (650°C used to bond Pyrex, 1100°C for fused silica) [3]. In all cases, the planarity and the cleanliness of wafer surfaces are critical to achieve a uniform sealing. Generally, glass wafers are cleaned with acetone and 2-propanol for 5 min each and then with fuming HNO_3 or H_2O_2-H_2SO_4 mixture for 10 min. The resulting surfaces have a hydrophilic layer consisting of OH groups. If the surfaces are mated immediately after cleaning, these silanol groups undergo hydrogen bonding and the wafer can be prebonded even at room temperature [56]. Efforts to lower the temperature required for bonding have also been reported [57, 58].

An example of classical micromachining technology is the process for the fabrication of glass microfluidic networks. The standard process steps used at IMT for this are outlined in Figure 1-3. More details related to this technology can be found in [59-61]. The sequence starts with the double-sided deposition on the glass wafer of poly-silicon (400 nm) by low pressure chemical vapor deposition (LPCVD) at 570°C. The deposition is done in two separate steps of 200 nm each to prevent pinhole formation in the wet etching process. Photoresist (i.e. AZ 1518 (positive)) is spin-coated on the wafer and exposed using a chromium mask. The wafer is then dipped in a developer solution (AZ 351 developer: DI water, 1:4), to dissolve the exposed resist. The pattern is then transferred to the polysilicon by a dry etching step (RIE). After photoresist stripping in acetone, the wafer is immersed in a solution of 50% hydrofluoric acid (HF) for wet, isotropic etching of the exposed glass areas. The poly-Si mask is then removed in a 40% KOH bath at 60°C for 5 min. The structured wafer and a coverplate containing holes to serve as reservoirs are cleaned, hydrated and bonded as described above.

Photolithographic processes facilitate the mass production of complicated microstructures, which can be manufactured in the same batch with excellent precision and reproducibility. The inconvenience of micromachining is that it requires cleanroom conditions and high-tech instrumentation. For these reasons

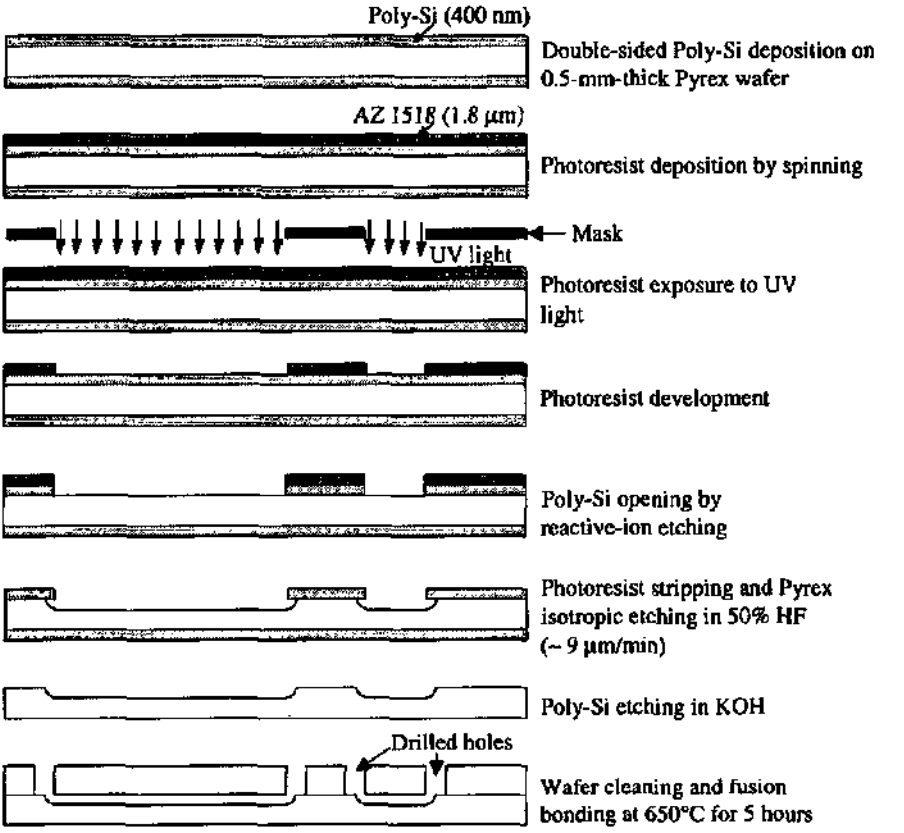

Figure 1-3 Process steps for standard, one-mask glass etching.

new materials and new technologies have been investigated in the last few years as alternatives to work outside the cleanroom and produce low cost, disposable devices [52].

1.2.2 Alternative methods

To overcome the expensive and time-consuming fabrication processes introduced in the previous section, alternative materials and technologies have been investigated. An excellent review about these new methods for microdevice

fabrication has been published by Becker et al. [52]. Polymers appear to be the most promising materials for low cost, and large-scale production of microfluidic devices. This is because they are applicable to mass fabrication processes such as injection molding and hot embossing. Moreover, polymers have a wide range of mechanical, chemical and optical properties, so that it should be possible to find a polymer suited to nearly every application.

Replication technologies are already well known in the macro world, and, for the case of injection molding, represent a standard process for macroscopic plastic component fabrication. It is worth mentioning that microfluidic structures have been realized on a compact disc (CD) platform, with the advantage of using CD manufacturing (low cost and rapid) and centrifugal pumping (connection-free) [62-66]. The expensive step of these technologies is the fabrication of the master structure (i.e. by electroplating or silicon technologies). However, once this master is available, it can be replicated many times into the substrate. In addition to the low cost, another advantage of replication technology is the freedom in design, which overcomes the geometric limitations typical of wet etching processes mentioned above (i.e. undercutting). Injection molding, hot embossing and casting technologies are briefly described below.

Injection molding This process starts with the raw polymer material in granular form. These granules start melting in a cylinder before being transported towards the mold cavity containing the master structure. The molten material is injected in this cavity under a high pressure (typically 600-1000 bar). For macroscopic components, the temperature of the cavity is kept below the solidification temperature of the polymer. In the case of micro-components, the cavity is heated up close to the melting point of the polymer material to allow the polymer to flow into all of the microstructures of the mold. The cavity is then cooled to allow the ejection of the component part. The fabrication cycle takes several seconds.

Hot embossing In this process, the master and a planar polymer substrate are heated separately in a vacuum chamber to a temperature just above the glass transition temperature of the polymer material (usually between 100-200°C). Master and substrate are then brought into contact and embossed with a controlled force (in the order of 0.5-2 kN/cm^2).

Casting This process is widely used in the academic world for the fabrication of planar channel microstructures in silicon-based elastomers. The most commonly used is poly(dimethylsiloxane) (PDMS), a silicone rubber, commercially available as Sylgard 184 (Dow Corning, Midland, MI). Effenhauser et al. published in 1997 the first miniaturized CE system in PDMS [67]. Since then, several groups have used this elastomer for fabrication of microdevices [68-70]. PDMS is inexpensive and UV transparent. Moreover, its fabrication process represents the simplest method to produce microstructures by replication, once a master is available. PDMS is an exceptionally good material for this purpose, as it faithfully reproduces the surfaces with which it has been in contact, with nm resolution. Thanks to this type of fabrication process, the channel geometry is flexible and different channel profiles can be obtained. Besides these useful features, PDMS has other characteristics related to its polymeric nature. Its hydrophobicity can create wettability problems and promote bubble formation in microsystems. Hydrophobic compounds could stick to the silicone rubber surface, and in certain cases be absorbed into the bulk polymer, as occurred with the neutral fluorescent dye, BODIPY [71]. These sorptive properties could negatively interfere with some kinds of applications, such as separations and immunoassays. Surface passivation methods have been investigated to prevent these problems. Examples of PDMS devices for separations [67, 68, 72, 73], immunoassay [74, 75], patterning of biological material (cells, proteins) [76, 77], and components for integrated systems (detectors, sensors, microswitches, valves) [78] have been published. In the following subsection some details about PDMS device fabrication are given.

1.2.2.1 PDMS devices

PDMS devices are fabricated by replica molding, which is simply the generation in PDMS of the negative replica of the master. The fabrication process is depicted in Figure 1-4. To elaborate, prepolymer and its curing agent are vigorously stirred in a 10:1 ratio, degassed using vacuum and poured onto the previously silanized master. To degas the pre-polymer mixture, it can also be left standing for 1-2 hours at room temperature. The PDMS is then heated at 65°C for 4 hours. PDMS may also be cured at room temperature overnight. However, to get well-polymerized slabs and reproducible properties of the material, and to avoid problems during the peeling, the polymerisation is performed in the oven under the mentioned conditions, as indicated by the specifications given by Dow Corning. After polymerization, the PDMS is peeled from the masters and reservoirs are punched through the silicon rubber at the ends of the channels using a hole punch. The PDMS slab is then cleaned with 2-propanol and water in an ultrasonic bath, 5 min each, dried with filtered nitrogen and sealed onto a flat and clean glass wafer. Alternatively, a second PDMS slab may be used to seal the microfluidic channels. The sealing can be reversible if the substrates (PDMS-glass or PDMS-PDMS) are brought together by mere adhesion. This seal is good enough to create tight systems in which solutions can be moved without leakage. When the device gets clogged, it can be easily peeled off the support, rinsed with water and used again. For some applications where, for instance, fluidic connections are inserted into the reservoirs, an irreversible bonding is preferred to avoid fluidic leakage due to mechanical stress. To realize an irreversible seal, the PDMS slab and the cover wafer are oxidized for 0.8 min in an oxygen plasma-based cleaner and brought immediately into contact. Clean, flat and quite large (> 3 × 3 cm) surfaces are absolutely necessary for both types of sealing. Two approaches for the fabrication of masters for PDMS casting are described in Chapter 2. The optical properties of this elastomer are described in Chapter 6.

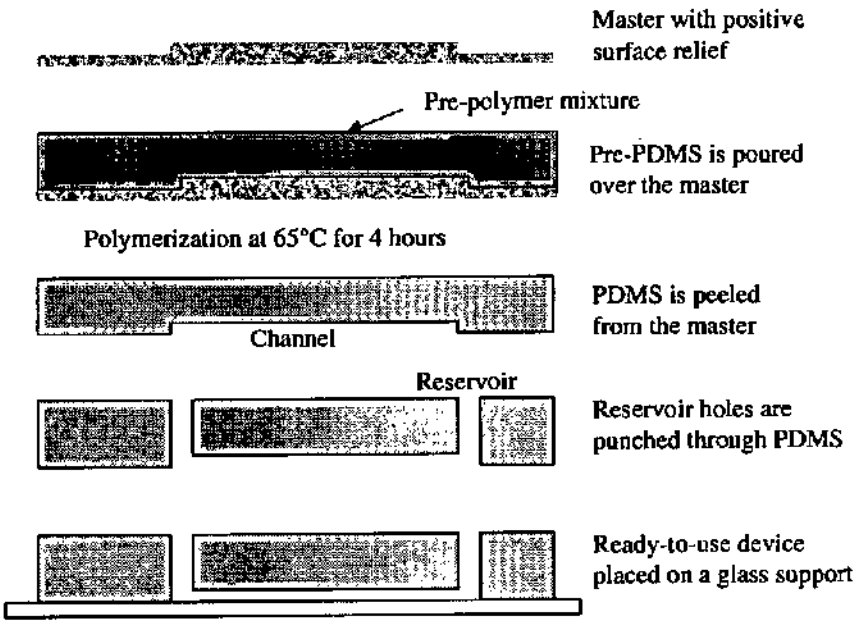

Figure 1-4 PDMS device fabrication by replica molding.

1.3 Introduction to separation techniques based on electromigration

The manipulation of liquids within a microchannel network is still a challenging aspect in the development of μTAS. Fluids are moved in microsystems mainly by using an electric field (E) for the generation of the electroosmotic flow (EOF) or by using a mechanical pump connected to the device or integrated in it. In this section the generation of electroosmosis and its role in CE and microCE analysis is presented. In next section pressure-driven systems will be introduced.

1.3.1 Electroosmosis and electrophoresis

Electroosmosis is a bulk phenomenon, which involves the pumping of fluid through a capillary tube by an externally applied electric field. A prerequisite for electroosmosis is the presence of immobilized surface charges at the wall in contact with the solution. The walls of fused-silica capillaries as well as of etched glass channels generally have a negative charge because of surface silanol groups (SiOH) exhibiting acid-base chemistry in aqueous solution, with a certain fraction becoming charged upon deprotonation. Clearly, the buffer pH determines the fraction of the silanol groups that will be ionized. At pH 2, few groups are ionised, and surface charge is low. At high pH, the opposite is true. In any case, fixed negative charges are compensated by cations in solution, which results in a layer of strongly absorbed counterions on the surface. This layer is termed the "Stern Layer" and is essentially static. A more diffuse layer formed distal to the Stern layer is mobile, and is known as the "Helmholz layer". The double layer model is schematised in Figure 1-5. When the electric field is

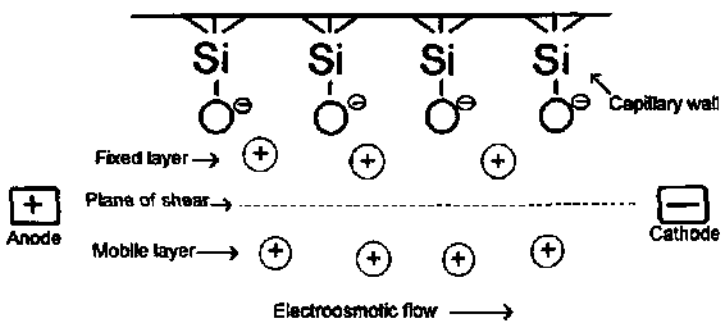

Figure 1-5 Diagram of the double ionic layer formed at bare silica capillary walls, which is critical for generating the electroosmotic flow. (Design from D.R.Baker, Capillary Electrophoresis, John Wiley & Sons, New York, 1995).

applied along the capillary, the cations of the Helmholz layer migrate toward the cathode, dragging their hydration shells with them. Due to viscous forces, the fluid in the center of the channel is also accelerated until the velocity gradient in the radial direction is zero, and all the fluid in the channel moves at a constant velocity. This bulk flow of buffer solution in a capillary under an electric field is known as the electroosmotic flow, or EOF. Since the thickness of the ionic double layer at the wall (several nm) is almost negligible compared with the inner diameter of the column (usually > 10 μm), the velocity profile of the electrosmotic flow is uniform over the cross-section of the capillary. Only at close proximity to the wall does the profile deviate from uniformity, due to frictional forces. Good explanations of EOF may be found in [79-81].

The relationship between the electroosmotic velocity, v_{eo}, and the zeta potential, ζ, at the plane of shear between the static and mobile layers is given by the following formula:

$$v_{eo} = -\mu_{eo}E = -\left(\frac{\varepsilon\zeta}{4\pi\eta}\right)E \qquad (1)$$

where μ_{eo} is the electroosmotic mobility, E is the electric field strength, ε is the buffer dielectric constant, and η is buffer viscosity. The negative sign means that the ζ is negative and the electroosmotic flow is toward the cathode. The direction of the flow is defined by the orientation of the electric field. The flow velocity can be controlled by changing the E through application of a different potential, or by affecting the ζ near the wall by changing pH or ionic strength, I. In untreated microchannels, the buffer pH affects the surface charge by controlling the degree of deprotonation of SiOH groups and, hence, ζ. In fact, ζ can be expressed as a function of the charge density, σ, (pH-dependent) at the plane of shear, and ε, (ionic strength-dependent) as follows:

$$\zeta = \frac{4\pi\sigma\delta}{\varepsilon} \qquad (2)$$

where δ is the double layer thickness. The ionic strength, I, also affects ζ, since δ shrinks when I is increased. Moreover, high I could produce high current with generation of Joule heat, resulting in higher temperatures inside the column and consequently lower solution viscosities. The ζ potential can also be modified using a surface coating or by varying the chemical composition of the aqueous solution (e.g. by addition of polymers or surfactants) [82]. Coatings are commonly used to prevent protein-wall interaction [83-86] and to suppress the EOF in the case of DNA capillary gel electrophoresis [87].

When charged species are placed under the influence of an externally applied electric field, they are separated by electrophoresis. The differential migration velocity of species in an electric field arise from their differing charge-to-mass ratios. For a spherical ion, the electrophoretic velocity, v_{ep}, is defined as follows:

$$v_{ep} = \mu_{ep}E = \left(\frac{q}{6\pi\eta r}\right)E \qquad (3)$$

where q is the particle charge and r is the Stokes' radius of the particle. Electroosmosis and electrophoresis combine for ionic species. Therefore, the net velocity, v_{app}, of the analyte in solution under an applied electric field is the sum of its electrophoretic velocity and the velocity due to electroosmosis (combination of equation (1) and (3)):

$$v_{app} = \mu_{app}E = (\mu_{ep} + \mu_{eo})E \qquad (4)$$

If v_{eo} is greater in magnitude than v_{ep} of all the anions in the buffer, all molecules will migrate in the same direction toward the cathode, where the detector is placed. Differences in μ_{ep} of the individual analytes define the separation of the individual analytes. Neutral species co-migrate with the same velocity of the EOF, v_{eo}.

The migration time of the analyte, t, can be predicted by the following formula:

$$t = \frac{L}{\mu appE} \qquad (5)$$

where L is the distance between the point of sample injection and the detector.

1.3.2 Resolution and efficiency for CE separations

As mentioned in the previous section, molecular species in solution become mobile when placed in an electric field and can be separated by capillary electrophoresis (CE). CE can be performed in fused-silica capillaries (conventional CE) or in a microchannels (microCE). In both cases, capillary and microchannel are filled with an appropriate separation solution at the desired pH. Capillary ends are immersed in buffer-filled reservoirs where the electrodes are placed. Likewise, reservoirs are glued at the channel ends and filled with buffer. The electrodes are then inserted into these reservoirs. The analysis starts with the introduction of the sample plug, ideally rectangular in shape, into a stream of background buffer. In conventional capillaries, the injection can be performed by applying an electric field along the capillary or a pressure at the inlet of the capillary for few seconds. In the case of microfluidic systems, the sample is loaded at a channel intersection and then electrokinetically injected into the separation channel, as discussed later. As electrophoresis ensues, the analytes

separate according to their individual electrophoretic mobilities and move toward the detector as "analyte zones". During migration, the solute zone progressively deteriorates in shape from having a sharp, flat front to a more diffuse, less well-defined boundary. The most important parameter influencing this process is diffusion, and the solute zone can be described as a Gaussian curve. The maximum of this curve is dependent on the initial solute concentration, while its width depends on the length of the injection plug, on the time the sample is in the system and on its diffusion coefficient, D_i.

The separation process is usually described in terms of resolution (how well two components are separated) and efficiency (width of the analyte band: the narrower, the better).

The resolution, *Res*, can be calculated by the difference in migration times of two analytes (t_i) divided by the sum of their peak base widths in time units (w_i) as follows:

$$Res = \frac{2(t_2 - t_1)}{w_1 + w_2} \qquad (6)$$

The efficiency of the process can be expressed using the width at half-height, $w_{1/2}$, of the Gaussian peak:

$$N = 5.54\left(\frac{t}{w_{1/2}}\right)^2 \qquad (7)$$

where t is the migration time of the component and $w_{1/2}$ has units of time. N is a convenient way to describe the analyte peak sharpness and is used to compare the efficiency of separations performed on one or several columns. Alternatively, the

efficiency may be characterized using the height equivalent to a theoretical plate (H), which is simply defined in CE as:

$$H = L/N = \sigma^2_{tot}/L \qquad (8)$$

where σ is the deviation standard of the peak (4σ is the base width of a Gaussian curve) and L is the effective separation length. H relates N to L, and can be regarded as a constant for a particular column.

The total variance, σ^2, includes multiple phenomena which influence the mobile analyte. In fact, it includes not only diffusion, but also the difference in mobility or diffusion due to viscosity changes generated by Joule heating as mentioned above, the finite sample plug length, the interaction of the analytes with the capillary wall, and the finite detection window length. Thus, the total variance, σ^2_{tot}, can be expressed as the sum of the variances due to these different parameters or processes:

$$\sigma^2_{tot} = \sigma^2_{diff} + \sigma^2_T + \sigma^2_{inj} + \sigma^2_{wall} + \sigma^2_{det} \qquad (9)$$

where

σ^2_{diff} = variance due to diffusion

σ^2_T = variance due to Joule heating effects

σ^2_{inj} = variance due to injection plug of finite length

σ^2_{wall} = variance due to analyte interaction with the wall

σ^2_{det} = variance due to finite detection window length

Each single source of variance has been investigated. In particular, σ^2_{diff}, which is derived from Fick's 2nd law of diffusion, can be expressed as:

$$\sigma^2_{diff} = 2D_i t \qquad (10)$$

The variance due to injected plug length, a function of plug volume, is defined as:

$$\sigma^2_{inj} = l^2_{inj}/12 \qquad (11)$$

where l_{inj} is the injection plug length. The variance due to the finite detection volume is described as:

$$\sigma^2_{det} = l^2_{det}/12 + (\mu_i E\tau)^2 \qquad (12)$$

where l_{det} is the detection volume length and $\tau = 1/2\pi f$ is defined as the time constant of the detection system [9]. For a typical CE system under ideal conditions, diffusion is the dominant source of band broadening.

1.3.3 On-chip electrophoresis

As introduced in Section 1.1.2, the first analysis performed in microfluidic systems was the separation of dyes [2, 10] and fluorescently labeled amino acids [88] by capillary electrophoresis (CE). This separation technique is particularly suited to miniaturization for different reasons. First of all, it uses electroosmosis to move liquids from one end of the channel to the other without the need for pumps and valves. As described above, electroosmosis is generated by applying a potential along the electrolyte-filled channel, as long as the walls possess a fixed charge. To mobilize fluids, all is needed is to make electrical contacts to the chip via electrodes immersed in the buffer-filled reservoirs. Secondly, because the separation mechanism is based on *q/r* (formula (3)), CE does not require any stationary phase, unlike HPLC and capillary electrochromatography (CEC), or buffer additives as in micellar electrokinetic chromatography (MEKC). For these

reasons, a large number of applications integrated into microdevices are based on CE separations [89-91]. In addition, branched channel networks are a basic part of microfluidic devices, making them fundamentally different from fused-silica capillaries. This allows the definition and manipulation of pL volumes of sample, as described below, for ultrafast analysis.

Buffer and sample flows within the channel manifold are precisely controlled by means of potentials applied at the reservoirs. For example, at a cross intersection discrete plugs of material can be reproducibly produced and introduced into the channel as described in Figure 1-6. Two types of schemes have been developed for sample loading and injection, namely the "pinched" and the "gated" injection methods. In the "pinched injection" scheme, the sample is electrokinetically transported from the sample reservoir towards the sample waste reservoir in order to fill a channel intersection. This intersection may be a simple cross geometry, or a so-called double-T, due to the 2 side channels being off-set to form 2 T-shaped injections with the main channel [9]. The geometry shown in Figure 1-6 is a double-T intersection. The sample volume is confined at the intersection by a flow of buffer electrokinetically pumped from buffer and buffer waste reservoirs (Figure 1-6a). The sample plug is then injected into the channel by applying the voltage along the separation channel (Figure 1-6b). To prevent sample leakage, which is defined as the unwanted flow of analyte sample from the injection channel into the separation channel, a potential is applied to the sample and sample waste reservoirs. This causes a small backflow of solution away from the separation channel, which minimizes leakage (Figure 1-6b). The pinched injection method dispenses a constant volume of sample, independent of sample loading time, electrophoretic mobilities and electric field [10, 92, 93]. In the "gated injection" scheme, the sample is continually driven from the sample reservoir towards the sample waste reservoir through the injection zone. At the same time, buffer is pumped from the buffer reservoir at the side channel towards the buffer waste, preventing sample leakage into the separation channel

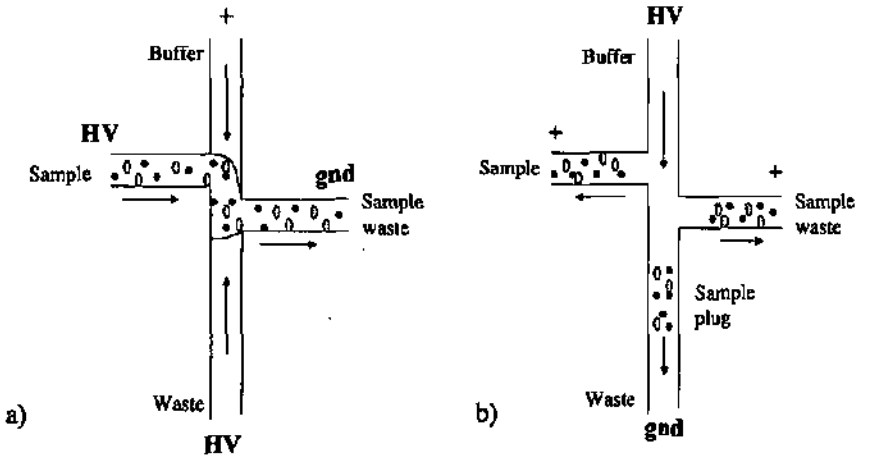

Figure 1-6 Schematic of pinched injection. a) The sample is loaded into the double-T intersection and confined by buffer flows from buffer and buffer waste reservoirs. b) The sample plug is injected onto the separation channel while potential fields are applied at the side arms to prevent sample leakage. Arrows indicate the direction of flow for the sample and buffer, HV and gnd stand for high-voltage and ground, respectively.

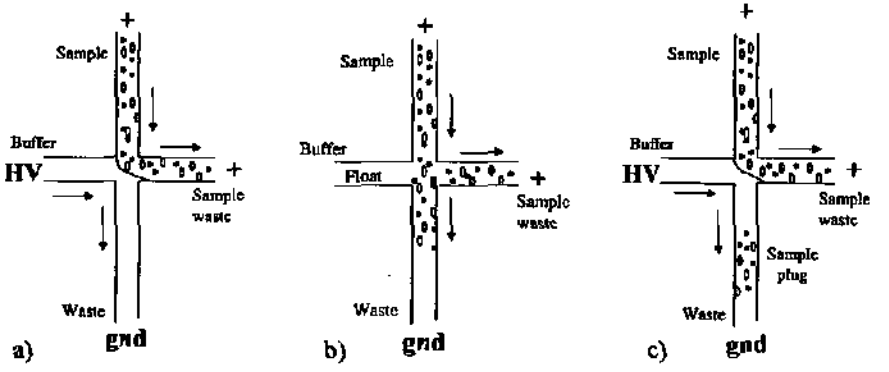

Figure 1-7 Schematic of gated injection. a) Sample is loaded into the cross-injector. b) The sample plug migrates onto the separation channel by removing the potential at the buffer reservoir. c) The sample plug is injected onto the separation channel after reapplying the potential at the buffer reservoir. Arrows indicate the direction of flow for the sample and buffer.

(Figure 1-7a). Sample injection is carried out by electrically floating the high-voltage buffer reservoir for a certain amount of time. This time defines the injection volume (Figure 1-7b). To break off the injection plug, the potential is reapplied at the buffer reservoir (Figure 1-7c) [94]. Although gated injection offers the advantage of injection volume flexibility, plug shape is not as controlled in this mode. Usually the structures we worked with contained a double-T injector and the injection scheme used is similar to the pinch mode described here. To prevent sample dilution and avoid the reduction of sample volume due to the buffer flows coming from the two sides of the separation channel, we often did not apply a potential at the buffer and waste reservoir during the loading step. The injection therefore was not pinched in these cases. However, the push-back flows in the side channels were maintained to prevent sample leakage during injection. Also, this kind of non-pinched injection scheme works well [9]. Fluorescently labelled samples were electrokinetically injected into fused silica (Chapter 2), Pyrex (Chapter 3) and PDMS (Chapter 4) microchannels using this type of volume-defined injection, usually in the non-pinched mode.

1.3.4 Capillary electrochromatography

Capillary electrochromatography (CEC) has emerged in the past few years as a promising, high-performance separation technique [95]. In CEC, the electroosmotic flow drives the mobile phase through the column. The capillary column can be packed with particles (usually porous) coated with stationary phase (packed CEC). Alternatively, the stationary phase can be attached to the inner walls of the capillary (open-tubular CEC). If the analytes are charged, they can be influenced by the electric field, resulting in electrophoretic separation. Thus, oeutral and charged species can be separated by differential migration through the column, based on the analyte partitioning between the mobile and the

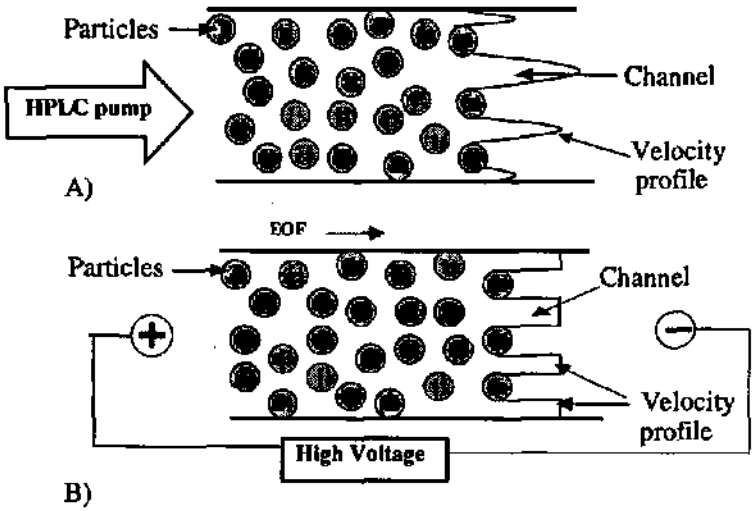

Figure 1-8 Schematic representation of flow profile through a packed bed in A) HPLC and B) CEC.

stationary phase, or a combination of such interactions and electrophoresis. The interest in CEC results from the advantages of performing analytical separations using electrically driven flows on chromatographic beds:

- the use of plug-like flow profiles (as in CE) reduces dispersion of the band of solute as it passes through the column, increasing column efficiency (see Figure 1-8);
- the availability of well-characterized stationary phases extends the range of available selectivities for the separation, analogous to HPLC.

Moreover, the electrically driven flow rate is independent of particle diameter and column length so that, in principle, smaller particles and longer columns can be used in CEC than in HPLC. This contrasts with pressure-driven flow rates through a packed bed, which depend on the square of the particle diameter and inversely on column length (see Section 1.4). Since the efficiency

increases by reducing particle diameter, as a result of decreased flow velocity discontinuities, bigh efficiencies are expected for CEC using particles size < 3 μm [96-98]. It is worth mentioning that particulate stationary phases are now in part being replaced by monolithic phases [99-102]. The combination of flat elution profile, low eddy diffusion (that arises from the different axial flow paths that solute molecules can take through the packed bed), reduced particle diameter and increased column length can lead to CEC efficiencies of up to 500,000 plates/meter or more [95]. These high efficiencies are not possible for conventional pressure-driven HPLC. The integration of a particulate stationary phase into a microchannel for on-chip CEC will be discussed in Chapter 4.

The range of applications for CEC is likely to overlap with both CE and HPLC. These would include impurity analysis, phenylthiohydantoin(PTH)-amino acids, peptide and chiral analysis, trace level determinations and drug and intermediate analysis [103]. Up to now, the effectiveness of CEC in the analysis of biological samples has not been fully exploited. One of the main challenges for CEC is in the field of bioanalysis, where concentrations are usually low and the sample may contain varying types and amounts of endogenous compounds. Moreover, the surface area of the packing material is small so that only small amounts of sample can be loaded and detection systems of high sensitivity are required. However, various researchers have been able to show that CEC can be successfully used to separate a range of compounds in various biological matrices such as urine and plasma, using preconcentration techniques [97, 104-106].

1.4 Introduction to pressure-driven systems

Electroosmotic pumping was the first method integrated into microdevices. Unfortunately, it is not fool-proof. When several channels are interconnected, it becomes difficult to prevent electroosmotic flow in one channel

from drawing fluids from other channels [107]. Careful design, impedance modelling [108] and active voltage control (i.e. pinching) [92] have to be considered to control "liquid cross-talk". In addition, electroosmotic pumping is not compatible with high-ionic-strength buffers, and is pH sensitive. Moreover, its use in conjunction with complex samples such as physiological matrices or bioreactor suspensions proves to be very ineffective. This is because of the generation of excessive or inadequate current to support the EOF, or the adsorption of sample components to the walls, which could mask or alter the charges necessary for EOF generation. The sample itself (e.g. brain tissue, cells) or the chemical reaction (e.g. ionisation) may be sensitive to an applied field. Therefore, it could be desirable to avoid the presence of electrodes in the "sample reservoir" and eliminate the electric field in the reaction zone.

To overcome these issues and realize on the same device regions where a field is applied in addition to field-free zones, different approaches have been adopted. One method, so-called "indirect electro-osmotic pumping" (IEOP), has been described by Guijt et al. [109, 110]. These researchers realized a microfluidic glass network in which side channels are electrically connected to a main channel by electrical breakdown of the glass barrier between them. A voltage applied between the side channels results in an electric field in the main channel, and therefore the generation of EOF. Electrical displacement of liquid in a portion of the main channel induces hydraulic flow in the other, field-free sections of the channel network (IEOP). Combination of electroosmotic pumping and IEOP was successfully used for cross injection of fluorescein [110]. Another approach to keep separate the pumping device and the chemical reaction system has been reported by Guenat et al. [111]. In this case, a Nafion membrane was placed between a nanopump and a sensor/actuator cell. The sample reservoir was on the other side of the cell. The nanopump consisted of a single channel with two electrodes in the reservoirs. When the electric field was applied along the channel, the EOF caused a pressure reduction at the interface between the channel

and the cell. This induced a movement of sample from the sample reservoir towards the cell, where the coulometric titration was accomplished [111]. A similar approach, involving the use of a porous membrane, has been used as interface between a microfluidic channel and a fused silica capillary. In this case, the EOF generated in the channel served as pump for the electrospray ionization, which took place at the tip of the capillary [112]. The use of porous bead-packed beds for the electrokinetic generation of high pressures (up to 500 bars) has been considered as a potential approach for electrokinetic-based micropump fabrication [113, 114].

As mentioned in Section 1.2.2, polymers are an attractive substrate for microfluidic device fabrication by replication methods. There are only a few reports on the electrophoretic properties of plastics [115, 116]. The use of these materials, which have surface properties completely different from fused silica (often, polymers bear little charge and are hydrophobic), has in fact pushed towards new approaches for fluid propulsion. Capillary forces [117-119], centrifugal forces [62-66, 120], or simply pumping the solution from one end of the column (pressure-driven pumping) and using valves have been employed to control flow in plastic microdevices. While a leak-proof valve incorporable into a microsystem is not yet available, the combination of hydrophobic and hydrophilic patches were successfully used to construct passive valves for pressure-driven systems [29, 121]. Polymeric valves, whose structures are sensitive to parameters such as pH, temperature or pressure, have also been reported for flow control inside microchannels [78, 122, 123].

Typically, pressure-driven systems fabricated in plastic as well as in glass use syringe or peristaltic pumps to move the liquids in the fluidic network [124-126]. In contrast with electroosmotic flow, which has a flat profile [79], the flow generated, for example, by a mechanical or electrokinetic pump (i.e. in IEOP), has a parabolic profile. This means that in the case of a pressure-driven separation, the dispersion of the solute zone is increased compared to separation

using electroosmotic pumping [124]. This fact compromises the separation efficiency, as mentioned above when comparing HPLC and CEC [96].

In a hydrodynamic flow system with an incompressible fluid medium, the pressure difference along the channel, ΔP, is described by the Hagen-Poiseuille law as follows:

$$\Delta P = QR \qquad (13)$$

where Q is the volumetric flow rate of the liquid and R the hydrodynamic resistance. The flow resistance for an open tube can be calculated on the basis of the tube geometry and reagent viscosity, η. In the case of a circular tube, R is calculated as follows:

$$R = \frac{8\eta L}{\pi r^4} \qquad (14)$$

where L is the length of the tube and r its radius. In the case of microchannels, which usually do not have circular cross-sections, other formulas should be considered. For a V-shaped channel having a hydraulic diameter r, for instance, R is calculated as follows:

$$R = \frac{17.4\eta L}{r^4} \qquad (15)$$

Once the hydrodynamic resistance is known and the flow rate decided it is easy to calculate the ΔP necessary to move the solution through the tube using Equation (13). This pressure drop should of course be compatible with the pressure capacity of the pumping system (syringe pump, peristaltic pump). Since ΔP is

inversely proportional to the fourth power of the radius for an open tubular system, the microchannel is very sensitive to back pressure. However, Chien et al. have reported that it is possible to control hydrodynamic flow with high precision even in a complex microfluidic network by varying the pressure applied at the reservoir wells [124]. (Recall that in the case of electroosmotic flow, the control is exercised by varying the applied voltage [127]). Solution mixing, reagent dilution, enzyme assays and chemical reactions can be successfully accomplished also in a pressure-driven system [124, 125]. However, prior to fabrication, the channel resistance must be considered to make the structures operable at the desired flow rate. In this work, long microchannels were fabricated for nucleic acid extraction (see Chapter 5). For this application a large surface was desired, since the nucleic acids bind to the silica surface under particular salt conditions [128]. To have a convenient surface available for the nucleic acid binding, channels of different lengths up to 1 m were designed. However, to pump fluids in such long channels without generating high back pressures, which would have been incompatible with the pump and the simple fluidic connections used, the channel cross-section dimensions were kept quite large. Channels were 50 μm deep and 130 μm and 50 μm wide across the top and bottom, respectively. For the 1-m long channel with this cross-section, a surface area of 3 cm^2 was available for nucleic acid binding and a pressure drop around 1 atm was calculated. This ΔP was obtained from Equation (13) using R calculated from Equation (14) and Q= 1 μL/min. The other parameters were: η= 0.001 Ns/m^2, L= 1 m, r= 2.5 10^{-5} m. The peristaltic pump delivers differential pressure drops of up to 6 atm.

In the case of a packed bed, the pressure drop depends on the square of the particle diameter, d, as follows:

$$\Delta P = \frac{Q\phi\eta L}{d^2} \qquad (16)$$

where ϕ is the column resistance factor. Therefore, to have practical pressures in HPLC, particle diameters are usually larger than 3 μm and column lengths are restricted to approximately 25 cm. In this work, a packed bead bed and a peristaltic pump were coupled for nucleic acid extraction. The bed was about 4 mm long, 500 μm wide, and 160 μm deep. Using 15-to-35 μm beads, the fluidic system worked well. Using beads smaller than 5 μm, however, resulted in back pressures, which were too high, and the pumping did not succeed.

In general, fluid flows are classified as being laminar or turbulent. Under laminar flow conditions, the velocity at any one point in a channel is well-defined (hence, EOF is also laminar). The Poiseuille equation (Equation (13)) is valid only in the case of laminar flows. The flow conditions under which the transition from laminar to turbulent flow occurs in a system can be predicted using the Reynolds number, *Re*, which is defined as:

$$Re = v\rho l/\eta \qquad (17)$$

where v is the linear velocity, ρ is the solution density and l the channel diameter. Laminar flow prevails at $Re < 2000$. Because of the small dimensions of the channels, low velocities are required to move liquids in microstructures, so that laminar flow is the norm in microsystems under pressure-driven conditions. This flow enables different streams of fluid to flow side-by-side without the need for a physical barrier between them. Their mixing occurs only at the interface through diffusion [43, 46, 129-133]. Micromixing devices based on diffusive transport and flow lamination operate in low *Re* number regimes and usually have mixing times on the order of seconds. A phenomenon known as chaotic advection has been introduced to passively enhance mixing even at low *Re* numbers (< 100) [134-136]. In this case, the occurrence of chaotic advection in a three-dimensional serpentine microchannel structures is used to help fluid stirring and

diffusion, leading to rapid mixing [134-136]. Another way to improve the mixing is the use of high flow velocity. Although turbulent flows are very difficult to generate, there is at least one example in the literature of its use [137]. In this work a silicon device containing two "T" mixers was employed to initiate and quench a chemical reaction in a submillisecond period of time. The mixing relied on turbulent flow achieved at flow velocities higher than 0.5 mL/s [137].

In Chapter 5 of this thesis, the use of pressure-driven systems to pump solutions through a device for nucleic acid extractor will be described. For this application the use of electroosmosis was prevented by the high salt concentration of the initial sample, which was prepared in lysis buffer (8-10 M guanidine isothiocyanate). Few papers have been published to date about nucleic acid extraction in miniaturized systems. All of them use pressure-driven flow to move the solutions through the extractor, independent of chip substrate and fabrication method [126, 135, 138].

1.5 Laser induced fluorescence detection systems

Fluorescence is an exquisitely sensitive detection technique. For this reason, fluorescence is widely used in immonoassay, flow cytometry, chromatography, electrophoresis and automated DNA sequencing. Detection limits from 10^3 to 10^7 fluorescent molecules have been regularly demonstrated, depending on the application [139]. A common mode of fluorescence detection is laser-induced fluorescence (LIF) detection. To improve LIF detection and give a theoretical basis for the analysis and optimisation of different fluorescent detection schemes and conditions, some parameters (e.g. laser intensity and illumination time) can be considered [140]. Studies were performed using an Ar^+-laser focused to a 8-μm-diameter spot in a capillary tube through which a sample solution was flowed. The resulting fluorescence was collected at a 90° angle and

passed through spatial and spectral filters to the detection system (photomultiplier tube and amplifier/discriminator). With such a system, single-molecule fluorescence detection was possible [139].

LIF detection is the most common detection method for chip-based separations because of its high sensitivity, which does not suffer with reduced path length. LIF detection systems generally require a set-up similar to the one mentioned above [139]. Several groups have performed on-channel LIF detection by directing a laser beam onto the separation channel and collecting the fluorescence with a microscope mounted perpendicular to the chip [8, 9, 94, 141]. Typically, a microscope objective with moderate numerical aperture has been used, so that both lens and beam are closed to the chip. A system like this has been used for the microchip CE experiments, that will be described later in this thesis. The set-up is depicted in Figure 1-9. An Ar^+-laser (Ion Technologies, Salt Lake City, UT) at 488 nm, coupled to a optical fiber (200 μm core diameter), is used for excitation at 45° with respect to the bottom of the wafer. The laser beam is collimated and focused with glass lenses to a ~50-μm spot on the separation microchannel. The fluorescence signal is collected and detected using an inverted microscope comprising an objective (NPL FL, 25 ×, NA 0.35, Leica AG, Glattbrugg, Switzerland), a band-pass filter (514 nm, 10 nm FWHM, Melles-Griot, Irvine, CA), and a pinhole (1 mm diam., Melles Griot). The filter and the pinhole are used to reject the scattered light. The fluorescence is then measured by a photomultiplier tube (PMT) (model H5701-50, Hamamatsu Photonics K.K., Schüpfen, Switzerland). The use of a detection system where the laser beam and PMT are positioned below the chip facilitates the channel-objective alignment. Because blue laser light is barmful to the eyes, special safety glasses should be worn. In particular, when the laser is oriented from underneath, laser light is directed up into the space above the bench. This can pose a safety hazard for those working near by. Thus, the set-up is usually isolated in a black box when the laser is on. This precaution also improves system performance by reducing

interference from environmental light. For the same reason, the lights in the laboratory are switched off during the experiments. The output signal of the photomultiplier is filtered with an R-C low-pass filter (cut-off at 33 Hz) and a numerical algorithm on the computer (cut-off at 50 Hz). Two high-voltage power supplies, high-voltage relays and a data acquisition card (AT-MIO-16-XE-50, PC-DIO-24, National Instruments, Austin, TX) were used. Data acquisition and instrument control were accomplished using in-house software written in LabView (National Instruments, Austin, TX, USA). For the analysis, the chip is mounted on an *x-y* translation stage to allow chip–optical system alignment. Electrical contacts with solutions in the reservoirs were made using Pt wire electrodes. The limit of detection of the set-up is 20 nM for the FITC-labelled amino acids for a signal-to-noise ratio (SNR) of 3. A detection limit of 3 nM has been reported for similar set-up by Liang et al. [142].

To extend on-chip detection to lower concentration detection limits, which are particularly important for clinical anaylsis, the use of confocal epifluorescence microscopy has been investigated [143, 144]. In this approach, high NA microscope objectives allow for high excitation and collection efficiency. In a confocal epifluorescence apparatus, the illumination and fluorescent light collection are performed on the same side of the chip. The excitation light coming from an Ar^+ laser is filtered, reflected by a dichroic mirror, and focused onto a glass device by a 0.6 NA, × 40, long working-distance lens. The fluorescence signal is collected by the same microscope objective, passed through the dichroic mirror and focused with a tube lens onto a pinhole. The signal is measured by a PMT after spectral filtering. Capillary zone electrophoresis of 1 pM fluorescein was achieved with a mean SNR of 5.8 [143]. With the same set-up in combination with a red diode laser, a limit of detection (LOD) of 9 pM for Cy5 was obtained, which corresponds to the detection of 900 molecules in a probe volume of 1.6 pL [144]. Working with a confocal microscope equipped with a 100 × 1.3 NA oil immersion objective, ultrasensitive

LIF detection of separated rhodamine 6G and rhodamine B with LOD of 1.7 pM and 8.5 pM, respectively, and even single molecule detection of R6G, has been achived [145]. With a similar detection system, single molecule detection of DNA has been also reported by Haab et al. [146]. In the method developed by these researchers, both physical focusing (realized by tapering the channel at the detection point) and electrokinetic focusing were used to improve mass and detection limits [146]. For sensitivity reasons and to have a high depth of field, an adapted confocal microscope has been used in our lab to characterize the formation of fluorescent bead clusters in microstructures with integrated diffusers [147]. In both the LIF set-ups described (simple and confocal), the optical system is quite complicated and big. A first attempt to integrate optical elements for fluorescence detection has been recently reported by Roulet et al. [148]. The use

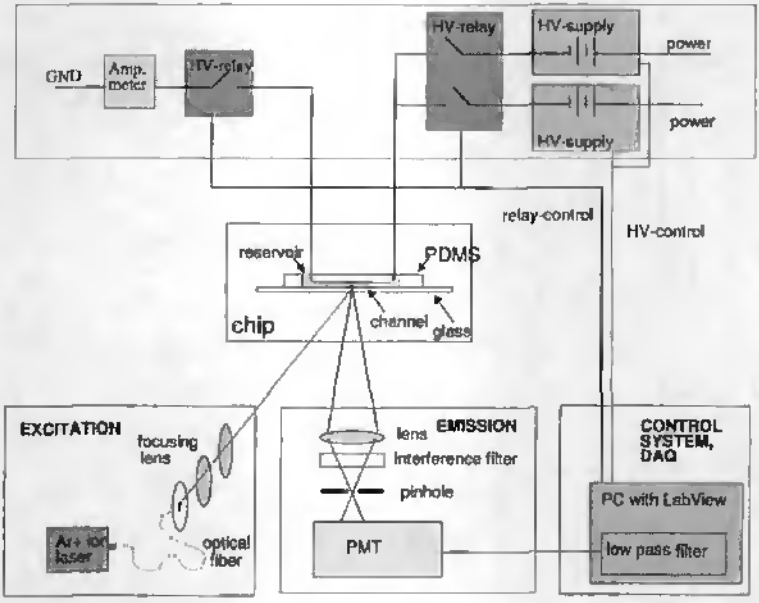

***Figure 1-9** Schematic representation of the CE apparatus with LIF detection and data acquisition systems. In this case a hybrid PDMS-glass chip is presented.*

of a photodiode instead of a PMT could be useful to decrease system size. Other lower sensitivity than fluorescence.methods which are menable to miniaturization and which are therefore interesting for the fabrication of POC systems are conductivity [149-152] and electrochemical detection [37, 153]. However, these detection methods have lower sensitivity than fluorescence.

During the course of the present thesis, LIF detection has been predominantly used. However, the technologies for the fabrication of rectangular channels through which UV detection can be performed have been investigated as an alternative to fluorescence for biological sample detection. This approach and a general overview of on-chip UV detection will be presented in Chapter 6.

REFERENCES

[1] A. Manz, Y. Miyahara, J. Miura, Y. Watanabe, H. Miyagi, and K. Sato, "Design of an open-tubular column liquid chromatograph using silicon chip technology," *Sensors and Actuators B*, vol. 1, pp. 249-255, 1990.

[2] A. Manz, D. J. Harrison, E. M. J. Verpoorte, J. C. Fettinger, A. Paulus, H. Ludi, and H. M. Widmer, "Planar chips technology for miniaturization and integration of separation techniques into monitoring systems - Capillary electrophoresis on a chip," *J. Chomatogr.*, vol. 593, pp. 253-258, 1992.

[3] M. Madou, *Fundamentals of Microfabrication*, first ed. Boca Raton, Florida: CRC Press, 1997.

[4] P. Rai-Choudhury, Handbook of Microlithography, Micromachining, and Microfabrication, Bellingham, Wa: SPIE Press, 1997.

[5] D. J. Harrison, A. Manz, Z. H. Fan, H. Ludi, and H. M. Widmer, "Capillary electrophoresis and sample injection systems integrated on a planar glass chip," *Anal. Chem.*, vol. 64, pp. 1926-1932, 1992.

[6] C. S. Effenhauser and A. Manz, "Miniaturizing a whole analytical laboratory down to chip size," *American Laboratory*, vol. 26, pp. 15-&, 1994.

[7] D. J. Harrison, P. G. Glavina, and A. Manz, "Towards miniaturized electrophoresis and chemical-analysis systems on silicon - an alternative to chemical sensors," *Sensors and Actuators B-Chemical*, vol. 10, pp. 107-116, 1993.

[8] K. Seiler, D. J. Harrison, and A. Manz, "Planar glass chips for capillary electrophoresis - repetitive sample injection, quantitation, and separation efficiency," *Anal. Chem.*, vol. 65, pp. 1481-1488, 1993.

[9] C. S. Effenhauser, A. Manz, and H. M. Widmer, "Glass chips for high-speed capillary electrophoresis separations with submicrometer plate heights," *Anal. Chem.*, vol. 65, pp. 2637-2642, 1993.

[10] S. C. Jacobson, R. Hergenröder, L. B. Koutny, and J. M. Ramsey, "High-speed separations on a microchip," *Anal. Chem.*, vol. 66, pp. 1114-1118, 1994.

[11] M. Marsh, O. Tu, V. Dolnik, D. Roach, N. Solomon, K. Bechtol, P. Smietana, L. P. Wang, X. D. Li, P. Cartwright, A. Marks, D. Barker, D. Harris, and J. Bashkin, "High-throughput DNA sequencing on a capillary array electrophoresis system," *Journal of Capillary Electrophoresis*, vol. 4, pp. 83-89, 1997.

[12] Y. N. Shi, P. C. Simpson, J. R. Scherer, D. Wexler, C. Skibola, M. T. Smith, and R. A. Mathies, "Radial capillary array electrophoresis microplate and scanner for high-performance nucleic acid analysis," *Anal. Chem.*, vol. 71, pp. 5354-5361, 1999.

[13] Z. Nemoda, Z. Ronai, A. Szekely, E. Kovacs, S. Shandrick, A. Guttman, and M. Sasvari-Szekely, "High-throughput genotyping of repeat polymorphism in the regulatory region of serotonin transporter gene by gel microchip electrophoresis," *Electrophoresis*, vol. 22, pp. 4008-4011, 2001.

[14] Q. Gao, Y. Shi, and S. Liu, "Multiple-channel microchips for high-throughput DNA analysis by capillary electrophoresis," *Fresenius Journal of Anal. Chem.*, vol. 371, pp. 137-45, 2001.

[15] A. T. Woolley, G. F. Sensabaugh, and R. A. Mathies, "High-speed DNA genotyping using microfabricated capillary array electrophoresis chips," *Anal. Chem.*, vol. 69, pp. 2181-2186, 1997.

[16] P. C. Simpson, D. Roach, A. T. Woolley, T. Thorsen, R. Johnston, G. F. Sensabaugh, and R. A. Mathies, "High-throughput genetic analysis using microfabricated 96-sample capillary array electrophoresis microplates," *Proc. Nat. Acad. Sci. USA*, vol. 95, pp. 2256-2261, 1998.

[17] S. Liu, H. Ren, Q. Gao, D. J. Roach, R. T. J. Loder, T. M. Armstrong, Q. Mao, I. Blaga, D. L. Barker, and S. B. Jovanovich, "Automated parallel DNA sequencing on multiple channel microchips," *Proc. Nat. Acad. Sci. USA*, vol. 97, pp. 5369-5374, 2000.

[18] B. M. Paegel, C. A. Emrich, G. J. Wedemayer, J. R. Scherer, and R. A. Mathies, "High throughput DNA sequencing with a microfabricated 96-lane capillary array electrophoresis bioprocessor.," *Proc. Nat. Acad. Sci. USA*, vol. 99, pp. 574-579, 2002.

[19] S. Yao, D. S. Anex, W. B. Caldwell, D. W. Arnold, K. B. Smith, and P. G. Schultz, "SDS capillary gel electrophoresis of proteins in microfabricated channels," *Proc. Nat. Acad. Sci. USA*, vol. 96, pp. 5372-5377, 1999.

[20] C. Wang, R. Oleschuk, F. Ouchen, J. Li, P. Thibault, and D. J. Harrison, "Integration of immobilized trypsin bead beds for protein digestion within a microfluidic chip incorporating capillary electrophoresis separations and an electrospray mass spectrometry interface," *Rapid Communications in Mass Spectrometry*, vol. 14, pp. 1377-83, 2000.

[21] Y. Jiang and C. S. Lee, "On-line coupling of micro-enzyme reactor with micro-membrane chromatography for protein digestion, peptide separation, and protein identification using electrospray ionization mass spectrometry," *J. Chromatogr. A*, vol. 924, pp. 315-22, 2001.

[22] C. S. Effenhauser, A. Paulus, A. Manz, and H. M. Widmer, "High-speed separation of antisense oligonucleotides on a micromachined capillary electrophoresis device," *Anal. Chem.*, vol. 66, pp. 2949-2953, 1994.

[23] S. C. Jacobson and J. M. Ramsey, "Integrated microdevice for DNA restriction fragment analysis," *Anal. Chem.*, vol. 68, pp. 720-723, 1996.

[24] F. T. Han, B. H. Huynh, Y. F. Ma, and B. C. Lin, "High efficiency DNA separation by capillary electrophoresis in a polymer solution with ultralow viscosity," *Anal. Chem.*, vol. 71, pp. 2385-2389, 1999.

[25] L. A. Colón, K. J. Reynolds, R. Alicea-Maldonado, and A. M. Fermier, "Advances in capillary electrochromatography," *Electrophoresis*, vol. 18, pp. 2162-2174, 1997.

[26] L. Ceriotti, N. F. de Rooij, and E. Verpoorte, "An integrated fritless column for on-chip capillary electrochromatography with conventional stationary phases," *Anal. Chem.*, vol. 74, pp. 639-647, 2002.

[27] L. Ceriotti, J. Lichtenberg, S. Clément, P. Nussbaum, E. Verpoorte, R. Dändliker, and N. F. de Rooij, "Visible and UV detection through square deep PDMS channels", Proceedings of Micro Total Analysis Systems 2001, Monterey, CA, USA, 2001, 339-340.

[28] M. A. Burns, B. N. Johnson, S. N. Brahmasandra, K. Handique, J. R. Webster, M. Krishnan, T. S. Sammarco, P. M. Man, D. Jones, D. Heldsinger, C. H. Mastrangelo, and D. T. Burke, "An integrated nanoliter DNA analysis device," *Science*, vol. 282, pp. 484-487, 1998.

[29] R. C. Anderson, X. Su, G. J. Bogdan, and J. Fenton, "A miniature integrated device for automated multistep genetic assays," *Nucleic Acids Res.*, vol. 28, pp. e60, 2000.

[30] M. T. Taylor, P. Belgrader, R. Joshi, G. A. Kintz, and M. A. Northrup, "Fully automated sample preparation for pathogen detection performed in a microfluidic cassette", Proceedings of Micro Total Analysis Systems 2001, Monterey, CA, USA, 2001, 670-672.

[31] B. H. Weigl, R. Bardell, T. Schulte, F. Battrell, and J. Hayenga, "Design and rapid prototyping of thin-film laminate-based microfluidic devices," *Biomedical Microdevices*, vol. 3, pp. 267-274, 2001.

[32] L. B. Koutny, D. Schmalzing, T. A. Taylor, and M. Fuchs, "Microchip electrophoretic immunoassay for serum cortisol," *Anal. Chem.*, vol. 68, pp. 18-22, 1996.

[33] N. Chiem and D. J. Harrison, "Microchip-based capillary electrophoresis for immunoassays: analysis of monoclonal antibodies and theophylline," *Anal. Chem.*, vol. 69, pp. 373-378, 1997.

[34] A. Ramseter, F. von Heeren, and W. Thormann, "Analysis of fluorescein isothiocyanate derivatized amphetamine and analogs in human urine by capillary electrophoresis in chip-based and fused-silica capillary instrumentation," *Electrophoresis*, vol. 19, pp. 2967-2975, 1998.

[35] K. Sato, M. Tokeshi, H. Kimura, and T. Kitamori, "Determination of carcinoembryonic antigen in human sera by integrated bead bed immunoassay in a microchip for cancer diagnosis," *Anal. Chem.*, vol. 73, pp. 1213-1218, 2001.

[36] H. Nakamura, Y. Murakami, K. Yokoyama, E. Tamiya, I. Karube, M. Suda, and S. Uchiyama, "A compactly integrated flow cell with a chemiluminescent FIA system for determining lactate concentration in serum," *Anal. Chem.*, vol. 73, pp. 373-378, 2001.

[37] J. C. Fanguy and C. S. Henry, "The analysis of uric acid in urine using microchip capillary electrophoresis with electrochemical detection," *Electrophoresis*, vol. 23, pp. 767-773, 2002.

[38] H. M. Sorouraddin, A. Hibara, M. A. Proskurnin, and T. Kitamori, "Integrated FIA for the determination of ascorbic acid and dehydroascorbic acid in a microfabricated glass channel by thermal lens microscopy," *Analytical Sciences*, vol. 16, pp. 1033-1037, 2000.

[39] Y. Deng, J. Henion, J. Li, P. Thibault, C. Wang, and D. J. Harrison, "Chip-based capillary electrophoresis/mass spectrometry determination of carnitines in human urine," *Anal. Chem.*, vol. 73, pp. 639-46, 2001.

[40] N. J. Munro, Z. Huang, D. N. Finegold, and J. P. Landers, "Indirect fluorescence detection of amino acids on electrophoretic microchips," *Anal. Chem.*, vol. 72, pp. 2765-2773, 2000.

[41] M. Zuborova, M. Masar, D. Kaniansky, M. Jöhnck, and B. Stanislawski, "Determination of oxalate in urine by zone electrophoresis on a chip with conductivity detection," *Electrophoresis*, vol. 23, pp. 774-781, 2002.

[42] I. R. Lauks, "Microfabricated biosensors and microanalytical systems for blood analysis," *Accounts of Chemical Research*, vol. 31, pp. 317-324, 1998.

[43] E. A. Schilling, A. E. Kamholz, and P. Yager, "Cell lysis and protein extraction in microfluidic device with detection by a fluorogenic enzyme assay," *Anal. Chem.*, vol. 74, pp. 1798-1804, 2002.

[44] L. D. Hutt, D. P. Glavin, J. L. Bada, and R. A. Mathies, "Microfabricated capillary electrophoresis amino acid chirality analyzer for extraterrestrial exploration," *Anal. Chem.*, vol. 71, pp. 4000-4006, 1999.

[45] P. A. Walker, M. D. Morris, M. A. Burns, and B. N. Johnson, "Isotachophoretic separations on a microchip. Normal Raman spectroscopy detection," *Anal. Chem.*, vol. 70, pp. 3766-3769, 1998.

[46] A. Daridon, M. Sequeira, G. Pennarun-Thomas, H. Dirac, J. P. Krog, P. Gravesen, J. Lichtenberg, D. Diamond, E. Verpoorte, and N. F. de Rooij, "Chemical sensing using an integrated chemical system based on the Berthelot reaction," *Sensors & Actuators B-Chemical*, vol. 76, pp. 235-243, 2001.

[47] P. Belgrader, W. Benett, D. Hadley, J. Richards, P. Stratton, R. J. Mariella, and F. Milanovich, "Infectious disease - PCR detection of bacteria in seven minutes," *Science*, vol. 284, pp. 449-450, 1999.

[48] M. B. Esch, L. E. Locascio, M. J. Tarlov, and R. A. Durst, "Detection of viable Cryptosporidium parvum using DNA-modified liposomes in a microfluidic chip," *Anal. Chem.*, vol. 73, pp. 2952-8, 2001.

[49] P. Belgrader, M. Okuzumi, F. Pourahmadi, D. A. Borkholder, and M. A. Northrup, "A microfluidic cartridge to prepare spores for PCR analysis," *Biosensors & Bioelectronics*, vol. 14, pp. 849-852, 2000.

[50] P. Belgrader, S. Young, B. Yuan, M. Primeau, L. A. Christel, F. Pourahmadi, and M. A. Northrup, "A battery-powered notebook thermal cycler for rapid multiplex real time PCR analysis," *Anal. Chem.*, vol. 73, pp. 286-289, 2001.

[51] R. F. Wolffenbuttel, "Silicon micromachining for integrated radiant sensors," *Sensors & Actuators A*, vol. 30, pp. 109-115, 1992.

[52] H. Becker and C. Gärtner, "Polymer microfabrication methods for microfluidic analytical applications," *Electrophoresis*, vol. 21, pp. 12-26, 2000.

[53] S. M. Sze, *Semiconductor Devices. Physics and Technology*, 1 ed: John Wiley & Sons, 1985.

[54] T. Rogers and J. Kowal, "Selection of glass, anodic bonding conditions material compatibility for silicon-glass capacitive sensors," *Sensors & Actuators A*, vol. 46-47, pp. 113-120, 1995.

[55] T. Laurell, J. Drott, and L. Rosengren, "Silicon wafer integrated enzyme reactors," *Biosensors and Bioelectronics*, vol. 10, pp. 289-299, 1995.

[56] M. Shimbo, K. Furukawa, and K. Tanzaka, "Silicon-to-silicon direct bonding method," *J. Appl. Phys.*, vol. 60, pp. 2987-2989, 1986.

[57] N. Chiem, L. Lockyear-Shultz, P. Andersson, C. Skinner, and D. J. Harrison, "Room temperature bonding of micromachined glass devices for capillary electrophoresis," *Sensors and Actuators B*, vol. 63, pp. 147-152, 2000.

[58] T. Nishimoto, Y. Fujiyama, H. Abe, M. Kanai, H. Nakanishi, and A. Arai, "Microfabricated CE chips with optical slit for UV absorption detection", Proceedings of Micro Total Analysis Systems 2000, Enschede, The Netherlands, 2000, 395-398.

[59] A. Daridon, V. Fascio, J. Lichtenberg, R. Wütrich, H. Langen, E. Verpoorte, and N. F. de Rooij, "Multi-layer microfluidic glass chips for microanalytical applications," *Fresenius Journal of Anal. Chem.*, vol. 371, pp. 261-269, 2001.

[60] J. Lichtenberg, E. Verpoorte, and N. F. de Rooij, "Sample preconcentration by field amplification stacking for microchip-based capillary electrophoresis," *Electrophoresis*, vol. 22, pp. 258-271, 2001.

[61] B. H. Weiller, L. Ceriotti, T. Shibata, D. Rein, M. A. Roberts, J. Lichtenberg, J. B. German, N. F. de Rooij, and E. Verpoorte, "Analysis of lipoproteins by capillary zone electrophoresis in microfluidic devices: assay development and surface roughness measurements," *Anal. Chem.*, vol. 74, pp. 1702-1711, 2002.

[62] A. Eckersten, A. E. Örlefors, C. Ellström, K. Erickson, E. Löfman, A. Eriksson, S. Eriksson, A. Jorsbeck, N. Tooke, H. Derand, G. Ekstrand, J. Engström, A.-K. Honerud, A. Aksberg, H. Hedsten, L. Rosengren, M. Stjernström, T. Hultman, and P. Andersson, "High-throughput SNP scoring in a disposable microfabricated CD device", Proceedings of Micro Total Analysis Systems 2000, Enschede, The Netherlands, 2000, 521-524.

[63] G. Ekstrand, C. Holmquist, A. E. Örlefors, B. Hellman, A. Larsson, and P. Andersson, "Microfluidics in a rotating CD", Proceedings of Micro Total Analysis Systems 2000, Enschede, The Netherlands, 2000, 311-314.

[64] N. Thomas, A. Ocklind, I. Blikstad, S. Griffiths, M. Kenrick, H. Derand, G. Ekstrand, C. Ellström, A. Larsson, and P. Andersson, "Integrated cell based assays in microfabricated disposable CD devices", Proceedings of Micro Total Analysis Systems 2000, Enschede, The Netherlands, 2000, 249-252.

[65] A. Palm, S. R. Wallenborg, M. Gustafsson, A. Hedström, E. Togan-Tekin, and P. Andersson, "Integrated sample preparation and MALDI MS on a disc", Proceedings of Micro Total Analyis Systems 2001, Monterey, CA, USA, 2001, 216-118.

[66] G. Jesson and P. Andersson, "Multiple separations at nanoliter scale using gradient elution", Proceedings of Micro Total Analysis Systems 2001, Monterey, CA, USA, 2001, 551-552.

[67] C. S. Effenhauser, G. J. M. Bruin, A. Paulus, and M. Ehrat, "Integrated capillary electrophoresis on flexible silicone microdevices - Analysis of DNA restriction fragments and detection of single DNA molecules on microchips," *Anal. Chem.*, vol. 69, pp. 3451-3457, 1997.

[68] D. C. Duffy, J. C. McDonald, O. J. A. Schueller, and G. M. Whitesides, "Rapid prototyping of microfluidic systems in poly(dimethylsiloxane)," *Anal. Chem.*, vol. 70, pp. 4974-4984, 1998.

[69] J. C. McDonald, D. C. Duffy, J. R. Anderson, D. T. Chiu, H. Wu, O. J. A. Schueller, and G. M. Whitesides, "Fabrication of microfluidic systems in poly(dimethylsiloxane) [Review]," *Electrophoresis*, vol. 21, pp. 27-40, 2000.

[70] G. Ocvirk, M. Munroe, T. Tang, R. Oleschuk, K. Westra, and D. J. Harrison, "Electrokinetic control of fluid flow in native poly(dimethylsiloxane) capillary electrophoresis devices," *Electrophoresis*, vol. 21, pp. 107-115, 2000.

[71] V. Linder, E. Verpoorte, W. Thormann, N. F. de Rooij, and H. Sigrist, "Surface biopassivation of replicated poly(dimethylsiloxane) microfluidic channels and application to heterogeneous immunoreaction with on-chip fluorescence detection," *Anal. Chem.*, vol. 73, pp. 4181-4189, 2001.

[72] R. S. Martin, A. J. Gawron, B. A. Fogarty, F. B. Regan, E. Dempsey, and S. M. Lunte, "Carbon paste-based electrochemical detectors for microchip capillary electrophoresis/electrochemistry," *Analyst*, vol. 126, pp. 277-80, 2001.

[73] J. W. Hong, T. Fujii, M. Seki, T. Yamamoto, and I. Endo, "Integration of gene amplification and capillary gel electrophoresis on a poly(dimethylsiloxane)-glass hybrid microchip," *Electrophoresis*, vol. 22, pp. 328-333, 2001.

[74] V. Linder, E. Verpoorte, N. F. de Rooij, H. Sigrist, and W. Thormann, "Application of surface biopassivated disposable poly(dimethylsiloxane)/glass chips to a heterogeneous

competitive human serum immunoglobulin G immunoassay with incorporated internal standard," *Electrophoresis*, vol. 23, pp. 740-749, 2002.

[75] E. Eteshola and D. Leckband, "Development and characterization of an ELISA assay in PDMS microfluidic channels," *Sensors and Actuators B-Chemical*, vol. 72, pp. 129-133, 2001.

[76] R. S. Kane, S. Takayama, E. Ostuni, D. E. Ingber, and G. M. Whitesides, "Patterning proteins and cells using soft lithography," *Biomaterials*, vol. 20, pp. 2363-2376, 1999.

[77] B. Michel, A. Bernard, A. Bietsch, D. E., M. Geisseler, D. Juncker, H. Kind, J.-P. Renault, H. Rothuizen, H. Schmid, P. Schmidt-Winkel, R. Stutz, and H. Wolf, "Printing meets lithography: soft approaches to high-resolution patterning," *J. Res. & Dev.*, vol. 45, pp. 697-719, 2001.

[78] M. A. Unger, H.-P. Chou, T. Thorsen, A. Scherer, and S. R. Quake, "Monolithic microfabricated valves and pumps by multilayer soft lithography," *Science*, vol. 288, pp. 113-116, 2000.

[79] C. L. Rice and R. Whitehead, "Electrokinetic flow in a narrow cylindrical capillary," *Journal of Physical Chemistry*, vol. 69, pp. 4017-4024, 1965.

[80] P. D. Grossman and J. C. Colburn, *Capillary electrophoresis : theory & practice*. San Diego: Academic Press, 1992.

[81] J. P. Landers, *Handbook of capillary electrophoresis*, 2nd ed. ed. Boca Raton, FL: CRC Press, 1997.

[82] P. G. Righetti, C. Gelfi, B. Verzola, and L. Castelletti, "The state of the art of dynamic coatings," *Electrophoresis*, vol. 22, pp. 603-611, 2001.

[83] E. Cordova, J. M. Gao, and G. M. Whitesides, "Noncovalent polycationic coatings for capillaries in capillary electrophoresis of proteins," *Anal. Chem.*, vol. 69, pp. 1370-1379, 1997.

[84] J. K. Towns and F. E. Regnier, "Capillary eletrophoretic separations of proteins using nonionic surfactant coatings," *Anal. Chem.*, vol. 63, pp. 1126-1132, 1991.

[85] K. Srinivasan, G. Pohl, and N. Avdalovic, "Cross-linked polymer coatings for capillary electrophoresis and application to analysis of basic proteins, acidic proteins, and inorganic ions," *Anal. Chem.*, vol. 69, pp. 2798-2805, 1997.

[86] N. E. Baryla and L. C.A., "Simultaneous separation of cationic and anionic proteins using zwitterionic surfactants in capillary electrophoresis," *Anal. Chem*, vol. 72, pp. 2280-2284, 2000.

[87] M. Chiari and A. Gelain, "Developments in capillary coating and DNA separation matrices," in *Analysis of nucleic acids by capillary electrophoresis*, C. E. Heller, Ed. Braunschweig, Wiesbaden Germany: Vieweg and Sohn, 1997, pp. 133-171.

[88] D. J. Harrison, K. Fluri, K. Seiler, Z. H. Fan, C. S. Effenhauser, and A. Manz, "Micromachining a miniaturized capillary electrophoresis-based chemical analysis system on a chip," *Science*, vol. 261, pp. 895-897, 1993.

[89] E. Verpoorte, "Microfluidic chips for clinical and forensic analysis," *Electrophoresis*, vol. 23, pp. 677-712, 2002.

[90] C. S. Effenhauser, G. J. M. Bruin, and A. Paulus, "Integrated chip-based capillary electrophoresis," *Electrophoresis*, vol. 18, pp. 2203-2213, 1997.

[91] G. J. M. Bruin, "Recent developments in electrokinetically driven analysis on microfabricated devices," *Electrophoresis*, vol. 21, pp. 3931-3951, 2000.

[92] S. C. Jacobson, R. Hergenröder, L. B. Koutny, R. J. Warmack, and J. M. Ramsey, "Effects of injection schemes and column geometry on the performance of microchip electrophoresis devices," *Anal. Chem.*, vol. 66, pp. 1107-1113, 1994.

[93] L. L. Shultz-Lockyear, C. L. Colyer, Z. H. Fan, K. J. Roy, and D. J. Harrison, "Effects of injector geometry and sample matrix on injection and sample loading in integrated capillary electrophoresis devices," *Electrophoresis*, vol. 20, pp. 529-538, 1999.

[94] S. C. Jacobson, L. B. Koutny, R. Hergenröder, A. W. Moore, and J. M. Ramsey, "Microchip capillary electrophoresis with an integrated postcolumn reactor," *Anal. Chem.*, vol. 66, pp. 3472-3476, 1994.

[95] M. M. Dittmann, K. Wienand, F. Bek, and G. P. Rozing, "Theory and practice of capillary electrochromatography," *LC-GC*, vol. 13, pp. 800-808, 1995.

[96] J. H. Knox and I. H. Grant, "Electrochromatography in packed tubes using 1.5 to 50 µm silica gels and ODS bonded silica gels," *Chromatographia*, vol. 32, pp. 317-328, 1991.

[97] D. A. Stead, R. G. Reid, and R. B. Taylor, "Capillary electrochromatography of steroids - Increased sensitivity by on-line concentration and comparison with high- performance liquid chromatography," *J. Chromatogr. A*, vol. 798, pp. 259-267, 1998.

[98] S. E. van den Bosch, S. Heemstra, J. C. Kraak, and H. Poppe, "Experiences with packed capillary electrochromatography at ambient pressure," *J. Chromatogr. A*, vol. 755, pp. 165-177, 1996.

[99] J.-L. Liao, N. Chen, C. Ericson, and S. Hjertén, "Preparation of continuous beds derivatized with one-step alkyl and sulfonate groups for capillary electrochromatography," *Anal. Chem.*, vol. 68, pp. 3468-3472, 1996.

[100] Y. Fintschenko, W.-Y. Choi, S. M. Ngola, and T. J. Shepodd, "Chip electrochromatography of polycyclic aromatic hydrocarbons on an acrylate-based UV-initiated porous polymer monolith," *Fresenius Journal of Anal. Chem.*, vol. 371, pp. 174-181, 2001.

[101] E. C. Peters, M. Petro, F. Svec, and J. M. J. Frechet, "Molded rigid polymer monoliths as separation media for capillary electrochromatography. 1. Fine control of porous properties and surface chemistry," *Anal. Chem.*, vol. 70, pp. 2288-2295, 1998.

[102] E. C. Peters, M. Petro, F. Svec, and J. M. J. Frechet, "Molded rigid polymer monoliths as separation media for capillary electrochromatography. 2. Effect of chromatographic conditions on the separation," *Anal. Chem.*, vol. 70, pp. 2296-2302, 1998.

[103] G. Vanhoenacker, T. Van den Bosch, G. P. Rozing, and P. Sandra, "Recent applications of capillary electrochromatography," *Electrophoresis*, vol. 22, pp. 4064-4103, 2001.

[104] M. R. Taylor, P. Teale, S. A. Westwood, and D. Perrett, "Analysis of corticosteroids in biofluids by capillary electrochromatography with gradient elution," *Anal. Chem.*, vol. 69, pp. 2554-2558, 1997.

[105] C. J. Paterson, R. J. Boughtflower, D. Higton, and E. Palmer, "An investigation into the application of capillary electrochromatography mass spectrometry (CEC-MS) for the analysis and quantification of a potential drug candidate in extracted plasma," *Chromatographia*, vol. 46, pp. 599-604, 1997.

[106] D. F. Chollet, "Determination of antiepileptic drugs in biological material," *J. Chromatogr. B Biomed. Sci. Appl.*, vol. 767, pp. 191-233, 2002.

[107] K. Seiler, Z. H. H. Fan, K. Fluri, and D. J. Harrison, "Electroosmotic pumping and valveless control of fluid flow within a manifold of capillaries on a glass chip," *Anal. Chem.*, vol. 66, pp. 3485-3491, 1994.

[108] A. Manz, C. S. Effenhauser, N. Burggraf, D. J. Harrison, K. Seiler, and K. Fluri, "Electroosmotic pumping and electrophoretic separation for miniaturised chemical analysis systems," *J. Micromech. Microeng.*, vol. 4, pp. 257-265, 1994.

[109] R. M. Guijt, J. Lichtenberg, E. Baltussen, E. Verpoorte, N. F. de Rooij, and G. W. K. van Dedem, "Indirect electro-osmotic pumping for direct sampling from bioreactors", Proceedings of Micro Total Analysis Systems 2001, Monterey, CA, USA, 2001, 399-400.

[110] R. M. Guijt, J. Lichtenberg, N. F. de Rooij, E. Verpoorte, E. Baltussen, and G. W. K. van Dedem, "Indirect Electro-Osmotic Pumping," *Journal of the Association for Laboratory Automation*, vol. 7, pp. 62-64, 2002.

[111] O. T. Guenat, D. Ghiglione, W. E. Morf, and N. F. de Rooij, "Partial electroosmotic pumping in complex capillary systems - Part 2: Fabrication and application of a Micro Total Analysis Systems (μTAS) suited for continuous volumetric nanotitrations," *Sensors and Actuators B-Chemical*, vol. 72, pp. 273-282, 2001.

[112] I. M. Lazar, R. S. Ramsey, S. C. Jacobson, R. S. Foote, and J. M. Ramsey, "Novel microfabricated device for electrokinetically induced pressure flow and electrospray ionization mass spectrometry," *J. Chromatogr. A*, vol. 892, pp. 195-201, 2000.

[113] P. H. Paul, D. W. Arnold, and D. J. Rakestraw, "Electrokinetic generation of high pressure using porous microstructures", Proceedings of Micro Total Analysis Systems '98, Banff, Canada, 1998, 49-52.

[114] P. H. Paul, D. W. Arnold, D. W. Neyer, and K. B. Smith, "Electrokinetic pump application in micro total analysis systems: mechanical actuation to HPLC", Proceedings of Micro Total Analysis Systems 2000, Enschede, The Netherlands, 2000, 583-590.

[115] H. Bayer and H. Engelhardt, "Capillary electrophoresis in organic polymer capillaries," *J. Microcolumn Sep.*, vol. 8, pp. 479-484, 1996.

[116] L. Martynova, L. E. Locascio, M. Gaitan, G. W. Kramer, R. G. Christensen, and W. A. MacCrehan, "Fabrication of plastic microfluid channels by imprinting methods," *Anal. Chem.*, vol. 69, pp. 4783-4789, 1997.

[117] L. Song, D. Fang, R. K. Kobos, S. J. Pace, and B. Chu, "Separation of double-stranded DNA fragments in plastic capillary electrophoresis chips using E99P69E99 as separation medium," *Electrophoresis*, vol. 20, pp. 2847-2855, 1999.

[118] I. Caelen, A. Bernard, D. Juncker, B. Michel, H. Heinzelmann, and E. Delamarche, "Formation gradient of proteins on surfaces with microfluidic networks," *Langmuir*, vol. 16, pp. 9125-9130, 2001.

[119] D. Juncker, H. Schmid, A. Bernard, I. Caelen, B. Michel, N. F. de Rooij, and E. Delamarche, "Soft and rigid two-level microfluidic networks for patterning surfaces," *J. Micromech. Microeng.*, vol. 11, pp. 532-541, 2001.

[120] D. C. Duffy, H. L. Gillis, J. Lin, N. F. Sheppard, Jr., and G. J. Kellogg, "Microfabricated centrifugal microfluidic systems: Characterization and multiple enzymatic assays," *Anal. Chem.*, vol. 71, pp. 4669-4678, 1999.

[121] B. Zhao, J. S. Moore, and D. J. Beebe, "Surface-directed liquid flow inside microchannels," *Science*, vol. 291, pp. 1023-1026, 2001.

[122] D. J. Beebe, J. S. Moore, J. M. Bauer, Q. Yu, R. H. Liu, C. Devadoss, and B.-H. Jo, "Functional hydrogel structures for autonomous flow control inside microfluidic channels," *Nature*, vol. 404, pp. 588-590, 2000.

[123] Y. Liu, C. B. Rauch, R. L. Stevens, L. R., J. Yang, D. B. Rhine, and P. Grodzinski, "DNA amplification and hybridization assay in integrated plastic monolithic devices," *Anal. Chem.*, vol. 74, pp. 3063-3070, 2002.

[124] R.-L. Chien and J. W. Parce, "Multiport flow-control system for lab-on-a-chip microfluidic devices," *Fresenius Journal of Anal. Chem.*, vol. 371, pp. 106-11, 2001.

[125] M. Kerby and R.-L. Chien, "A fluorogenic assay using pressure-driven flow on a microchip," *Electrophoresis*, vol. 22, pp. 3916-23, 2001.

[126] K. A. Wolfe, M. C. Breadmore, J. P. Ferrance, M. E. Power, J. F. Conroy, P. M. Norris, and J. P. Landers, "Toward a microchip-based solid-phase extraction method for isolation of nucleic acids," *Electrophoresis*, vol. 23, pp. 727-733, 2002.

[127] J. P. Kutter, S. C. Jacobson, N. Matsubara, and J. M. Ramsey, "Solvent-programmed microchip open-channel electrochromatography," *Anal. Chem.*, vol. 70, pp. 3291-3297, 1998.

[128] R. Boom, C. J. A. Sol, M. M. M. Salimans, C. L. Jansen, P. M. E. Wertheim-van Dillen, and J. van der Noordaa, "Rapid and simple method for purification of nucleic acids," *J. Clin. Microbiol.*, vol. 28, pp. 495-503, 1990.

[129] E. M. J. Verpoorte, B. H. van der Schoot, S. Jeanneret, A. Manz, H. M. Widmer, and N. F. de Rooij, "Three-dimensional micro flow manifolds for miniaturized chemical analysis systems," *J. Micromech. Microeng.*, vol. 4, pp. 246-256, 1994.

[130] J. P. Brody, P. Yager, R. E. Goldstein, and R. H. Austin, "Biotechnology at low Reynolds numbers," *Biophysical Journal*, vol. 71, pp. 3430-3441, 1996.

[131] S. M. Flockhart and R. S. Dhariwal, "Experimental and numerical investigation into the flow characteristics of channels etched in < 100 > silicon," *Journal of Fluids Engineering-Transactions of the Asme*, vol. 120, pp. 291-295, 1998.

[132] P. J. A. Kenis, R. F. Ismagilov, and G. M. Whitesides, "Microfabrication inside capillaries using multiphase laminar flow patterning," *Science*, vol. 285, pp. 83-85, 1999.

[133] M. Surmeian, M. N. Slyadnev, H. Hisamoto, A. Hibara, K. Uchiyama, and T. Kitamori, "Three-layer flow membrane system on a microchip for investigation of molecular transport," *Anal. Chem.*, vol. 74, pp. 2014-2020, 2002.

[134] R. H. Liu, M. A. Stremler, K. V. Sharp, M. G. Olsen, J. G. Santiago, R. J. Adrian, H. Aref, and D. J. Beebe, "Passive mixing in a three-dimensional serpentine microchannel," *Journal of Microelectromechanical Systems*, vol. 9, pp. 190-196, 2000.

[135] J. H. Kim, B. G. Kim, H. Nam, D. E. Park, K. S. Yun, J. B. Yoon, J. You, and E. Yoon, "A disposible DNA sample preparation microfluidic chip for nucleic acid probe assay", Proceedings of 15th Annual IEEE International MEMS 2002, Las Vegas, Nevada, 2002, 133-136.

[136] M. H. Oddy, J. G. Santiago, and J. C. Mikkelsen, "Electrokinetic instability micromixing," *Anal. Chem.*, vol. 73, pp. 5822-5832, 2001.

[137] D. Bökenkamp, A. Desai, X. Yang, Y. C. Tai, E. M. Marzluff, and S. L. Mayo, "Microfabricated silicon mixers for submillisecond quench-flow analysis," *Anal. Chem.*, vol. 70, pp. 232-236, 1998.

[138] L. A. Christel, K. Petersen, W. McMillan, and M. A. Northrup, "Rapid, automated nucleic acid probe assays using silicon microstructures for nucleic acid concentration," *Journal of Biomechanical Engineering-Transactions of the ASME*, vol. 121, pp. 22-27, 1999.

[139] K. Peck, L. Stryer, A. N. Glazer, and R. A. Mathies, "Single-molecule fluorescence detection: Autocorrelation criterion and experimental realization with phycoerythrin," *Proc. Nat. Acad. Sci. USA*, vol. 86, pp. 4087-91, 1989.

[140] R. A. Mathies, K. Peck, and L. Stryer, "Optimization of high-sensitivity fluorescence detection," *Anal. Chem.*, vol. 62, pp. 1786-91, 1990.

[141] F. von Heeren, E. Verpoorte, A. Manz, and W. Thormann, "Micellar electrokinetic chromatography separations and analyses of biological samples on a cyclic planar microstructure," *Anal. Chem.*, vol. 68, pp. 2044-2053, 1996.

[142] Z. Liang, N. H. Chiem, G. Ocvirk, T. Tang, K. Fluri, and D. J. Harrison, "Microfabrication of a planar absorbance and fluorescence cell for integrated capillary electrophoresis devices," *Anal. Chem.*, vol. 68, pp. 1040-1046, 1996.

[143] G. Ocvirk, T. Tang, and D. J. Harrison, "Optimization of confocal epifluorescence microscopy for microchip-based miniaturized total analysis systems," *Analyst*, vol. 123, pp. 1429-1434, 1998.

[144] G. F. Jiang, S. Attiya, G. Ocvirk, W. E. Lee, and D. J. Harrison, "Red diode laser induced fluorescence detection with a confocal microscope on a microchip for capillary electrophoresis," *Biosensors & Bioelectronics*, vol. 14, pp. 861-869, 2000.

[145] J. C. Fister, S. C. Jacobson, L. M. Davis, and J. M. Ramsey, "Counting single chromophore molecules for ultrasensitive analysis and separations on microchip devices," *Anal. Chem.*, vol. 70, pp. 431-437, 1998.

[146] B. B. Haab and R. A. Mathies, "Single-molecule detection of DNA separations in microfabricated capillary electrophoresis chips employing focused molecular streams," *Anal. Chem.*, vol. 71, pp. 5137-5145, 1999.

[147] G.-L. Lettieri, E. Verpoorte, and N. F. de Rooij, "Planar microfluidic devices for controlled vortex generation", Proceedings of Transducers '01, Munich, Germany, 2001, 1510-1513.

[148] J.-C. Roulet, R. Völkel, H. P. Herzig, E. Verpoorte, N. F. de Rooij, and R. Dändliker, "Performance of an integrated micro-optical system for fluorescence detection in microfluidic systems," *Anal. Chem.*, vol. 74, pp. 3400-3407, 2002.

[149] B. Graß, A. Neyer, M. Jöhnck, D. Siepe, F. Eisenbeiß, G. Weber, and R. Hergenröder, "A new PMMA microchip device for isotachophoresis with integrated conductivity detector," *Sensors and Actuators B*, vol. 72, pp. 249-258, 2001.

[150] Y. Liu, D. O. Wipf, and C. S. Henry, "Conductivity detection for monitoring mixing reactions in microfluidic devices," *Analyst*, vol. 126, pp. 1248–1251, 2001.

[151] J. Lichtenberg, N. F. de Rooij, and E. Verpoorte, "A microchip electrophoresis system with integrated in-plane electrodes for contactless conductivity detection," *Electrophoresis*, vol. 23, in press, 2002.

[152] M. Galloway, W. Stryjewski, A. Henry, S. M. Ford, S. Llopis, R. L. McCarley, and S. A. Soper, "Contact conductivity detection in poly(methylmethacrylate)-based microfluidic devices for analysis of mono- and polyanionic molecules," *Anal. Chem.*, vol. 74, pp. 2407-15, 2002.

[153] R. P. Baldwin, T. J. Roussel, M. M. Crain, V. Bathlagunda, D. J. Jackson, J. Gullapalli, J. A. Conklin, R. Pai, J. F. Naber, K. M. Walsh, and R. S. Keyton, "Fully integrated on-chip electrochemical detection for capillary electrophoresis in a microfabricated device," *Anal. Chem.*, vol. 74, pp. 3690-3697, 2002.

2 Technology for rectangular channels

2.1 Introduction

Most of the work in the field of miniaturized CE so far has been done on glass substrates. Glass has many advantages, such as its optical transparency and well-known chemical properties for electroosmosis and regeneration processes. However, the fabrication process is time consuming and requires a relatively dust-free environment. For instance, a simple, one-step photolithographic process, followed by glass wet etching and substrate cleaning for the bonding, requires at least eight hours of work in the cleanroom. The bonding process itself is also time consuming and critical, requiring pristine wafer surfaces and high temperatures. Moreover, glass itself is fragile and in general too expensive for disposable devices, though Capiler Technologies sells glass devices for rapid DNA analysis (*www.chem.agilent.com*). Polymers offer an interesting alternative to glass as substrates for mass fabrication of microfluidic systems [1]. Polymers are usually inexpensive (0.2-2 cents per cm^2), while the boro-float glass (e.g. Corning Pyrex) price is in the order of 10-20 cents/cm^2 [1] and the price for the standard Pyrex wafers we use (Pyrex 7740, Bullen Ultrasonics) is about 40 cents/cm^2. Plastic devices are also easy to handle and robust. Moreover, the fabrication processes are based on replication (casting, embossing or injection molding) ensuring good

device reproducibility at considerably lower costs than for glass [2-8]. The combination of photolithographically made masters and these new technologies allows the fabrication of high-aspect-ratio structures, which means large height: width ratios, imparting a greater freedom in the choice of the channel profile than available for isotropically etched glass channels. The bonding protocols used for the fabrication of polymeric devices are also less demanding, even if the bonding process is not always immediate. All these features make polymeric devices very attractive for generating integrated disposable devices for point-of-care applications [9-13]. However, the transfer of separation methods from glass chips to plastic devices is not as direct and easy as first thought, due to the native hydrophobicity of most plastic surfaces. In fact, working in these devices is often a challenge, due to wetting and adsorption problems. Moreover, the electroosmotic flow is not always well characterized in plastic devices, and much effort has been spent to stabilize and control it [14-19]. It is also worth mentioning that plastic stability at high temperatures and high pH values is reduced. Some plastics are incompatible with solvents and/or are autofluorescent, properties that make polymeric devices unsuitable for certain applications and LIF detection.

The profile of plastic channels depends on the master structures. In this chapter, two approaches that can be used for the fabrication of narrow, tall master features are presented. These masters will be used for the fabrication of poly(dimethylsiloxane) (PDMS) devices by replica molding. In the first approach, the master consists of a silicon wafer structured by deep reactive-ion etching (DRIE). In the second, the master is made by structuring SU-8, a negative epoxy-based resist, on a glass substrate. The fabrication processes are described in detail, while the use of the replicated PDMS structures will be discussed in Chapter 4 (CEC separation in PDMS packed channels), Chapter 5 (nucleic acid extraction in PDMS packed beds) and Chapter 6 (UV absorbance detection through PDMS channels).

In this technology-oriented chapter, the use of dry etching to create high-aspect-ratio channels directly in fused silica wafers will be also presented and discussed. Although possible, our results indicate that this technology will require a significant development effort before being generally applicable to fabrication of microfluidic devices for lab-on-a-chip applications. At present, this approach is still quite expensive, and more time consuming than other related dry etching methods for silicon micromachining.

2.1.1 Reagents

Tris(hydroxymethyl)aminomethane (Tris), boric acid and 0.1 M NaOH (0.2-μm-filtered) were obtained from Fluka (Buchs, Switzerland). Acetone (MOS grade), 2-propanol (MOS grade) and hexamethyldisilazane (HMDS) were purchased from Laporte Electronic Chemicals (Riddings, England). Hexane and 100% fuming HND_3 were purchased from Merck (Darmstadt, Germany), while toluene and dimethyloctadecylchlorosilane were obtained from Aldrich (Buchs, Switzerland). Amino acids, fluorescein sodium and fluorescein isothiocyanate isomer I (FITC) were purchased from Sigma (Buchs, Switzerland). The Dow Corning PDMS kit Sylgard 184 was obtained from Distrelec (Nänikon, Switzerland). AZ 1518 and AZ 4562 photoresists, and AZ 351 developer were purchased from Clariant (Frankfurt, Germany). SU-8 was obtained from MicroChem (Newton, MA, local distributor in Rapperswil, Switzerland) and SU-8 developer, propylene glycol monomethyl ether acetate (PGMEA puriss.), was purchased from Fluka (Buchs, Switzerland).

2.2 Master for poly(dimethylsiloxane) devices

As introduced in Chapter 1, poly(dimethylsiloxane) (PDMS) has been used for several applications [2]. It is commercially available (Sylgard 184, Dow

Corning, Midland, MI), inexpensive and UV/visible transparent (see Chapter 6). Fabrication of PDMS devices represents the easiest method to produce microstructures, once a master is available (as described in Chapter 1). For the replication, neither cleanroom facilities nor expensive instrumentation, as required for hot embossing and injection molding, are necessary. An oven for curing of the polymer is enough.

In the next sections, two different approaches chosen for the fabrication of the master are presented and discussed.

2.2.1 Micromachined silicon masters by DRIE

As reported in [20], masters for PDMS replicas can be fabricated in silicon by DRIE. In our case, 10-cm-diameter, ⟨100⟩-oriented silicon wafers (Siltronix, Vernier-Genève, Switzerland) were used. The fabrication process is described in Figure 2-1 and detailed in the following points.

1. **Silicon wafer cleaning**. The Si wafer is cleaned sequentially with acetone and 2-propanol for 5 min each and fuming HNO_3 for 10 minutes, rinsed in deionised, 18-MΩ (DI-18 MΩ) water, and rinsed and dried in the wafer washing machine. The wafer is then dehydrated at 200°C for at least 30 min.
2. **Photolithography process**. The Si wafer is silanized with gaseous hexamethyldisilazane (HMDS) to prevent water adsorption and improve resist adhesion. AZ 1518 positive photoresist is spin-coated onto the silicon wafer at 500 rpm for 3 s followed by 4000 rpm for 40 s to define a 1.8-μm-thick photoresist layer. Thicker photoresists can be used, in particular when deep structures and long etching times are required. The wafer is prebaked at 85°C for 30 min, or alternatively on a hot-plate at 100°C for 1 min. The photoresist-coated wafer is then placed into a mask aligner (Electronic Vision AL 6, Schaarding, Austria), where it is aligned

with respect to the mask and exposed to UV radiation. The exposure time is calculated as the ratio between the energy necessary to achieve a good exposition of the photoresist (55 mJ in the case of the AZ 1518) and the lamp intensity (mJ/sec, measured weekly). The distance between mask and substrate, and the precision of mask-substrate alignment, depend on the kind of mask used. When a resolution of ~1 μm is required, 0.5-mm-thick chromium masks (from Delta Mask, Enschede, Holland) are used and contact mode with wedge error 1 (very clean mask) or 2 (dirty or scratched mask) is chosen. Note that the wedge error defines the precision with which the aligner tries to adjust the mask and chuck. For rapid prototyping, transparency masks (from DIP SA, Lausanne, Switzerland) are preferred. The transparency is cut to size and attached on a cleaned 500-μm-thick, 5-by-5 inch quartz plate (final thickness of plate + transparency= 0.8 mm). In this case, contact mode is also used, but a wedge error of 5 is necessary. The resolution is limited to 7 μm by the laser printer used at DIP SA. The zone of photoresist exposed to the UV light, in this case all the wafer except for the microfluidic network, is removed in developing solution (AZ 351 developer: DI water, 1:4). The wafer is dipped and agitated in this solution for 1 min. The wafer is then rinsed with DI-18 MΩ water and dried. After the definition of the features in the photoresist has been checked with a microscope, the wafer is *postbaked in the oven at 120°C for 30 min.*

3. **Deep reactive-ion etching.** To realize the channel structure as a relief on the master, the wafer is processed by DRIE in a Surface Technology Systems machine (STS, Newport, U.K.). During the DRIE, the ions in the chamber are directed perpendicularly at the wafer surface so that the areas surrounding the patterned photoresist channels are etched anisotropically. The etching rate for DRIE of Si is about 5 μm/min.

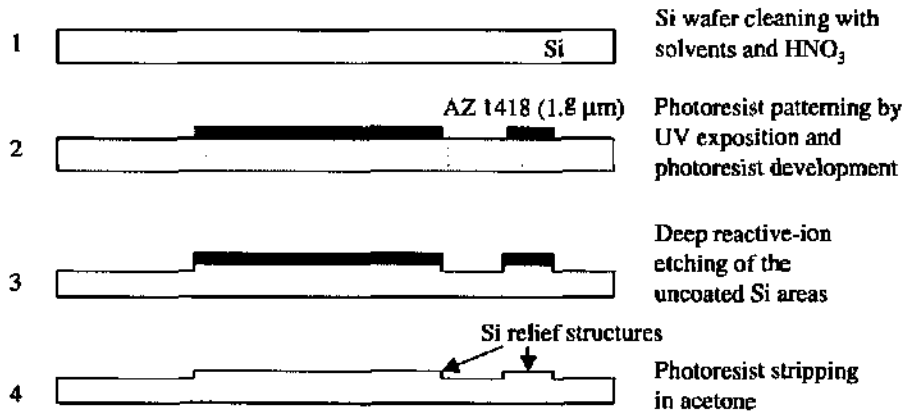

Figure 2-1 DRIE process for Si master fabrication.

4. **Master cleaning.** After DRIE the photoresist is stripped in acetone.

Vertical, high-aspect-ratio, smooth-walled profiles are achieved with DRIE. Usually the masters have 30 to 70-µm-high features. Silicon masters fabricated by DRIE using transparency and Cr masks are presented in Figure 2-2A and 2-2B, respectively. The different resolutions of the masks are faithfully transferred to the master and consequently to the plastic replica. In Figure 2-2A the structures have a scalloped edge while in Figure 2-2B they look very smooth. In both cases the walls are almost perfectly vertical.

All channel geometries can be transferred from a mask to the silicon wafer by DRIE as mentioned in Chapter 1, Section 1.2.1. Moreover, narrow and high-aspect-ratio structures can be realized with this process [21]. Silicon masters, like nickel molds, are suitable templates for hot embossing and injection molding, both processes which are widely used to fabricate polymeric parts [1].

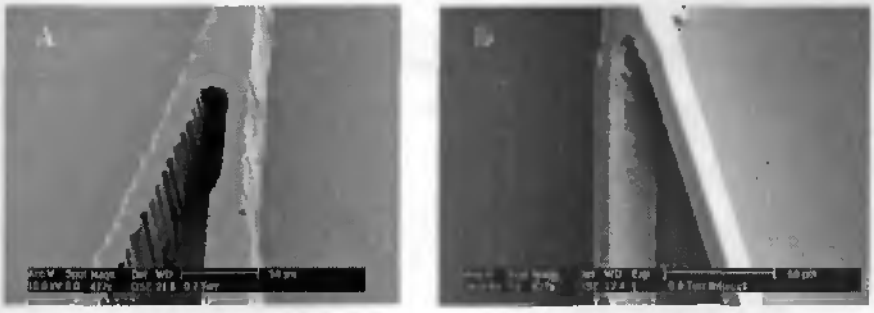

***Figure 2-2** ESEM images (720 × 484 pixel, standard definition) of the 50-μm-high injector element on a silicon master fabricated by DRIE using A) a transparency mask and B) a chromium mask during the photolithography process.*

2.2.2 SU-8 masters for rapid prototyping

Whitesides' group used masters made in photoresist for rapid prototyping [22], which consists of the use of transparency masks to pattern SU-8 epoxy layers. SU-8 is an epoxy-based, negative photoresist developed by IBM [23-25]. It can be patterned using a standard mask aligner to form thick features, having aspect ratios approaching 20. This photoresist is a low-cost material consisting of an epoxy (the monomer, which contains 8 epoxy groups is presented in Figure 2-3a), an organic solvent (γ-butyrolactone) and a photoinitiator (triaryl-sulfonium salt). It is deposited on a surface by spinning to produce films with thicknesses of 1 to 2000 μm, depending on the viscosity of the resist used and on the spinning rate. The deposition is followed by a softbake to evaporate the solvent. SU-8 is then polymerised by a cationic photopolymerization to create a cross-linked structure, as represented in Figure 2-3b. The polymerization reaction is schematised in Figure 2-4. The process starts with the formation of a Lewis acid from the triaryl-sulfonium salt under UV light exposure (Figure 2-4a).

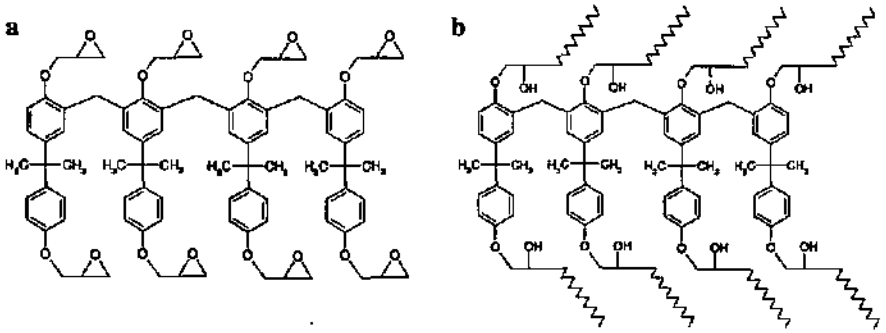

Figure 2-3 Structure of a) the SU-8 monomer and b) the SU-8 polymer.

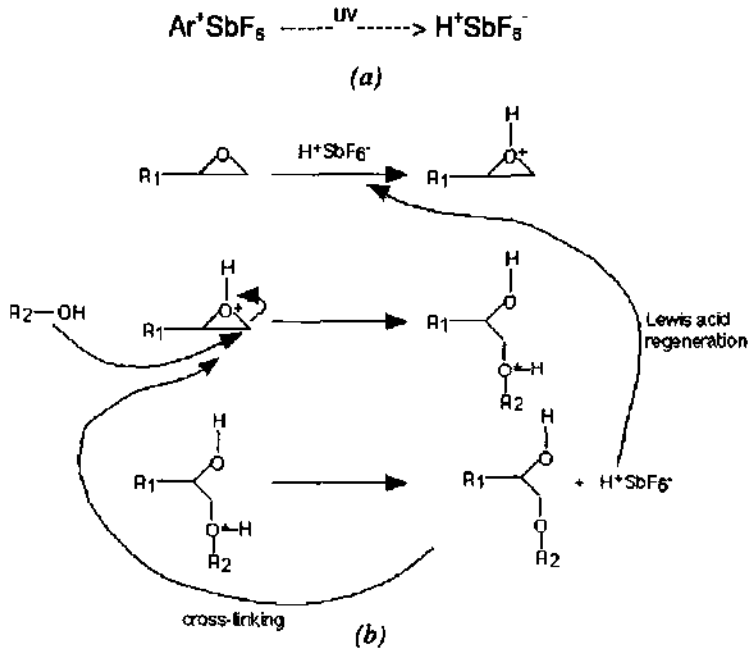

Figure 2-4 (a) Photolysis of the triaryl-sulfonium hexafluorantimonium which generates the Lewis acid. (b) Cationic polymerisation with epoxy group opening and chain propagation (www.somisys.ch/cationic.htm).

The polymerisation then continues with the ring-opening of the 1,2-epoxy, Lewis acid regeneration and propagation of the chain cross-linking (Figure 2-4b). The cross-linking takes place during the post-bake, which could be several minutes to a few hours, depending on the layer thickness. After polymerization, the SU-8 resist becomes relatively resistent to most organic solvents, making it suitable for applications that other polymers could not withstand. SU-8 devices have been used for the fabrication of low-cost, monolithic flow sensors [26], a laminar flow mixer [27], a device for solution delivery to neurons [28], and UV/visible detection systems [29]. For these applications, at least four methods have been developed for the fabrication of closed SU-8 channels for microfluidic devices [27, 29].

During the course of this thesis, SU-8 was employed for master fabrication. The process actually was optimized to obtain a multi-layer master for microfluidic devices containing features with different depths, to act as weirs for bead retention. Weir-based chambers were realized in glass by Oleschuk et al. and used to create a bead-packed bed for CEC and solid phase extraction [30]. For the fabrication of each structure, two photolithographic steps were required. In our case, once the two-layer SU-8 master is available, several structures can be replicated from it. Two designs were realized in SU-8:

i. a deep, 300 to 700-μm-wide channel with a weir on one side,

ii. a 400 × 400 (or 500 × 500) μm chamber defined by two weirs on either side placed in the channel along the flow direction.

The process developed for the master fabrication on a glass wafer consisted of three photolithographic steps. The first one was used to define the alignment marks on the backside of the wafer, while the other two allowed the patterning of the two SU-8 layers on the topside of the wafer. Thus, the alignment is backside, and each SU-8 layer is aligned by means of the backside marks to the mask to which it will be exposed. Obviously, the three masks contain the same

alignment marks at the same position. Moreover, structures in the second SU-8 layer were formed on top of previously formed structures in the first layer.

The SU-8 was purchased from MicroChem Corp. and the exposure and bake parameters used were obtained from their literature (*www.microchem.com*). The process is described in detailed below and depicted in Figure 2-5.

1. **Glass wafer cleaning**. A 525-μm-thick Pyrex wafer is cleaned in acetone and 2-propanol for 5 min each and in HNO_3 for 10 min, rinsed in DI-18 MΩ water, dried and dehydrated at 200°C for at least 30 min.
2. **Backside photolithography**. For the backside alignment, a first photolithography was performed on the backside of the wafer using AZ 1518 as described previously. The marks were patterned but not etched.
3. **1st SU-8 layer photolithography**. The first thin layer of SU-8 (MicroChem, SU8-10, optimized for layers up to 30 μm) is spin-coated at 500 rpm for 10 s and then at 3000 rpm for 30 s. With these conditions a 10-μm-thick SU-8 layer is obtained. The wafer is pre-baked on a hotplate programmed to increase the temperature from 35°C to 65°C in 5 min. After dwelling for 5 min at 65°C, the wafer is heated up to 95°C in 5 min, remaining at 95°C for 4 min before gently cooling down on the open hotplate. Before exposure, the wafer is aligned with the mask containing the first level of the structures by means of the backside alignment marks. The mask is aligned with the chuck, and at this point the cross hairs of the aligner optical system are positioned exactly over the mask alignment marks. Then, when the substrate is loaded, the backside marks are aligned with the cross hairs on the screen. The SU-8 is exposed to UV light using an energy of 200 mJ/cm^2, contact mode, 1/10 contact force. The wafer is then post-baked on the hotplate. The program used is the same as for the pre-bake, but stopped after 2 min at 95°C.

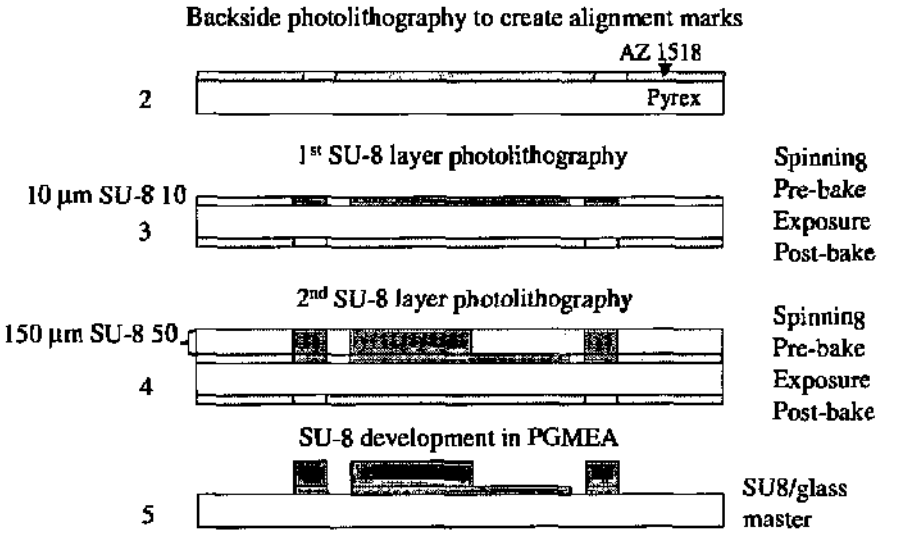

***Figure 2-5** SU8/glass master fabrication.*

4. **2nd SU-8 layer photolithography.** The second layer of SU-8 (Microchem, SU-8-50, optimized for layers up to 100 µm) is then spin-coated at 1000 rpm for 10 s, followed by 1200 rpm at 30 s. These conditions allow the formation of a 150-µm-thick SU-8 layer. Since this layer is spun over another SU-8 layer, the rpm used is higher than the value reported in the datasheet for deposition on bare wafers. This is because the adhesion of SU-8 to SU-8 is higher than the adhesion of SU-8 to silicon or to glass. Note that for SU-8 layers thicker than 100 µm, MicroChem suggests SU-8 100, which is very viscous and difficult to handle. For these reasons in our lab the use of the SU-8 50 spun at lower spin rates is also preferred for the fabrication of thick (> 100 µm) layers. The wafer is pre-baked on the hotplate, which is heated up from 35°C to 65°C in 12 min and dwells at 65°C for 10 min. The wafer is then heated up to 90°C in the oven, at which temperature it remains for 10 min. The oven is used for this second

pre-bake to prevent stress from being induced in the thin, first layer during the pre-bake of the second layer. In the oven, in fact, the temperature is more uniform than on the hot plate, where the heat comes from underneath the wafer. Afterwards, the wafer is left to cool down overnight. Before the second exposure, the wafer is aligned with the mask by means of the backside alignment marks, as described for the first layer. The wafer is exposed using an energy of 640 mJ/cm^2, while the other conditions remain the same as in Point 3 above. The post-exposure-bake is performed on the hotplate. The hotplate is programmed to heat up from 35°C to 65°C in 12 min, dwell at 65°C for 12 min, before heating up to 95°C in 12 min and remaining there for other 20 min. The wafer cools down on the hotplate, which is switched off for one to two hours.

5. **SU-8 development**. For the development of the SU-8, the wafer is immersed backside up in a beaker containing propylene glycol monomethyl ether acetate (PGMEA) (wear chemically resistent gloves: it is toxic) for 10 min. In this case, it was not necessary to agitate the wafer during the development. The wafer is then transferred to new PGMEA solution for 5 min, and then rinsed with a pipette using the same developer. It is then rinsed in 2-propanol for 5 min and dried. PGMEA dissolved also the AZ 1518 resist, leaving only the 3D structures on the front side of the wafer.

The thickness of the two SU-8 layers is checked using an inductive stylus-based profilometer (Carycompar). The first SU-8 layer is 10 µm thick, while the overall thickness resulting from the two superimposed layers is about 160 µm thick, as expected. Images of the SU-8 master are presented in Figure 2-6. The adhesion of the structures on the glass wafer is good, so that the master can be used several times.

Although the process described here is quite long because of the heating and cooling steps, the results achieved confirm that SU-8 can be used for master

fabrication, in particular for rapid prototyping and, of course, when a DRIE process is not available. The SU-8 structures fabricated with the process just described are quite wide (300-500 μm), and are wider than high (160 μm), with an aspect ratio < 0.6. However, as mentioned above, SU-8 is widely used for the fabrication of narrow, high structures, so that it can be employed to create high-aspect-ratio channels as well.

Both silicon and SU-8 masters have to be silanized to make the surface hydrophobic and facilitate PDMS peeling from the master after the polymerization. Before silanization, the master is dried under vacuum for 1 hour. It is then immersed in 3%(v/v) dimethyloctadecylchlorosilane in dry toluene for 2 hours. The master is then cleaned with hexane, 2-propanol and DI water before casting.

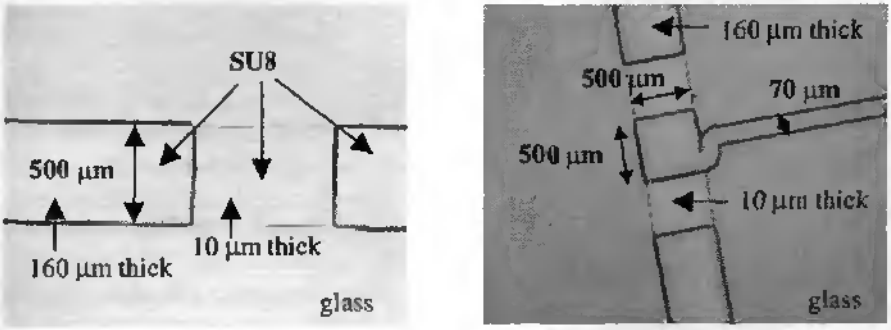

Figure 2-6 *Images of the PDMS master realized by structuring 2 SU-8 layers on a glass substrate. The thin photoresist layer is 10 μm thick while the thick one is about 160 μm thick. Transparencies were used as masks.*

2.3 Fused silica dry etching

Another approach considered to improve channel depth was the use of dry etching processes of SiO_2. In particular, we investigated the plasma etching of non-crystalline quartz wafers (100 × 0.525 mm, Guinchard, Yverdon-les-Bains, Switzerland) to create rectangular channels with optical pathlengths suitable for transverse UV detection [31]. A simple channel layout for CE separation was employed (Figure 2-7). It consists of a 5-cm-long separation channel and two 1-cm-long side channels defining a 200-µm-long double-T injector.

As with silicon and glass, wet and dry etching can be applied for micromachining quartz wafers. However, only dry etching, in particular reactive-ion etching (RIE), can be used to achieve high-aspect-ratio profiles. The RIE process results from the combination of physical sputtering, which is necessary

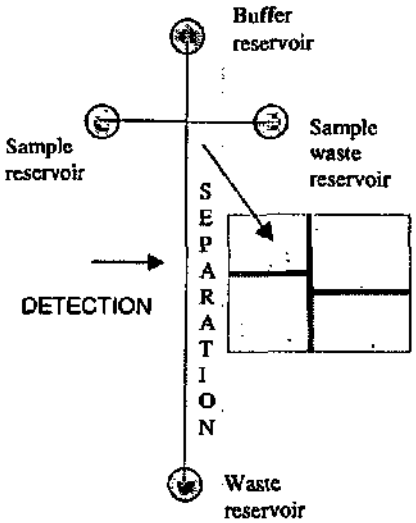

Figure 2-7 Structure layout and close-up of the double-T intersection of the quartz structure etched by RIE.

for the substrate etching but is not selective, and the dry chemical etching, which is material selective [32]. Different parameters influence the RIE process, such as gas pressure, platen power, gas composition and gas density. Process optimisation is therefore empirical and time-consuming. For our process we used C_3F_8 as gas, a coil power of 750 W and a nickel mask. The coil power used ensured a sufficient plasma density for the etch process. The voltage applied to the platen, or substrate bias electrode, was varied (though always kept low), to control the energy with which ions bombarded the sample. The use of the nickel mask and low platen power increased the selectivity of the etch process to about 1:40 (nickel: quartz), compared with the 1:1 reported for a photoresist mask [33].

The process for the fabrication of quartz structures by RIE is illustrated in Figure 2-8 and described below:

1. **Metal deposition.** Thin films of titanium (200 Å) followed by copper (3000 Å) are deposited on a clean quartz wafer by vacuum evaporation.
2. **Photolithography**. A positive photoresist (AZ 4562) is spin-coated (500 rpm for 3 s followed by 4000 rpm for 40 s) onto the metal layer and patterned by photolithography to obtain 8-μm-thick structures.
3. **Nickel electrodeposition**. 4 μm of nickel is electroplated onto the exposed parts of the titanium/copper film around the patterned photoresist, using a commercially available bath (Nickel Sulfamate type from Lea Ronal, Littau, Switzerland).
4. **Mask opening.** After photoresist stripping in acetone, the channels are selectively opened by etching the copper and titanium with sodium persulfate (20 mg of $Na_2S_2O_8$ in 100 mg of Df water) for 1 min and buffered HF (BHF) for 20 s, respectively. Figure 2-9 is a photograph of the open, cleaned structure defined by the nickel mask, which will be transferred into the substrate in the following step.
5. **Dry etching.** Finally, RIE is carried out with C_3F_8 as the gaseous etching agent in a Surface Technology System (STS) ICP machine.

6. **Nickel mask etching**. After etching, the nickel mask is removed using Aqua Regia (37% HCl: 69% HNO_3, 3:1).

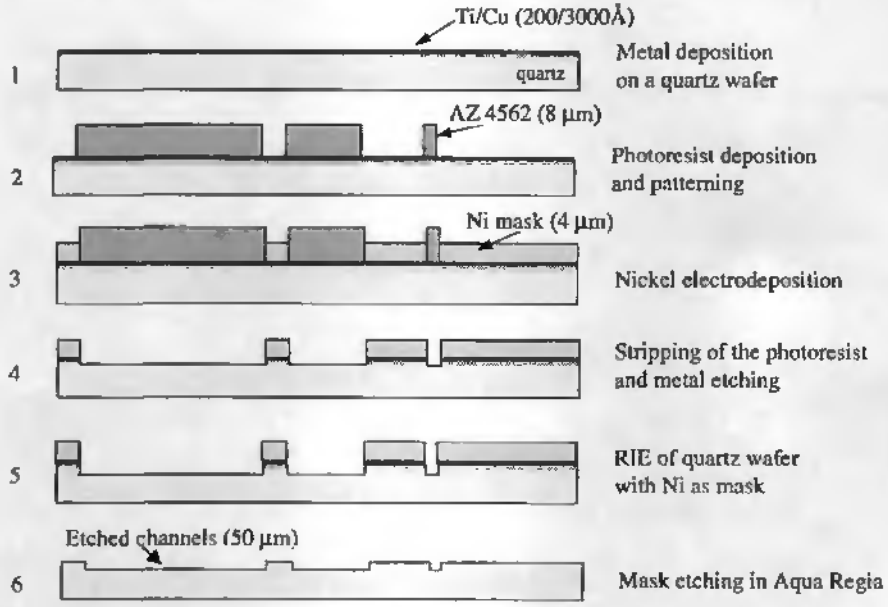

Figure 2-8 Quartz microchannel fabrication by ICP-RIE.

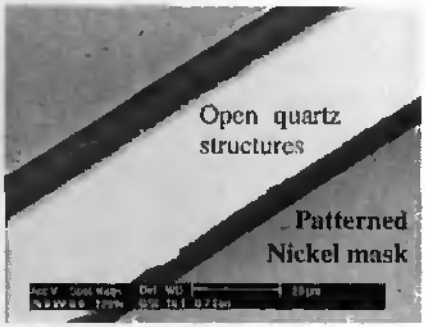

Figure 2-9 Nickel mask on quartz wafer after Ti/Cu etching and before ICP-RIE (XL 30, ESEM-FEG, Philips).

The ESEM images of Figure 2-10 show the results for 50-μm-deep, 50-μm-wide channels etched in quartz with an etch rate of 190 nm/min. The etching process therefore takes more than 4 hours. This etch rate is lower than the etch rate reported for other optimized ICP-RIE systems (1 μm/min) [34]. The nickel mask was used in all the examples shown, but the gas conditions were varied slightly from one test to the next. C_3F_8 was always employed but O_2 was added in test A, while CH_4 was added in test B. The addition of O_2 and CH_4 was introduced to improve mask selectivity with respect to the substrate. It is known, in fact, that O_2 addition accomplishes this when aluminium masks are used (STS personal communication). No effect, however, was observed when using the nickel mask, and following tests were performed with C_3F_8 only. From the ESEM photos it is clear that channel profile and roughness are very irreproducible. As discussed for the DRIE process (Figure 2-2), the low resolution of the transparency mask is transferred to the quartz channels, and results in scalloped channel profiles (Figure 2-10A and 2-10B), while well-defined walls derive from the use of chromium masks (Figure 2-10C and 2-10D). The initial test (Figure 2-10A) suffers from non-uniform etching, which results in a saddle-shaped channel base. This effect may be due to a sloped mask profile, which is responsible for ion reflection as reported for dry etching of Pyrex in SF_6 (Figure 2-11) [34]. However, the problem was not encountered again using the same type of nickel mask. In Figure 2-10B the significant channel roughness can be attributed to the low power applied to the platen, a condition which was chosen to preserve the integrity of the nickel mask. As a result, the physical ion impact necessary to break SiO_2-bonds was not enough, and the etching was not effective. By increasing the platen power, a 50 × 50 μm channel was obtained, but wall verticality was not very good (Figure 2-10C). The best results achieved for ICP-RIE of a fused silica wafer using higher platen power and chamber pressure are presented in Figure 2-10D. In this case the verticality of the walls and the

A

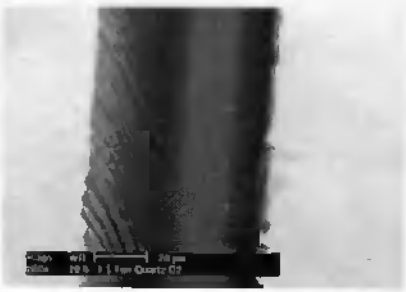

B

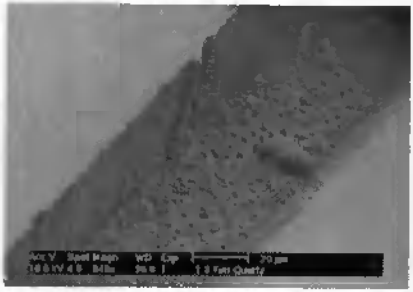

C

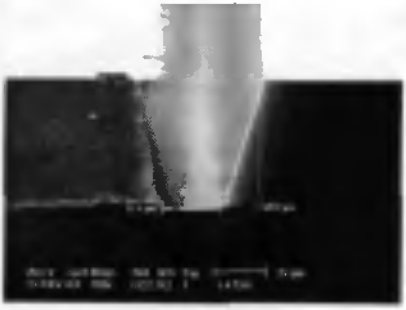

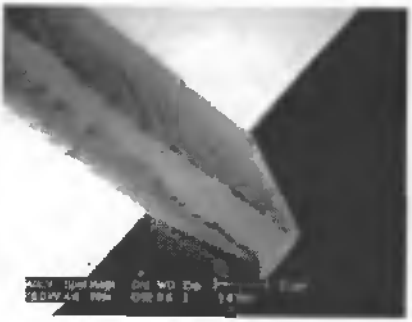

D

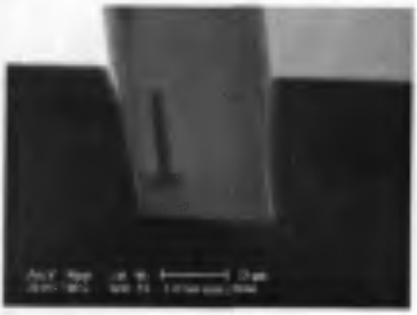

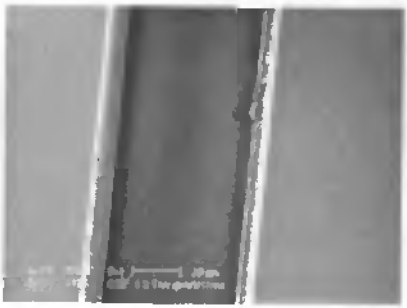

***Figure 2-10** (opposite page) ESEM images of ICP-RIE etched quartz channels and their profiles. A nickel mask prepared as described in the text was used for all cases, while the plasma conditions were slightly different: A) Coil: 750 W, platen: 150 W, 5 mTorr chamber press., 20°C, C_3F_8 with O_2; B) Coil: 750 W, platen: 50 W, 5 mTorr chamber press., 20°C, C_3F_8 with CH_4; C) Coil: 750 W, platen: 120 W, 2.5 mTorr chamber press., 20°C, C_3F_8 only; D) Coil: 750 W, platen: 180 W, 3.5 mTorr chamber press., 20°C, C_3F_8 only.*

roughness of the surfaces look very promising. The apparent non-verticality of the left channel wall is an optical effect. Some needle-like structures were observed in these channels. These could be due to deposition of fluorocarbon (CFx) particles in the channel, which would act as a micromask as reported in the literature [35, 36]. However, this type of needle-like structures was never reproduced. Clearly, then, the ICP-RIE is not yet reliable and further studies are necessary for the process optimization. However, significant progress was made in this work with respect to the development of a highly selective and reproducible nickel mask.

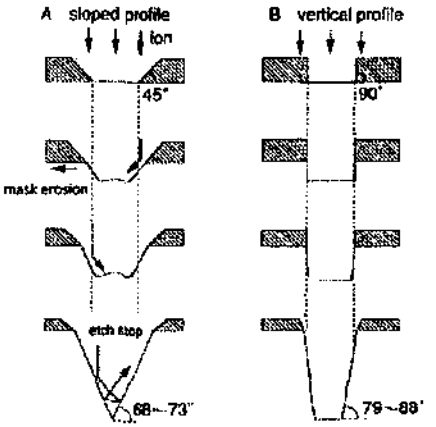

***Figure 2-11** Schematic illustration of the observed profiles caused by use of sloped or vertical masks in Pyrex dry etching with SF_6 [34].*

The deep etching of fused silica continues to be of interest both in our group and others. In Oki et al. [36], microcapillaries of 30 × 30 μm cross-section were dry-etched with a mixture of 70% CF_4 and 30% C_3F_8 and using a 1.5-μm-thick Cr mask. They noted that the use of C_3F_8 alone causes defects at the bottom surface of the quartz channel, probably due to the deposition of fluorocarbon polymeric particles formed during the long etching period. These residues then acted as masking material, preventing further etching at localized spots. The addition of CF_4 reduced the formation of the polymer precursor in the gas phase, preserving the surface quality. It is probable that the same polymer masking effect is occurring in our channels. However, at the moment we cannot introduce CF_4 together with the C_3F_8, because this gas is not available in our RIE system. Its use would require an additional gas line or the replacement of a currently installed gas.

2.3.1 CE in plasma etched quartz channels

To perform CE in the quartz structures presented in the previous Section, the channels had to be sealed. The fabrication of reservoirs in a quartz wafer, and the fusion bonding of quartz-quartz wafers (which requires the usual wafer cleaning and temperature of 1000-1100°C) are both tedious. To avoid these procedures, we decided to use as coverplate a slab of PDMS with reservoir holes punched at positions corresponding to the ends of the channels. In this way, the resulting sealed channels have 3 walls of quartz and one of PDMS. Before sealing, the etched quartz wafer was cleaned with acetone and 2-propanol for 5 min each, followed by fuming HNO_3 for 10 minutes to activate the surface. The wafer was then reversibly sealed on a slab of PDMS, and the structure was conditioned sequentially with 0.1 M NaOH, DI water and 100 mM Tris- 20 mM boric acid (pH 9.2) for 5 min each before CE. The 10-cm device neither fits in the UV system that will be presented in Chapter 6 nor has the thin optical window

required for the UV detection. Thus, we decided to test the channels simply by using the LIF detection system described in Chapter 1, Figure 1-9, to detect amino acids separated by CE [20, 37]. The electro-osmotic flow mobility, μ_{eof}, in these devices was measured from the elution time of fluorescein and were quite low, in the order of 2×10^{-4} $cm^2/Vsec$. Hence, the labelled amino acids, which are negatively charged, migrated against the flow towards the anode, which in this case is placed at the waste reservoir. The sample plug formed at the intersection was injected onto the separation column and driven towards the detection point placed 1.5 cm below the intersection by applying high voltage along the separation channel. During the CE separation, push-back voltages were applied at the side channels, preventing sample leakage into the separation channel as described in Chapter 1. The electropherogram of 10 μM gly-FITC and ser-FITC is presented in Figure 2-12. The serine peak exhibits an efficiency of 90,000 N/m, with a theoretical plate height, H, of 11 μm. Note that the order of the separated peaks is reversed, since the electrophoretic mobilities of the species, rather than the electro-osmotic flow, determine the overall direction of analyte movement in the chip. Although elution times are reproducible for this example, the efficiency is lower than expected when compared to that obtained in glass devices [37]. The contribution to H of the injection plug is not negligible in this design (0.3 μm), but it alone does not explain the poor performance. The use of a hybrid quartz/PDMS device can partially contribute to band broadening, due to ζ potentials which differ from quartz channel walls to the PDMS channel ceiling. This will lead to variations in electro-osmotic velocity from the top to the bottom of the channel, and a resulting deformation of the expected flat electro-osmotic flow profile [38]. Taylor dispersion of the analyte will increase as a consequence of the non-uniform velocity distribution over the channel cross-section [38, 39]. Other sources of dispersion associated with low column performance could be related to surface roughness (the separation shown in Figure 2-12 was achieved in

a quartz channel similar to the one reported in Figure 2-10B) and a possible fluorocarbon film deposited on the structures during the RIE etching process [36, 40]. The presence of this coating is supported by the low value of μ_{eof} measured in this hybrid quartz/PDMS device. This mobility is 2×10^{-4} cm^2/Vs for the 100 mM Tris- 20 mM boric acid used in this test, a value which is much lower than that measured for PDMS channels at a similar pH, namely 4.3×10^{-4} cm^2/Vs at pH 9.2 [41]. Channels in glass or quartz are also normally characterized by higher μ_{eof} at this pH. The low μ_{eof} observed therefore strongly suggests that charge sites on the quartz have been suppressed in some way, and that surface effects are primarily to blame for the increased band broadening. In [36], the biocompatible polymer 2-methacryloyloxyethylphosphorycholine (MPC) was used as coating of the quartz channels to prevent protein adsorption. Electroosmotic pumping was used to move serum into the channel, and the serum flow was monitored by UV detection. In this paper, therefore, the integration of CE analysis of a complex

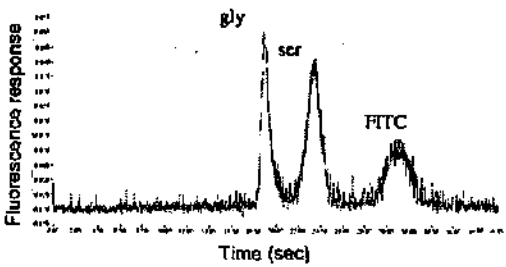

***Figure 2-12** Electropherogram of 10 μM gly-FITC and ser-FITC. Device= 50-μm-deep quartz channels and PDMS coverplate. Running buffer= 100 mM Tris-20 mM boric acid buffer, pH 9.2; L_{tot}= 5 cm; L_{eff}=1.5 cm; E_{sep}= 3 kV. Detection system non-optimised.*

matrix and UV detection was accomplished. Continued development of RIE in our labs thus could prove to be a promising route to clinically useful devices.

REFERENCES

[1] H. Becker and C. Gärtner, "Polymer microfabrication methods for microfluidic analytical applications," *Electrophoresis*, vol. 21, pp. 12-26, 2000.

[2] C. S. Effenhauser, G. J. M. Bruin, A. Paulus, and M. Ehrat, "Integrated capillary electrophoresis on flexible silicone microdevices - Analysis of DNA restriction fragments and detection of single DNA molecules on microchips," *Anal. Chem.*, vol. 69, pp. 3451-3457, 1997.

[3] B. Graβ, A. Neyer, M. Jöhnck, D. Siepe, F. Eisenbeiβ, G. Weber, and R. Hergenröder, "A new PMMA microchip device for isotachophoresis with integrated conductivity detector," *Sensors and Actuators B*, vol. 72, pp. 249-258, 2001.

[4] J. Xu, L. Locascio, M. Gaitan, and C. S. Lee, "Room-temperature imprinting method for plastic microchannel fabrication," *Anal. Chem.*, vol. 72, pp. 1930-1933, 2000.

[5] Y.-H. Chen and S.-H. Chen, "Analysis of DNA fragments by microchip electrophoresis fabricated on poly(methyl methacrylate) substrates using a wire-imprinting method," *Electrophoresis*, vol. 21, pp. 165-170, 2000.

[6] K. E. Petersen, W. A. McMillan, G. T. A. Kovacs, M. A. Northrup, L. A. Christel, and F. Pourahmadi, "Toward next generation clinical diagnostic instruments: Scaling and new processing paradigms," *Biomedical Microdevices*, vol. 1, pp. 71-79, 1998.

[7] L. Martynova, L. E. Locascio, M. Gaitan, G. W. Kramer, R. G. Christensen, and W. A. MacCrehan, "Fabrication of plastic microfluid channels by imprinting methods," *Anal. Chem.*, vol. 69, pp. 4783-4789, 1997.

[8] R. M. McCormick, R. J. Nelson, M. G. Alonso-Amigo, D. J. Benvegnu, and H. H. Hooper, "Microchannel electrophoretic separations of DNA in injection-molded plastic substrates," *Anal. Chem.*, vol. 69, pp. 2626-2630, 1997.

[9] A. P. Sassi, A. Paulus, I. D. Cruzado, T. Bjornson, and H. H. Hooper, "Rapid, parallel separations of D1S80 alleles in a plastic microchannel chip," *J. Chromatogr. A*, vol. 894, pp. 203-217, 2000.

[10] R. C. Anderson, X. Su, G. J. Bogdan, and J. Fenton, "A miniature integrated device for automated multistep genetic assays," *Nucleic Acids Res.*, vol. 28, pp. e60, 2000.

[11] J. C. Fanguy and C. S. Henry, "The analysis of uric acid in urine using microchip capillary electrophoresis with electrochemical detection," *Electrophoresis*, vol. 23, pp. 767-773, 2002.

[12] J. Wang, M. Pumera, M. P. Chatrathi, A. Escarpa, R. Konrad, A. Griebel, W. Dörner, and H. Löwe, "Towards disposable lab-on-a-chip: poly(methylmethacrylate) microchip electrophoresis device with electrochemical detection," *Electrophoresis*, vol. 23, pp. 596-601, 2002.

[13] Y. Liu, C. B. Rauch, R. L. Stevens, L. R., J. Yang, D. B. Rhine, and P. Grodzinski, "DNA amplification and hybridization assay in integrated plastic monolithic devices," *Anal. Chem.*, vol. 74, pp. 3063-3070, 2002.

[14] H. Bayer and H. Engelhardt, "Capillary electrophoresis in organic polymer capillaries," *J. Microcolumn Sep.*, vol. 8, pp. 479-484, 1996.

[15] Y. Liu, J. C. Fanguy, J. M. Bledsoe, and C. S. Henry, "Dynamic coating using polyelectrolyte multilayers for chemical control of electroosmotic flow in capillary electrophoresis microchips," *Anal. Chem.*, vol. 72, pp. 5939-5944, 2000.

[16] S. C. Wang, C. E. Perso, and M. D. Morris, "Effects of alkaline hydrolysis and dynamic coating on the electroosmotic flow in polymeric microfabricated channels," *Anal. Chem.*, vol. 72, pp. 1704-1706, 2000.

[17] S. L. R. Barker, M. J. Tarlov, H. Canavan, J. J. Hickman, and L. E. Locascio, "Plastic microfluidic devices modified with polyelectrolyte multilayers," *Anal. Chem.*, vol. 72, pp. 4899-4903, 2000.

[18] N. J. Munro, A. F. Huhmer, and J. P. Landers, "Robust polymeric microchannel coatings for microchip-based analysis of neat PCR products," *Anal. Chem.*, vol. 73, pp. 1784-94, 2001.

[19] V. Linder, E. Verpoorte, W. Thormann, N. F. de Rooij, and H. Sigrist, "Surface biopassivation of replicated poly(dimethylsiloxane) microfluidic channels and application to heterogeneous immunoreaction with on-chip fluorescence detection," *Anal. Chem.*, vol. 73, pp. 4181-4189, 2001.

[20] L. Ceriotti, N. F. de Rooij, and E. Verpoorte, "An integrated fritless column for on-chip capillary electrochromatography with conventional stationary phases," *Anal. Chem.*, vol. 74, pp. 639-647, 2002.

[21] P. A. Clerc, L. Dellmann, F. Gretillat, M. A. Gretillat, P. F. Indermühle, S. Jeanneret, P. Luginbuhl, C. Marxer, T. L. Pfeffer, G. A. Racine, S. Roth, U. Staufer, C. Stebler, P. Thiébaud, and N. F. de Rooij, "Advanced deep reactive ion etching: a versatile tool for microelectromechanical systems," *J. Micromech. Microeng.*, vol. 8, pp. 272-278, 1998.

[22] D. C. Duffy, J. C. McDonald, O. J. A. Schueller, and G. M. Whitesides, "Rapid prototyping of microfluidic systems in poly(dimethylsiloxane)," *Anal. Chem.*, vol. 70, pp. 4974-4984, 1998.

[23] H. Lorenz, M. Despont, N. Fahrni, N. LaBianca, P. Renaud, and P. Vettiger, "SU-8: a low-cost negative resist for MEMS," *J. Micromech. Microeng.*, vol. 7, pp. 121-124, 1997.

[24] H. Lorenz, M. Despont, N. Fahrni, J. Brugger, P. Vettiger, and P. Renaud, "High-aspect-ratio, ultrathick, negative-tone near-UV photoresist and its applications for MEMS," *Sensors and Actuators A*, vol. 64, pp. 33-39, 1998.

[25] J. M. Shaw, J. D. Gelorme, N. C. LaBianca, W. E. Conley, and S. J. Holmes, "Negative photoresists for optical lithography," *IBM Journal of Research and Development*, vol. 41, pp. 81-94, 1997.

[26] L. J. Guérin, M. Bossel, M. Demierre, S. Calmes, and P. Renaud, "Simple and low cost fabrication of embedded micro-channels by using a new thick-film photoplastic", Proceedings of Transducers '97, Chicago, 1997, 1419-1422.

[27] P. Renaud, H. van Lintel, M. Heuschkel, and L. Guérin, "Photo-polymer microchannel technologies and applications", Proceedings of Micro Total Analysis Systems '98, Banff, Canada, 1998, 17-22.

[28] M. O. Heuschkel, L. Guerin, B. Buisson, D. Bertrand, and P. Renaud, "Buried microchannels in photopolymer for delivering of solutions to neurons in a network," *Sensors & Actuators B-Chemical*, pp. 356-361, 1998.

[29] R. J. Jackman, T. M. Floyd, R. Ghodssi, M. A. Schmidt, and K. F. Jensen, "Microfluidic systems with on-line UV detection fabricated in photodefinable epoxy," *J. Micromech. Microeng.*, vol. 11, pp. 263-269, 2001.

[30] R. D. Oleschuk, L. L. Shultz-Lockyear, Y. Ning, and D. J. Harrison, "Trapping of bead-based reagents within microfluidic systems: on-chip solid-phase extraction and electrochromatography," *Anal. Chem.*, vol. 72, pp. 585-590, 2000.

[31] L. Ceriotti, E. Verpoorte, K. J. Weible, and N. F. de Rooij, "High aspect ratio channels for capillary electrophoresis", Proceedings of Transducers '01, Munich, Germany, 2001, 1174-1177.

[32] M. Madou, *Fundamentals of Microfabrication*, first ed. Boca Raton, Florida: CRC Press, 1997.

[33] P. Nussbaum, K. J. Weible, M. Rossi, and H. P. Herzig, "Potential of dry etching for the fabrication of fused silica micro-optical elements", Proceedings of SPIE Conference on Micromachine Technology for diffractive and Holographic Optics, Santa Clara, CA, USA, 1999, 63-70.

[34] X. D. Li, T. Abe, and M. Esashi, "Deep reactive ion etching of Pyrex glass using SF_6 plasma," *Sensors & Actuators A*, vol. 87, pp. 139-145, 2001.

[35] W. W. Stoffels, E. Stoffels, G. M. W. Kroesen, M. Haverlag, J. H. G. den Boer, and F. J. de Hoog, "Infrared spectroscopy of a dusty RF plasma," *Plasma Sources Sci. Technol.*, vol. 3, pp. 320-324, 1994.

[36] A. Oki, S. Adachi, Y. Takamura, K. Ishiara, H. Ogawa, Y. Ito, T. Ichiki, and Y. Horiike, "Electroosmosis injection of blood serum into biocampatible microcapillary chip fabricated on quartz plate," *Electrophoresis*, vol. 22, pp. 341-347, 2001.

[37] C. S. Effenhauser, A. Manz, and H. M. Widmer, "Glass chips for high-speed capillary electrophoresis separations with submicrometer plate heights," *Anal. Chem.*, vol. 65, pp. 2637-2642, 1993.

[38] F. Bianchi, F. Wagner, P. Hoffman, and H. H. Girault, "Electroosmotic flow in composite microchannels and implications in microcapillary electrophoresis systems," *Anal. Chem.*, vol. 73, pp. 829-836, 2001.

[39] G. I. Taylor, "Dispersion of soluble matter in solvent flowing slowly through a tube," vol. 219: *Proc. Roy. Soc. London Sect. A*, 1953, pp. 186-203.

[40] M. Haverlag, E. Stoffels, W. W. Stoffels, G. M. W. Kroesen, and F. J. de Hoog, "Measurments of radicals densities in radio-frequency fluorocarbon plasmas using infrared absortion spectroscopy," *J. Vac. Sci. Technol. A*, vol. 12, pp. 3102-3106, 1994.

[41] G. Ocvirk, M. Munroe, T. Tang, R. Oleschuk, K. Westra, and D. J. Harrison, "Electrokinetic control of fluid flow in native poly(dimethylsiloxane) capillary electrophoresis devices," *Electrophoresis*, vol. 21, pp. 107-115, 2000.

3 On-chip lipoprotein analysis

3.1 Introduction

Lipoproteins (LP) are nanometer-size complexes of lipids and proteins held together by hydrophobic and electrostatic forces. The particle core consists of cholesteryl esters, free cholesterol and triglycerides, while the surface is made up of proteins (apolipoproteins, i.e. apoB-100) and phospholipid headgroups (Figure 3-1). Cholesterol is the major component of the eukaryotic cell membrane, where it participates in modulation of membrane fluidity. Triglycerides are used in our body as fuel or stored energy. Neither cholesterol nor triglycerides can be transported in blood alone because they are not soluble (in contrast to sugars and most proteins). Therefore, they are combined with proteins, making lipoproteins, and transported in the blood in such packages. LP are classified by the type and ratio of proteins and fats they contain, which determines their size and density. The largest LP complexes are chylomicrons and very low-density lipoproteins (VLDL). The intermediate, low- and high-density lipoproteins (ILD, LDL, HDL, respectively) are smaller in size. Some of the properties of human plasma lipoprotein classes are reported in Table 3-1. LDL and HDL specifically carry the cholesterol. The LDL-cholesterol is called "bad" cholesterol, because it is the main source of damaging buildup and blockage in the arteries. Thus, the higher is the LDL-cholesterol concentration in blood (> 100 mg/dL) the greater is the risk of heart disease. The HDL-cholesterol is called "good" cholesterol since HDL acts as a cholesterol scavenger, carrying surplus

cholesterol from tissues to the liver and preventing lipid accumulation in the arterial walls. Thus, HDL concentrations below 40 mg/dL could be associated with a high risk of heart disease. The ratio of the cholesterol in LDL to that in HDL is the most commonly accepted indicator of risk for coronary heart disease [1]. Together with the mentioned LP classes, there are some other modified LP forms of clinical interest. LDL particles are usually harmless. However, they can undergo progressive oxidative modification of the lipid and protein components. The oxidized LDL have a reduced binding affinity for the LDL scavenger receptors and thus escape capture and removal by phagocytic cells, prolonging their residence in blood plasma. These modified particles can interact dangerously with the artery walls, producing a harmful inflammatory response which leads to the accumulation of blood cells in the arterial tissue and the formation of atherosclerotic plaques [2, 3]. High plasma levels of oxidized LDL have been found in patients with acute myocardial infarction, unstable angina and thrombogenic carotid atherosclerosis [4, 5]. Glycosylation and enzymatic degradation are other modifications, which could impart atherogenicity to the

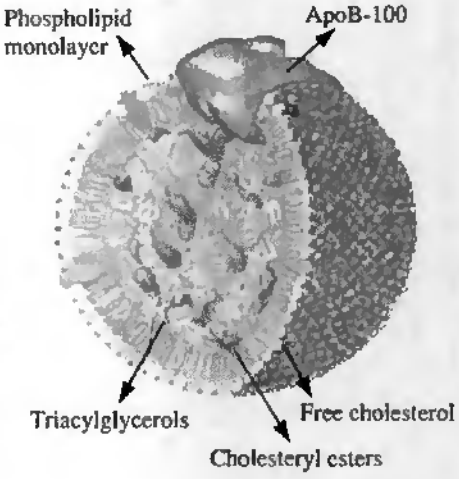

Figure 3-1 *Schematic presentation of LDL particle structure (from « Principles of Biochemistry », Lehninger, A.L., Nelson, D.L. and Cox, M.M., 2nd edn., 1993, North, New York)*

Table 3-1 Properties of major human plasma protein classes (from «Biochemistry», Mathews, C.K. and van Holde, K.E., 1st edn., 1990).

Lipoprotein	Density (g/cm^3)	Composition (wt%)			
		Protein	Cholesterol ester	Triacyl-glicerols	Size (nm)
chylomicrons	0.92-0.96	1-2	2-4	90-95	80-500
VLDL	0.95-1.006	10.4	13.9	53.4	30-80
IDL	1.006-1.019	17.8	22.5	31.4	25-35
LDL	1.019-1.063	25.0	41.9	3.5	18-25
HDL_2	1.063-1.120	42.6	20.3	2.2	8.7-12.9
HDL_3	1.12-1.21	54.9	16.1	1.4	7.2-8.7

LDL [6, 7]. Therefore, there is an interest in developing a method for the rapid separation, identification and quantification of LP forms. A microfluidic device could be an ideal platform to accomplish this analysis. Moreover, the micro-format could guarantee the integration of other assay steps (i.e. sample concentration and labelling) and a high sample throughput, which is particular interesting for clinical diagnostics [8].

Different methods have been used to characterize and resolve lipoproteins classes as presented in Table 3-2. The method traditionally used for LP separation is ultracentrifugation, which allowed the classification of LP in the classes mentioned above [9]. This method is time consuming, requiring more than 5 hours. Contamination of fractions with traces of other LP is also common, due to manual pipetting being used to sequentially remove the lipoprotein fractions from the ultracentrifuge tubes [10]. Lipoprotein separation obtained by gel electrophoresis is also time-consuming (more than 8 hours) [11]. Using this technique, however, lipoprotein subclasses associated, for instance, with an

increased risk of coronary heart disease [12] and insulin resistance syndrome [13] may be identified. Lipoprotein complexes can also be analysed by immunoassay such as ELISA [14, 15]. Antibodies are required in this case and, because of the heterogeneity of the particles, standardization and comparison between samples is difficult. Lipoproteins can be separated and quantified using high-performance liquid chromatography (HPLC) on a gel exclusion column [16]. Recently, lipoproteins from human serum were separated by HPLC using a hydroxyapatite column and ^{1}H NMR spectroscopy for LP class identification. The separation was completed in 90 min and the supramolecular structure of the particles was maintained [17]. Capillary electrophoresis has been used as a simple method for lipoprotein separation, which is based on the differential electrophoretic mobilities of these particles. Using CE, the separation time is reduced to less than20 min [18-20]. Finally, application of isotachophoresis (ITP) and capillary

Table 3-2 *Separation methods for lipoprotein analysis.*

Separation technique	*Ref.*	*Lipoprotein classes identification*	*Comments*
Ultracentrifugation	[9]	LDL, VLDL, HDL	Time-consuming process, evidence of contamination in the fractions
Gradient gel electrophoresis	[11]	3 LDL and 2 HDL subclasses	Identification of subclasses of clinical interest
Immunoassay	[14, 15]	LDL, Lipoprotein (a), apolipoproteins	Antibodies are required, standardization is difficult
HPLC	[16, 17]	HDL, LDL, VLDL	Non destructive and sensitive method
CE	[18-20]	LDL, oxidized LDL, Lipoprotein (a), HDL	Simple method
Capillary isotachophoresis	[7, 21-24]	LDL subclasses	High resolution method

ITP (cITP) has resulted in some promising electrophoretic methods for serum protein analysis on the basis of their charge-to-mass ratios. The high resolution due to the self-focusing effect on the sample make this method an attractive tool for reliable quantitation of lipoprotein subpopulations in the clinical laboratory [7, 21-24]. In 1994, Schmitz and Möllers reported for the first time an analytical method based on ITP for the separation of lipoprotein subclasses [21]. Up to fourteen lipoprotein subclasses were detected and, thanks to the specific staining procedure used, lipoprotein metabolism could be studied and pathological cases could be identified [22, 23]. In short, the electrophoretic methods appear to be more effective for the analysis of lipoproteins than separation using gels or immunoassay tests, due to 1) the reduction of the analysis time (less than 30 min), 2) the sensitivity of the coupled detection system (absorbance, fluorescence) and 3) the possibility to simultaneously determine LP concentrations and resolve LP isoforms.

In collaboration with the Nestlè Research Centre (Vers-Chez-les-Blanc, Lausanne), we have developed a CE-based separation method for LP analysis in conventional systems (Beckman Instruments, Nestlè Research Centre) and in a miniaturized format (home-made glass chip). The CE approach was chosen because of the simplicity of this method, in particular if compared to ITP where particular electrolyte solutions are required. Moreover, previous experience with on-chip CE in our laboratory made this approach our first choice. The results of this work were presented at the μTAS 2001 Conference, Monterey, CA [25, 26] and more in detail in 2 separate papers, which are included as Appendix 1 and Appendix 2 in this manuscript [10, 27]. The first paper is focused on the development of a CE method for separation of lipoprotein samples in a conventional system, and its subsequent application to the microchip format. HDL and LDL particles were separated in capillaries and microchannels using a dynamic coating to prevent LP adsorption to the wall, and detected by LIF detection after LP fluorescent staining. Similar results were achieved in both

formats, suggesting the possibility of using the microsystem for LP separation and quantification. The second paper is focused on LDL analysis on chip. It demonstrates that LDL analysis can be performed in an uncoated microchannel. Significant improvement in peak efficiency was observed by adding SDS at a concentration well below the critical micellar concentration to the sample. This peak sharpening effect is probably due to a mobility gradient created between the sample and the running buffer when SDS is added only to the sample. Laser light scattering experiments demonstrated that the low concentration of SDS does not significantly alter lipoprotein particles, so that the properties of diagnostic interest are maintained. The results achieved in this study suggest that microchips have the potential for rapid analysis and sensitive detection of serum components [28], and they could specifically be used as diagnostic tool for atherogenic lipoprotein analysis. In the following sections the main results about on-chip LP analysis will be summarized, and completed with some details not presented in the papers.

3.2 Experimental section

3.2.1 Samples and reagents

The lipoprotein samples were prepared from fresh blood by ultracentrifugation and then dialyzed against phosphate-buffered saline (pH 7.2) and frozen and stored until use [10]. Lipoproteins were stained before analysis using the fluorescent, uncharged, lipophilic dye, NBD-ceramide (from Molecular Probes). The structure of NBD-ceramide is presented in Figure 3-2A. This dye associates with lipoprotein particles through hydrophobic interactions with the phospholipid/cholesterol membrane. After association, NBD-ceramide becomes fluorescent with an absorbance maximum at 466 nm and emission maximum at 536 nm. It is therefore compatible with the LIF detection system available in the lab, which is based on an Ar^+ laser emitting at 488 nm and a band-pass filter centred at 516 nm for fluorescence detection (see Chapter 1). NBD-ceramide was identified as a good fluorescent dye for specific lipoprotein labelling and lipoprotein class and cholesterol quantification [22, 23]. It shows a saturable labelling for LP in serum, reaching a plateau above 0.7 mg NBD-ceramide per mL serum. At higher concentrations, the LP peak areas do not increase [22, 23]. We worked in the saturating regime of the dye (about 1 mg NBD-ceramide for mL sample). The staining protocol used in our experiments is described in the paper [10]. Briefly, 1 mg of NBD-ceramide is dissolved in 200 µL of dimethylsulfoxide (DMSO) (Merck, Darmstadt, Germany) and diluted with 1800 µL of ethylene glycol (Merck) to a final concentration of 0.5 mg/mL of dye. The lipoprotein solution (25 µL) is diluted with deionized water (75 µL) and then vortexed in the presence of NBD-ceramide solution (50 µL) for 1 min. The running buffer (250 µL) is finally added to the solution. Sample aliquots

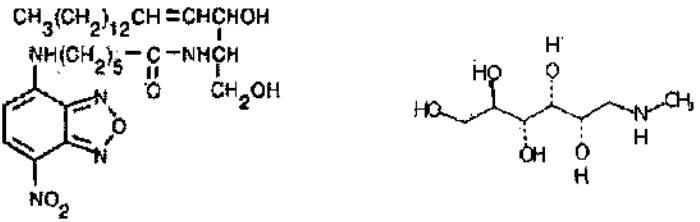

A B

Figure 3-2 A) Structure of NBD-ceramide. B) Structure of methylglucamine.

(50 µL) are then analysed either on chip or in a fused-silica column by CE. As running buffer, 40 mM Tricine (pH 9.1) was used. For the first part of the study, 40 mM methylglucamine (Sigma) was added to the buffer as a dynamic coating. The molecular structure of methylglucamine is presented in Figure 3-2B.

3.2.2 Glass microdevice fabrication

Glass channels were fabricated in 100-mm-diameter, 500-µm-thick borosilicate glass wafers using the standard technology available at IMT: photolithography, wet etching in 50% HF using poly-Si as etch mask, and fusion bonding. The fabrication process is described in Chapter 1, Section 1.2.1. Once the etched wafer and the drilled coverplate were bonded together, plastic tubes of 3 mm internal diameter and 9 mm length were glued over each hole of the coverplate to serve as fluidic reservoirs. Volumetric micropipettes (Eppendorf AG, Hamburg, Germany) were employed to load the same volume of solution (typically 50 µL) into each reservoir to prevent hydrostatic pressure differences, which could lead to broadened peaks and irreproducible peak elution times [29].

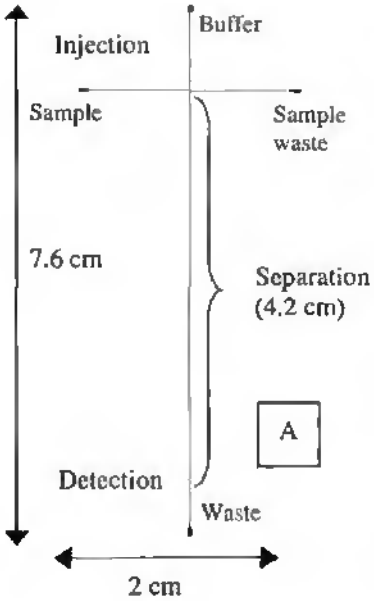

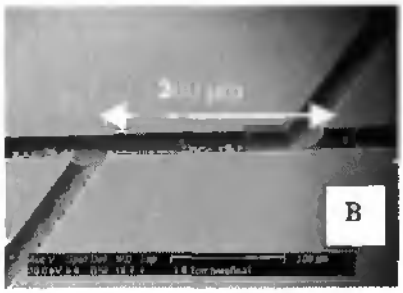

Figure 3-3 A) Layout of the chip employed for CE separations. B) ESEM image of the double-T intersection, which is 200 µm long. Note the rounded profile of the channels due to isotropic etching.

The chip layout is shown in Figure 3-3A. It consists of a straight 7.6-cm-long channel with two 1-cm-long side channels used to form a 200-µm-long double-T intersection (Figure 3-3B). This intersection defines the volume of sample to be injected into the separation channel. Since the etched structures are about 18 µm deep, the resulting injection volume is about 165 pL. The effective separation length is kept fixed at 4.2 cm.

3.2.3 Channel alignment with detection system

The detection set-up for microchip CE experiments was described in Chapter 1, Section 1.5. The following points, in chronological order, summarize the steps that are usually performed to optimize chip and detection system conditions before running the sample of interest (e.g. peptides, proteins).

1. The channels are usually rinsed with 0.1 M NaOH for 4 min and water for 3 min by applying vacuum at one reservoir to draw the solution in question from all the reservoirs, which have been filled prior to rinsing. This cleaning allows regeneration of the charged surface, which is necessary to get high, reproducible electroosmotic flow. Water is finally rinsed away with the running buffer. After this, 50 μL of buffer is loaded into the buffer, buffer waste and sample waste reservoirs, and 50 μL of sample is loaded to the sample reservoir. Filling the reservoirs to the same level is very important to prevent hydrostatic pressure effects during the separation.
2. The chip is then positioned on the chip holder and the separation channel is aligned with the microscope body below by means of an eye piece. This last is then replaced with the photomultiplier tube (PMT). The distance between the injector and the detection point (where the PMT is aligned) defines the effective separation length of the channel, L_{eff}.
3. A fluorescein-containing sample is used to optimize the alignment of the channel with the laser and the PMT. By applying voltage between sample and waste, 10 μM fluorescein (FL) is pumped into the separation column. While fluorescein is running in the separation channel, the laser and collection objective are slowly moved to find the highest PMT signal on the screen. The fluorescein is then removed from the separation channel by applying an electric field along it to introduce buffer.
4. To really inject a plug of fluorescein into the separation column, –2000 V are applied between sample and sample waste reservoirs for 30 s while the separation channel is left floating (no pinching). Then, –6000 V are applied along the separation channel to drive the sample plug towards the detector, while –2000 V are applied at the sample and sample waste reservoirs to push back the sample and prevent its leakage into the

separation channel. The fluorescein peak is detected in 20 *s* for an L_{eff} of 4.2 cm.

When the fluorescein peak is symmetric, sharp and reproducible, the fluorescein sample can be replaced with the sample to be analysed, while maintaining system alignment. To assure chip performance, a sample containing a known mixture of fluorescein isothiocyanate (FITC)-labeled amino acids was used. To replace one sample with another, in this case fluorescein with the amino acid mixture, the sample reservoir is rinsed three times with buffer and then the buffer is electroosmotically injected into the separation column. Once the signal reaches the background level, the buffer is replaced with the next sample in the sample reservoir. If the fluorescein is not completely removed from the sample reservoir, a fluorescence peak will appear in the following electropherogram(s) as contamination when the sample is injected (FL peak in Figure 3-4). The amino acids are labeled by adding 100 µL of a 1 mM solution of FITC in acetone to 1 mL of 1 mM amino acid solution prepared in a basic solution (i.e. Tris/boric buffer, pH 9). After reaction overnight at room temperature, the FITC-labeled amino acid solutions are diluted in the background electrolyte (BGE) to a concentration of 10 µM with respect to FITC. The electropherogram of the four amino acids at a concentration of 5 µM each is presented in Figure 3-4. Peak efficiencies were calculated using the formula reported in Chapter 1 (Equations (7) and (8)) and plate heights of about 1 to 1.2 µm could be obtained. Once this type of data was achieved, good chip performance was demonstrated, and the device would be used for LP analysis.

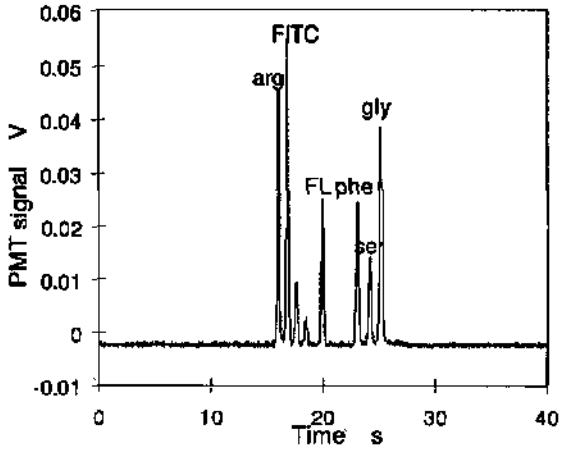

Figure 3-4 Electrophorogram of 4 amino acids (arg, phe, ser and gly) separated in an etched glass channel. FL is the fluorescein contamination identified by its elution time. BGE= 100 mM Tris-20 mM Boric, pH 9.1, E= 780 V/cm, L_{tot}= 7.6 cm, L_{eff}= 4.2 cm, Sample concentration= 5 μM of each amino acid, Injection time= 30 s, Push-back voltage= -2000 V, LIF detection (λ_{ex}= 488 nm, λ_{em}= 515 nm). Detection system not optimized. When optimized, amino acid concentrations down to 20 nM can be detected.

3.3 Results and discussion

3.3.1 Analysis of HDL and LDL

A new assay for lipoprotein analysis was developed based on CE using, as BGE, Tricine buffer containing methylglucamine as a dynamic coating to prevent LP adsorption at the capillary or channel walls (Appendix 1). The same BGE was used by Stocks and Miller for CE analysis of native and LDL oxidized forms [18]. However, they did not analyze HDL, and a separation of LDL and HDL was not demonstrated with their capillary system. Lipoproteins are usually detected by UV absorbance. However, some papers reported the possibility of staining them with fluorescent dyes, such as NBD-ceramide and Sudan Black, making their

detection by LIF possible [22, 24]. Since LIF detection is the more common detection method coupled with on-chip CE separation, NBD-ceramide was chosen for LP fluorescent staining in our method. We worked with dye concentrations high enough to saturate the LP sites available for the labelling, so that heterogeneity due to tagging was minimized [22, 23]. The CE assay was performed in a conventional CE system and in a glass microchip with qualitatively comparable results. The electropherograms obtained by injecting a mixture of LDL: HDL (1:1) in a 75-μm-i.d. capillary and in a microchannel are presented in Figure 3-5A and Figure 3-5B, respectively. The first sharp eluting peak is the LDL; the broad one is the HDL peak as demonstrated by injecting the single fractions alone and by varying the volume ratios of the two fractions in the mixture [10]. The broader HDL peak is likely due to a greater heterogeneity of HDL particles compared to the LDL ones. HDL has more proteins of different structure on its surface, which leads to a greater range of mobilities and a larger peak width for HDL compared to LDL. As expected, the analysis time is 26 times shorter in the microchannel than in the capillary column, and the peak efficiency was also improved. The plate height for the LDL peak obtained on chip, in fact, was 1.4 μm while in the capillary it was calculated to be 3 μm after correction for the lower electric field applied in the capillary format. The better performance obtained on-chip could be attributed to the smaller sample plug injected and the fast analysis, which limits the time available for LP-wall interaction. Comparison of the 2 electropherograms also leads to the observation that the signal is reduced in a microdevice. The low sensitivity observed for the chip can be attributed to the different detection system used and the smaller sample volume injected into the microcolumn. In fact, a sample volume of 2.65×10^{-8} L was calculated for the capillary (considering a sample plug of 6 mm) and of 1.66×10^{-10} L for the chip. The sample plug loaded into the chip is therefore 160 times smaller than the plug injected in the capillary column. This is one reason for the lower SNR in microchannel. As a consequence, sensitivity in microsystems could be an issue

for POC devices. The electropherogram in Figure 3-5B represents the first separation and detection of LP in a microfluidic device. A serum sample was also stained with the same procedure used for the lipoprotein fractions and injected into the capillary. The electropherogram obtained is shown in Figure 3-6. The peak migration times adjusted for the applied voltage do not correlate with the data achieved when injecting the single LP fractions. However, the fact that a

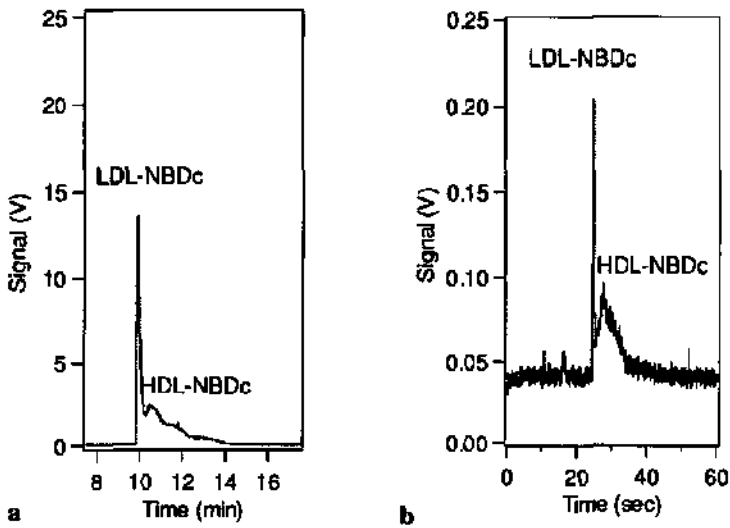

***Figure 3-5** Electrophorogram of a mixture of LDL:HDL (1:1) achieved in a) 75-µm-i.d. capillary (Beckman Instruments, Ltd) (L_{eff}= 50 cm, E= 333 V/cm); b) 18-µm-deep glass channel (L_{eff}= 4.2 cm, E= 714 V/cm). In both cases, BGE= 40 mM Tricine, 40 mM methylglucamine, pH= 9; Sample staining with NBD-ceramide; LIF detection (λ_{ex}= 488 nm, λ_{em}= 515 nm).*

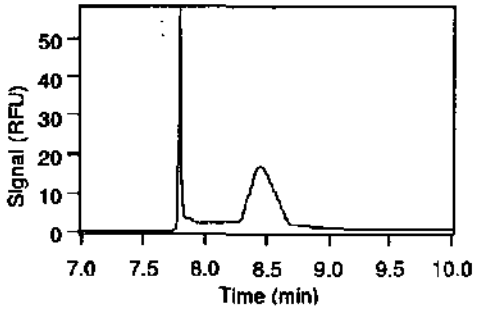

***Figure 3-6** Electropherogram of fluorescently stained serum injected in a capillary. L_{eff}= 50 cm, E= 476 V/cm. For other conditions see Figure 3-5.*

lipophilic dye specific for LP was used and a peak shape similar to the one for the separated LDL and HDL fractions was observed suggests that the two peaks in Figure 3-6 could be the LP. Hence, it appears that LP can be separated directly from serum samples using this method. Unfortunately, when the stained serum sample was injected into the microchannel, the channel got clogged quickly, probably because the sample was too concentrated. Under these conditions, no peaks were detected.

3.3.2 Analysis of LDL in uncoated glass microchannels

After the first promising separations of LDL and HDL fractions in a miniaturized CE system, further work was done to develop a method that could be of clinical interest for reproducible and efficient analysis of LDL particles on chip. The details of this work are included in this manuscript as Appendix 2 [27]. Working with LP samples in the microsystem, we realized that LDL peaks could also be detected also in an uncoated microchannel (Figure 3-7), in contrast with what has been reported for untreated capillaries [18]. This suggests that highly

adsorptive compounds can be detected in microsystems, using BGE conditions different from those optimized for conventional columns. The area of the LDL peak detected in an untreated channel is half of the peak area obtained in presence of 40 mM MG (data not shown). This suggests that the particle adsorption without coating is increased, as expected. The fact that we still detect the LP particles is primarily due to the short effective separation length of 4.2 cm in the microchannel as compared to the 30-50 cm effective length of the capillary. Since the diffusion coefficient of the particles, D_{LDL}, is low (1.8×10^{-7} cm^2s^{-1}) [30] and the resident time of LDL in the untreated microchannel is limited to about 20 s (LDL peak migration time, t_{el}), an average diffusion distance, d_{diff}, can be calculated, using the Einstein-Smoluchowski equation [31]:

$$d_{diff} = (2\, D_{LDL} \times t_{el})^{1/2} \qquad (1)$$

The calculated d_{diff} is about 25 µm. Since this value is on the order of the channel cross-section dimensions, the probability of LDL diffusing to the walls of the microchannel before reaching the detection point is reduced if compared to the analysis on the 75-µm-i.d. capillary. In the latter case, an average d_{diff} of 150 µm is calculated for the 10-min LDL migration time. Hence, more LDL passes the detector in the chip without loss to the uncoated channel walls than in the fused-silica capillary case. In fact, the vast majority of LP particles are adsorbed to the bare capillary walls in the latter case, leading to no signal being recorded at all [18].

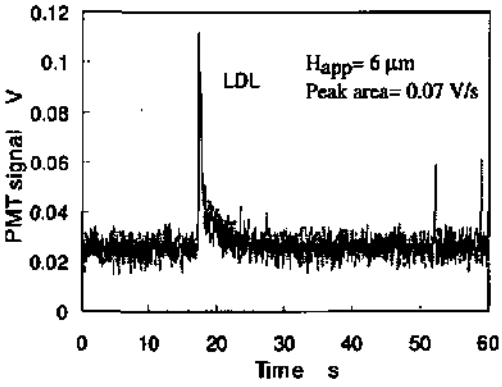

***Figure 3-7** Electropherogram of LDL(NBD-ceramide) in an untreated microchannel (no dynamic coating used). BGE= 40 mM Tricine buffer, pH 9.1; E= 750 V/cm; L_{eff} = 4.2 cm; L_{tot}= 6.7 cm; LIF detection (λ_{ex}= 488 nm, λ_{em}= 515 nm).*

To improve LDL solubilization, we added a small amount of SDS to the sample and not to the BGE prior to injection. As reported in the literature, SDS has been used at a concentration of 0.5 mM in both BGE and sample to enhance the repulsion between the negatively charged particles and the negatively charged walls during CE separations [19]. The use of SDS at higher concentration (> 2.7 mM) for apolipoprotein dissociation [32] and lipoprotein delipidation [19] has also been reported. In our case, SDS was added to the sample at a low concentration of 0.3 mM in order to minimize particle delipidation, particle adsorption and aggregation. With SDS added, a sharp peak was obtained as shown in Figure 3-8a. An apparent efficiency of 816,600 plates (N) was calculated for the peak, corresponding to a plate height, H, of 0.05 µm and an N/m of almost 2×10^7 plates/m. A number of observations support the hypothesis that this sharp peak is due to intact LDL(NBD-ceramide)-SDS complexes and not to SDS micelles or apolipopoteins.

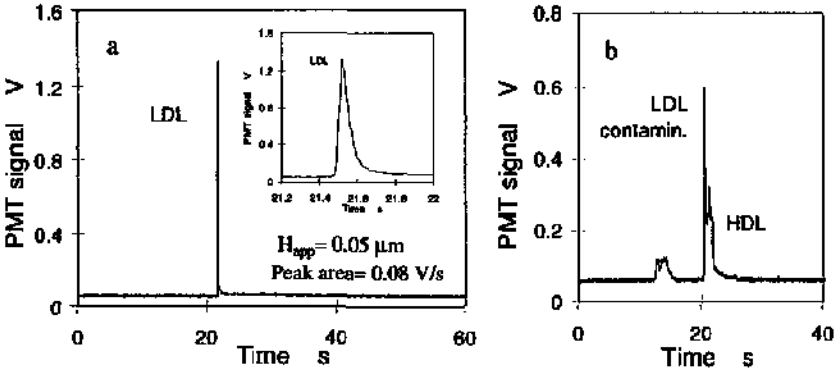

Figure 3-8 *Electropherogram of a) LDL(NBD-ceramide)-SDS and b) HDL(NBD-ceramide)-SDS complexes. 0.3 mM SDS was added to the sample and not to the BGE. Note the LDL contamination in the HDL sample. BGE= 40 mM Tricine buffer, pH 9.1. Separation conditions as described in Figure 3-7.*

i. Since we worked at an SDS concentration much lower than the critical micelle concentration (8.1 mM), micelles are not present in the sample.

ii. Literature reports state that 0.5 mM SDS is not enough to delipidate LDL particles [19]. However, it has been reported that apolipoproteins have a high affinity for SDS molecules and tend to interact with SDS molecules at detergent concentrations < 10^{-4} M [32].

iii. The areas of the peaks in Figure 3-7 and Figure 3-8a are similar, suggesting that the integrity of the particles is preserved.

Moreover, laser light scattering (LLS) experiments confirmed that HDL (and presumably also LDL) particles are not destroyed in the presence of SDS at this low concentration. The LLS results will be discussed in the following section.

The sharpening effect observed for LDL after addition of SDS to the sample was also observed for HDL samples under the same conditions. The electropherogram of the HDL sample containing 0.3 mM SDS is presented in Figure 3-8b. The sharp peak that appears before the HDL peak is the LDL

contamination, which is present in the sample due to the poor zone separation after the ultracentrifugation process. The broad peak eluting before the LP is an unidentified contamination present in the HDL sample. For both LDL and HDL the migration time in presence of 0.3 mM SDS in the sample is shifted to higher values (see Table 3-3 for the HDL migration times). This observation suggests that SDS interacts with the LP, changing their charge and size and therefore their electrophoretic mobilities. However, the sharpening effect observed for the LP peaks is probably due to a mobility gradient created between sample and BGE when the SDS is added solely to the sample and not by binding of SDS to the LP particles. This electrolyte focusing effect has been reported in the literature by Kenndler et al. for a CE separation of two proteins, conalbumin and ovalbumin [33]. These researchers found that the presence of SDS in a protein-containing sample, even at low concentrations (1.7 mM), and not in the BGE, led to a loss of separation resolution. At the same time, a sharpening effect of the single peak obtained for the mixture of the two proteins at an SDS concentration of 3.4 mM or more was observed. This focusing effect was not observed when SDS was present at the same level in both the sample and the BGE [33]. Similarly, we did not observe peak sharpening for LP when both sample and BGE contain the same concentration of SDS, which agrees with the results reported for the LP CE analysis by Macfarlane et al [19]. Though the proteins considered by Kennedler et al. are different from the LP particles we worked with, the difference in conductivity between the SDS-containing sample and the BGE (SDS-free) could be responsible for the sharpening effect observed also for our LP peaks. The loss of separation resolution reported in [33] for addition to the sample of SDS at concentrations higher than 1.7 mM would be an undesirable effect in our lipoprotein analysis, since our interest is to resolve different lipoprotein forms. However, the concentration of SDS we used, 0.3 mM, would most likely not be sufficient for a complete loss of resolution between LP forms. The observed

focusing effect could therefore by quite useful for the preconcentration of lipoproteins present at low concentrations, as is often the case in clinical samples.

3.3.3 HDL-SDS complex characterization

In the paper reproduced in Appendix 2 [27], we focused our interest on LDL particles and their analyis, since these particles and in particular their oxidized forms are related to high atherosclerosis risk. In this section, attention is focused on HDL particles, and how the data obtained from the electropherograms and from laser light scattering (LLS) experiments can be combined to get more information about particle size and charge. Unfortunately we could not get the same data for LDL samples because of particle aggregation, which made the sample solution turbid and the LLS results difficult to interpret. LLS experiments were performed on the HDL sample as described in the paper in Appendix 2. Three samples consisting of HDL (375 µL) in deionized water (50 µL) and further diluted in 40 mM Tricine buffer (1000 µL) were prepared. Note the large volume required for these experiments compared to the few µL necessary for the CE experiment on chip! Fresh blood and serum samples should be easily obtainable in quite large volumes. However, we did not established contacts with hospitals or clinical labs, and so did not have easy access to good-quality samples. The first sample was analyzed without any additives. NBD-ceramide (375 µL) was added to the second sample. Both NBD-ceramide (375 µL) and 3 mM SDS (200 µL) for a final SDS concentration of 0.3 mM were added to the third one. Each sample was freshly made. The measurements were started 1 minute after sample preparation and made at increasingly long time intervals, starting with a 1-minute interval and ending with a 10-minute-long interval over a 30-minute total measuring time. This was done to have a better idea of any changes at the very beginning of the reaction due to the interaction of different additives with HDL. The light scattering experimental data were used to measure

correlation functions, which are curves of scattered light intensity vs decay time, where the decay time depends on the fluctuations of light when it is scattered by the particles in the solution. It is thus a measure of how fast the particles move. The refractive index of these LP particle-containing samples was determined separately using a refractometer (Bellingham + Stanley, UK, Type RFM340). Refractive index and correlation curves were used to calculate the diffusion coefficients of the particles. Diffusion coefficients of 2.5×10^{-7} and 2.1×10^{-7} cm^2/s were found for the HDL samples without and in presence of 0.3 mM SDS, respectively. These values are comparable to the diffusion coefficient of 1.8×10^{-7} cm^2/s reported in the literature for LDL particles [30]. The particle size was then calculated from the diffusion coefficient using the Stokes-Einstein equation:

$$D = \frac{kT}{6\pi\eta r} \qquad (2)$$

where D is the diffusion coefficient, T is temperature, k is the Boltzmann constant, η is viscosity, and r is the radius of the particle. HDL particles demonstrated a mean particle radius of circa 10 nm. This agrees well with values measured using electron microscopy [34]. The addition of NBD to the solution had no effect, but particles swelled to about 12 nm radius with the subsequent addition of SDS, which is an increase to dimensions equivalent to SDS micelles. The LLS results are shown in Figure 3-9.

The HDL elution time obtained from the electropherograms and the data achieved from the light scattering experiments (Stokes radius) can be combined to get more information about HDL charge. The binding of the negative SDS molecules (the molecule length is about 1.5 nm) to the particles will alter the Stokes radius, r, and charge, q, causing a change in electrophoretic mobility, μ_e, according to [35]:

$$\mu e = \frac{q}{r}\left(\frac{1}{6\pi\eta}\right) \qquad (3)$$

The μ_e of the LDL particles with and without SDS in the sample were determined experimentally using the following Equation:

$$\mu e = \frac{LtotLeff}{V}\left(\frac{1}{teo} - \frac{1}{t}\right) \qquad (4)$$

where L_{tot} and L_{eff} are total channel length and effective length to the detection point, respectively; V is the applied voltage; and t_{eo} and t are the neutral marker and analyte retention times, respectively. The value of t_{eo} was found to be 14 s, using BODIPY as a neutral marker. We used the same value of t_{eo} for the neutral marker in both cases since it has been reported that SDS at concentrations up to 1.75 mM do not adsorb on negatively charged, bare silica [36]. Without SDS present, the HDL migration time was 18.2 s, resulting in a $\mu_e = 0.9 \times 10^{-8}$ m^2/Vs. In presence of 0.3 mM SDS, the migration time was 21.4 s, corresponding to a $\mu_e = 1.4 \times 10^{-8}$ m^2/Vs.

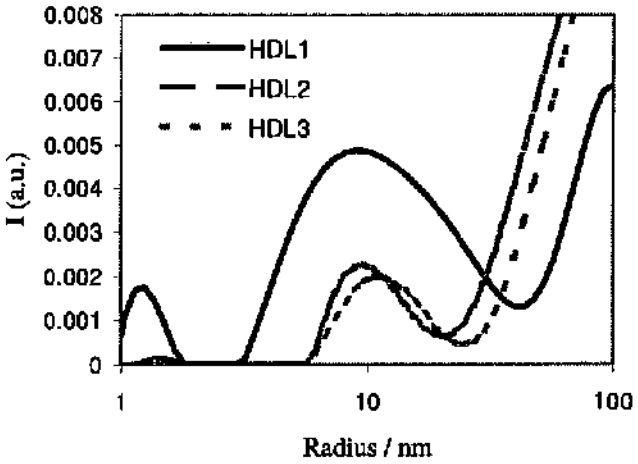

***Figure 3-9** LLS experiments results for HDL sample (HDL1) without additive, (HDL2) in presence of NBD ceramide, (HDL3) in presence of NBD-ceramide and 0.3 mM SDS. The peaks at high radius size (> 30 nm) represent particle aggregates present in all the samples considered. The particle radius reported corresponds to the radius at the maximum intensity, I.*

HDL particle charge was then calculated using Equation (3), the particle size data from the LLS experiments (10 nm and 12 nm diameter before and after the addition of SDS, respectively) and a value for the viscosity of water at 25°C of 8.91×10^{-4} kg $m^{-1}s^{-1}$. A charge of -9 was obtained for native HDL particles and -18 for the HDL particles in the presence of 0.3 mM SDS. While the first value corresponds to the data reported by Cruzado et al. [34], the second value relative to the 0.3 mM SDS is higher than the value of -14 reported in the same reference and calculated in the presence of 3.5 mM SDS. This may be explained by the fact that Cruzado et al. did not consider particle swelling upon exposure to SDS and used the same radius for all the different conditions considered. Our calculations are most likely more accurate, demonstrating the utility of combining different methods in Table 3-3.

Table 3-3 HDL peak characteristics without and in presence of SDS in the sample.

	Without SDS	*With 0.3 mM SDS added to the sample*
Migration time (s)	18.2	21.4
Mobility (10^{-8} m^2/Vs)	0.9	1.4
Size (nm)	10	12
Charge	-9	-18

The increased negative charge of HDL upon addition of SDS was expected because of the high affinity that the LP particles (in particular the apolipoproteins) have for the detergent molecules [37]. Whether SDS molecules are integrated into the particles by interacting with the proteins or with the lipidic core, the result is a change in particle charge, dimension and electrophoretic mobility. While the electropherogram gives an indirect idea of this LP-SDS interaction, the LLS experiments give direct proof of the presence of SDS on the LP particles and the consequent particle swelling. Moreover, LLS data suggest that the particles are not destroyed at this low SDS concentration. As mentioned, for the LDL samples the LLS experimental results were not so informative because of bad sample quality of the sample. However, the conclusion drawn for the HDL-SDS samples could be applied to LDL-SDS samples as well, due to the similarity of the LP composition and their electrophoretic behaviour in the presence of 0.3 mM SDS. In conclusion, it is hypothesized that the SDS non-destructively coats the LP particles, and at the same time modifies the sample sufficiently with respect to the BGE to cause a focusing effect on the sample. Since the integrity of the particle is maintained, different LDL modified forms could be resolved and detected in an untreated channel, using LIF detection and adding a small amount of SDS to the sample to improve the method sensitivity.

3.4 Conclusions and outlook

A discussion of the lipoprotein work and an outlook of how LP analysis in miniaturized systems could be further improved are presented in the following points.

- We demonstrated that complex particles such as lipoproteins could be analysed in the chip-format. The lipoprotein samples used in this work were derived from fresh serum, which was first separated from blood by clotting and centrifugation. Lipoprotein particles were then fractionated on the basis of their density by micro-ultracentrifugation and finally dialysed against phosphate-buffered saline (PBS, pH 7.4). This means that the samples are pretreated before being analysed by CE. Analysis of serum directly was tried in both fused silica and microchip formats. For the capillary format, two peaks corresponding mostly likely to HDL and LDL were detected for this sample (Figure 3-6). Injection of serum directly onto chip resulted in clogging of the microchannels. This different behaviour can be attributed to the higher surface-to-volume ratio in the microchannel compared to a 75-μm-i.d. capillary. Thus the complex matrix sticks easily to the wall of the side channels used to load the sample at the injector. This was confirmed by observation of fluorescence signal at the channel walls using the fluorescence microscope, and by the difficulty of rinsing the structure and regenerating the channel surface after serum injection. Sample dilution probably would facilitate the serum analysis on-chip, but more time was not invested in examining this possibility. It suffices to say that, although the first papers have been recently published about analysis of complex samples in miniaturized systems as mentioned in Section 1.1.3, the possibility to deal with complex matrices on chip is still an open challenge [38]. The development of POC devices for the analysis of crude samples is still, in fact, not trivial. Moreover, for the development of an

actual PDC device, sample loading onto the chip should be also simple and rapid and require a minimum of human handling in order to minimize contamination. The use of microneedles for taking a few μL of blood and guiding it directly into the fluidic network could be an interesting approach.

- Although fluorescence detection is still the most sensitive detection method [39-42] widely coupled to microsystems, analytes are often not intrinsically fluorescent, and a covalent or noncovalent labelling step is necessary for their detection. To avoid off-chip sample manipulations, the staining of LP with NBD-ceramide could be integrated directly into the microdevice as on-column [43, 44] or post-column [28, 45, 46] reaction step. Probably LP labelling can be integrated on-chip due to the simple and rapid staining protocol and the high affinity between LP and NBD-ceramide. However, labelling usually requires an extra channel for dye loading and a portion of the separation channel dedicated to the labelling reaction. Thus, a channel layout more complex than the one presented in Figure 3-3A and larger dye volumes would be required. Moreover, the dye is not soluble in the usual aqueous buffers, and thus problems with its loading into the channels could occur. Another problem associated with labelling is the heterogeneity caused by the multiple-tagging, which could compromise separation performance and decrease peak efficiency.

  Alternatively, a detection system different from the LIF method could be employed. Conductivity detection, for instance, seems to be a good choice because it does not require any sample derivatization and can be easily integrated into the chip format as reported in the literature [47-49]. Optical systems still tend to be large (i.e. laser, microscope lenses, photomultiplier tube) and therefore not as amenable to miniaturization. The only requirement for conductivity detection is that the migrating analyte zones possess a conductivity that is different from that of a carrier electrolyte.

This method was easily integrated into a microdevice. Although suffering from lower sensitivity than fluorescence (in the order of μM) [50, 51], conductivity was successfully employed to detect small inorganic ions and low-molecular-weight organic ions usually isolated via isotachophoresis [47, 51, 52] or via zone electrophoresis [53, 54]. Only recently, peptides, proteins and double-stranded DNA ladders were detected by conductivity detection using different electrophoretic methods for their separation [55]. These species were detected as negative peaks, due to the lower conductivity of the analyte bands compared to the background carrier electrolyte. Lipoproteins could also be detected in such a way.

- Although microchip CE is quite well established, the use of CE in a fused-silica format is still important for method development. For this reason the collaboration with a laboratory where conventional systems are available (the Nestlè Research Centre in this case), was invaluable for getting a first idea of LP electrophoretic behaviour (peak identity, peak shape and elution order). These results helped the interpretation of the electropherograms obtained from a miniaturized device, at least for a qualitative assessment. From a quantitative point of view (i.e. detection limits, signal-to-noise ratio) the two system results are difficult to compare, due in part to the different optical and electronic components of the detection set-up.
- The direct comparison between the conventional and the microchip suggests that microCE chips could be better for protein analysis than conventional capillaries. At the very least, different BGE conditions are required for the two systems, due primarily to the short effective length and therefore the short analyte retention time in the microchip. Moreover, the application of higher electric fields along the microchannel during the separation could also reduce protein adsorption at the wall. This is due to the faster LP migration, which reduces the LP residence time and perhaps

orients the particles in such a way as to prevent their interaction with the walls. Although for the moment there is no evidence for the latter hypothesis, it would be interesting to systematically study protein adsorption in an electroosmotically-driven system under different electric fields and compare the results with those achieved for the same study in a pressure-driven system. This would reveal if the electric field and flow profile could play a role in protein-wall interaction. In any case, the simplicity of the integrated CE system makes it very attractive for on-chip protein separations.

- The sharpening effect observed for the LDL peak in the presence of 0.3 mM SDS added to the sample and not to the running buffer could be useful for the detection of species present in the sample at low concentration, such as oxidized LDL forms. The focusing effect in fact enhances peak signal height, improving method sensitivity. Moreover, lipoprotein integrity is maintained, as supported by the literature and laser light scattering (LLS) experiments. This fact suggests that the particles can be retained throughout separation, and can undergo other kinds of analysis. These could include cholesterol or triglyceride concentration measurements, which would increase the amount of extractable information for LP characterization and diagnostics. These features make the method an attractive choice for the detection of low concentrations of lipoproteins of clinical interest, such as oxidized LDL forms [7, 18]. Moreover, the information obtained from the LP electropherograms and from the LLS experiments could be further used to better characterize the sample as demonstrated for HDL particles.
- A good method for lipoprotein analysis should neither modify or destroy the particles, nor create unknown peaks. It should also guarantee the resolution necessary for the separation of different LP subclasses. It would be also of interest to identify the species of clinical interest and their

concentrations on-line. It is worth recalling that the higher the SDS concentration in the sample, the lower the separation resolution seems to be [33]. In case the differences in mobilities between the modified LDL forms were so small as to not be resolved in the presence of SDS, even at low concentration, isotachophoresis (ITP) could be an interesting approach to investigate. It has been, in fact, demonstrated that capillary ITP has the power to resolve different subclasses of lipoproteins [7, 21-24]. This technique has been recently integrated in a microdevice, but used so far only for analysis of organic acids [47, 51] or pesticides [56]. With further efforts, on-chip ITP could become a potential diagnostic tool for LP subclass analysis.

- A potential POC device for LP analysis, for instance, should contain structures for sample loading and analyis (e.g. separation columns). Once the sample is loaded, the device could be inserted into an instrument equipped with power supply sources, detection elements (e.g. laser diode and photodiode) and software system for data acquisition and storage. Standards should also be available for result evaluation. Such a system could be used directly in surgery, and provide real-time answers about patient health.

REFERENCES

[1] H. Buchwald, J. R. Boen, P. A. Nguyen, S. B. Williams, and J. P. Matts, "Plasma lipids and cardiovascular risk: a POSCH report. Program on the surgical control of the hyperlipidemias.," *Atherosclerosis*, vol. 154, pp. 221-227, 2001.

[2] D. Steinberg, S. Parthasarathy, T. E. Carew, J. C. Khoo, and J. L. Witztum, "Beyond cholesterol. Modifications of low-density lipoprotein that increase its atherogenicity," *New England J. Med.*, vol. 320, pp. 915-24, 1989.

[3] H. Hakamata, A. Miyazaki, M. Sakai, Y. Sakamoto, and S. Horiuchi, "Cytotoxic effect of oxidized low density lipoprotein on macrophages," *J. Atheroscler. Thromb.*, vol. 5, pp. 66-75, 1998.

[4] G. Bittolo-Bon, G. Cazzolato, and P. Avogaro, *Does circulating oxidized LDL exist and can it be detect?*: Bellomo, G.; Finardi, G.; Maggi, E.; Rice-Evans, C. editors. Ricelieu, London, 1995.

[5] P. Halvoet, G. Perez, Z. Zhao, E. Brouwers, H. Bernar, and D. Collen, "Malondialdehyde-modified low density lipoproteins in patients with atherosclerotic disease," *J. Clin. Invest.*, vol. 95, pp. 2611-2619, 1995.

[6] T. J. Lyons, "Glycation and oxidation: a role in the pathogenesis of atherosclerosis," *Am. J. Cardiol.*, vol. 71, pp. 26B-31B, 1993.

[7] G. Bittolo-Bon and G. Cazzolato, "Analytical capillary isotachophoresis of total plasma lipoproteins: a new tool to identify atherogenic low density lipoproteins," *J. Lipid Res.*, vol. 40, pp. 170-7, 1999.

[8] C. L. Colyer, T. Tang, N. Chiem, and D. J. Harrison, "Clinical potential of microchip capillary electrophoresis systems," *Electrophoresis*, vol. 18, pp. 1733-1741, 1997.

[9] R. J. Havel, H. A. Eder, and J. H. Bragdon, "The distribution and chemical composition of ultracentrifugally separated lipoproteins in human serum," *J. Clin. Invest.*, vol. 34, pp. 1345-1353, 1955.

[10] B. H. Weiller, L. Ceriotti, T. Shibata, D. Rein, M. A. Roberts, J. Lichtenberg, J. B. German, N. F. de Rooij, and E. Verpoorte, "Analysis of lipoproteins by capillary zone electrophoresis in microfluidic devices: assay development and surface roughness measurements," *Anal. Chem.*, vol. 74, pp. 1702-1711, 2002.

[11] M. A. Austin, J. L. Breslow, C. H. Hennekens, J. E. Buring, W. C. Willet, and R. M. Krauss, "Low density lipoprotein subclass pattern and risk of myocardial infarction," *J. Am. Med. Assoc.*, vol. 260, pp. 97-104, 1988.

[12] M. A. Austin, "Small, dense low-density lipoprotein as a risk factor for coronary heart disease," *Int. J. Clin. Lab. Res.*, vol. 24, pp. 184-192, 1994.

[13] G. M. Reaven, Y. D. Chen, J. Jeppesen, P. Maheux, and R. M. Krauss, "Insulin resistence hyperinsulinemia in individuals with small, dense low density lipoprotein particles," *Clin. Invest.*, vol. 92, pp. 141-146, 1993.

[14] C. Labeur, J. Shepherd, and M. Rossenen, "Immunological assays of apolipoproteins in plasma: methods and instrumentation," *Clin. Chem.*, vol. 36, pp. 591-597, 1990.

[15] W. C. Taddei-Peters, B. T. Butman, G. R. Jones, T. M. Venetta, P. F. Macomber, and J. H. Ransom, "Quantification of lipoprotein(a) particles containing various apolipoprotein(a) isoforms by a monoclonal anti-Apo(a) capture antibody and a polyclonal anti-apolipoprotein B detection antibody sandwich enzyme immunoassay," *Clin. Chem.*, vol. 39, pp. 1382-1389, 1993.

[16] R. Vercaemst and M. Rossenen, "Separation and quantitation of plasma lipoproteins by high-performance liquid chromatography," *J. Chomatogr.*, vol. 276, pp. 174-181, 1983.

[17] C. A. Daykin, O. Corcoran, S. H. Hansen, I. Bjornsdottir, C. Cornett, S. C. Connor, J. C. Lindon, and J. K. Nicholson, "Application of directly coupled HPLC NMR to separation and characterization of lipoproteins from human serum," *Anal. Chem.*, vol. 73, pp. 1084-1090, 2001.

[18] J. Stocks and N. E. Miller, "Capillary electrophoresis to monitor the oxidative modification of low density lipoproteins," *J. Lipid Res.*, vol. 39, pp. 1305-9, 1998.

[19] R. D. Macfarlane, P. V. Bondarenko, S. L. Cockrill, I. D. Cruzado, W. Koss, C. J. McNeal, A. M. Spiekerman, and L. K. Watkins, "Development of a lipoprotein profile using capillary electrophoresis and mass spectrometry," *Electrophoresis*, vol. 18, pp. 1796-806, 1997.

[20] A. Z. Hu, I. D. Cruzado, J. W. Hill, C. J. McNeal, and R. D. Macfarlane, "Characterization of lipoprotein a by capillary zone electrophoresis," *J. Chromatogr. A*, vol. 717, pp. 33-9, 1995.

[21] G. Schmitz and C. Möllers, "Analysis of lipoproteins with analytical capillary isotachophoresis," *Electrophoresis*, vol. 15, pp. 31-9, 1994.

[22] G. Schmitz, C. Möllers, and V. Richter, "Analytical capillary isotachophoresis of human serum lipoproteins," *Electrophoresis*, vol. 18, pp. 1807-13, 1997.

[23] K. Inano, S. Tezuka, T. Miida, and M. Okada, "Capillary isotachophoretic analysis of serum lipoproteins using a carrier ampholyte as spacer ion," *Ann. Clin. Biochem.*, vol. 37, pp. 708-716, 2000.

[24] A. Schlenck, B. Herbeth, G. Siest, and S. Visvikis, "Characterization and quantification of serum lipoprotein subfractions by capillary isotachophoresis: relationships with lipid, apolipoprotein, and lipoprotein levels," *J. Lipid Res.*, vol. 40, pp. 2125-33, 1999.

[25] B. H. Weiller, T. Shibata, L. Ceriotti, M. A. Roberts, D. Rein, J. B. German, J. Lichtenberg, E. Verpoorte, and N. F. de Rooij, "Development of a new, chip-based method for lipoprotein

analysis by capillary electrophoresis", Proceedings of Micro Total Analysis Systems 2001, Monterey, CA, USA, 2001, 426-428.

[26] T. Shibata, L. Ceriotti, B. H. Weiller, M. A. Roberts, E. Verpoorte, and N. F. de Rooij, "Low density lipoprotein (LDL) analysis in a chip-based system", Proceedings of Micro Total Analysis Systems 2001, Monterey, CA, USA, 2001, 513-514.

[27] L. Ceriotti, T. Shibata, B. Folmer, B. H. Weiller, M. A. Roberts, N. F. de Rooij, and E. Verpoorte, "Low-density lipoprotein analysis in microchip capillary electrophoresis systems," *Electrophoresis*, vol. 23, pp. 3615-3622, 2002.

[28] C. L. Colyer, S. D. Mangru, and D. J. Harrison, "Microchip-based capillary electrophoresis of human serum proteins," *J. Chromatogr. A*, vol. 781, pp. 271-276, 1997.

[29] H. J. Crabtree, E. C. S. Cheong, D. A. Tilroe, and C. J. Backhouse, "Microchip injection and separation anomalies due to pressure effects," *Anal. Chem.*, vol. 73, pp. 4079-4086, 2001.

[30] V. Hlady, J. Rickel, and J. D. Andrade, "Quantitative analysis of protein adsorption kinetics," *Colloids Surf.*, vol. 34, pp. 171, 1988/89.

[31] I. N. Levine, *Physical Chemistry*, 2nd Edition ed. New York: McGraw-Hill, 1983.

[32] T. Tadey and W. C. Purdy, "Effect of detergents on the electrophoretic behaviour of plasma apolipoproteins in capillary electrophoresis," *J. Chromatogr. A*, vol. 652, pp. 131-138, 1993.

[33] E. Kenndler and K. Schmidt-Beiwl, "Effect of dodecyl sulphate in protein samples on separation with free capillary zone electrophoresis," *J. Chomatogr.*, vol. 545, pp. 397-402, 1991.

[34] I. D. Cruzado, A. Z. Hu, and R. D. Macfarlane, "Influence of dodecyl sulfate ions on the electrophoretic mobilities of lipoprotein particles measured by HPCE," *Journal of Capillary Electrophoresis*, vol. 3, pp. 25-9, 1996.

[35] Y. Walbroehl and J. W. Jorgenson, "Capillary zone electrophoresis for the determination of electrophoretic mobilities and diffusion coefficients of proteins," *J. Microcolumn Sep.*, vol. 1, pp. 41-45, 1989.

[36] M. Y. Badal, M. Wong, N. Chiem, H. Salaimi-Moosavi, and D. J. Harrison, "Protein separation and surfactant control of electroosmotic flow in poly(dimethylsiloxane)-coated capillaries and microchips," *J. Chromatogr. A*, vol. 947, pp. 277-286, 2002.

[37] S. Mikano, C. Tanford, and J. A. Reynolds, "The interaction of polypeptide components of human high density serum lipoprotein with detergents," *J. Biol. Chem.*, vol. 249, pp. 7379-7382, 1974.

[38] A. Oki, S. Adachi, Y. Takamura, K. Ishiara, H. Ogawa, Y. Ito, T. Ichiki, and Y. Horiike, "Electroosmosis injection of blood serum into biocampatible microcapillary chip fabricated on quartz plate," *Electrophoresis*, vol. 22, pp. 341-347, 2001.

[39] C. S. Effenhauser, G. J. M. Bruin, A. Paulus, and M. Ehrat, "Integrated capillary electrophoresis on flexible silicone microdevices - Analysis of DNA restriction fragments and detection of single DNA molecules on microchips," *Anal. Chem.*, vol. 69, pp. 3451-3457, 1997.

[40] J. C. Fister, S. C. Jacobson, L. M. Davis, and J. M. Ramsey, "Counting single chromophore molecules for ultrasensitive analysis and separations on microchip devices," *Anal. Chem.*, vol. 70, pp. 431-437, 1998.

[41] B. B. Haab and R. A. Mathies, "Single-molecule detection of DNA separations in microfabricated capillary electrophoresis chips employing focused molecular streams," *Anal. Chem.*, vol. 71, pp. 5137-5145, 1999.

[42] M. B. Wabuyele, S. M. Ford, W. Stryjewski, J. Barrow, and S. A. Soper, "Single molecule detection of double-stranded DNA in poly(methylmethacrylate) and polycarbonate microfluidic devices," *Electrophoresis*, vol. 22, pp. 3939-3948, 2001.

[43] S. C. Jacobson and J. M. Ramsey, "Integrated microdevice for DNA restriction fragment analysis," *Anal. Chem.*, vol. 68, pp. 720-723, 1996.

[44] L. J. Jin, B. C. Giordano, and J. P. Landers, "Dynamic labeling during capillary or microchip electrophoresis for laser-induced fluorescence detection of protein-SDS complexes without pre- or postcolumn labeling," *Anal. Chem.*, vol. 73, pp. 4994-99, 2001.

[45] K. Fluri, G. Fitzpatrick, N. Chiem, and D. J. Harrison, "Integrated capillary electrophoresis devices with an efficient postcolumn reactor in planar quartz and glass chips," *Anal. Chem.*, vol. 68, pp. 4285-4290, 1996.

[46] Y. Liu, R. S. Foote, S. C. Jacobson, R. S. Ramsey, and J. M. Ramsey, "Electrophoretic separation of proteins on a microchip with noncovalent, postcolumn labeling," *Anal. Chem.*, vol. 72, pp. 4608-4613, 2000.

[47] B. Graβ, A. Neyer, M. Jöhnck, D. Siepe, F. Eisenbeiβ, G. Weber, and R. Hergenröder, "A new PMMA microchip device for isotachophoresis with integrated conductivity detector," *Sensors and Actuators B*, vol. 72, pp. 249-258, 2001.

[48] Y. Liu, D. D. Wipf, and C. S. Henry, "Conductivity detection for monitoring mixing reactions in microfluidic devices," *Analyst*, vol. 126, pp. 1248–1251, 2001.

[49] J. Lichtenberg, E. Verpoorte, and N. F. de Rooij, "A miniaturized analysis system based on capillary electrophoresis and contactless conductivity detection", Proceedings of Transducers '01, Munich, Germany, 2001, 408-411.

[50] M. Pumera, I. Wang, F. Opekar, I. Jelínek, J. Feldman, H. Löwe, and S. Hardt, "Contactless conductivity detector for microchip capillary electrophoresis," *Anal. Chem.*, vol. 74, pp. 1968-1971, 2002.

[51] D. Kaniansky, M. Masar, J. Bielcikova, F. Ivanyi, F. Eisenbeiß, B. Stanislawski, B. Graβ, A. Neyer, and M. Jöhnck, "Capillary electrophoresis separations on a planar chip with the column-coupling configuration of the separation channels," *Anal. Chem.*, vol. 72, pp. 3596-3604, 2000.

[52] M. Masar, M. Zuborova, J. Bielcikova, D. Kaniansky, M. Jöhnck, and B. Stanislawski, "Conducovity detection and quantitation of isotachophoretic analytes on a planar chip with on-line coupled separation channels," *J. Chromatogr. A*, vol. 916, pp. 101-111, 2001.

[53] R. M. Guijt, E. Baltussen, G. van der Steen, R. B. M. Schasfoort, S. Schlautmann, H. A. Billiet, J. Frank, G. W. van Dedem, and A. van den Berg, "New approaches for fabrication of microfluidic capillary electrophoresis devices with on-chip conductivity detection," *Electrophoresis*, vol. 22, pp. 235-41, 2001.

[54] J. Lichtenberg, N. F. de Rooij, and E. Verpoorte, "A microchip electrophoresis system with integrated in-plane electrodes for contactless conductivity detection," *Electrophoresis*, vol. 23, in press, 2002.

[55] M. Galloway, W. Stryjewski, A. Henry, S. M. Ford, S. Llopis, R. L. McCarley, and S. A. Soper, "Contact conductivity detection in poly(methylmethacrylate)-based microfluidic devices for analysis of mono- and polyanionic molecules," *Anal. Chem.*, vol. 74, pp. 2407-15, 2002.

[56] P. A. Walker, M. D. Morris, M. A. Burns, and B. N. Johnson, "Isotachophoretic separations on a microchip. Normal Raman spectroscopy detection," *Anal. Chem.*, vol. 70, pp. 3766-3769, 1998.

4 On-chip fritless capillary electrochromatography

4.1 Introduction

As presented in reviews by Bruin [1] and Kutter [2], the chromatographic separation mode has not been explored much in the area of chip-based systems, though clearly it is of interest, as it is the mode most commonly applied in separation sciences. A quite recent chromatographic method is capillary electrochromatography (CEC), where EOF is used to drive the mobile phase and sample through the stationary phase [3, 4]. The basic features of CEC were introduced in Chapter 1, Section 1.3.4. In principle, CEC is more suited to miniaturization than HPLC, where the connection between microdevice and high performance pump is still a challenge [5-8]. However, for both separation methods the packing and its stabilization within the channel represent a big challenge. For these reasons, the first on-chip CEC was performed in an open-channel (O-CEC), as described by Jacobson et al. [9]. These researchers separated coumarin dyes in a glass channel, in which the surface was chemically modified with octadecylsilane to function as a stationary phase. The same approach was reported by Kutter et al. [10], who demonstrated control of selectivity, resolution and analysis times of the dye test mixture using both isocratic and gradient conditions. These conditions were easily realized in the miniaturized format by

simply computer-controlling the applied voltage at the ends of the channels. O-CEC has also been integrated on chip to act as the first dimension of a two-dimensional separation system, while CE was used for the second dimension [11]. The utilization of the sol-gel technique to easily produce micro O-CEC columns was described by Constantin et al. [12]. In this paper, the channel walls were coated with a stationary phase containing tetraethoxysilane (TEOS) and *n*-octyltriethoxysilane (C_8-TEOS). Such co-monomers guarantee the presence on the channel walls of both silanol groups for the EOF generation and organic moieties for the chromatographic interaction. Polycyclic aromatic hydrocarbons (PAHs) were successfully separated in these coated channels.

The open channel approach suffers from low sample capacity and retention capabilities. To improve this, CEC separations are mostly performed in channels packed with stationary phases. In conventional CEC, the most used stationary phases are particulate in nature, based on surface-modified silica particles 5 µm or less in diameter. The performance and the stability of the capillary column are dependent on the quality of the retaining frits at the ends of the column. Frit fabrication is problematic in capillaries and it is also more inconvenient on chips. An alternative fritless approach for CEC on chip was introduced by He et al. [13, 14]. To mimic the packed bed, they fabricated so-called collocated monolith support structures (COMOSS) by deep reactive-ion etching (DRIE) in quartz. The approach is innovative, since the COMOSS provide a large interface between the stationary (bonded to the monolith structures) and mobile phases for analyte partitioning, frits are not required and several columns can be constructed on a single wafer. Moreover, the COMOSS structure design is often mentioned in review papers as an example of the potential of microfabrication to realize complex, well-defined structures. Integrated COMOSS were also replicated in PDMS and used for CEC separation of a peptide mixture after surface derivatization [15, 16].

Another way to circumvent the bead packing is represented by the so-called "monolith approach", which uses continuous polymer beds instead of particles as stationary phases [17, 18]. The first paper to use a continuous bed for on-chip chromatography was published by Ericson et al. [19]. The monolithic bed was polymerised using ammonium persulfate and N,N,N`N`-tetramethylethylenediamine (TEMED) in the microchannel itself, and was used as a stationary phase for electrochromatography and ion-exchange chromatography. Low-molecular-weight (alkyl phenones, antidepressants) and high-molecular-weight substances (proteins) were separated in these microbeds with efficiencies higher than 300,000 plates/m and separation times usually shorter than 20 s [19]. More recently, porous acrylate-based polymer monoliths have been patterned in channels by photopolymerization using a mask and a UV lamp as for conventional photolithography [20, 21]. In the last reference, bioactive peptides and amino acids were separated by CEC achieving efficiencies up to 600,000 plates/m. The monolith characteristics can be easily controlled in terms of charge, hydrophobicity and pore size. As a result, different types of chromatography can be performed to separate different classes of analytes. The monolithic phase can also be removed from the glass channel and be regenerated [21].

Although the monolithic approaches are worth pursuing, conventional silica-based phases remain attractive due to their easy availability and well-characterized properties. In the literature only two examples of bead-packed beds have been reported for CEC. The first one, reported by Oleschuk et al. [22], described a weir-based approach to reversibly trap modified silica beads in a 200-μm-long glass chamber. Fluorescein and BODIPY were separated in less than 15 s with an efficiency of 500,000 plates/m for the fluorescein peak. The creation of packed particle beds in narrow channels is not trivial; however, this approach works well and the chamber can be reversibly packed using electrokinetic pumping. The second paper is the one we published in Anal. Chem. [23]. In our work, particulate stationary phases were employed, with the aim of comparing the

results achieved in the micro-format with the ones achieved in conventionally packed capillaries by our partners at Novartis Pharma (Basel, Switzerland). To pack this kind of stationary phase, a simple, tapered channel geometry was employed. In this chapter our approach for fritless CEC will be summarized and discussed. For a detailed description of this study, see the paper reproduced in Appendix 3.

4.2 Experimental section

4.2.1 Chip fabrication and layout

The devices developed to perform on-chip CEC were realized in PDMS using replica molding as described in Chapter 1, Section 1.2.2.1. The details of the channel layout are presented in Figure 4-1. The 16-μm-wide side channels are curved and intersect with the separation channel to form a 150-μm-long double-T intersection. The 5.5-cm-long separation channel was designed for fritless CEC. It includes a gradual tapering just below the intersection, where the separation channel width changes from 16 to 70 μm over distances of 0.5, 0.8 or 1 mm, depending on the layout. Particles could be trapped in this taper to create packing, as described below. The design was transferred to a chromium mask (Delta Mask, Enschede, Holland) and then patterned as a relief (30-50 μm high) on a silicon wafer by DRIE, as described in Chapter 2, Section 2.2.1. The PDMS replica was sealed with a clean glass wafer after 0.8-min-long exposure of both substrates in an oxygen plasma-based cleaner (Tegal Asher 6, Tegal Corp., Novato, CA). This bonding is irreversible, since the plasma discharge converts $-OSi(CH_3)_2O-$ groups at the surface to $-O_nSi(OH)_{4-n}$. The condensation of these silanol groups (Si-OH) to covalent siloxane (-O-Si-O-) bonds when the two oxidized surfaces are put

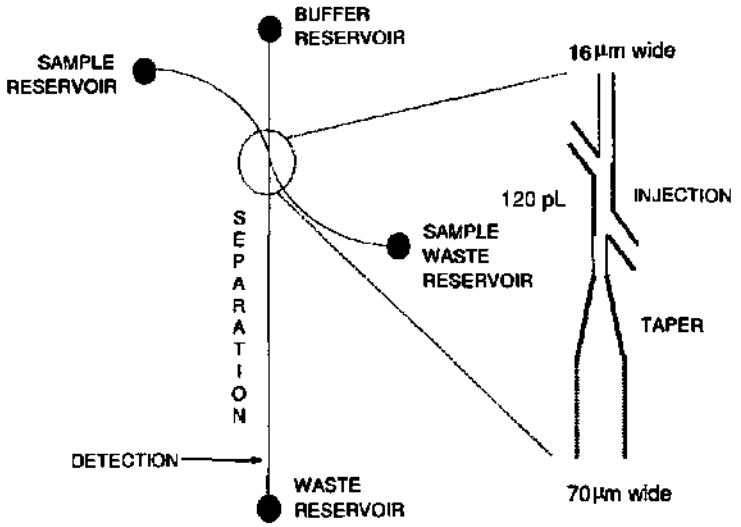

Figure 4-1 Chip loyout for fritless CEC in poly(dimethylsiloxane) (PDMS). The channel structure consists of two side channels entering the main channel to form slanted T-intersections. This so-called "double-T" injection scheme allows pinched injection of small, well-defined volumes (about 120 pL for 50-µm-deep structures) of sample into the straight column. As shown in the close-up, the separation column includes o gradual tapering just below the intersection, which is used to stop stationary phase particles, leaving the injector particle-free.

together is responsible for the irreversibility of the sealing [24]. In our case, the PDMS structure was sealed on a glass wafer to form a hybrid device. In another report, PDMS structures were irreversibly sealed to flat PDMS slabs [24]. This kind of bonding is not only fast but can be carried out at room temperature and pressures. Channel geometry is also maintained, in contrast to other bonding methods for plastic devices. These latter methods are based on heating the substrates to their softening temperatures before bringing them in contact, which may introduce distortion to the channel geometry [25].

4.2.2 Channel packing and conditioning

The PDMS structures include a gradual tapering of the separation channel width just below the injector. This taper was used as an alternative to frits to block and confine the stationary phase in the separation channel. To pack, a suspension of octadecylsilanized particles (ODS, 3 μm particles, 2% slurry in acetone) is driven by vacuum from the waste reservoir into the separation channel. At the taper, the density of the particles increases, and they aggregate and act as "keystones". These particles block the others and allow the packing to grow in the opposite direction toward the buffer waste. In this way, the chip can be packed without requiring retaining frit structures, leaving the intersection and the injection channels particle-free. In our case, the ratio of particle size to taper width is about 5, close to the values reported in the literature, where 10-15 μm i.d. capillaries or capillary portions were used to retain 3 μm silica particles [26, 27].

Once packed, the column is flushed with deionized water for two hours by applying vacuum at the sample waste reservoir and intermittent manual pressure at the waste reservoir. The packing is then stabilized by a thermal treatment at 115°C overnight. To carry out the separation, the column is flushed with methanol, deionized water and finally with the mobile phase, consisting of 5 mM phosphate: acetonitrile (80:20) (pH 7), and containing 1 mM sodium fluorescein for indirect fluorescence detection.

4.2.3 Sample injection

The samples were loaded electroosmotically from the sample reservoir to the sample waste reservoir in order to fill the injector formed at the double-T intersection. The sample was confined to the intersection by a counterflow of buffer from the waste reservoir to the sample waster reservoir (pinching scheme, see Chapter 1, Section 1.3) [28, 29], while the buffer reservoir was left floating to

prevent sample dilution. To inject the sample plug (~120 pL) into the separation channel, the potential was reconfigured in order to have the main flow from the buffer reservoir to the waste, and a smaller flow towards the side channel reservoirs to prevent sample leakage into the main channel. The injection procedure is described in detail in Appendix 3.

4.2.4 Indirect fluorescence detection

To detect small neutral molecules, such as benzene and thiourea, which have no derivatizable sites, the fluorescein was added to the running buffer, and the compounds were detected as negative peaks. Indirect laser-induced fluorescence (IDLIF) detection has been reported by Wallenborg et al. for the separation and detection of explosives in an integrated micellar electrokinetic chromatography (MEKC) system [30]. Indirect detection has been reported in ref. [9], where a negative peak of water was used to characterize the mobile-phase velocity in an O-CEC microsystem. In the same work, the same coumarin dyes used for the fluorescent background were then separated and detected by direct LIF detection. In our study, the laser was focused into the packed portion of the channel. In-column (through the packing) detection has some advantages over the detection performed just below the packing (on-column detection). It lends flexibility in the choice of the effective length. It also avoids the band-broadening introduced when a separated sample zones enters the open channel below the packing because of the mismatch of ζ potential between packed and open segment [31, 32]. However, in-column detection can suffer from scattering effects, which compromise detection sensitivity, although it has been reported that multiple scattered light through the packed bed could increase the optical pathlengh, enhancing therefore the detection performance [33]. Moreover, in the case of polymeric monoliths, a high fluorescent background could occur when the

laser is focused in the monolith, due to the autofluorescence of most of the organic polymers [21].

4.3 Results and discussion

4.3.1 CE separation in hybrid structures

Before packing, the empty, oxidized, hybrid structures were employed to perform CE separations of FITC-labeled amino acids [23]. The electropherogram obtained is presented in Figure 4-2 with the relevant experimental conditions. This electropherogram can be compared with the one obtained for the same sample mixture in a glass channel (Chapter 3, Figure 3-4). In the hybrid PDMS/glass device, the FITC peak exhibits an apparent mobility, μ_{app}, of 3.1×10^{-4} cm^2/Vs. In the glass device, the same FITC peak has a μ_{app} of 1.5×10^{-4} cm^2/Vs. This means that the electroosmotic flow in the hybrid channel is two times lower than in the glass structure, due to the lower density of ionized silanols on the plastic walls. In the case of the hybrid device the peak plate height was about 5 μm for the amino acids, 5 times higher than in the glass device. The lowered efficiency has different causes:

- While the injection plug length in the hybrid device is shorter than in the glass structure (150 compared to 200 μm), the plastic channel contained a taper just below the injector, which contributes to sample diffusion [34].
- PDMS surface properties are unstable after plasma treatment [24, 35] as confirmed by the poor separation time reproducibility (migration times in native PDMS are more reproducible [36]) and by the increased peak broadening due to increased analyte-surface interaction [37].

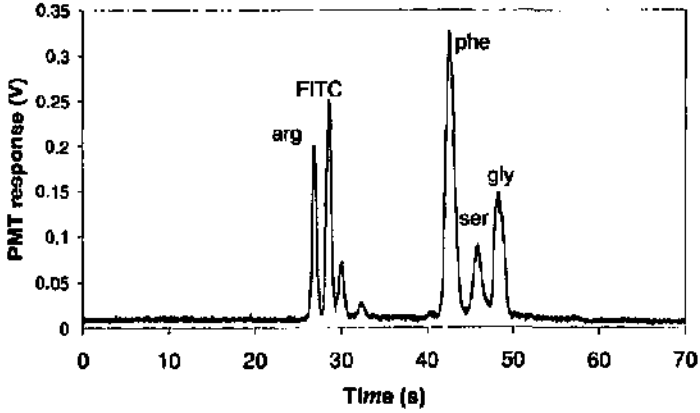

***Figure 4-2** Electropherogram of a mixture of 10 μM FITC-labeled amino acids, achieved in an oxidized PDMS/glass device. L_{tot}= 6 cm; L_{eff}= 2.5 cm; E= 580 V/cm; Running buffer= 100 mM Tris-20 mM boric acid (pH 9); Detection system= Ar^+ laser (488 nm) and bandpass filter at 515 nm; Control system= PC with LabVIEW™.*

- The difference in ζ potential at the PDMS walls and glass coverplate could resulted in non-uniform velocity distribution over the channel cross-section, resulting in a skewed plug front, which leads to increased analyte dispersion and band broadening [38].

4.3.2 Packing conditions and performance

The "keystone effect" can be a very simple way to retain particles in a microcolumn. In our case, a 2% suspension of 3-μm-sized particles could be retained with good reproducibility in a taper 16 μm wide at the narrow end. On the other hand, the "keystone effect" is sensitive to many parameters. Particle concentration in the suspension is one such parameter, which has to be optimised as a function of the taper design. Moreover, the sonication of the dry beads prior to making the acetone suspension, and of the suspension itself, is also critical.

Taper profile proved also to be important. The smooth-sided taper obtained using a chromium mask (the respective silicon master is presented in Chapter 2, Figure 2-2B) was more effective for bead packing than the scalloped one resulting from the use of the transparency mask (Chapter 2, Figure 2-2A).

As mentioned above, a thermal treatment at 115°C of the packed column is absolutely necessary to make the bed stable when exposed to pressure and to the high electric fields typically employed to generate the EOF. This treatment probably determines interparticle bonding and stabilization by a hydrothermal treatment, as reported in reference [39]. Briefly, it is proposed that, upon heating, silica at the outer surface of the particles dissolves in water to form a saturated solution of polysilic acids. This redeposits as silica between the particles upon cooling, thereby bonding particles to one another. The thermal treatment probably also promotes particle-wall interaction.

Using indirect fluorescence detection, a linear relationship between field strength, E, and linear velocity was determined by injecting thiourea (1 mg/mL) as unretained compound in the thermally stabilized packed column. Plate heights of ~5 μm were achieved for this marker at linear mobile phase velocities from 0.5 mm/s up to 3 mm/s, a behaviour which is expected for CEC separations [40, 41]. This flat curve is in contrast with the one reported for pressure-driven systems, for which the plate height increases rather steeply with increasing linear velocity [3]. The different behaviour arises from the greater contribution of the eddy diffusion to the band broadening in the pressure-driven than in the electro-driven system. This is because the flat profile of the mobile phase in CEC ensures a smaller variation in the flow velocities in the individual paths across the bed, limiting the eddy diffusion, as compared to the parabolic flow profile of HPLC [41]. Data at velocities < 0.5 mm/s could not be obtained due to significant axial diffusion of the sample zones, which resulted in concentrations too low to be detected.

The baseline separation of methanol, used as unretained compound, and benzaldehyde was achieved in less than 10 s for an effective length of 1.7 cm and an E of 500 V/cm. The electropherogram is presented in Figure 4-3. Efficiencies of 120,000 and 290,000 plates/m for the unretained and the retained compounds were obtained, respectively. Other neutral compounds, such as phenol, benzaldeyde, benzene, benzyl alcohol and toluene, were tested, though these generally resulted in channel clogging due to analyte adsorption by PDMS. The efficiency values achieved in the packed PDMS channels are close to those reported for other on-chip CEC systems [19, 21, 22]. In particular, Oleschuk et al. obtained a 500,000 plates/m for the fluorescein peak eluting from a 200-μm-long bed, which was packed with silica beads similar to the ones used in our study [22]. The higher efficiency obtained in that system can be in part explained by the fact that the packing was realized in a glass device, limiting the interference of the substrate on the separation. However, the principal difference between the two systems is the injection scheme used. In our system, the sample is driven towards the intersection to fill it and form a defined sample plug, which will be injected into the separation channel without any further treatment (i.e. preconcentration). The structure used in ref. [22] does not contain an intersection for the injection. Thus, the loading step is used to introduce the large-volume (> 100 nL) sample in the channel and preconcentrate it at the front of the packed bed, for which the sample has a high affinity [22]. The concentrated sample begins to undergo chromatography and elute from the bed only when the mobile phase reaches the bed. The preconcentration step will improve the efficiency of the eluting peak by confining analyte to a narrow band, though the potential applied during the separation is lower (about 300 V/cm) than the 500 V/cm employed for the separation presented in Figure 4-3. This injection scheme therefore is more "sophisticated" if compared to the injection schemes conventionally used in microsystems because it allows sample preconcentration, but also less "flexible" because it requires a packed bed and analyte with a high

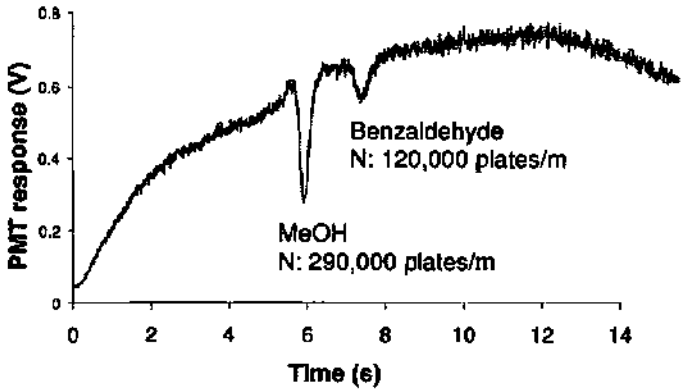

Figure 4-3 CEC separation of methanol and benzaldehyde in the plastic packed microcolumn. L_{tot}= 5 cm; L_{eff}= 1.7 cm; E= 2.5 kV; Stationary phase= 3 µm, Nucleosil, ODS-modified particles; Mobile phase= 5 mM phosphate:acetonitrile (80:20, pH 7) and 1 mM fluorescein for indirect fluorescence detection.

affinity for it. In the case of the monolithic approach, the properties of the acrylate-based stationary phases and the high electric fields applied (up to 770 V/cm) are responsible for efficiency up to 600,000 plates/m achieved for bioactive peptide separation [21].

4.4 Conclusions

- The use of tapered channels to retain the particles in the column originated in conventional systems, where tapered capillaries were used for fritless CEC [26, 27]. Actually, the expression "keystone effect", that we and others have used to define the behaviour of the beads at the taper comes from the architecture domain. The keystone is the central and bearing stone of an arch. If this stone is removed, the arch will collapse. The design of a keystone of a medieval arch (like the ones of the Colosseo in

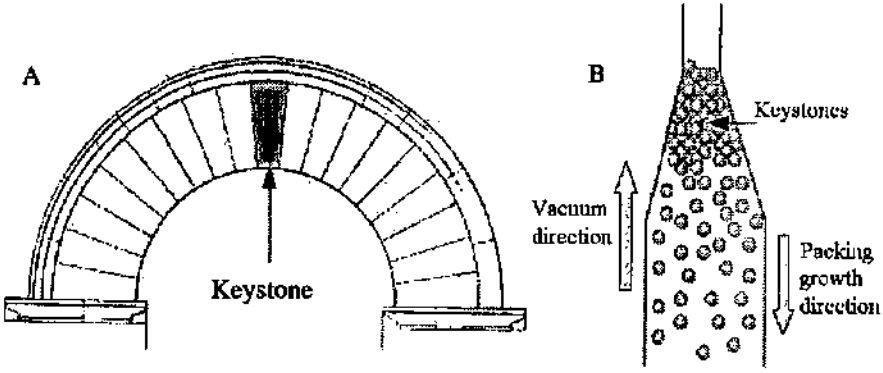

***Figure 4-4** A) Keystone in the medieval architecture. It is important structurally because it makes the apex of the vault and supports the other stones. B) "Keystones" in the tapered channel. They are the first particles that reach the taper. They aggregate at the taper and block the other particles allowing the packing to grow in the direction of the waste.*

Rome) is presented in Figure 4-4A. In an analogous way, it is presumed that just a few particles form a barrier at the taper, and that their aggregate (Figure 4-4B) is strong enough to withhold a packing under flow conditions. If these particles were to be removed, the packing would in all likelihood collapse (as observed when the electric field was applied along the separation channel without thermal treatment).

- The high-aspect-ratio tapered structures realized for this application could not be realized in glass by wet-etching technology. The last, in fact, is isotropic, meaning that the etch rate is equal in all directions, leading to the generation of channels that are at least two times as wide as they are deep. This means that 16-μm-wide channels in glass must be less than 8 μm deep, depending on the mask design dimensions. Using DRIE of silicon, it was possible to obtain masters and therefore channels with rectangular and bigh-aspect-ratio profiles of the desired dimensions. These

high-aspect-ratio channels are also attractive for performing on-chip UV detection, since narrow, deep channels ensure both small detection volumes and reasonable optical path lengths. In Chapter 6 of the present thesis, an approach developed for transverse UV detection through PDMS rectangular channels will be described.

- Tapered capillaries are usually made using a laser-based micropipette puller and the fabrication process, though optimized, is not very reproducible [27]. However, in microdevices, tapers or other geometric features can be integrated in the column design and transferred to a substrate by photolithography with excellent reproducibility, in particular when dry etching techniques (such as DRIE) are employed. Thus, it is much easier to experiment with new channel geometries in microdevices than in fused-silica capillaries. The effect of the geometry (i.e. taper aperture angle and length, turn radius and width) on column performance and fluidic behaviour can be studied more systematically as a result [34, 42].
- The choice of PDMS for this work was dictated by the freedom of channel profile that replica molding can offer, as well as by the good optical characteristics of this polymer. On the other hand, it is known that PDMS is not compatible with many analytes and organic solvents [43]. In our experiments, neutral compounds were tested, with channel clogging often resulting, particularly at the intersection. For this reason, most of the chips were used for 1 day only and comparison with the separation data achieved in bead-packed capillaries at Novartis Pharma was not possible. It is clear that a surface modification is necessary to prevent channel clogging and loss of analytes to this substrate. The plastic substrate thus limits device performance and utility. Passivation of the PDMS [16, 37, 44, 45] or a different substrate altogether would be preferable.

- The use of a direct detection method would also simplify the system, increasing the sensitivity for in-column (through the packing) detection. Note that the analytes mentioned above are usually detected by UV absorbance [33, 46]. Direct fluorescence detection [47] and mass spectrometry [48] have also been coupled with conventional CEC. In microchip CEC systems, UV absorbance [12, 19] and direct fluorescence detection [10, 14, 16, 21] have been used.
- The use of miniaturized systems can enhance among other things the chromatographic separation mode. In particular, from what has been reported recently in the literature, the potential of the monolithic column approach for CEC and other pressure-driven separation methods is emerging [49]. Unfortunately, we have no experience with polymer synthesis and derivatization in our lab. However, polymeric matrices, in particular photopolymerized sol-gel monoliths, represent a promising solution to prepare microbeds of the length and pore size desired, and with high mechanical strength. These monoliths can be created rapidly at a local area on the chip and used to perform all sorts of chromatographic separations (reverse phase, ionic exchange, affinity, chiral and so on) with high resolution and selectivity. The same polymeric beds could be also useful for extraction and concentration steps to further improve sample pretreatment and diagnostic monitoring [50].
- Packing beads into a microdevice is not easy. However, bead-based microbeds are still largely employed for different assays, from immunoassay [51] and enzymatic reactions [52] to solid phase DNA analysis [53], DNA hybridization [54] and extraction methods [22, 55]. Beads with functionalized surfaces are commercially available with a wide range of size and porosity, so that they represent a first good approach before embarking on the investigation of new, less known and less available polymeric matrices. The fritless approach presented here for

bead retention in a microcolumn is quite original. Of course, it should work for applications other than CEC as well, making device fabrication and bead packing easy.

- In general, the integration of chromatography into microdevices can involve also chromatographic techniques other than CEC. Micellar electrokinetic chromatographic (MEKC) separations of fluorescent dyes [56, 57], amino acids [58], explosives [30], and serum theophylline [59] were performed on chip with high efficiency. Attempts to miniaturize pressure-driven chromatography [5, 60] and gas chromatography [61-65] have been reported, as well as integration of the novel hydrodynamic chromatography separation method [66, 67]. From these examples it is evident that progress is ongoing to develop chromatographic systems which are capable of rapid and efficient analysis of biological samples [21, 65], and which are easy to fabricate and handle.

REFERENCES

[1] G. J. M. Bruin, "Recent developments in electrokinetically driven analysis on microfabricated devices," *Electrophoresis*, vol. 21, pp. 3931-3951, 2000.

[2] J. P. Kutter, "Current developments in electrophoretic and chromatographic separation methods on microfabricated devices," *Trac-Trends in Anal. Chem.*, vol. 19, pp. 352-363, 2000.

[3] L. A. Colón, K. J. Reynolds, R. Alicea-Maldonado, and A. M. Fermier, "Advances in capillary electrochromatography," *Electrophoresis*, vol. 18, pp. 2162-2174, 1997.

[4] K. D. Altria, N. W. Smith, and C. H. Turnbull, "A review of current status of capillary electrochromatography technology and applications," *Chromatographia*, vol. 46, pp. 664-674, 1997.

[5] G. Ocvirk, E. Verpoorte, A. Manz, M. Grasserbauer, and H. M. Widmer, "High performance liquid chromatography partially integrated onto a silicon chip," *Analytical Methods and Instrumentation*, vol. 2, pp. 74-82, 1995.

[6] M. McEnery, A. M. Tan, J. Alderman, J. Patterson, S. C. O'Mathuna, and J. D. Glennon, "Liquid chromatography on-chip: progression towards a μ-total analysis system," *Analyst*, vol. 125, pp. 25-27, 1999.

[7] M. Aiello and R. McLaren, "A sensitive small-volume UV/vis flow cell and total absorbance detection system for micro-HPLC," *Anal. Chem.*, vol. 73, pp. 1387-1392, 2001.

[8] P. H. Paul, D. W. Arnold, D. W. Neyer, and K. B. Smith, "Electrokinetic pump application in micro total analysis systems: mechanical actuation to HPLC", Proceedings of Micro Total Analysis Systems 2000, Enschede, The Netherlands, 2000, 583-590.

[9] S. C. Jacobson, R. Hergenröder, L. B. Koutny, and J. M. Ramsey, "Open-channel electrochromatography on a microchip," *Anal. Chem.*, vol. 66, pp. 2369-2373, 1994.

[10] J. P. Kutter, S. C. Jacobson, N. Matsubara, and J. M. Ramsey, "Solvent-programmed microchip open-channel electrochromatography," *Anal. Chem.*, vol. 70, pp. 3291-3297, 1998.

[11] N. Gottschlich, S. C. Jacobson, C. T. Culbertson, and J. M. Ramsey, "Two-dimensional electrochromatography/capillary electrophoresis on a microchip," *Anal. Chem.*, vol. 73, pp. 2669-2674, 2001.

[12] S. Constantin, R. Freitag, D. Solignac, A. Sayah, and M. A. M. Gijs, "Utilizatioo of the sol-gel technique for the development of novel stationary phases for capillary electrochromatography on a chip," *Sensors and Actuators B*, vol. 78, pp. 267-272, 2001.

[13] B. He and F. E. Regnier, "Microfabricated liquid chromatography columns based on collocated monolith support structures," *Journal of Pharmaceutical and Biomedical Analysis*, vol. 17, pp. 925-932, 1998.

[14] B. He, J. Ji, and F. E. Regnier, "Capillary electrochromatography of peptides in a microfabricated system," *J. Chromatogr. A*, vol. 853, pp. 257-262, 1999.

[15] B. E. Slentz, N. A. Penner, E. Lugowska, and F. Regnier, "Nanoliter capillary electrochromatography columns based on collocated monolithic support structures molded in poly(dimethylsiloxane)," *Electrophoresis*, vol. 22, pp. 3736-43, 2001.

[16] B. E. Slentz, N. A. Penner, and F. E. Regnier, "Capillary electrochromatography of peptides on microfabricated poly(dimethylsiloxane) chips modified by cerium(IV)-catalyzed polymerization," *J. Chromatogr. A*, vol. 948, pp. 225-233, 2002.

[17] C. Yu, F. Svec, and J. M. J. Frechet, "Towards stationary phases for chromatography on a microchip: molded porous polymer monoliths prepared in capillaries by photoinitiated in situ polymerization as separation media for electrochromatography," *Electrophoresis*, vol. 21, pp. 120-127, 2000.

[18] S. M. Ngola, Y. Fintschenko, W.-Y. Choi, and T. J. Shepodd, "Conduct-as-cast polymer monolith as separation media for capillary electrochromatography," *Anal. Chem.*, vol. 73, pp. 849-856, 2001.

[19] C. Ericson, J. Holm, T. Ericson, and S. Hjertén, "Electroosmosis- and pressure-driven chromatography in chips using continuous beds," *Anal. Chem.*, vol. 72, pp. 81-87, 2000.

[20] Y. Fintschenko, W.-Y. Choi, S. M. Ngola, and T. J. Shepodd, "Chip electrochromatography of polycyclic aromatic hydrocarbons on an acrylate-based UV-initiated porous polymer monolith," *Fresenius Journal of Anal. Chem.*, vol. 371, pp. 174-181, 2001.

[21] D. J. Throckmorton, T. J. Shepodd, and A. K. Singh, "Electrochromatography on chip: reversed-phase separation of peptides and amino acids using photopatterned rigid polymer monoliths," *Anal. Chem.*, vol. 74, pp. 784-789, 2002.

[22] R. D. Oleschuk, L. L. Shultz-Lockyear, Y. Ning, and D. J. Harrison, "Trapping of bead-based reagents within microfluidic systems: on-chip solid-phase extraction and electrochromatography," *Anal. Chem.*, vol. 72, pp. 585-590, 2000.

[23] L. Ceriotti, N. F. de Rooij, and E. Verpoorte, "An integrated fritless column for on-chip capillary electrochromatography with conventional stationary phases," *Anal. Chem.*, vol. 74, pp. 639-647, 2002.

[24] D. C. Duffy, J. C. McDonald, O. J. A. Schueller, and G. M. Whitesides, "Rapid prototyping of microfluidic systems in poly(dimethylsiloxane)," *Anal. Chem.*, vol. 70, pp. 4974-4984, 1998.

[25] L. Martynova, L. E. Locascio, M. Gaitan, G. W. Kramer, R. G. Christensen, and W. A. MacCrehan, "Fabrication of plastic microfluid channels by imprinting methods," *Anal. Chem.*, vol. 69, pp. 4783-4789, 1997.

[26] G. A. Lord, D. B. Gordon, P. Myers, and B. W. King, "Tapers and restrictors for capillary electrochromatography and capillary electrochromatography mass spectrometry," *J. Chromatogr. A*, vol. 768, pp. 9-16, 1997.

[27] M. Mayer, E. Rapp, C. Marck, and G. J. M. Bruin, "Fritless capillary electrochromatography," *Electrophoresis*, vol. 20, pp. 43-49, 1999.

[28] L. L. Shultz-Lockyear, C. L. Colyer, Z. H. Fan, K. 1. Roy, and D. J. Harrison, "Effects of injector geometry and sample matrix on injection and sample loading in integrated capillary electrophoresis devices," *Electrophoresis*, vol. 20, pp. 529-538, 1999.

[29] S. C. Jacobson, R. Hergenröder, L. B. Koutny, and J. M. Ramsey, "High-speed separations on a microchip," *Anal. Chem.*, vol. 66, pp. 1114-1118, 1994.

[30] S. R. Wallenborg and C. G. Bailey, "Separation and detection of explosives on a microchip using micellar electrokinetic chromatography and indirect laser-induced fluorescence," *Anal. Chem.*, vol. 72, pp. 1872-1878, 2000.

[31] A. S. Rathore, E. Wen, and C. Horvath, "Electroosmotic mobility and conductivity in columns for capillary electrochromatography," *Anal. Chem.*, vol. 71, pp. 2633-2641, 1999.

[32] A. S. Rathore and C. Horvath, "Axial nonuniformities and flow in columns for capillary electrochromatography," *Anal. Chem.*, vol. 70, pp. 3069-3077, 1998.

[33] P. K. Owens and J. Johansson, "Light-scattering studies of packed stationary phases for capillary electrochromatography," *Anal. Chem*, vol. 72, pp. 740-746, 2000.

[34] Y. J. Xue and E. S. Yeung, "Characterization of band broadening in capillary electrophoresis due to nonuniform capillary geometries," *Anal. Chem.*, vol. 66, pp. 3575-3580, 1994.

[35] M. Morra, E. Occhiello, R. Marola, F. Garbassi, P. Humphrey, and D. Johnson, "On the aging of oxygen plasma-treated polydimethylsiloxane surfaces," *Journal of Colloid and Interface Science*, vol. 137, pp. 11-24, 1990.

[36] G. Ocvirk, M. Munroe, T. Tang, R. Oleschuk, K. Westra, and D. J. Harrison, "Electrokinetic control of fluid flow in native poly(dimethylsiloxane) capillary electrophoresis devices," *Electrophoresis*, vol. 21, pp. 107-115, 2000.

[37] V. Linder, E. Verpoorte, W. Thormann, N. F. de Rooij, and H. Sigrist, "Surface biopassivation of replicated poly(dimethylsiloxane) microfluidic channels and application to heterogeneous immunoreaction with on-chip fluorescence detection," *Anal. Chem.*, vol. 73, pp. 4181-4189, 2001.

[38] F. Bianchi, F. Wagner, P. Hoffman, and H. H. Girault, "Electroosmotic flow in composite microchannels and implications in microcapillary electrophoresis systems," *Anal. Chem.*, vol. 73, pp. 829-836, 2001.

[39] T. Adam, K. K. Unger, M. M. Dittmann, and G. P. Rozing, "Towards the column bed stabilization of columns in capillary electroendosmotic chromatography. Immobilization of

microparticulate silica columns to a continuous bed," *J. Chromatogr. A*, vol. 887, pp. 327-337, 2000.

[40] J. H. Knox and I. H. Grant, "Electrochromatography in packed tubes using 1.5 to 50 μm silica gels and ODS bonded silica gels," *Chromatographia*, vol. 32, pp. 317-328, 1991.

[41] M. M. Dittmann, K. Wienand, F. Bek, and G. P. Rozing, "Theory and practice of capillary electrochromatography," *LC-GC*, vol. 13, pp. 800-808, 1995.

[42] J. I. Molho, A. E. Herr, B. P. Mosier, J. G. Santiago, T. W. Kenny, R. A. Brennen, G. B. Gordon, and B. Mohammadi, "Optimization of turn geometries for microchip electrophoresis," *Anal. Chem.*, vol. 73, pp. 1350-1360, 2001.

[43] J. C. McDonald, D. C. Duffy, J. R. Anderson, D. T. Chiu, H. Wu, O. J. A. Schueller, and G. M. Whitesides, "Fabrication of microfluidic systems in poly(dimethylsiloxane) [Review]," *Electrophoresis*, vol. 21, pp. 27-40, 2000.

[44] Y. Liu, J. C. Fanguy, J. M. Bledsoe, and C. S. Henry, "Dynamic coating using polyelectrolyte multilayers for chemical control of electroosmotic flow in capillary electrophoresis microchips," *Anal. Chem.*, vol. 72, pp. 5939-5944, 2000.

[45] T. Yang, S.-y. Jung, H. Mao, and P. S. Cremer, "Fabrication of phospholipid bilayer-coated microchannels for on-chip immunoassays," *Anal. Chem.*, vol. 73, pp. 165-169, 2001.

[46] C. Yan, D. Schaufelberger, and F. Erni, "Electrochromatography and micro high-performance liquid chromatography with 320 μm i.d. packed columns," *J. Chromatogr. A*, vol. 670, pp. 15-23, 1994.

[47] C. Yan, R. Dadoo, H. Zhao, R. N. Zare, and D. J. Rakestraw, "Capillary electrochromatography: analysis of polycyclic aromatic hydrocarbons," *Anal. Chem.*, vol. 67, pp. 2026-2029, 1995.

[48] G. A. Lord, D. B. Gordon, T. W. Tetler, and C. M. Carr, "Electrochromatography-electrospray mass spectrometry of textile dyes," *J. Chromatogr. A*, vol. 700, pp. 27-33, 1995.

[49] N. Tanaka, H. Kobayashi, K. Nakanishi, H. Minakuchi, and N. Ishizuka, "A new type of chromatographic support could lead to higher separation efficiencies," *Anal. Chem.*, pp. 421-429 A, 2001.

[50] K. G. Olsen, D. J. Ross, and M. J. Tarlov, "Immobilization of DNA hydrogel plugs in microfluidic channels," *Anal. Chem.*, vol. 74, pp. 1436-1441, 2002.

[51] K. Sato, M. Tokeshi, T. Odake, H. Kimura, T. Ooi, M. Nakao, and T. Kitamori, "Integration of an immunosorbent assay system: Analysis of secretory human immunoglobulin A on polystyrene beads in a microchip," *Anal. Chem.*, vol. 72, pp. 1144-1147, 2000.

[52] C. Wang, R. Oleschuk, F. Ouchen, J. Li, P. Thibault, and D. J. Harrison, "Integration of immobilized trypsin bead beds for protein digestion within a microfluidic chip incorporating

capillary electrophoresis separations and an electrospray mass spectrometry interface," *Rapid Communications in Mass Spectrometry*, vol. 14, pp. 1377-83, 2000.

[53] H. Andersson, W. van der Wijngaart, P. Enoksson, and G. Stemme, "Micromachined flow-through filter-chamber for chemical reactions on beads," *Sensors and Actuators B*, vol. 67, pp. 203-208, 2000.

[54] Z. H. Fan, S. Mangru, R. Granzow, P. Heaney, W. Ho, Q. Dong, and R. Kumar, "Dynamic DNA hybridization on a chip using paramagnetic beads," *Anal. Chem.*, vol. 71, pp. 4851-4859, 1999.

[55] K. A. Wolfe, M. C. Breadmore, J. P. Ferrance, M. E. Power, J. F. Conroy, P. M. Norris, and J. P. Landers, "Toward a microchip-based solid-phase extraction method for isolation of nucleic acids," *Electrophoresis*, vol. 23, pp. 727-733, 2002.

[56] A. W. Moore, S. C. Jacobson, and J. M. Ramsey, "Microchip separations of neutral species via micellar electrokinetic capillary chromatography," *Anal. Chem.*, vol. 67, pp. 4184-4189, 1995.

[57] J. P. Kutter, S. C. Jacobson, and J. M. Ramsey, "Integrated microchip device with electrokinetically controlled solvent mixing for isocratic and gradient elution in micellar electrokinetic chromatography," *Anal. Chem.*, vol. 69, pp. 5165-5171, 1997.

[58] C. T. Culbertson, S. C. Jacobson, and J. M. Ramsey, "Microchip devices for high-efficiency separations," *Anal. Chem.*, vol. 72, pp. 5814-5819, 2000.

[59] F. von Heeren, E. Verpoorte, A. Manz, and W. Thormann, "Micellar electrokinetic chromatography separations and analyses of biological samples on a cyclic planar microstructure," *Anal. Chem.*, vol. 68, pp. 2044-2053, 1996.

[60] M. Seki, M. Yumada, R. Ezaki, R. Aoyama, and J. W. Hong, "Chromatographic separation of proteins on a PDMS-polymer chip by pressure flow", Proceedings of Micro Total Analysis Systems 2001, Monterey, CA, 2001, 48-50.

[61] S. C. Terry, J. H. Jerman, and J. B. Angel, "A gas chromatographic air analyzer fabricated on a silicon wafer," *IEEE Trans. Electron. Devices*, vol. 26, pp. 1880-1887, 1979.

[62] R. R. Reston and E. S. Kolesar, "Silicon-micromachined gas-chromatography system used to separate and detect ammonia and nitrogen-dioxide. 1. Design, fabrication, and integration of the gas-chromatography system," *Journal of Microelectromechanical Systems*, vol. 3, pp. 134-146, 1994.

[63] E. S. Kolesar and R. R. Reston, "Silicon-micromachined gas-chromatography system used to separate and detect ammonia and nitrogen-dioxide. 2. Evaluation, analysis, and theoretical modeling of the gas-chromatography system," *Journal of Microelectromechanical Systems*, vol. 3, pp. 147-154, 1994.

[64] U. Lehmann, "Micro machined gas chromathograph based on a plasma polymerised stationary phase", Proceedings of Micro Total Analysis Systems 2000, Enschede, The Netherlands, 2000, 171-174.

[65] G. Frye-Mason, R. Kottenstette, C. Mowry, C. Morgan, R. Manginell, P. Lewis, C. Matzke, G. Dulleck, L. Anderson, and D. Adkings, "Expanding the capabilities and applications of gas phase miniature chemical analysis systems", Proceedings of Micro Total Analysis Systems 2001, Monterey, CA, 2001, 658-659.

[66] M. T. Blom, E. Chmela, J. G. E. Gardeniers, R. Tijssen, M. Elwenspoek, and A. van den Berg, "Design and fabrication of a hydrodynamic chromatography chip," *Sensors & Actuators B-Chemical*, vol. 82, pp. 111-116, 2002.

[67] E. Chmela, R. Tijssen, M. T. Blom, J. G. E. Gardeniers, and A. van den Berg, "A chip system for size separation of macromolecules and particles by hydrodynamic chromatography," *Anal. Chem.*, vol. 74, pp. 3470-3475, 2002.

5 On-chip nucleic acid extraction

5.1 Introduction

Genomic analysis represents a powerful tool for detecting and treating disease states. Traditional diagnostics relying on DNA sequence information involve extraction of DNA from whole blood, its purification, amplification by polymerase chain reaction (PCR), and fragment separation using slab gel electrophoresis. This procedure is time-consuming and has a high risk of contamination. The need for new, reliable and timesaving methods has increased, particularly because POC devices for personalized medicine are increasingly desired. For these reasons, DNA analysis, in particular the Human Genome Project, has been a big driver of microtechnology [1].

Initial efforts to make genomic analysis a clean and fast process were focused on the electrophoresis step, which saw a big improvement in terms of time and sample consumption with the development of capillary electrophoresis (CE) instrumentation. In the last few years, CE has been miniaturized to a microchip format, allowing the separation of DNA in a few minutes compared to the hours required for slab gel [2-5]. Parallel samples can be analyzed on the same micro device without diagnostic capability being lost [6-9]. DNA sequencing [10-13] and DNA amplification by PCR [14, 15] have also been successfully integrated into microchips [16]. However, it is only recently that efforts have been invested in the miniaturization of DNA purification methods in order to speed up sample preparation and therefore the whole diagnostic process.

The ability to integrate the lysis of cells and the extraction of nucleic acid and other cell compounds (i.e. enzymes) into a microdevice would greatly increase the power and the applicability of the microsystem [17-21]. Moreover, by interfacing the sample treatment element to PCR and electrophoresis units, the integrated device would become an efficient and autonomous tool for rapid POC diagnostics and environmental testing.

Historically, the time necessary for DNA purification was greatly reduced by switching from phenol extraction procedures to chromatographic resins and solid-phase extraction on silica. In particular, the latter approach, based on the method proposed by Boom in 1990 [22], received particular interest because of its simplicity. The method is based on the lysing and nuclease-inactivation properties of a chaotropic agent, together with the nucleic acid-binding properties of silica particles in the presence of this agent. Chaotropic agents, such as urea, guanidine hydrocloride and sodium iodide, can reduce the activity of water by forming hydrated ions, leaving dehydrated biological molecules behind. In concentrated solutions, these agents can denature proteins and double-stranded DNA by reducing the hydrophobic interactions in their 3D structure. Moreover, they can cause the lysis of mammalian cells, viruses and gram-negative bacterial species, with consequent nucleic acid release in the solution and their binding on the silica surfaces [22]. The process of DNA adsorption on a silica surface is not completely understood. However, it seems that this adsorption of DNA is based on hydrogen bonds, which explains why the highest adsorption efficiencies are achieved in solutions having high ionic strength, low pH and high chaotropic agent concentration [23, 24]. The first two conditions, in fact, cooperate to reduce the electrostatic repulsion between DNA and silica by decreasing the charge on the silica surface. The high concentration of the chaotropic agent rids the DNA and silica of their hydration shells and causes biomolecular denaturation, as mentioned above. In these conditions, the binding between silica and DNA becomes energetically favorable. Unbound components can be removed from the

silica by washing with solvents. DNA purification is finally accomplished by eluting the nucleic acids from the surface with solutions of low ionic strength and quite basic pH (pH= 8), or even water. This method is therefore simple and rapid, and it allows the recovery of undamaged and highly pure nucleic acids that can then be used as a reagent in molecular biological reactions, such as amplification by PCR or NASBA, digestion by restriction nucleases, and Southern Blot. The data acquired are useful in diagnostics of bacterial and viral infections, as well as in gene polymorphism studies and prenatal diagnostics.

A large number of nucleic acid extraction kits available on the market are based on the Boom method and use beads as binding material (examples include kits from Qiagen Inc., Biorad Labs, Promega). This is because beads supply a large available surface area for nucleic acid binding. Usually centrifugation is chosen to separate the solid phase (i. e. particles) from the supernatant solution during the various sample loading, washing and elution steps. Although centrifugation has been successfully integrated in microchips for multiple assay microfluidic systems [19, 25-29], the same goal (separation of stationary and mobile phase) can be achieved by driving different solutions through an extraction matrix, which is physically retained in a macro- or microfluidic structure. Alternatively, magnetic beads can be utilized as solid phase, and a magnetic field in this case is used to immobilize particles and separate them from the solution. Suppliers of these beads include Polysciences Inc., Seradyne Inc., Dynal, and Abgene North America.

Tian et al. published the first miniaturized bead-based system for micro solid-phase extraction (μSPE) for adsorption of human DNA from different matrices [24]. The μSPE device contained 0.2-0.3 mg of silica particles, which were retained in a polyethylene sleeve between two glass fiber frits to define a total volume of around 500 nL. In spite of the small dimensions of the extractor, it turned out to be efficient for the adsorption and desorption of DNA in the picogram-to-nanogram range. The protocol used for the extraction is based on the

Boom method [22, 30]: guanidine HCl-based buffer, alcohols and Tris-EDTA buffer were used for sample loading, washing and elution, respectively. A syringe pump was used to move the solutions with a flow rate usually on the order of a few μL/min. Fluorescence spectroscopy was employed to analyze the DNA recovered from the solid phase, as well as the protein eluting during the loading and the washing phases from the column. PCR and capillary electrophoresis were then used to evaluate the amplificability, and thus the purity, of the eluted DNA. A DNA recovery of roughly 70% from white cells was demonstrated, while more than 80% of the proteins was removed during the loading and washing steps, which took less than 10 min. Although this work was not done on a chip, the dimensions of the capillary used suggest that extraction can be transferred successfully to the microchip format.

On the basis of Tian's work, Landers' group have gone on to trap silica beads within a microchip for NA extraction [31]. In order to retain the particles in a microchamber, they worked with etched glass structures in which the beads are retained by a weir placed at the outlet of the 30-μm-deep cavity [32]. A gap of 12 μm remains between the weir and the cavity coverplate to allow solution flow through the bead bed. It was found that 15-μm silica beads alone can extract DNA with high efficiency, but with low reproducibility for repeated extractions on the same chip, and from chip to chip. The packed devices also had a short lifetime, arising from increased back pressure and decreased flow with time due to gradual compression of the bed with use. To overcome these problems, beads were stabilized with a sol solution, which was then converted into a gel matrix directly in the microchannel. With these silica bead/sol-gel microdevices, high extraction efficiency in stable and reproducible systems was achieved. The channel design was also modified by replacing the weir with a silica bead/sol-gel frit polymerized in situ. Nucleic acids were eluted in less than 10 μL, the extraction process took less than 30 min, and the DNA extracted was suitable for

PCR amplification. The samples extracted were rather academic in nature, consisting of digested λ-phage DNA. Crude lysate was not tested.

The use of magnetic beads has in the last few years received great interest for applications in microfluidics, since the use of magnetic fields to trap magnetic beads in a precise place is an attractive solution. Paramagnetic Dynal beads were used to capture by affinity synthetic poly(A)-tailed DNA samples within a microfluidic device [33]. Jiang et al. published promising work in which paramagnetic oligo-$(dT)_{25}$ beads (diameter of 2.8 μm) were used for mRNA isolation from total RNA in a microfluidic glass device [34]. The results suggest that rare RNA can be isolated on-chip in concentrations and with a quality good enough for constructing cDNA libraries.

Besides beads, Anderson et al. have packed cellulose into a microchamber and employed it for nucleic acid extraction by the Boom method [35]. In this paper, a miniaturized device for multistep genetic assays was developed. This device is realized in polycarbonate by computer-controlled machining or injection molding with overall dimensions of 8 × 40 × 70 mm. It automatically carries out DNA/RNA purification from serum lysate, RT-PCR, nested PCR, nucleic acid hybridization, Dnase fragmentation, and dephosphorylation, labelling and washing steps. Integrated porous hydrophobic membranes work as fluid barriers in conjunction with pneumatically controlled diaphragm valves. Gas pressure is used to move, position and mix reagents under PC control. Nested PCR confirmed the good performance of the purification units. This plastic system for multistep assays promises flexibility and broad applicability, together with high throughput and low cost (10$ for the cartridge and less than 20,000$ for the instruments, GeneChips and scanner excluded). A picture of this multi-assay device is presented in Chapter 7, Figure 7-2.

Since in the presence of chaotropic agents nucleic acids bind on silica surfaces, simple open channels could work as extractor. However, the low surface area available for the binding limits this approach. Two different approaches were

developed to increase surface area-to-volume ratios and improve extraction efficiency in open microstructures. The first approach used deep reactive-ion etching (DRIE) to fabricate pillar-like structures (200 μm high and 18 μm in diameter, for a total area of 0.36 cm^2) to use as binding substrate for DNA adsorption [36]. On-chip PCR and fluorescence detection were employed for eluted DNA evaluation. DNA quantities approaching the binding capacity of the system (40 ng/cm^2 as predicted for glass by Vogelstein and Gillespie [37]) were recovered. Although this approach shows some potential, it relies on expensive and complex technology for chip fabrication. The second approach is reported by Kim et al. [38]. They used photosensitive glass, which was easily structured to again realize pillar-like structures (200 μm high and 25 μm in diameter for a total area of 2 cm^2). In this case, a binding capacity of 15 ng/cm^2 was reported for prepurified plasmid DNA. In both cases a syringe pump was used to move liquids through the extractor.

As a part of a complex and challenging project to develop an automated unit for DNA diagnostics, our laboratory has been involved in the design and realization of a unit for nucleic acid extraction and fragmentation in a miniaturized system. More precisely, the goal was the development of a simple, low cost microdevice able to extract nucleic acids from 10-100 μL of complex matrix, such as blood, saliva and smear. The extract must be representative of the nucleic acid species present in the original sample, and contain good-quality nucleic acids with the lengths on the order of a few kbp. This chapter describes the ongoing development of a device for nucleic acid extraction based on the Boom method protocol. Two different types of devices have been developed for this purpose: long, open glass channels and a silica bead-packed bed. The results obtained in the former approach were less promising than the latter, due to the low extraction recovery exhibited by the open structures. Though the packed bed approach is quite similar to the one published by Wolfe et al. [31], there are some important differences. First of all, our packed bed is realized in a plastic device,

with the aim of producing disposable and low cost systems. Moreover, the device should also concentrate the extracted nucleic acids in a volume of just 1 or 2 µL, providing a sample which could be easily implemented in a downstream application (i.e. PCR, NASBA) for totally integrated DNA analysis. For the enrichment process, the idea is to electrokinetically collect the negatively charged, eluting nucleic acids at electrodes integrated into the same device. Electrodes have already been employed for DNA concentration [39-42]. Khandurina et al. [39] and Lin et al. [40] used integrated electrodes to concentrate DNA at an intersection of microchannels. The enriched sample plug was then injected into the separation channel for CGE analysis. DNA oligomers have been used in a microelectronic array by Stelzle et al. [41] and Heller et al. [42] to concentrate samples and thus promote oligonucleotide hybridization. In these cases, the accumulation of labeled DNA molecules was visualized by using a fluorescent imaging system. Moreover, integrated electrodes have been used for bioparticle and macromolecule separation and preconcentration by Huang et al. [43]. These papers suggest that electrodes can be used for reversible biomolecule accumulation. Electrodes have been also integrated in glass [44-48], in PDMS [49] and in PMMA [50, 51] devices for electrochemical or conductivity detection.

5.2 Experimental section

5.2.1 Glass devices

Glass structures for nucleic acid extraction were fabricated using standard technology available at IMT in 100-mm-diameter, 525-µm-thick wafers (Pyrex 7740, Bullen Ultrasonic, Inc.). The fabrication description is presented in Chapter 1, Figure 1-3. Transparency masks were used in this project. Three different layouts were realized: 1-, 0.5- and 0.13-m long, U-shaped microchannels. These

channels are 50 μm deep, 130 μm wide at the top and 50 μm wide at the bottom. This means a surface area of 3, 1.5 and 0.4 cm^2, and a channel volume of 5.5, 1.5 and 0.4 μL for the different decreasing channel lengths, respectively. The layout of the longest chip is presented in Figure 5-1 and a photo of parallel section of this U-shaped channel is presented in Figure 5-2. Four layouts were fabricated on a single Pyrex wafer and separated by dicing after fusion bonding. Each chip is 44 × 32 mm in size. These chips were positioned in a PMMA chip holder and connected by means of ferrules and fittings (Upchurch, Oak Harbor, WA) to the peristaltic pump.

Other open glass channels, kindly provided by R. M. Guijt (TU, Delft, The Netherlands), were also tested for extraction. These channels were fabricated by powder blasting. With this technique, channel etching is achieved by directing a strong stream of micron-sized Al_2O_3 particles (9 μm in this case) at the surface of the substrate through an open mask [45]. As a consequence of this process, channel walls are very rough, with the roughness visible through the microscope and probably in the order of μm (Figure 5-3). As a comparison, the surface roughness of isotropically etched glass channels was measured with the atomic force microscope (AFM) to be about 10 nm [52]. The channel layout of the structure in Figure 5-3 consisted of a single 6-cm-long, U-shaped channel, which was 85 μm wide at the top and 22 μm deep. These chips were 9 × 17 mm in size.

5.2.2 PDMS structures

PDMS structures for nucleic extraction were realized using a two-layer SU-8 master, whose fabrication is detailed in Chapter 2, Section 2.2.2. Two layouts were investigated: a channel with a single weir (Figure 5-4A), and a chamber with weirs at both ends, having an extra side channel for the packing (Figure 5-4B). The second layout is similar to the one reported in the literature and employed for solid-phase extraction in packed glass chambers [32]. For both

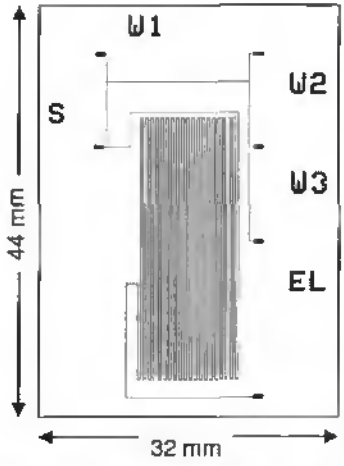

Figure 5-1 Layout of 1-m-long channel used for nucleic acid extraction. The channel is 50 μm deep, 130 μm wide at the top and 50 μm wide at the bottom for a surface area of 3 cm^2. The chip is 44 × 32 mm. Four chips were obtained from a single structured and bonded, 100-mm-diameter Pyrex wafer.

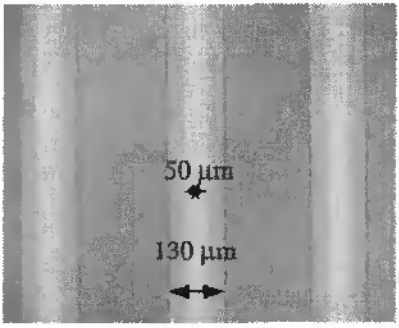

Figure 5-2 Close-up of U-shaped Pyrex channels realized by isotropic etching in 50% HF. The channels are 50 μm deep, and 130 μm and 50 μm wide at the top and bottom, respectively.

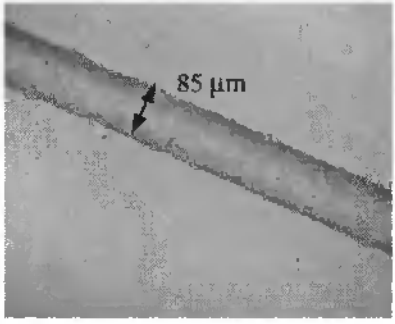

Figure 5-3 Powder-blasted channel realized in glass substrate using 9 μm beads (Micronit, Enschede, The Netherlands). The channel is 22 μm deep and 85 μm wide at the top.

layouts, the 160-μm-thick structures on the master will give rise to the 160-μm-deep PDMS channels or chambers that would be packed. These deep structures have at one end (for the channel), or at two ends (for the chamber), a weir with a 10-μm gap which serves to block the beads while allowing fluid flow. The channels are usually 12 mm long and 300-500 μm wide. The portion that would

be packed is about 4-6 mm long. The chamber is 400 by 400 μm in size, and the lateral channel is 70 μm wide, 3 mm long and also 160 μm deep. At the ends of each channel, reservoirs 1.2 mm in diameter are punched through the PDMS. The structured PDMS slab and a flat PDMS wafer are cleaned with isopropanol and dried with nitrogen. They are then exposed to an oxygen plasma treatment for 0.8 min, before bringing the two PDMS pieces into contact. The irreversible sealing that results is important to prevent PDMS lifting at the channel ends when fluidic connections are inserted into the reservoirs. Without oxidation, in fact, leakage occurs at the reservoirs. The connections between chip and pump consist of PVC tubes (Semadeni SA, Ostermundigen, Switzerland), which fit perfectly into the reservoirs and can be connected directly to the pump tube. This makes the fluidic system very simple to realize, and at the same time tight enough to prevent solution leakage and allow the controlled introduction of 5-to-10 μL plugs.

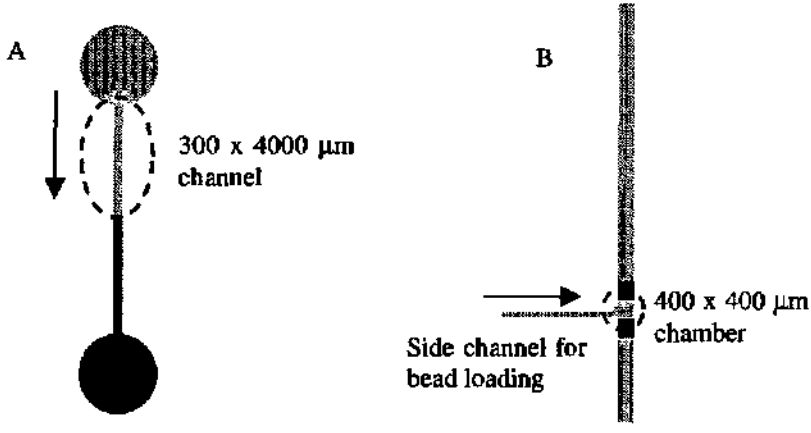

Figure 5-4 A) Channel and B) chamber layouts of PDMS structures used for nucleic acid extraction. The deep portions of the structures that will be packed are circled. The black areas represent the 10-μm-thin sections, which serve to block the beads while allowing fluid flow. The arrows indicate the direction followed by the beads to pack the deep channel or chamber.

5.2.3 PDMS structure packing

In a departure from the usual slurry-based methods, channels and chambers are packed simply by drawing in dry, 15-to-35 μm silica beads (Fluka Chemie, Buchs, Switzerland) using vacuum. A plastic tube is dipped in a vial containing dry silica particles. For the channel (single weir) layout, the bead-containing tube is then positioned in the reservoir at the deep channel end and vacuum is applied at the other reservoir, allowing the beads to fill the deep portion up to the weir. For the chamber layout, the beads are loaded from the lateral channel. The packing process is simple and takes only a few seconds. Images of a PDMS channel before and after packing are presented in Figure 5-5.

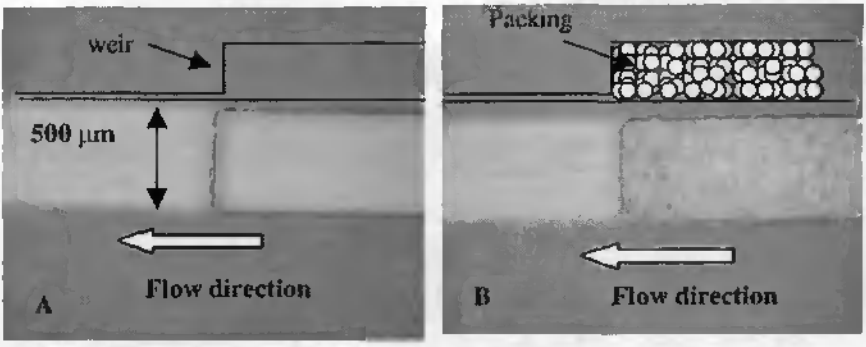

***Figure 5-5** Photo of a PDMS single-weir channel realized using the double-layer SU-8 master. A) Empty channel. B) Channel packed with 15-to-35 μm silica beads.*

5.2.4 Electrode fabrication

Platinum electrodes were integrated into a Pyrex wafer with the process described in Figure 5-6. Briefly, standard photolithography was used to pattern the electrode design in a positive photoresist layer, which was deposited by

spinning onto a clean glass wafer. After development and post-bake at 120°C for 3 min, the wafer was etched in buffered HF (BHF) for 3.5 min to get a 150-nm-deep sink where the electrodes are to be integrated. A 30-nm-thick tantalum adhesion layer was deposited on top of the wafer by evaporation, followed by a 120-nm-thick platinum layer. A lift-off process in acetone was performed to leave the surface of the metal electrodes level with the wafer surface. In this way no steps are present on the surface and a good seal with the structured PDMS slab is possible. The wafer with integrated electrodes was manually aligned with the PDMS channels used for the extraction. Figure 5-7 shows the electrodes integrated just below the packed channel. The electrodes were connected by means of conductive wires to a potentiostat, and a potential difference of 1-to-1.5 V was applied between them for nucleic acid concentration. This work is ongoing. The results presented in the following sections were realized using PDMS-PDMS devices without integrated electrodes.

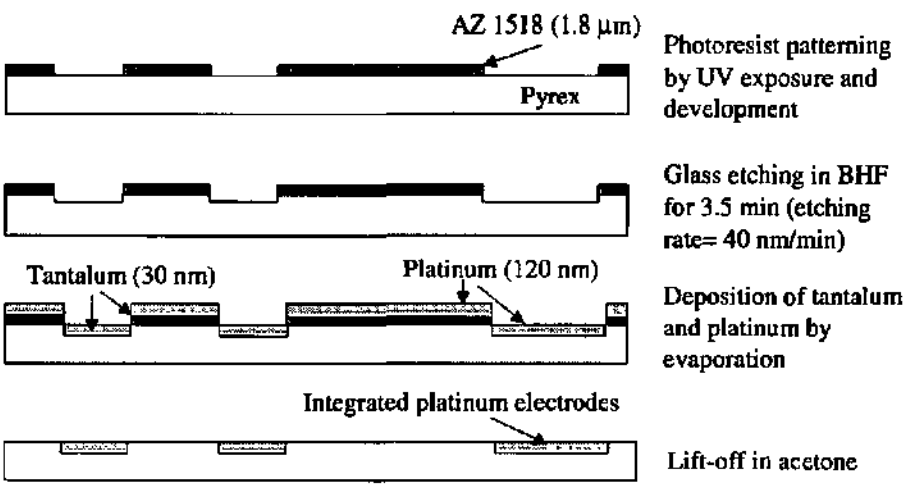

Figure 5-6 Fabrication process for platinum electrode integration into a glass wafer.

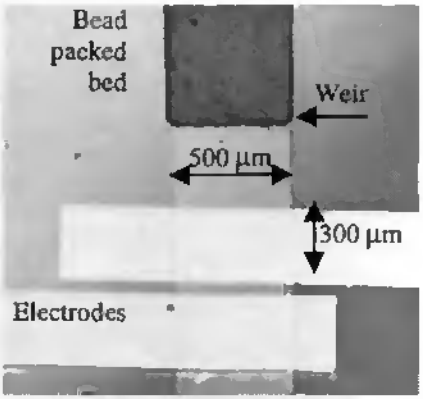

Figure 5-7 Platinum electrodes integrated in a glass wafer and aligned with a PDMS channel. Note the deep, packed portion of the channel just above the electrodes.

5.2.5 Pump

To drive solutions through the packed channel, a peristaltic pump (BVP Model, Isostac) was connected to the chip. To achieve low flow rates, we selected a 130-µm internal-diameter pump tube, which is the smallest tube size available. By measuring the time required to move a known volume of solution from one vial at one end of the tube to another vial at the other end, we calculated the flow rate (µL/min) corresponding to different turning rates of the pump. In the experiments, we worked usually with flow rates between 1 and 4 µL/min. The use of the peristaltic pump proved to be much easier and more practical than the syringe pump, for which syringes and quite sophisticated interconnections are required.

5.2.6 Sample preparation and loading

To investigate the efficiency of the extraction in the open glass channel as well in the packed PDMS channel, we used as sample a purified 48 kbp double-stranded λ DNA (Invitrogen AG, Basel, Switzerland). Lambda DNA is widely

used for research studies because it is well known and easily available. An aliquot of the initial 500 μg/mL λ DNA sample was diluted to 2 μg/mL in 8-10 M guanidine isothiocyanate (GuSCN) (Fluka, Buchs, Switzerland), which was prepared weekly in 100 mM Tris/HCl, pH 6.4. After vortexing, 20 μL of sample containing enough DNA to saturate the packed bed (40 ng) was pumped into the dry packed channel at a flow rate of 2 μL/min. Two biological samples provided by NorChip SA (Klokkarstua, Norway) were also tested in the miniaturized extraction unit. They consisted of human cell and Human Papilloma Virus (HPV) lysates in chaotropic lysis buffer. 50 μL of human cell lysate and 30 μL of HPV lysate were loaded into the packed chamber under the same experimental conditions reported for the test with λ DNA sample.

5.2.7 Extraction method

After sample loading, in order to wash the packing and remove salts and other components present in a complex matrix, 30 μL of 2-propanol followed by other 30 μL of ethanol were pumped into open channels or through packed beds at a flow rate of 4 μL/min. The extractor was then dried by flushing with air first and then placing the chip into an oven at 60°C for 5 min.

The elution buffer consisted of 10 mM Tris/HCl, 1 mM EDTA Na_2 (Fluka) pH 8. At this low salt concentration, the DNA bound at the surface of the sllica beads is released in the solution. Normally the elution solution contained 1 μM of the intercalating dye YOYO-1 (Molecular Probes) from a 10-μM stock solution in DMSO. This dye is essentially nonfluorescent in the absence of nucleic acids and exhibits significant fluorescence enhancement upon intercalation with DNA (λ_{ex}= 491 nm and λ_{em}= 509 nm). Therefore, if nucleic acids are present in the eluate, the dye becomes fluorescent, with the fluorescent signal proportional to the DNA concentration. To better understand the elution kinetics and define the smallest volume required to recover all the DNA, 5-μL

elution plugs were loaded onto the packing, collected in separated vials and analyzed as described in the following section.

5.2.8 Detection method

To quantify the fluorescence, a fluorometer is usually used [24, 31]. Because no fluorometer was available for the analysis of samples of a few microliters, we adopted a different approach based on the use of a fluorescent microscope and a pixel-intensity analysis program called Lispix. The microscope (Axiovert S 100; Carl Zeiss, Zurich, Switzerland) was equipped with a mercury lamp, filters and dichroic mirrors for fluorescein excitation, and a CCD camera (Kappa, Gleichen, Germany) and software developed by Kappa for signal analysis. A droplet (3 μL) of sample was dispensed onto a microscope slide. After focusing the objective on the droplet, images were taken quickly at the centre of the droplet and stored. The emission was then quantified using Lispix. This was done for samples from each of the collecting vials. Calibration curves like the one in Figure 5-8 could be obtained in the same way, using solutions with known

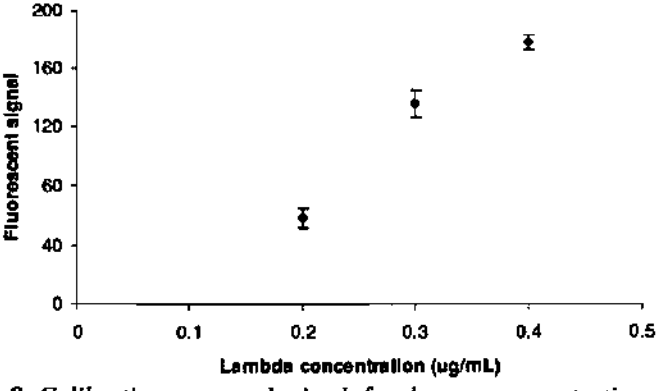

Figure 5-8 Calibration curve obtained for known concentration of λ DNA labelled with YOYO-1.

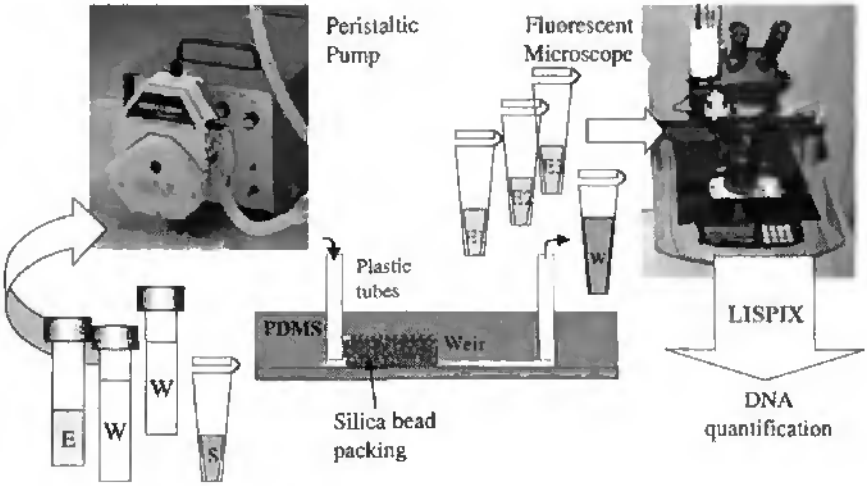

Figure 5-9 *Schematic representation of the set-up employed for nucleic acid extraction in PDMS bead-packed channels. On the left side: S, W, E stand for sample, washing and elution solutions, respectively. In the centre: w stands for waste, while E1, E2 and E3 are the vials collecting the eluate.*

λ DNA concentrations. These curves can be used to interpret the data from the eluate. It should be noted that the fluorescence obtained for nucleic acid-free buffer containing YOYO served as reference. This background value was in fact used to correct the values obtained for the samples. The schematic presentation of the entire set-up used for extraction is presented in Figure 5-9.

5.3 Results and discussion

5.3.1 Extraction in open structures

The use of beads guarantees good binding capacities [31], but requires a packing step. Since microdevices can themselves be made in glass, the ideal solution would be to structure the chip substrate itself to increase the binding surface area, while keeping small chip dimensions. A very simple approach is to use the glass wall of a microchannel as binding surface. For this purpose, 1-, 0.5-, and 0.13-m-long, 50-μm-deep glass microchannels were fabricated. The extraction process described in the Experimental Section was applied to these open channels using purified λ DNA. 4 ng of the λ DNA was, for example, collected from the medium length channel (histogram in Figure 5-10). This recovery is much lower than the expected 60 ng, which is calculated by considering the 1.5 cm^2 surface area and assuming 40 ng/cm^2 as the binding capacity of glass [37].

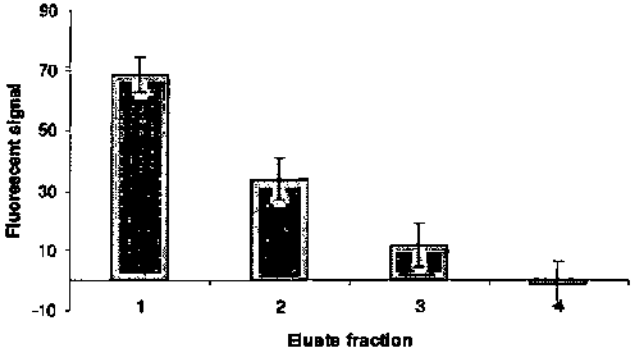

***Figure 5-10** Fluorescent signal from 10-μL elution fractions from a 0.5-m-long open glass channel.*

We tested also open channels fabricated by powder blasting. The channels in this case were 6 cm long, 85 µm wide at the top and 22 µm deep. Their surface was very rough as a consequence of the fabrication process. While this roughness could compromise CE separations, it should improve extraction efficiency by providing an increased binding surface. About 0.5 ng of λ DNA were recovered, again a value lower than the expected 4.8 ng, calculated as before considering 0.12 cm^2 as binding surface and neglecting increased surface area due to surface roughness.

The poor results achieved working with open structures are due to the large dimensions of the channels and the low diffusion coefficient of the DNA ($D= 0.5 \times 10^{-8}$ cm^2s^{-1}) [53], which reduces the probability that the DNA reaches the surface while resident in the microchannel. The time, *t*, necessary for the DNA to diffuse from the center of the channel to the channel walls can be calculated by the following formula:

$$t= \frac{d^2}{2D} \qquad (1)$$

where *d* is the channel radius (we assume that the channel fabricated at IMT has a circular cross-section with a radius of 25 µm) and D the diffusion coefficient mentioned above. The resulting diffusion time is about 10 min. The flow velocity, *v*, can be calculated using the following formula:

$$v= \frac{Q}{A} \qquad (2)$$

where *Q* is the flow rate (µL/min) and *A* the area of the channel cross-section. For a flow rate of 2 µL/min (0.03 mm^3/s), typically used to pump the sample through the device, a flow velocity of 8.3 mm/s was calculated. This means that the

resident time of the sample in the 1-m-long channel at this flow rate was only 2 min. Therefore, the probability that the DNA diffuses and binds to the channel surface is reduced.

Since decreasing channel size would imply higher fluidic resistance, open channels with larger cross-sections become interesting if they are structured in such a way as to have a high surface-to-volume ratio. For this purpose, as mentioned before, pillar-like structures were realized in silicon [36] and in photosensitive glass [38] and effectively used for nucleic acid extraction in microdevices. Although the fabrication process of high surface-to-volume structures could be critical and more time consuming than the preparation of a packed bed, these open devices can be used several times because the surface can be easily regenerated. A good inter- and intra-column reproducibility is also guaranteed.

5.3.2 Extraction in PDMS packed channels

After the poor DNA recovery achieved in open structures, we decided to work with bead-packed channels, an approach which is very similar to the one recently published by Wolfe et al. [31]. However, our packed beds were realized in PDMS and not in glass devices, making the fabrication process easier (replica-based) and practical (no clean environment required). A very simple and rapid method of packing was developed, as described in the Experimental Section. Moreover, a simple system of fluidic tubes, which do not require fittings and ferrules, was adopted to connect the PDMS chips and the peristaltic pump. The channel layout (Figure 5-4A) was preferred to the chamber layout (Figure 5-4B), because of solution leakage in the lateral channel in the latter case during the extraction process through the chamber. Therefore, the results reported below are for extractions performed in channel structures.

Sample, wash and elution solutions were pumped through the packed bed as described in the Experimental Section. The extraction performed in an open PDMS channel (without bead packing) does not result in a measurable amount of eluted nucleic acid, suggesting that these molecules are not absorbed appreciably on bare PDMS surfaces. For the extraction performed through the packed bed, some fluorescent signal was measured in the eluate fractions. Using the calibration curve, it was estimated that from 1 to 3 ng of λ DNA could be extracted in our packed device as a function of the packed channel dimensions and quality. As reported in [31], the reproducibility of the extraction in a packed bed is low, and the lifetime is usually reduced because of increased backpressure with use. The same bed can be used 3-4 times with the λ-phage sample, but only once with the biological lysate. However, the chip-to-chip reproducibility for the first extraction, expressed in term of binding capacity, is quite good, at about 12,5% (Table 5-1).

Figure 5-11A shows the fluorescent signal resulting from eluate fractions collected for a λ DNA sample extraction experiment (chip 1). It appears that most of the DNA is eluted in the first 10 uL of buffer. Considering this volume, around 2.7 ng of DNA were extracted from the device packed with 0.3 mg beads. Therefore, we could estimate a binding capacity of about 9 ng/mg of beads. Only in a few cases, the binding capacity was 20-24 ng/mg, in agreement with the values reported by Tian et al. [24]. These last data were achieved in structures replicated from a different master, but with similar structure layouts.

The fluorescent signal for a series of 5-μL eluate fractions from an HPV lysate sample is shown in the histogram of Figure 5-11B. Using this sample, around 2.5 ng of nucleic acids were extracted, with a recovery efficiency similar to the one achieved for the prepurified sample in a similar packed bed. Efficiency lower than the usual binding capacity of the system was found for human cell lysate sample. In this case, only 1.5 ng of nucleic acid were recovered. This may be explained by competition of the complex matrix with the nucleic acid for

Table 5-1 *Binding capacity for 5 different PDMS chips packed with 15-35 μm silica beads (about 0.4 mg). The binding capacity was determined for the first extraction performed in each chip using as sample the prepurified λ DNA (40 ng). The average binding capacity of these packed chips was of 9.6 ± 1.2 ng/mg beads.*

	Binding capacity (ng DNA/mg beads)
Chip 1	9
Chip 2	10
Chip 3	8
Chip 4	10
Chip 5	11,25

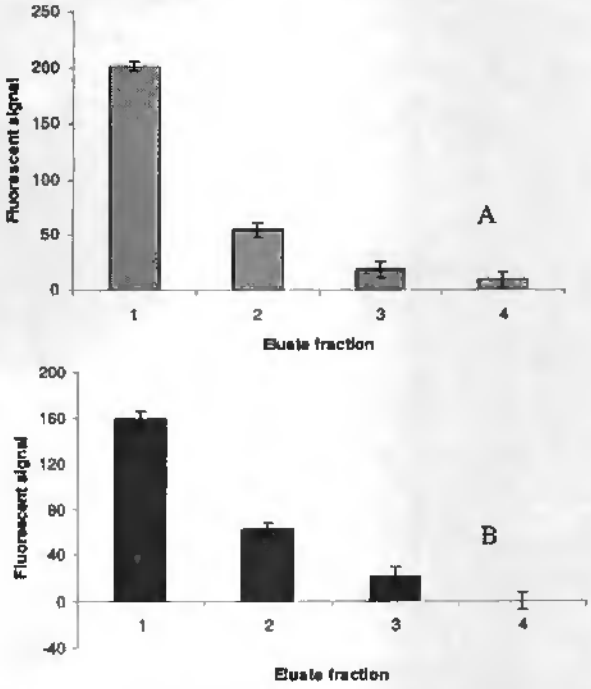

Figure 5-11 *Fluorescent signal of 5-μL elution fractions from a silica-bead packed PDMS channel. A) λ DNA sample. B) HPV lysate sample.*

binding on the surface [24]. However, it should be noted that the amount of nucleic acids in the biological sample was unknown. Unfortunately, we could not determine this beforehand.

The extraction process is itself an enrichment step, since the nucleic acids in the initial volume of 20, 30 or 50 µL can be extracted and eluted in only 10 µL of buffer. However, since our downstream application requires a volume of 1-to-2 µL of purified sample, the sample volume should be reduced. Two approaches can be taken to address this issue:

i. The collected NA could be divided into a few aliquots, which are supposed to be representative of the initial sample. This approach would not be effective if the target sequence is present in the sample at low concentration, as it could be for viral sequences.

ii. The purified NA could be concentrated into a small volume. In this case, a further on-chip enrichment step is required. Electrokinetic enrichment using integrated electrodes, whose fabrication was described above, is under investigation for this purpose.

5.4 Conclusions and outlook

From the preliminary results obtained, we can conclude that nucleic acid extraction can be performed in open glass channels and in bead-packed microbeds. In both cases, the extraction takes less that 40 min and uses a very simple pressure-driven fluidic system. The bead-based approach is preferable to the open structure because of the low binding capacity of the open channel chip. This is due to the low diffusion coefficient of nucleic acids and the large dimensions of the channel, the latter being dictated by hydrodynamic considerations. (The theory about hydrodynamic pumping is reported in Chapter 1, Section 1.4). Moreover, other factors have to be considered when the device is conceived as low-cost and disposable. Glass chip fabrication is not suited for

mass production, since it is time consuming, expensive and requires clean facilities. Moreover, fewer devices can be obtained from a single Pyrex wafer (4 in this case) if compared to the packed beds integrated on a plastic slab (> 10). In contrast with glass micromachining techniques, replica molding allows rapid prototyping and the fabrication of devices in a normal chemical lab. The elasticity of PDMS and the fact that PDMS devices can be easily bonded by oxygen plasma treatment were useful for the easy realization of a pressure-tight system. The same two-level structures could be replicated in plastics other than PDMS, which are suited for mass production technologies (i.e. injection molding). Since plastics are usually more rigid than PDMS, different connections and fittings as well as new bonding methods would be necessary.

The packing technique introduced, which uses dry beads and vacuum, is an easy, efficient and rapid way to prepare an extraction bed in a microdevice. A piece of 903 cellulose paper was integrated for the same application in a different study [35]. Bead or cellulose beds are thus preferable to silicon or glass micromachined beds [36, 38] for the fabrication of an extraction chamber in a low-cost, disposable device.

Promising results have been achieved using the packed bed and complex samples (e.g. cell lysates). However, some work is still needed. It is planned to evaluate soon the quality of the nucleic acids extracted in the packed bed. This test is conventionally performed using amplification methods, such as PCR [24, 36, 38]. At the same time, nucleic-acid enrichment will be investigated. This step is quite challenging, since nucleic acid collection at the electrodes should be carried out in a flowing system, during the elution step. The use of electrodes to concentrate nucleic acids has been reported for static systems [41, 42]. A different approach for nucleic acid concentration could involve the use of electroosmotic pumping in the elution step and the concentration of the eluting species at the anode, as reported for sample enrichment prior to CGE analysis [39, 40].

The other challenge for this project is the combination of the extraction-enrichment unit with on-chip sample lysis and amplification modules. The project is focused on a very particular application, namely the detection of Human Papilloma Virus (HPV) in cervical smears. The idea is to detect the viral infection using the nucleic acid sequence-based amplification (NASBA) process and primers specific for viral mRNA. To provide purified nucleic acids to the amplification unit, the epithelial cells of the smears have to be concentrated (e.g. by filtration) and lysed (e.g. by mixing with a lysis buffer). The nucleic acids obtained from the cells must be purified and concentrated for the amplification reaction. To accomplish these multiple assays on a single device, the integration of some valving functions is required to control liquid flow [35, 54]. The realization of a monolithic device that carries out a series of molecular processes starting from a crude sample is therefore not trivial, though devices with this capability exist for certain applications [35, 54]. The accumulation of the amplification products, which is usually followed by fluorescence detection and signal analysis, confirms the presence of the virus. Since some strains of HPV have been identified as the main cause of neoplastic changes in the cervix, this kind of screening test represents an important tool for the identification of women at risk for cervical cancer. The development of such a test on a microfluidic, low-cost, disposable and easy-to-use device could have a strong impact in those underdeveloped countries where conventional screening methods are not readily available to the population and mortality due to cervical cancer is high as a result. A more detailed discussion of this application is included in Chapter 7.

Acknowledgements

NorChip AS, Klokkarstua, Norway is acknowledged for both financial and scientific supports.

REFERENCES

[1] Y. Baba, "Development of novel biomedicine based on genome science," *European Journal of Pharmaceutical Science 2001*, vol. 13, pp. 3-4, 2001.

[2] C. S. Effenhauser, A. Paulus, A. Manz, and H. M. Widmer, "High-speed separation of antisense oligonucleotides on a micromachined capillary electrophoresis device," *Anal. Chem.*, vol. 66, pp. 2949-2953, 1994.

[3] S. C. Jacobson and J. M. Ramsey, "Integrated microdevice for DNA restriction fragment analysis," *Anal. Chem.*, vol. 68, pp. 720-723, 1996.

[4] D. J. Ehrlich and P. Matsudaira, "Microfluidic devices for DNA analysis," *Trends in Biotechnology*, vol. 17, pp. 315-19, 1999.

[5] H. Tian, A. Jaquins-Gerstl, N. Munro, M. Trucco, L. C. Brody, and J. P. Landers, "Single-strand conformation polymorphism analysis by capillary and microchip electrophoresis: a fast, simple method for detection of common mutations in BRCA1 and BRCA2," *Genomics*, vol. 63, pp. 25-34, 2000.

[6] A. T. Woolley and R. A. Mathies, "Ultra-high-speed DNA fragment separations using microfabricated capillary array electrophoresis chips," *Proc. Nat. Acad. Sci. USA*, vol. 91, pp. 11348-11352, 1994.

[7] P. C. Simpson, D. Roach, A. T. Woolley, T. Thorsen, R. Johnston, G. F. Sensabaugh, and R. A. Mathies, "High-throughput genetic analysis using microfabricated 96-sample capillary array electrophoresis microplates," *Proc. Nat. Acad. Sci. USA*, vol. 95, pp. 2256-2261, 1998.

[8] Y. N. Shi, P. C. Simpson, J. R. Scherer, D. Wexler, C. Skibola, M. T. Smith, and R. A. Mathies, "Radial capillary array electrophoresis microplate and scanner for high-performance nucleic acid analysis," *Anal. Chem.*, vol. 71, pp. 5354-5361, 1999.

[9] D. Schmalzing, L. Koutny, D. Salas-Solano, A. Adourian, P. Matsudaira, and D. Ehrlich, "Recent developments in DNA sequencing by capillary and microdevice electrophoresis," *Electrophoresis*, vol. 20, pp. 3066-77, 1999.

[10] S. Liu, H. Ren, Q. Gao, D. J. Roach, R. T. J. Loder, T. M. Armstrong, Q. Mao, I. Blaga, D. L. Barker, and S. B. Jovanovich, "Automated parallel DNA sequencing on multiple channel microchips," *Proc. Nat. Acad. Sci. USA*, vol. 97, pp. 5369-5374, 2000.

[11] B. M. Paegel, C. A. Emrich, G. J. Wedemayer, J. R. Scherer, and R. A. Mathies, "High throughput DNA sequencing with a microfabricated 96-lane capillary array electrophoresis bioprocessor.," *Proc. Nat. Acad. Sci. USA*, vol. 99, pp. 574-579, 2002.

[12] L. Koutny, D. Schmalzing, O. Salas-Solano, S. El-Difrawy, A. Adourian, S. Buonocore, K. Abbey, P. McEwan, P. Matsudaira, and D. Ehrlich, "Eight hundred base sequencing in a microfabricated electrophoretic device," *Anal. Chem.*, vol. 72, pp. 3388-3391, 2000.

[13] O. Salas-Solano, D. Schmalzing, L. Koutny, S. Buonocore, A. Adourian, P. Matsudaira, and D. Ehrlich, "Optimization of high-performance DNA sequencing on short microfabricated electrophoretic devices," *Anal. Chem.*, vol. 72, pp. 3129-3137, 2000.

[14] E. T. Lagally, I. Medintz, and R. A. Mathies, "Single-molecule DNA amplification and analysis in an integrated microfluidic device," *Anal. Chem.*, vol. 73, pp. 565-570, 2001.

[15] B. C. Giordano, J. Ferrance, S. Swedberg, A. F. Hühmer, and J. P. Landers, "Polymerase chain reaction in polymeric microchips: DNA amplification in less than 240 seconds," *Anal. Biochem.*, vol. 291, pp. 124-132, 2001.

[16] E. Verpoorte, "Microfluidic chips for clinical and forensic analysis," *Electrophoresis*, vol. 23, pp. 677-712, 2002.

[17] L. C. Waters, S. C. Jacobson, N. Kroutchinina, J. Khandurina, R. S. Foote, and J. M. Ramsey, "Microchip device for cell lysis, multiplex PCR amplification, and electrophoretic sizing," *Anal. Chem.*, vol. 70, pp. 158-162, 1998.

[18] G. Ocvirk, H. Salimi-Moosavi, R. J. Szarka, E. Arriaga, P. E. Andersson, R. Smith, N. J. Dovichi, and D. J. Harrison, "Single cell enzymatic analysis on a microchip: lysing of single cells and identification of their β-galactosidase activity", Proceedings of uTAS '98, Micro Total Analysis Systems '98, Banff, Canada, 1998, 203-206.

[19] A. Eckersten, A. E. Örlefors, C. Ellström, K. Erickson, E. Löfman, A. Eriksson, S. Eriksson, A. Jorsback, N. Tooke, H. Derand, G. Ekstrand, J. Engström, A.-K. Honerud, A. Aksberg, H. Hedsten, L. Rosengren, M. Stjernström, T. Hultmao, and P. Andersson, "High-throughput SNP scoring in a disposable microfabricated CD device", Proceedings of Micro Total Analysis Systems 2000, Enschede, The Netherlands, 2000, 521-524.

[20] E. A. Schilling, A. E. Kamholz, and P. Yager, "Cell lysis and protein extraction in microfluidic device with detection by a fluorogenic enzyme assay," *Anal. Chem.*, vol. 74, pp. 1798-1804, 2002.

[21] H. Lu, R. J. Jackman, S. Gaudet, M. Cardone, M. A. Schmidt, and K. F. Jensen, "Microfluidic devices for cell lysis and isolation of organelles", Proceedings of Micro Total Analysis Systems 2001, Monterey, CA, USA, 2001, 297-298.

[22] R. Boom, C. J. A. Sol, M. M. M. Salimans, C. L. Jansen, P. M. E. Wertheim-van Dillen, and J. van der Noordaa, "Rapid and simple method for purification of nucleic acids," *J. Clin. Microbiol.*, vol. 28, pp. 495-503, 1990.

[23] K. A. Melzak, C. S. Sherwood, R. F. B. Turner, and C. A. Haynes, "Driving forces for DNA adsorption to silica in perchlorate solutions," *J. Colloid Interface Sci.*, vol. 181, pp. 635-644, 1996.

[24] H. Tian, A. F. R. Hühmer, and J. P. Landers, "Evaluation of silica resins for direct and efficient extraction of DNA from complex biological matrices in a miniaturized format," *Anal. Biochem.*, vol. 283, pp. 175-191, 2000.

[25] D. C. Duffy, H. L. Gillis, J. Lin, N. F. Sheppard, Jr., and G. J. Kellogg, "Microfabricated centrifugal microfluidic systems: Characterization and multiple enzymatic assays," *Anal. Chem.*, vol. 71, pp. 4669-4678, 1999.

[26] N. Thomas, A. Ocklind, I. Blikstad, S. Griffiths, M. Kenrick, H. Derand, G. Ekstrand, C. Ellström, A. Larsson, and P. Andersson, "Integrated cell based assays in microfabricated disposable CD devices", Proceedings of Micro Total Analysis Systems 2000, Enschede, The Netherlands, 2000, 249-252.

[27] G. Ekstrand, C. Holmquist, A. E. Örlefors, B. Hellman, A. Larsson, and P. Andersson, "Microfluidics in a rotating CD", Proceedings of Micro Total Analysis Systems 2000, Enschede, The Netherlands, 2000, 311-314.

[28] A. Palm, S. R. Wallenborg, M. Gustafsson, A. Hedström, E. Togan-Tekin, and P. Andersson, "Integrated sample preparation and MALDI MS on a disc", Proceedings of Micro Total Analyis Systems 2001, Monterey, CA, USA, 2001, 216-118.

[29] G. Jesson and P. Andersson, "Multiple separations at nanoliter scale using gradient elution", Proceedings of Micro Total Analysis Systems 2001, Monterey, CA, USA, 2001, 551-552.

[30] W. R. Boom, H. M. A. Adriaanse, T. Kievits, and P. F. Lens, "Process for isolating nucleic acid." European Patent Office, EP 0.389 063 A2: Akzo Nobel N.V., 1990.

[31] K. A. Wolfe, M. C. Breadmore, J. P. Ferrance, M. E. Power, J. F. Conroy, P. M. Norris, and J. P. Landers, "Toward a microchip-based solid-phase extraction method for isolation of nucleic acids," *Electrophoresis*, vol. 23, pp. 727-733, 2002.

[32] R. D. Oleschuk, L. L. Shultz-Lockyear, Y. Ning, and D. J. Harrison, "Trapping of bead-based reagents within microfluidic systems: on-chip solid-phase extraction and electrochromatography," *Anal. Chem.*, vol. 72, pp. 585-590, 2000.

[33] Z. H. Fan, S. Mangru, R. Granzow, P. Heaney, W. Ho, Q. Dong, and R. Kumar, "Dynamic DNA hybridization on a chip using paramagnetic beads," *Anal. Chem.*, vol. 71, pp. 4851-4859, 1999.

[34] G. Jiang and D. J. Harrison, "mRNA isolation in a microfluidic device for eventual integration of cDNA library construction," *Analyst*, vol. 125, pp. 2176-2179, 2000.

[35] R. C. Anderson, X. Su, G. J. Bogdan, and J. Fenton, "A miniature integrated device for automated multistep genetic assays," *Nucleic Acids Res.*, vol. 28, pp. e60, 2000.

[36] L. A. Christel, K. Petersen, W. McMillan, and M. A. Northrup, "Rapid, automated nucleic acid probe assays using silicon microstructures for nucleic acid concentration," *Journal of Biomechanical Engineering-Transactions of the ASME*, vol. 121, pp. 22-27, 1999.

[37] B. Vogelstein and D. Gillespie, "Preparation of analytical purification of DNA from agarose," *Biochemistry*, vol. 76, pp. 615-619, 1978.

[38] J. H. Kim, B. G. Kim, H. Nam, D. E. Park, K. S. Yun, J. B. Yoon, J. You, and E. Yoon, "A disposible DNA sample preparation microfluidic chip for nucleic acid probe assay", Proceedings of 15th Annual IEEE International MEMS 2002, Las Vegas, Neveda, 2002, 133-136.

[39] J. Khandurina, S. C. Jacobson, L. C. Waters, R. S. Foote, and J. M. Ramsey, "Microfabricated porous membrane structure for sample concentration and electrophoretic analysis," *Anal. Chem.*, vol. 71, pp. 1815-1819, 1999.

[40] Y.-C. Lin, H.-C. Ho, C.-K. Tseng, and S.-Q. Hou, "A poly-methylmethacrylate electrophoresis microchip with sample preconcentrator," *J. Micromech. Microeng.*, vol. 11, pp. 189-194, 2001.

[41] M. Stelzle, M. Dürr, M. Cieplik, and W. Nisch, "On-chip electrophoretic accumulation of DNA oligomers and streptavidin," *Fresenius Journal of Anal. Chem.*, vol. 371, pp. 112-119, 2001.

[42] M. J. Heller, A. H. Forster, and E. Tu, "Active microelectronic chip devices which utilize controlled electrophoretic fields for multiplex DNA hybridization and other genomic applications," *Electrophoresis*, vol. 21, pp. 157-164, 2000.

[43] Y. Huang, K. L. Ewalt, M. Tirado, R. Haigis, A. H. Forster, D. Ackley, M. J. Heller, J. P. O'Connell, and M. Krihak, "Electric manipulation of bioparticles and macromolecules on microfabriated electrodes," *Anal. Chem.*, vol. 73, pp. 1549-1559, 2001.

[44] A. T. Woolley, K. Lao, A. N. Glazer, and R. A. Mathies, "Capillary electrophoresis chips with integrated electrochemical detection," *Anal. Chem.*, vol. 70, pp. 684-688, 1998.

[45] S. Schlautmann, H. Wensink, R. B. M. Schasfoort, M. Elwenspoek, and A. van der Berg, "Powder-blasting technology as an alternative tool for microfabrication of capillary electrophoresis chips with integrated conductivity sensors," *J. Micromech. Microeng.*, vol. 11, pp. 386-389, 2001.

[46] R. M. Guijt, E. Baltussen, G. van der Steen, J. Frank, H. A. H. Billiet, T. Schalkhammer, F. Laugere, M. J. Vellekoop, A. Berthold, P. M. Sarro, and G. W. K. van Dedem, "Capillary electrophoresis with on-chip four-electrode capacitively coupled conductivity detection for application in bioanalysis," *Electrophoresis*, vol. 22, pp. 2537-2541, 2001.

[47] J. Lichtenberg, N. F. de Rooij, and E. Verpoorte, "A microchip electrophoresis system with integrated in-plane electrodes for contactless conductivity detection," *Electrophoresis*, vol. 23, in press, 2002.

[48] R. P. Baldwin, T. J. Roussel, M. M. Crain, V. Bathlagunda, D. J. Jackson, J. Gullapalli, J. A. Conklin, R. Pai, J. F. Naber, K. M. Walsh, and R. S. Keyton, "Fully integrated on-chip

electrochemical detection for capillary electrophoresis in a microfabricated device," *Anal. Chem.*, vol. 74, pp. 3690-3697, 2002.

[49] A. J. Gawron, R. S. Martin, and S. M. Lunte, "Fabrication and evaluation of a carbon-based dual-electrode detector for poly(dimethylsiloxane) electrophoresis chips," *Electrophoresis*, vol. 22, pp. 242-248, 2001.

[50] B. Graβ, A. Neyer, M. Jöhnck, D. Siepe, F. Eisenbeiβ, G. Weber, and R. Hergenröder, "A new PMMA microchip device for isotachophoresis with integrated conductivity detector," *Sensors and Actuators B*, vol. 72, pp. 249-258, 2001.

[51] J. Wang, M. Pumera, M. P. Chatrathi, A. Escarpa, R. Konrad, A. Griebel, W. Dörner, and H. Löwe, "Towards disposable lab-on-a-chip: poly(methylmethacrylate) microchip electrophoresis device with electrochemical detection," *Electrophoresis*, vol. 23, pp. 596-601, 2002.

[52] B. H. Weiller, L. Ceriotti, T. Shibata, D. Rein, M. A. Roberts, J. Lichtenberg, J. B. German, N. F. de Rooij, and E. Verpoorte, "Analysis of lipoproteins by capillary zone electrophoresis in microfluidic devices: assay development and surface roughness measurements," *Anal. Chem.*, vol. 74, pp. 1702-1711, 2002.

[53] D. E. Smith, T. T. Perkins, and S. Chu, "Self-diffusion of an entangled DNA molecule by reptation," *The American Physical Society*, vol. 75, pp. 4146-4149, 1995.

[54] Y. Liu, C. B. Rauch, R. L. Stevens, L. R., J. Yang, D. B. Rhine, and P. Grodzinski, "DNA amplification and hybridization assay in integrated plastic monolithic devices," *Anal. Chem.*, vol. 74, pp. 3063-3070, 2002.

6 On-chip absorbance detection

6.1 Introduction

On-chip detection has relied predominantly on fluorescence, due to its high sensitivity. With the LIF detection system available in our lab (described in Chapter 1, Section 1.5), concentrations down to 20 nM fluorescein isothiocyanate (SNR= 3) can be detected [1]. The integrated microfluidic/microoptic device developed by Roulet et al. could reach a limit of detection (LOD) of 3.3 nM for a Cy5 solution in phosphate buffer (pH 7.4) [2]. This result is comparable with the LOD of 1.5 nM for Cy5, which was reached using a confocal epifluorescence microscope [3]. In an optimised confocal epifluorescence scheme, a peak of 1 pM fluorescein injected electrophoretically in microchannels was detected with a mean SNR of 5.8 [4]. Unfortunately, only a few compounds are intrinsically fluorescent and can be detected directly in the systems mentioned above. For non-fluorescent compounds, a reaction to associate them with fluorescent molecules is required. Fluorescent labelling can be easily achieved by using intercalating dyes for DNA fragments, or fluorescently labelled primers in the case of PCR. Peptides and proteins are generally labelled by covalently bonding a fluorescent molecule to an amino or other reactive group. Although protein labelling is quite common, it suffers from multiple-site labelling, which compromises peak efficiency by producing a number of labelled variants of the same proteins, all having slightly different charge-to-mass ratios. Fluorescence detection is not applicable to hormones and other small, drug-like molecules, which have no

derivatizable groups. One solution is the use of indirect fluorescence detection (IDLIF), as reported by Wallenborg et al. [5]. This approach sees the addition of a fluorescent marker to the background electrolyte, so that non-fluorescent analytes are detected as negative peaks or signals. Indirect fluorescence detection was also used for chip-based CEC in this thesis work (Chapter 4).

Absorbance detection for separation-based μTAS is an attractive alternative, since it is applicable to a larger variety of species than fluorescence. However, the strong dependence of signal strength on optical pathlength makes absorbance detection in small volumes difficult, since pathlength, and hence sensitivity, is generally reduced. To improve it, a U-type, multireflection cell for absorbance detection has been fabricated in silicon [6]. Optical waveguides have also been integrated into a structured silicon wafer for in-plane UV absorbance measurements across a 120-μm-wide separation channel [7]. However, to fabricate planar CE absorbance cells, glass is a better choice than Si, due to its nonconductive properties [8]. An example of a U-cell in glass is given in Liang et al. [9]. These researchers made a cell with a 120-to-140 μm pathlength parallel to the flow, which allowed good detection limits in the range of 6 μM for hydrolyzed fluorescein isothiocyanate dye. Unfortunately, optical fiber integration into this glass device complicated its manufacture, since fiber alignment grooves had to be deepened after chip fabrication by flowing an HF solution through them. An optical cuvette was realized in the middle wafer of a 3-layer glass chip for visible detection in the direction of the flow by Daridon et al. [10]. In this work, the vertical cuvette connected the microchannels etched in the top and bottom wafers, and optical fibers were employed to bring and recover light from the optical cell. Detection carried out vertically through a chip, perpendicular to the flow, generally yields insufficient sensitivity. This is because commonly used wet-etching techniques are isotropic, so that the resulting channels are at least twice as wide as they are deep. Channels with depths approaching reasonable optical path lengths would have volumes too large for

optimum separation performance. Therefore, channel depths are restricted to between 10 and 25 μm or so. To enhance absorbance sensitivity in the visible range through these rounded glass channels, the effective optical pathlength can be increased by integrating metal mirrors above and below the channel [11]. In this way, the light is bounced back and forth through the cell several times. To allow UV detection through isotropically etched quartz channels, an optical slit was integrated at the bonding interface between two quartz glass substrates, in order to effectively cut off the stray light [12]. This slit was fabricated by sputtering a Si film on a quartz substrate and coating it with SiO_2 to allow the bonding with hydrofluoric acid. The detection of 1 mg/mL of uracil (10 μM) was possible in this system.

In addition to limited pathlength, there is another problem associated with the integration of UV absorbance into microdevices, related to chip substrate material. The transmission of most materials from which microfluidic systems are made decreases dramatically below 300-350 nm. This property makes spectroscopy in the visible range possible in glass and in plastic devices, but makes UV spectroscopy very difficult to impossible. Therefore, to integrate UV absorbance effectively into a microfluidic system, the device has to include quartz windows or other UV transparent materials. Nakanishi et al. therefore had to work with quartz for their UV detection system mentioned above, which entailed amongst other things the development of a special quartz-to-quartz bonding procedure which was accomplished at 60°C [12]. Quartz windows were integrated in microfluidic systems by Jackman et al. [13]. They proved the feasibility of performing on-line UV detection through a 60-μm-deep microchannel having SU-8 sidewalls and quartz windows at the top and bottom. Transverse UV detection through a 40-μm-deep diamond channel [14] and a 20-μm-deep quartz channel [15] has also been reported. For these experiments, a modified HPLC detector cartridge was used, precluding the need for optical fibers

and minimizing coupling losses. The detection slit of a capillary cartridge of a conventional CE system was also employed for UV detection in O-CEC microsystems [16]. In this work, a mixture of uncharged polycyclic aromatic hydrocarbons at concentrations of 10 mM each were separated and detected at 280 nm. The low sensitivity of the system can be ascribed primarily to the unusual use of Pyrex, a poor UV transmitter, as chip substrate for UV absorbance. Transverse UV detection was also used to investigate adsorption of proteins from serum samples in dry-etched quartz microchannels [17].

Since our goal was to keep detection volumes small and chip layouts simple for CE separations, we decided to perform absorbance vertically through narrow microchannels. Two different ways to fabricate transparent, rectangular structures were investigated. One approach consisted of the fabrication of 50-μm-deep, rectangular quartz channels using inductively coupled plasma (ICP)-reactive-ion etching (RIE) [18]. The results of this fabrication process were described and discussed in Chapter 2 of the present thesis. In the second approach, the devices were fabricated in PDMS using replica molding and high-aspect-ratio relief patterns, which were dry-etched in silicon. These structures were integrated in an optical system with prealigned optical fibers to allow UV absorbance detection of amino acid and peptide samples that had been electrokinetically injected into the separation channel. The use of optical fibers represents a practical choice for microfluidic-detection system coupling [10, 13]. It eliminates the need for a bench for optical components and makes the system portable and therefore more suitable for point-of-care testing. The results achieved with the latter approach were presented at μTAS 2001 Conference [19]. In this chapter, this work is further detailed and discussed.

6.2 Experimental section

6.2.1 PDMS absorbance properties

The good optical transparency of PDMS at low wavelengths (< 300 nm) was mentioned in Chapter 1 and 4. This makes it an attractive material for applications where absorbance detection is required or preferred to other detection methods. The spectrum in Figure 6-1 shows that the optical transmission of PDMS is more than 70% for a 0.5-mm-thick slab at $\lambda > 240$ nm. We also discussed in Chapter 2 and 4 the freedom of choice for PDMS channel profile, which is made possible by the different methods that can be used for master fabrication (e.g. DRIE, Epon SU-8 technology). Therefore, high-aspect-ratio PDMS channels, if realized in thin layers, make transverse UV detection through the channel (and perpendicular to the flow) possible.

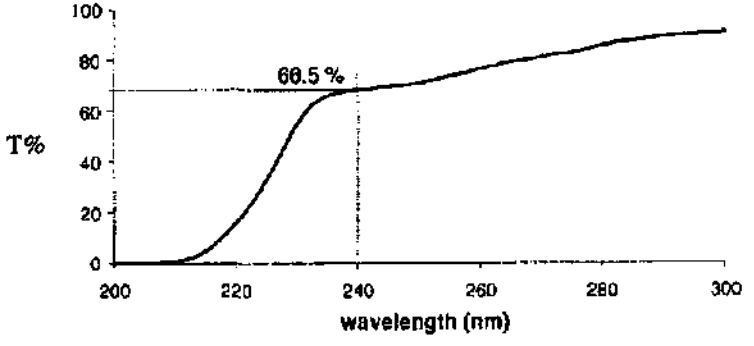

Figure 6-1 UV trasmission spectrum for a 0.5-mm-thick PDMS sample, measured with 2 nm resolution. (Spectrum courtesy of Stephanie Clément, Applied Optics Group (Prof. Dändliker), Institute of Microtechnology, University of Neuchâtel, Neuchâtel).

6.2.2 PDMS chip for absorbance detection

To test absorbance detection through PDMS channels, hybrid PDMS/quartz structures with a layout suitable for CE analysis were fabricated. The channel layout consisted of a 5-cm-long separation channel and 1-cm-long side channels. The structure contained a 200-μm-long double-T intersection, which was used to define sample plugs of about 500 pL for injection into the separation column as described earlier (Chapter 1, Section 1.3.3). Channels were 50 μm wide and 50 or 70 μm deep, depending on the master used.

The PDMS replica was made in a rectangular metallic mold (w × l × h= 5× 8 × 2 cm outer dimensions, 4 × 7 × 0.6 cm inner dimensions) (Figure 6-2A), at the base of which the silicon master (4 × 7 × 0.05 cm) was affixed using double-sided Scotch tape. The mold looks like a closed box, with two openings in one side through which the prepolymer is poured (Figure 6-2B and 6-2C). The mold frame consists of several steel pieces which are screwed together to contain the viscous pre-polymer solution, and which are unscrewed piece by piece after the polymerization to allow PDMS peeling from the master. The mold has a PMMA coverplate with a trapezoidal steel insert which is positioned with the small end directed towards the master. The surface of the small end is covered with a piece of silicon wafer sawed to the right dimensions (3 × 1 cm). This Si piece ensures that the thin PDMS film formed between it and the master is flat and smooth, and therefore suitable as a window for the optical detection. Thus, the polymerization in this mold allows the replication of microchannels in a 6-mm-thick elastomer slab and, at the same time, the formation of a thin window of PDMS (about 0.5 mm thick) towards the end of the separation channel. The prepolymer-curing agent mixture is poured gently through the two side openings while the mold is held vertically, using a glass pipette to guide the viscous solution into the mold (Figure 6-2B). Once filled, the mold is put into the oven at 65°C for 4 hours still

vertically positioned to allow the polymerization to take place. After the polymerization, the metallic parts are unscrewed, the PDMS is peeled from the

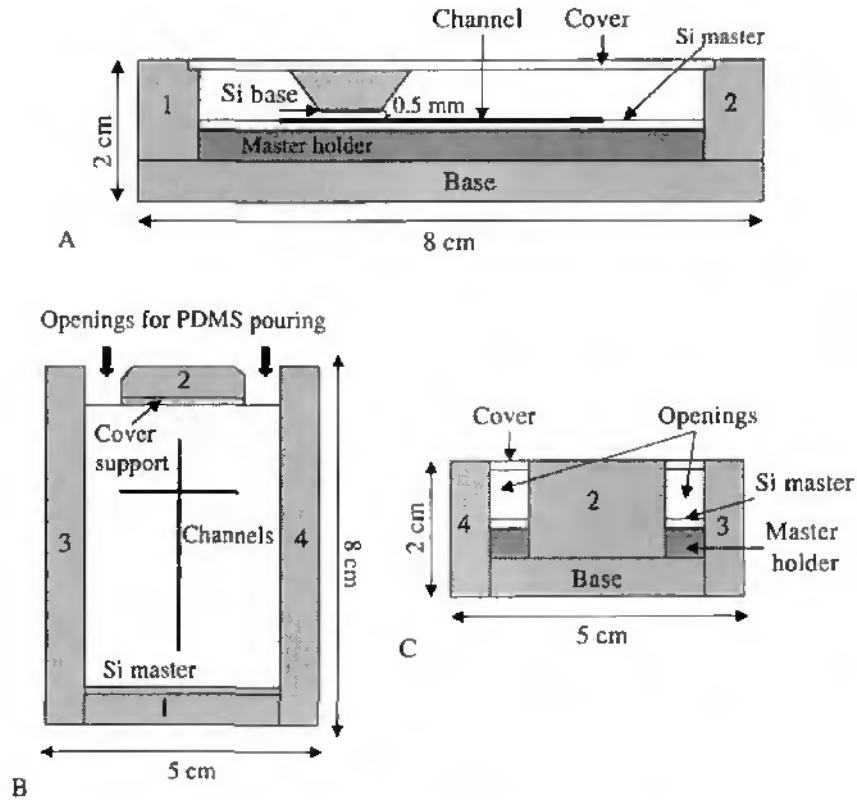

***Figure 6-2** Mold for replication of PDMS structures containing a thin optical window. A) Cross-section of the mold frame. The Si master is attached to the base of this frame. The mold is then closed with a PMMA cover containing a trapezoidal steel piece, which is directed downwards into the box, towards the master. The inside base of the trapezoid is covered with a piece of Si wafer cut to size. The distance between this base and the master defines the PDMS optical window thickness (0.5 mm in our case). B) Top view of the mold with the Si master fixed on its base. The mold is closed with the plastic cover. The prepolymer mixture can be introduced through the two side openings when the mold is held vertically. C) Cross-section of the side of the mold frame containing the openings for PDMS introduction.*

master, and fluidic reservoirs are punched through the PDMS at locations corresponding to the channel ends. The structured PDMS slab is cleaned in deionized water and 2-propanol (MOS-grade), dried with nitrogen and sealed by adhesion on a quartz wafer cut in a rectangle with appropriate dimentions (w × l × h= 4 × 8 × 0.05 cm, Guinchard, Yverdon-les-Bains, Switzerland). The top and cross-sectional views of the resulting hybrid PDMS/quartz chip are depicted in Figure 6-3A and 6-3B. The use of a thin polymer window and a quartz wafer to seal the structures ensures better system performance with respect to losses due to absorbance by materials, light scattering and divergence. The Si master was fabricated by DRIE (as described in Chapter 2), sawed and silanized before casting.

6.2.3 Optical detection system

The PDMS/quartz chip was incorporated into the detection system as shown in Figure 6-4A. The optical system, constructed in the IMT machine workshop, places the microfluidic device between two prealigned optical fibers. These fibers (GMP SA, Renens, Switzerland) are used to guide the light from the light source to the channel and to collect the transmitted light at the other side of the channel and guide it to the detector. The input optical fiber is 100 µm in diameter, while the output is 200 µm. The larger diameter of the output fiber should allow a more efficient recovery of the transmitted light. The two fibers are aligned and fixed using ferrules in a bulk piece, which is attached to a translation stage. The distance between the fibers is about 1.2 mm. The chip is placed on the chip holder with the optical window inserted between the fibers and the channel positioned close to the fiber core (Figure 6-4B). At this point, the optical axis, which is defined as the vertical path from the center of one fiber core to the other, can be aligned with respect to the stationary chip. This alignment is possible because the channel, whether filled with solution or air, has a different refractive

index than the chip, and hence exhibits a higher absorbance. The optical axis can therefore be slowly moved until the maximum absorbance signal is found.

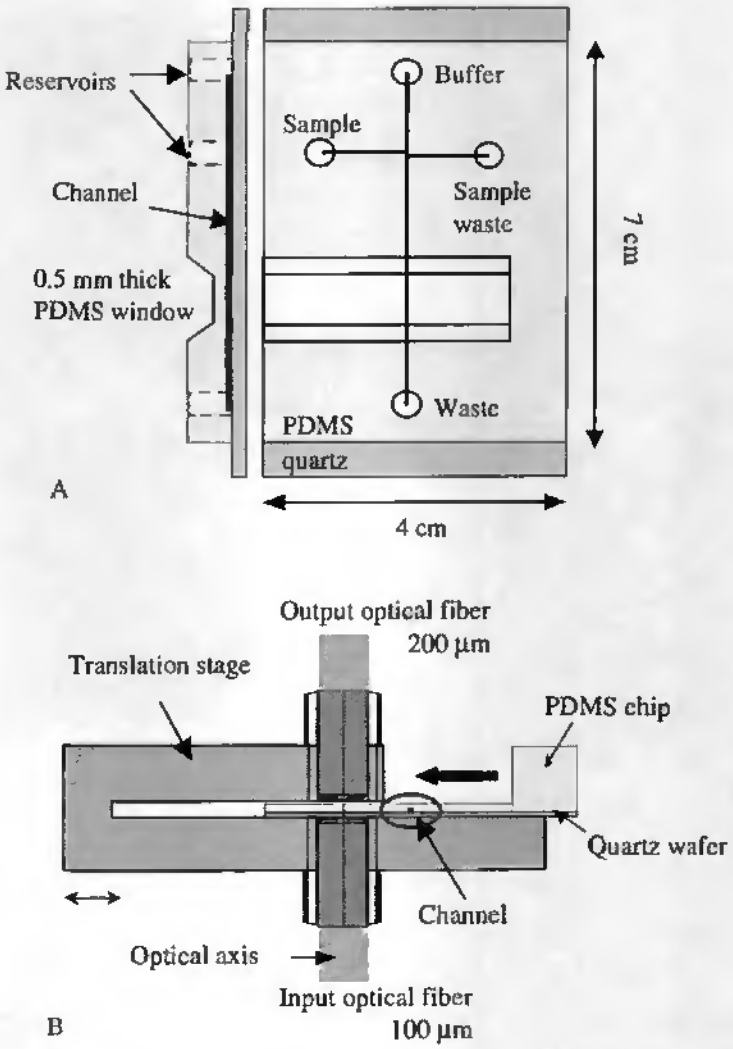

***Figure 6-3** A) Chip layout: (right) top view, (left) cross-sectional view. B) Cross-sectional view of chip alignment with respect to the optical axis (vertical dashed line). The channel is oriented out of the plane of the paper. The structured PDMS layer is sealed on a rectangular quartz wafer.*

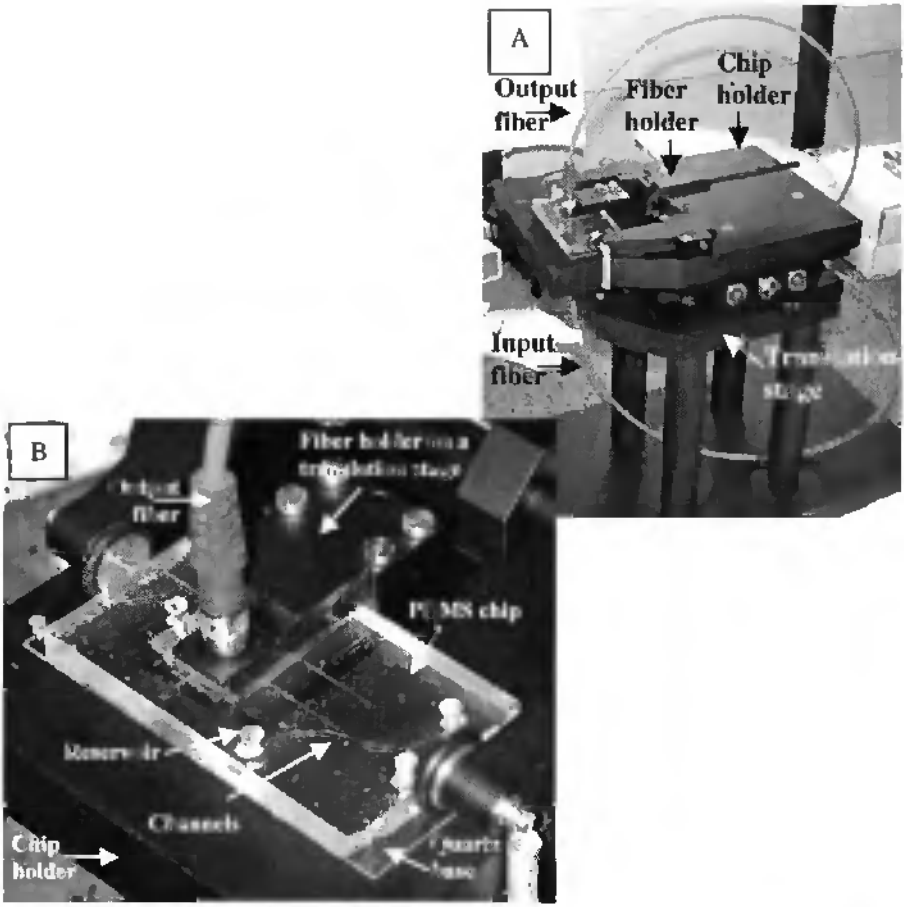

Figure 6-4 *A) (right) Optical system with prealigned optical fibers and translation platform. B) (left) Close up of the aligned PDMS/quartz chip. Channels and reservoirs are visible.*

Halogen and deuterium light sources (Ocean Optics Inc., supplied by GMP SA, Renens, Switzerland) were used for visible and UV detection, respectively. The transmitted light was transported by the output optical fiber to a detector with a bandpass filter that allowed selection of the wavelength range of interest: 632 nm for the visible (A43-081, Edmund Industrial Optics, Barrington, NJ, USA) and 240-400 nm for the UV (U-330 Hoya, Edmund Industrial Optics). The filter

was followed by a photodiode (OPT301, Burr-Brown Corporation), an amplifier and a low-pass electronic filter. The signal was finally analysed by LabView. A homemade high-voltage power supply using high-voltage components (Emco, Sutter Creek, CA, USA) was employed to inject sample plugs into the separation channel. To do this, 900 V were applied between sample and sample waste reservoirs for 40 s, followed by application of 2000 V between buffer and buffer waste (L_{tot}= 5 cm, L_{eff}= 2.5 cm). The power supply was connected with a homemade relay box and the potential was manually switched between sample loading and separation mode.

6.2.4 Reagents

A run buffer of 20 mM Tris/HCl (pH 7.4) was used. Methylene blue (MB), amino acids, glucose (all purchased from Sigma, Buchs, Switzerland) and a 6-amino-acid peptide (Leu-Trp-Met-Arg-Phe-Ala) (kindly donated by CSEM, Neuchâtel, Switzerland) were prepared in the running buffer and electrokinetically injected in the separation channel towards the detection window, as described above. The absorbance spectrum of methylene blue was measured using a spectrometer (Lambda 14, Perkin Elmer). It conveniently absorbs both in the red (600-700 nm) and in the UV. Since at 290 nm and 632 nm its absorbance is nearly the same (0.2 AU), MB was used to compare the sensitivity of the system in the UV and in the visible at these wavelengths.

6.3 Results and discussion

In initial tests, MB concentrations down to 5 μM were detected in the visible at 632 nm as shown in Figure 6-5A. At this wavelength, an LOD of about 1 μM was calculated. The peak height increased monotonically with the dye concentration, as shown in Figure 6-5B. The same dye at different concentrations was detected in the UV, as shown in Figure 6-6. Because of the reduced photodiode response in the UV (from 0.42 A/W for the red to 0.18 A/W for the UV range), the different filter bandwidth and light source used, the sensitivity of the system is limited in the UV, though 30 μM methylene blue could still be easily determined. The LOD for MB in the UV was estimated around 5 μM. While the reproducibility of the peak signal height is quite good (RSD= 0.34%), peak elution time is less reproducible (RSD= 1.64%), due to the manual control of the injection.

The UV detection system was employed for the detection of more interesting species. 0.1 mg/mL (0.5 mM) of the aromatic amino acid, tryptophan (ε_{279nm}= 5574 $cm^{-1}M^{-1}$, ε_{310nm}= 82 $cm^{-1}M^{-1}$) was detected as shown in Figure 6-7.

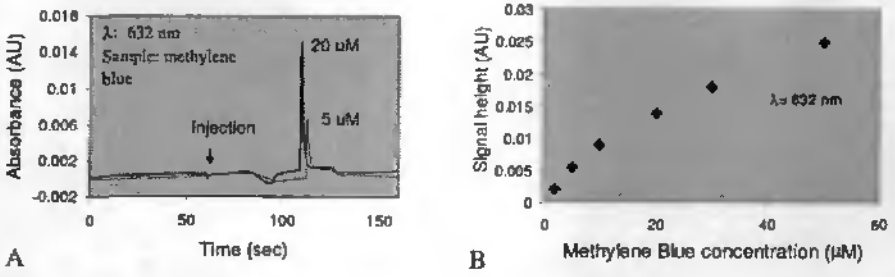

Figure 6-5 A) Detection of methylene blue at 632 nm (ε_{632nm}= 42,960 $cm^{-1}M^{-1}$) at concentrations down to 5 μM. B) MB concentration vs. peak height. Running buffer= 20 mM Tris/HCl, pH 7.6, E_{sep}= 400 V/cm, L_{eff}= 2.5 cm.

Note in the same figure that the absorbance signal grows, as expected, when channel depth increases from 50 to 70 μm. The peaks are quite broad (N= 84,000 plates/m, H= 12 μm), due principally to the manual switching. The peak signal intensity is also smaller than expected on the basis of the Lambert-Beer law. This can be explained in part by the fact that the band-pass filter is centred at 310 nm, while the $\lambda_{max\ abs}$ for tryptophan is 279 nm. The wide spectral bandwidth used probably also contributes to a lowered peak height, though improved SNR could also result [20].

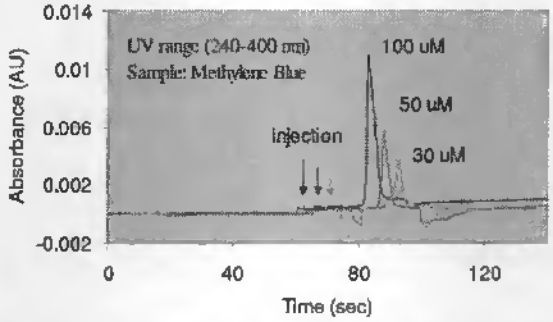

Figure 6-6 *UV absorbance peak of methylene blue. Experimental conditions described in Figure 6-5.*

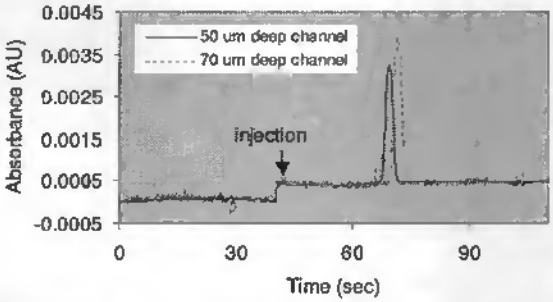

Figure 6-7 *UV absorbance peak of 0.1 mg/mL tryptophan (ε_{279}= 5574 $cm^{-1}M^{-1}$) through 50- and 70-μm-deep channels in different chips. Experimental conditions described in Figure 6-5.*

The amino acid tyrosine was detected in the same system but with lower sensitivity, due to the lower extinction coefficient at 310 nm (ε_{275nm}= 1400 cm^{-1} M^{-1}, ε_{310nm}= 40 $cm^{-1}M^{-1}$) than tryptophan. A peptide of 6 amino acids (Leu-Trp-Met-Arg-Phe-Ala) could be detected at a concentration of 1 mg/mL, and glucose was also detected at a 0.1 mg/mL level. The peptide peak (not shown) was relatively broad and tailed (peak asymmetry= 2), suggesting increased interaction of a sorptive nature with the PDMS walls.

6.4 Conclusions

The data reported demonstrate that UV detection of compounds of biological interest can be accomplished in microfluidic devices. However, the system is far from optimization. A system like the one described here, using optical fibers to bring light perpendicularly to and from a microdevice and then to the electronic components, was reported in [13]. In this case, the channel side walls were fabricated in SU-8 (another interesting approach to have vertical structures, 60 μm in this case), while the bottom and top walls consisted of quartz windows. Benzene and acetone prepared in hexane were pumped into these channels and their spectra were successfully obtained. Our PDMS/hybrid devices could be suitable for spectral characterization of samples. However, a monochromator and a different diode would be necessary. Moreover, the incompatibility of PDMS with many samples and solvents would make application to many real samples difficult.

Transverse UV detection through 40-μm-high diamond channels and 20-μm-deep quartz channels have been reported in the literature [14, 15]. For these experiments, a modified HPLC detector cartridge obviated the need for optical fibers. Peaks of proteins, drugs and alkyl phenones at concentrations on the order of 0.1-0.6 mg/mL were detected after anion-exchange and CEC separations [15].

Again, adsorption problems would occur with these kinds of analytes during analysis in PDMS channels. It is known that protein adsorption on the channel walls is a problem inherent to both glass and plastic substrates [17, 21]. The development of a good coating could resolve these issues and allow protein separation and detection in PDMS channels [22, 23]. The separation of a DNA ladder in PDMS chips has also been reported using LIF detection [24]. Our system could therefore be employed for UV detection of nucleic acids separated by CGE in the hybrid PDMS/quartz channels.

Finally, our detection system could be improved optically by incorporating microlenses to focus the light into the channel and integrating a slit to avoid interference from the stray light. From both an electronic and optical point of view, a reference signal to reduce system noise and therefore improve system sensitivity could be used. These modifications would lead to performance comparable or perhaps better than the other systems mentioned above.

REFERENCES

[1] B. H. Weiller, L. Ceriotti, T. Shibata, D. Rein, M. A. Roberts, J. Lichtenberg, J. B. German, N. F. de Rooij, and E. Verpoorte, "Analysis of lipoproteins by capillary zone electrophoresis in microfluidic devices: assay development and surface roughness measurements," *Anal. Chem.*, vol. 74, pp. 1702-1711, 2002.

[2] J.-C. Roulet, R. Völkel, H. P. Herzig, E. Verpoorte, N. F. de Rooij, and R. Dändliker, "Performance of an integrated micro-optical system for fluorescence detection in microfluidic systems," *Anal. Chem.*, vol. 74, pp. 3400-3407, 2002.

[3] G. F. Jiang, S. Attiya, G. Ocvirk, W. E. Lee, and D. J. Harrison, "Red diode laser induced fluorescence detection with a confocal microscope on a microchip for capillary electrophoresis," *Biosensors & Bioelectronics*, vol. 14, pp. 861-869, 2000.

[4] G. Ocvirk, T. Tang, and D. J. Harrison, "Optimization of confocal epifluorescence microscopy for microchip-based miniaturized total analysis systems," *Analyst*, vol. 123, pp. 1429-1434, 1998.

[5] S. R. Wallenborg and C. G. Bailey, "Separation and detection of explosives on a microchip using micellar electrokinetic chromatography and indirect laser-induced fluorescence," *Anal. Chem.*, vol. 72, pp. 1872-1878, 2000.

[6] E. Verpoorte, A. Manz, H. Ludi, A. E. Bruno, F. Maystre, B. Krattiger, H. M. Widmer, B. H. van der Schoot, and N. F. de Rooij, "A silicon flow cell for optical detection in miniaturized total chemical analysis systems," *Sensors and Actuators B-Chemical*, vol. 6, pp. 66-70, 1992.

[7] K. B. Mogensen, N. J. Petersen, J. Hübner, and J. P. Kutter, "Monolithic integration of optical waveguides for absorbance detection in microfabricated electrophoresis devices," *Electrophoresis*, vol. 22, pp. 3930-3938, 2001.

[8] D. J. Harrison, A. Manz, Z. H. Fan, H. Ludi, and H. M. Widmer, "Capillary electrophoresis and sample injection systems integrated on a planar glass chip," *Anal. Chem.*, vol. 64, pp. 1926-1932, 1992.

[9] Z. Liang, N. H. Chiem, G. Ocvirk, T. Tang, K. Fluri, and D. J. Harrison, "Microfabrication of a planar absorbance and fluorescence cell for integrated capillary electrophoresis devices," *Anal. Chem.*, vol. 68, pp. 1040-1046, 1996.

[10] A. Daridon, V. Fascio, J. Lichtenberg, R. Wütrich, H. Langen, E. Verpoorte, and N. F. de Rooij, "Multi-layer microfluidic glass chips for microanalytical applications," *Fresenius Journal of Anal. Chem.*, vol. 371, pp. 261-269, 2001.

[11] H. Salimi-Moosavi, Y. T. Jiang, L. Lester, G. McKinnon, and D. J. Harrison, "A multireflection cell for enhanced absorbance detection in microchip-based capillary electrophoresis devices," *Electrophoresis*, vol. 21, pp. 1291-1299, 2000.

[12] H. Nakanishi, T. Nishimoto, A. Arai, H. Abe, M. Kanai, Y. Fujiyama, and T. Yoshida, "Fabrication of quartz microchips with optical slit and development of a linear imaging UV detector for microchip electrophoresis systems," *Electrophoresis*, vol. 22, pp. 230-234, 2001.

[13] R. J. Jackman, T. M. Floyd, R. Ghodssi, M. A. Schmidt, and K. F. Jensen, "Microfluidic systems with on-line UV detection fabricated in photodefinable epoxy," *J. Micromech. Microeng.*, vol. 11, pp. 263-269, 2001.

[14] H. Bjorkman, C. Ericson, S. Hjertén, and K. Hiort, "Diamond microchip capillary chromatoghraphy of protein", Proceedings of Micro Total Analysis Systems 2000, Enschede, The Netherlands, 2000, 187-190.

[15] C. Ericson, J. Holm, T. Ericson, and S. Hjertén, "Electroosmosis- and pressure-driven chromatography in chips using continuous beds," *Anal. Chem.*, vol. 72, pp. 81-87, 2000.

[16] S. Constantin, R. Freitag, D. Solignac, A. Sayah, and M. A. M. Gijs, "Utilization of the sol-gel technique for the development of novel stationary phases for capillary electrochromatography on a chip," *Sensors and Actuators B*, vol. 78, pp. 267-272, 2001.

[17] A. Oki, S. Adachi, Y. Takamura, K. Ishiara, H. Ogawa, Y. Ito, T. Ichiki, and Y. Horiike, "Electroosmosis injection of blood serum into biocampatible microcapillary chip fabricated on quartz plate," *Electrophoresis*, vol. 22, pp. 341-347, 2001.

[18] L. Ceriotti, E. Verpoorte, K. J. Weible, and N. F. de Rooij, "High aspect ratio channels for capillary electrophoresis", Proceedings of Transducers '01, Munich, Germany, 2001, 1174-1177.

[19] L. Ceriotti, J. Lichtenberg, S. Clément, P. Hussbaum, E. Verpoorte, R. Dändliker, and N. F. de Rooij, "Visible and UV detection through square deep PDMS channels", Proceedings of Micro Total Analysis Systems 2001, Monterey, CA, USA, 2001, 339-340.

[20] M. Aiello and R. McLaren, "A sensitive small-volume UV/vis flow cell and total absorbance detection system for micro-HPLC," *Anal. Chem.*, vol. 73, pp. 1387-1392, 2001.

[21] M. Y. Badal, M. Wong, N. Chiem, H. Salaimi-Moosavi, and D. J. Harrison, "Protein separation and surfactant control of electroosmotic flow in poly(dimethylsiloxane)-coated capillaries and microchips," *J. Chromatogr. A*, vol. 947, pp. 277-286, 2002.

[22] D. C. Duffy, J. C. McDonald, O. J. A. Schueller, and G. M. Whitesides, "Rapid prototyping of microfluidic systems in poly(dimethylsiloxane)," *Anal. Chem.*, vol. 70, pp. 4974-4984, 1998.

[23] V. Linder, E. Verpoorte, W. Thormann, N. F. de Rooij, and H. Sigrist, "Surface biopassivation of replicated poly(dimethylsiloxane) microfluidic channels and application to heterogeneous immunoreaction with on-chip fluorescence detection," *Anal. Chem.*, vol. 73, pp. 4181-4189, 2001.

[24] J. W. Hong, K. Hosokawa, T. Fujii, M. Seki, and I. Endo, "An inexpensive PDMS (polydimethylsiloxane) microchip for capillary gel electrophoresis", Proceedings of Transducers '99, Sendai, Japan, 1999, 760-763.

7 Conclusions and outlook

Microfabrication technology has proven to be a valuable tool for creating miniaturized devices for applications in many chemical and biochemical assays. The attractive features associated with these devices include their potential for system integration (in which various assays are included onto the fluidic platform), speed, reduced sample and reagent consumption, high efficiency and automation. Moreover, microdevices are small, compact and easy to transport. They therefore represent a good route to achieve real-time analysis at the point-of-care (POC). In this thesis, different fabrication processes have been investigated with the aim of developing prototype devices useful for POC testing.

To date, most microfluidic devices have been fabricated in glass or silicon-based substrates. Photolithographic processing techniques are used to produce channels in a planar substrate. The channels are then sealed usually with a wafer of similar material. An advantage of using these materials is their well-known electrophoretic properties and surface derivatization chemistries. In Chapter 3, the analysis of lipoproteins (LP) by CE in a glass microdevice was demonstrated. The clinical interest for these complex particles is high, since their concentration and forms are directly related to increased risk of coronary heart diseases. Oxidized LDL forms, for instance, tend to stay longer in blood than the native forms. They can interact with the artery walls and activate a dangerous inflammatory response, which leads to the formation of atherosclerotic plaques. The method we developed for LP analysis is based on LP staining with NBD-ceramide for fluorescent detection and the use of a dynamic coating consisting of

methylglucamine to prevent particle adsorption to the wall. The CE method was developed in a conventional system and then transferred with success to the glass chip. The possibility to directly compare the two formats was important in the first part of the study to understand LP electrophoretic behaviour. The electropherograms obtained in the two systems are qualitatively similar. In the microsystem, however, the sensitivity is reduced, due mainly to the small sample volume injected. On the other hand, the short working distance used in microCE not only allows short analysis times but also higher sample recovery at the detection point, which makes the detection of LP peaks also possible in uncoated channels. Moreover, the focusing effect observed by adding a small concentration of SDS to the sample and not to the running buffer could be useful to concentrate and detect LP forms which are present in the sample at low concentrations. Unfortunately, the injection of serum into the microchannel resulted in channel clogging. With further efforts, it should be possible to separate, identify and quantify on-chip the different lipoprotein classes directly from serum samples. The LP study was developed on a glass device, which cannot be thought of as disposable because of the cost of the substrate and the fabrication process. However, the channels can be cleaned with NaOH after the separation and the same structure can be used several times. Several layouts can be also integrated on the same wafer so that high throughput can be achieved and sample and reagent consumption reduced.

Although the fabrication of glass microchannels is a standard process in our lab, it is time consuming, expensive and the bonding process is critical. Another limitation of this process is the channel cross section, which is restricted by the use of the isotropic etchiog technique, as discussed in Chapter 1, Section 1.2.1. In Chapter 2 we demonstrated that rectangular channels can be obtained in fused silica wafers using a dry etching process. This process, however, is again difficult and expensive.

To overcome the problems connected with classical planar technologies, polymer substrates have become increasingly popular as an alternative for the fabrication of microfluidic devices over the last few years [1, 2]. The use of plastics is primarily driven by the fact that these materials are less expensive and easier to manipulate than silicon-based substrates. As introduced in Chapter 1, Section 1.2.2, plastics devices can be fabricated en mass by replication technologies and without geometric (i.e. channel profile) restrictions.

In the course of the present thesis the use of poly(dimethylsiloxane) (PDMS) as an alternative to glass for the fabrication of prototype devices has been investigated. This elastomer is commercially available, cheap, UV transparent and can be easily structured by casting. In Chapter 2 we presented two methods for the fabrication of masters for PDMS casting. The first approach is based on silicon-micromachining by deep reactive-ion etching (DRIE). The second one is based on Epon SU-8 technology. Once a master is available, a new PDMS chip can be fabricated outside the cleanroom in 4 hours, which is the time required for its polymerization. Rectangular PDMS channels were employed for transverse UV/visible absorbance detection (Chapter 6). Because of the dependence of UV absorbance on the optical path length, this detection method is not commonly used in microsystems. However, this method is interesting since it is applicable to a wider range of molecules than fluorescence, and does not require a labelling step prior to analysis. We have demonstrated that amino acids and peptides can be analysed electrophoretically and detected by UV absorbance as sharp, rectangular channels, using optical fibers to guide light to the chip, and from the chip to the detector (Chapter 6). This system could be further improved to allow on-chip analysis of complex matrices by UV absorbance detection [3].

A new fritless method to retain beads in a PDMS microcolumn was presented in Chapter 4. This method is based on the use of high-aspect-ratio, tapered separation channels. When a suspension of beads is loaded into the column towards the taper, the beads agglomerate in the taper to form a stationary

plug behind which beads are retained. Tapered PDMS channels were successfully packed with 3-μm, octadecylsilanized (ODS) silica beads and used for capillary electrochromatography (CEC). The separation of neutral compounds was achieved in less than 15 s with efficiencies of 290,000 plates/m for the unretained compound MeOH. Unfortunately, PDMS has sorptive properties which limit the range of analytes that can be analysed. This problem could be solved using a coating to passivate the surface [4]. In general, chromatography is an interesting separation method to integrate in POC devices for diagnostics (i.e. CEC separation of hormones from biological matrices) and environmental monitoring (toxin and pesticide detection). Moreover, the work with a packed bed was interesting since many applications can be realized on bead beds as reported in the literature, namely immunoassays [5], solid-phase extraction [6], chromatographic separations [6, 7], affinity purification [8], enzymatic reactions [9], nucleic acid sequencing [10], hybridisation [11] and extraction [12]. This is in part because beads are available in different sizes, porosities and surface chemistries. Applications other than CEC can take advantage of the fritless packing method proposed here.

Together with separation methods, there are other applications that should be integrated and be of interest for POC testing. Sample pre-treatment (e.g. nucleic acid extraction) is one example that we have started investigating. A packed bed was presented in Chapter 5 for nucleic acid extraction using the Boom method. In this case, 15 to 35-μm-diameter silica beads were integrated into a PDMS channel with one or two weirs, realized using a 2-layer Epon SU-8 master. A peristaltic pump was used to move the solutions through the packed bed. Nucleic acids were extracted from prepurified DNA samples, and human cell and HPV lysate samples. Nucleic acid extraction is usually performed in big systems, which, though completely automated and efficient, requires mL volumes of reagents, long analysis times (about 1 hour), and a central laboratory housing all these instruments. Photos of conventional instruments used for nucleic acid

extraction and PCR amplification are presented in Figure 7-1. With the packed microbed, which is typically 500 µm wide and 4 mm long, the extraction was completed in less then 40 min using a few µL of each solution. The quality of the extracted nucleic acids and their on-chip concentration will be tested soon.

The extraction unit was developed as part of a more challenging project focused on the detection of Human Papilloma Virus (HPV) in cervical samples. Some strains of HPV have been identified as the main cause of neoplastic changes or cell transformation in the cervix. Deaths from cervical cancer account for approximately 2% of all cancer deaths and 18% of all gynecological cancer deaths. These percentages increase if underdeveloped nations, such as Mexico,

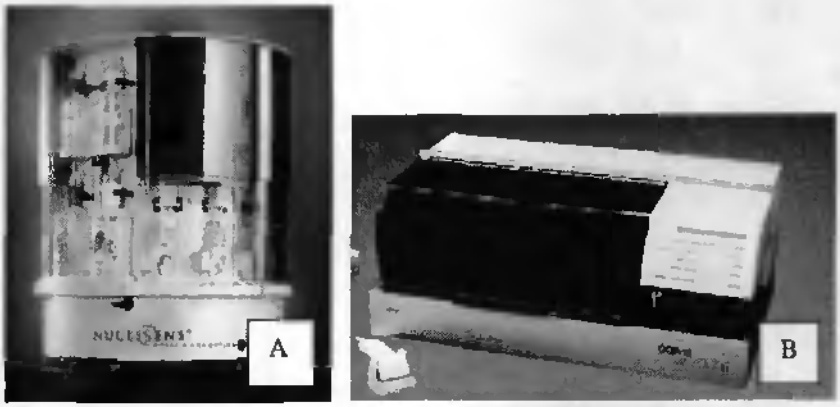

***Figure 7-1** Conventional instruments used for nucleic acid extraction and amplification. A) Organon Teknika Nuclisens Extractor, an automated nucleic acid isolation system well suited for applications in the fields of clinical analysis, routine in vitro diagnostic testing and blood safety testing. B) COBAS AMPLICOR Automated PCR system for molecular diagnostic testing. Polymerase chain reaction (PCR) provides accurate and sensitive technology for the detection of infectious diseases. Amplification, denaturation, hybridization, incubation, washing, colorimetric reading and result reporting are all performed automatically and all combined onto one simple, easy-to-use testing platform.*

Latin America, Africa, India and Eastern Europe, are considered. In these countries, in fact, cervical cancer is the leading cause of cancer death for women. The mortality rate for cervical cancer can be decreased by adopting routine pap screening. Conventionally, this test is based on cytological examination of the epithelial cells removed from the cervix by a gynecologist. Changes in cell and nucleus morphology indicate there may be a problem and that further diagnostic procedures (usually biopsy) should be done. There is another way to screen woman at risk, involving the detection of the HVP virus in epithelial cells. The amplification of viral nucleic acid sequences can be used to reveal the viral infection. The importance of developing an assay for detection of HPV infection in cervical smears could have a very strong impact on the populations of underdeveloped countries. A portable, easy-to-use-and-interpret pap test could represent, in fact, a very powerful tool for cervical cancer prevention, allowing the detection of women at risk and their treatment [13].

The challenges for the development of integrated systems for POC testing are multiple. An important step is the choice of the substrate for chip fabrication. For a disposable device, the use of plastic in conjunction with replication methods is the best choice. For our application, the plastic should be biocompatible, withstand solvents and high ionic-strength solutions used for nucleic acid extraction, and not be autofluorescent, since the detection of the amplified sequence is fluorescent-based. Cycloolefin copolymer (COC) is under investigation as substrate for the prototype device in this project. Device sealing is not always trivial and different bonding processes need to be tested and perhaps combined to get good and reproducible sealing. Solvents, glues, ultrasonication and laser welding are some examples of the possible bonding approaches. Once the type of assays that have to be integrated is clear, a first prototype could be designed and fabricated. In the literature there are two examples of highly integrated devices for diagnostics. Both have the dimensions of a credit-card [14, 15]. The first one is the monolithic device developed at Affymetrix Inc. [14]. A

picture of the chip is presented in Figure 7-2. It is realized in polycarbonate by computer-controlled machining or injection molding, and contains several chambers and channels for a complex series of assays (i.e. extraction, amplification, hybridization, labelling). Pneumatically controlled diaphragm valves and Peltier elements are also integrated for precise manipulation of reagents and precise control of temperature regions, respectively. The function of each element integrated into the device is described in the caption of Figure 7-2. Typically, the sample, 1 mL of serum mixed with lysis buffer, is drawn through the different assay steps. The chip was tested for detection of mutations in a 1.6-kbp region of the HIV genome using the GeneChip array. The sophistication of this device makes it useful for other applications, a flexibility that is often desirable.

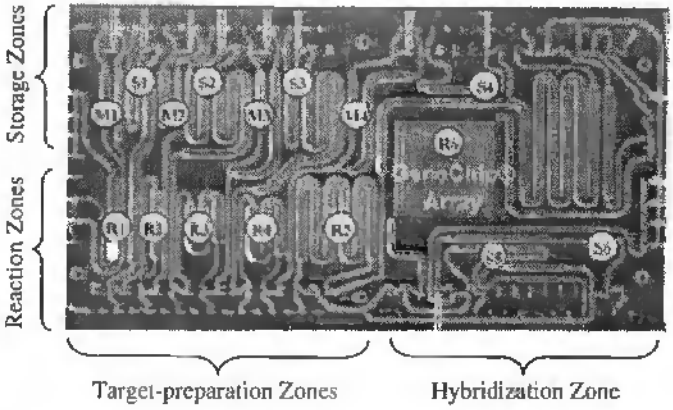

Figure 7-2 *Integrated polycarbonate device that automatically performs a multistep HIV genotyping assay. The cartridge measures 8 ×40 ×70 mm and was developed at Affymetrix Inc. (Santa Clara, CA, USA). At the beginning of the process, reagent mixtures are loaded into the storage chambers S1 to S6. The device carries out RNA purification from a serum lysate (extraction) (R1), RT-PCR (R2), nested PCR (R3), Dnase fragmentation (R4), labelling (R5), and hybridization (R6). Intermediate products are stored in chambers M1 to M4. The chip was tested for the detection of mutations in a 1.6-kbp region of the HIV [14].*

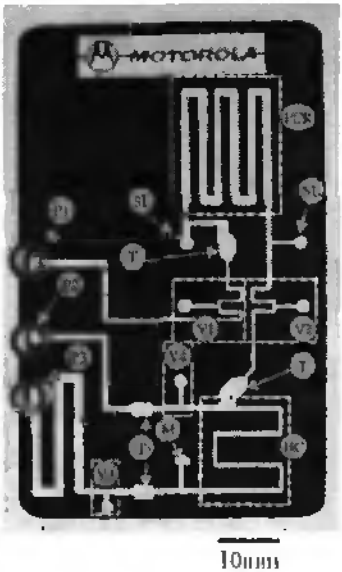

Figure 7-3 *Monolithic integrated polycarbonate DNA assay device developed at the Motorola Labs (Motorola, Inc., Tempe, Arizona, USA). Serpentine PCR channel (PCR), hybridization channel (HC), pluronic valves (V1-V4), pluronic traps (T), sample loading holes (SL), syringe pump connections (P1-P3). In this chip, the amplification and detection of specific genes from Escherichia coli and Enterococcus faecalis were demonstrated [15].*

In other cases, less complex systems in which only a few assays are integrated for a particular application may be preferable. An example of this kind of system is the monolithic DNA device developed by Motorola [15]. This device is presented in Figure 7-3. It contains the elements for PCR and DNA hybridisation. Novel Pluronic phase change valves and Peltier thermal elements are also integrated. Some gene sequences of *Escherichia coli* and *Enterococcus faecalis* have been amplified and detected by hybridisation in such systems [15].

For our application, the detection of HPV in cervical smears, the device should be able to perform cell lysis, nucleic extraction, amplification and detection. Moreover, since cervical smears are very heterogeneous samples and contain high concentrations of proteins, a filtration step could be useful to concentrate the epithelial cells and remove the unwanted material. The integrated device should then contain a filter, a chamber where samples and lysis buffer are mixed, a packed bed for nucleic acid extraction and a channel to deliver the

extracted nucleic acids to the amplification unit. After sample loading, the chip would be inserted in an instrument equipped with a detection system (i.e. laser diode for excitation and photodiode for detection) and system software for data analysis, quantification (i.e. using a calibration curve) and storage. Chip operations would be computer controlled. In the case where the device is used as a screening test for the presence of the viral infection in a non-quantitative way, a less sophisticated detection and analysis method could be used. For example, colourimetry could be employed to reveal if the amplification of the viral target sequence has occurred or not. A colour change of the solution in the amplification chamber would mean that the test is positive for the presence of viral sequences in the initial sample, and further analysis should be performed.

As amplification method, nucleic acid sequence-based amplification (NASBA) has been chosen. NASBA is a simple and rapid alternative to PCR for nucleic acid amplification, specifically designed for the detection of RNA targets [16-22]. The principle of NASBA is illustrated in Figure 7-4. The reverse transcriptase creates dsDNA from the mRNA target, when this last is present in the sample. The dsDNA serves as template for RNA polymerase, which makes many copies of RNA. These RNA transcripts are the species to detect. This amplification process is particularly interesting because it is isothermal (60°C). This means that the integration of NASBA should be less challenging than PCR, for which thermal cycles are necessary. Moreover, the RNA amplicons, which are generated during the amplification process, can be real-time detected using molecular beacons [13, 17, 21]. These molecules are DNA probes with modified ends as illustrate in Figure 7-5. In the folded state (stem-loop) the fluorescence is quenched, but, upon binding of the loop sequence to its complementary target sequence, the probe undergoes a conformational change and a fluorescent signal is emitted. This means that, if the molecular probes are opportunely designed to be complementary to the RNA amplicons, the amplification can be followed in

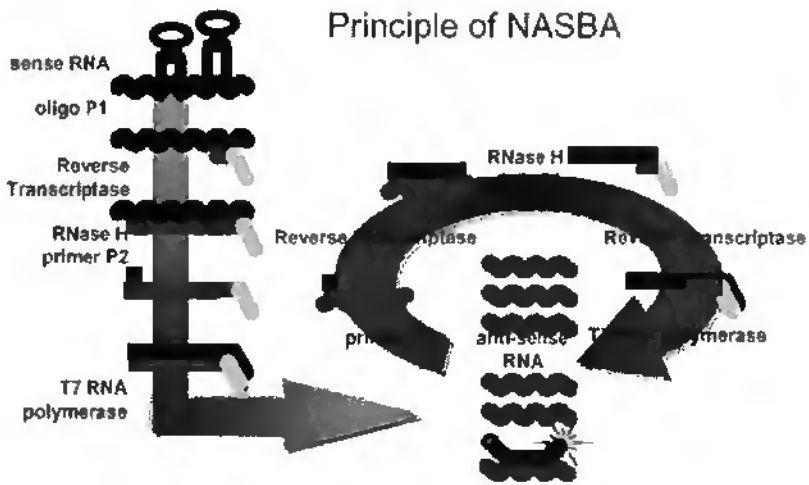

Figure 7-4 Principle of NASBA. Reverse transcriptase creates dsDNA from mRNA. dsDNA serves as template for RNA polymerase, which makes many copies of RNA .(Design from [13]).

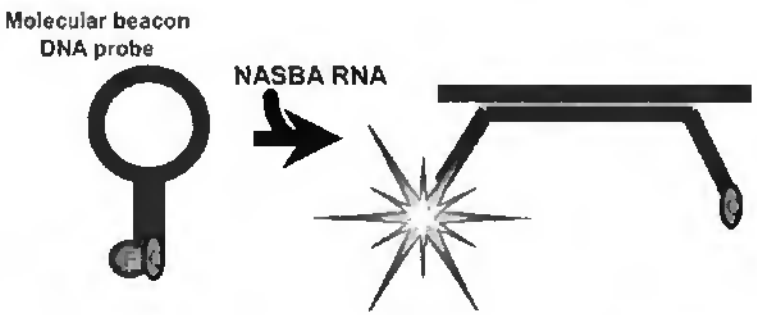

Figure 7-5 Molecular beacons are DNA probes with modified ends. In the folded configuration the fluorescence is quenched. Upon bonding with the complementary sequence the probes undergoes a conformational change and a fluorescence signal is emitted. Molecular beacons can be used for real time detection of the NASBA RNA products. (Design from [13]).

real-time using a fluorescent reader. The isothermal amplification process NASBA and the real-time detection with molecular beacons should have a great impact on the development of integrated and rapid POC diagnostic tests.

Progress in microtechnology (i.e. the fabrication of plastic chips and valves) and molecular biology, and new sample pre-treatment methods will all contribute to the development of fully integrated, low cost, efficient and reliable devices. The combination of microfluidic networks and sensors could also play an important role in the fabrication of such devices [23]. Portable, disposable, chip-based tools for POC medical diagnostics, environmental and food quality testing, and defensive biological agent detection will be a reality in the near future.

REFERENCES

[1] L. Martynova, L. E. Locascio, M. Gaitan, G. W. Kramer, R. G. Christensen, and W. A. MacCrehan, "Fabrication of plastic microfluid channels by imprinting methods," *Anal. Chem.*, vol. 69, pp. 4783-4789, 1997.

[2] H. Becker and C. Gärtner, "Polymer microfabrication methods for microfluidic analytical applications," *Electrophoresis*, vol. 21, pp. 12-26, 2000.

[3] A. Oki, S. Adachi, Y. Takamura, K. Ishiara, H. Ogawa, Y. Ito, T. Ichiki, and Y. Horiike, "Electroosmosis injection of blood serum into biocampatible microcapillary chip fabricated on quartz plate," *Electrophoresis*, vol. 22, pp. 341-347, 2001.

[4] B. E. Slentz, N. A. Penner, and F. E. Regnier, "Capillary electrochromatography of peptides on microfabricated poly(dimethylsiloxane) chips modified by cerium(IV)-catalyzed polymerization," *J. Chromatogr. A*, vol. 948, pp. 225-233, 2002.

[5] K. Sato, M. Tokeshi, T. Odake, H. Kimura, T. Ooi, M. Nakao, and T. Kitamori, "Integration of an immunosorbent assay system: Analysis of secretory human immunoglobulin A on polystyrene beads in a microchip," *Anal. Chem.*, vol. 72, pp. 1144-1147, 2000.

[6] R. D. Oleschuk, L. L. Shultz-Lockyear, Y. Ning, and D. J. Harrison, "Trapping of bead-based reagents within microfluidic systems: on-chip solid-phase extraction and electrochromatography," *Anal. Chem.*, vol. 72, pp. 585-590, 2000.

[7] M. Seki, M. Yumada, R. Ezaki, R. Aoyama, and J. W. Hong, "Chromatographic separation of proteins on a PDMS-polymer chip by pressure flow", Proceedings of Micro Total Analysis Systems 2001, Monterey, CA, 2001, 48-50.

[8] G. Jiang and D. J. Harrison, "mRNA isolation in a microfluidic device for eventual integration of cDNA library construction," *Analyst*, vol. 125, pp. 2176-2179, 2000.

[9] C. Wang, R. Oleschuk, F. Ouchen, J. Li, P. Thibault, and D. J. Harrison, "Integration of immobilized trypsin bead beds for protein digestion within a microfluidic chip incorporating capillary electrophoresis separations and an electrospray mass spectrometry interface," *Rapid Communications in Mass Spectrometry*, vol. 14, pp. 1377-83, 2000.

[10] H. Andersson, W. van der Wijngaart, P. Enoksson, and G. Stemme, "Micromachined flow-through filter-chamber for chemical reactions on beads," *Sensors and Actuators B*, vol. 67, pp. 203-208, 2000.

[11] Z. H. Fan, S. Mangru, R. Granzow, P. Heaney, W. Ho, Q. Dong, and R. Kumar, "Dynamic DNA hybridization on a chip using paramagnetic beads," *Anal. Chem.*, vol. 71, pp. 4851-4859, 1999.

[12] K. A. Wolfe, M. C. Breadmore, J. P. Ferrance, M. E. Power, J. F. Conroy, P. M. Norris, and J. P. Landers, "Toward a microchip-based solid-phase extraction method for isolation of nucleic acids," *Electrophoresis*, vol. 23, pp. 727-733, 2002.

[13] T. E. F. Molden, I. Kraus, P. Karlsen, M. Rabone, T. Nordstrom, P. Gronn, M. Oye, S. Hovland, and B. Hagmar, "A high throughput real-time assay for detection of HPV-RNA - a study of 4589 cervical specimens", Proceedings of 19th International Papillomavirus Conference, Florianópolis, Brazil, 2001, Poster presentation.

[14] R. C. Anderson, X. Su, G. J. Bogdan, and J. Fenton, "A miniature integrated device for automated multistep genetic assays," *Nucleic Acids Res.*, vol. 28, pp. e60, 2000.

[15] Y. Liu, C. B. Rauch, R. L. Stevens, L. R., J. Yang, D. B. Rhine, and P. Grodzinski, "DNA amplification and hybridization assay in integrated plastic monolithic devices," *Anal. Chem.*, vol. 74, pp. 3063-3070, 2002.

[16] J. Compton, "Nucleic acid sequence-based amplification," *Nature*, vol. 350, pp. 91-92, 1991.

[17] B. Deiman, v. A.P., and P. Sillekens, "Characteristics and applications of nucleic acid sequence-based amplification (NASBA)," *Mol. Biotechnol.*, vol. 20, pp. 163-179, 2002.

[18] A. Heim and J. Schumann, "Development and evaluation of nucleic acid sequence based amplification (NASBA) protocol for detection of enterovirus RNA in cerebrospinal fluid samples," *J. Virol Methods*, vol. 103, pp. 101-107, 2002.

[19] R. A. Collins, L. S. Ko, K. L. So, T. Ellis, L. T. Lau, and A. C. Yu, "Detection of highly pathogenic and low pathogenic avian influenza subtype H5 (Eurasian lieage) using NASBA," *J. Virol Methods*, vol. 103, pp. 213-125, 2002.

[20] J. Min and A. J. Baeumner, "Highly sensitive and specific detection of viral Escherochia coli in drinking water," *Anal. Biochem.*, vol. 303, pp. 186-193, 2002.

[21] S. Yates, M. Penning, J. Goudsmit, I. Frantzen, B. van de Weijer, D. van Strijp, and B. van German, "Quantitative detection of hepatitis B virus DNA by real-time nucleic acid sequence-based amplifiation with molecular beacon detection," *J. Clin. Microbiol.*, vol. 39, pp. 3656-3665, 2001.

[22] M. B. Esch, L. E. Locascio, M. J. Tarlov, and R. A. Durst, "Detection of viable Cryptosporidium parvum using DNA-modified liposomes in a microfluidic chip," *Anal. Chem.*, vol. 73, pp. 2952-8, 2001.

[23] I. R. Lauks, "Microfabricated biosensors and microanalytical systems for blood analysis," *Accounts of Chemical Research*, vol. 31, pp. 317-324, 1998.

Acknowledgments

It's difficult for me to express my thankfulness to everybody, here at the IMT. Of course, it was not easy to make the devices working in the lab (at the beginning I had a particular affection for high voltage short circuits), but I'm sure that the four years spent in Neuchâtel will remain in my mind as a nice and enriching experience for both the personal and the professional point of view.

First of all, I would like to thank Prof. Nico de Rooij, who gave me the possibility to work here although I did not have an engineering degree. He relied on me and encouraged me with my work. He also enables me to present my results at prestigious conferences of the microtechnological field around the world. Thank you for these opportunities that I enjoyed a lot.

Although Prof. Nico de Rooij was officially responsible for me, it was Dr. Elisabeth Verpoorte, who contacted me in August 1998 and followed me during my PhD. I would like to express to her my gratitude for her help and her support during these four years. I have learnt a lot from her, from writing a manuscript to how to deal with the Thanksgiving turkey. Thanks a lot, Sabeth, for the enthusiasm you put in all the things the μTAS group did and will go on doing. You made of your students not only a wonderful group of colleagues but also friends.

Thanks to the postdocs in Sabeth's team: Karl, Antoine, Jean-Christophe and Sander, the PhD students: Vincent, Jan, Arash, Gian-Luca, Roos, Alexandra,

and the visitors: Takayuki, Bruce, Mitra, Nathan. With them I'll not forget their families and partners. I would also like to acknowledge the "external" people involved in the projects I worked on: Stephanie, Fiona, Ken, Britta and their supervisors or collaborators, Prof. Dändliker (IMT), Dr. Djordjevic (Novartis Pharma) and Dr. Roberts (Nestlé).

Special thanks go to Peter, Olivier, Milena and Jean-Charles, who were my references for the personal, and as well as the chemical or technological problems. Many thanks to my ex-colleagues Laurent, Benny, Gregor, Marco, Sylvan, Patrick, Pierre, Vincent, Cornel, Eva, Cynthia, Florence, and Danick, Philippe, Quyen, Gaspar, Raphael, Schahrazede, Laure, Thomas, Giovanni, Teru, Andreas, Gio, Fernando, Patrick C., Michael, Sebastian, Vincent, Luca, Patrick W., Willy, Urs, Marc, Bart, who are still in the Samlab group. A particular thought goes to my office colleagues: Sylvan, Philippe, Lutz, Edith, Sabina and Maurizio. This last was so kind to help me with the editing of this thesis. Grazie Mau. The technical staff has also to be mentioned for their irreplaceable work: Gianni, Clairon, Sylviane, José, Edith, Pierre-André and Nicole. Many thanks also to the service of nanoscopy and microscopy of IMT, Mireille and M. Dadras, for the nice and explicit pictures I got of my channels. Thanks also to the secretaries, Magrit and Florence, for their availability and Claudio, who was always ready to solve my bizarre informatic problems.

Grazie ai miei genitori, che per quattro anni mi hanno chiamato per telefono quasi ogni giorno. Grazie perchè avete accettato le mie scelte e siete stati sempre pronti a venirmi a prendere alla stazione di Gallarate per portarmi a casa. Thanks to my friends, in particular Monica, Viviana, Marina, Sabrina, Isabella, Romo and Paolo, who kept me up date of what was going on in Dairago and in their life by mail, e-mail and visiting me in Neuchâtel.

Finally, I'd like to infinitely thank my boyfriend, Pierangelo, who patiently followed my staying here. He supported me and our wonderful relation, which grows with time despite of the four mountains so often between us. Grazie di tutto.

The IMT experience is almost finished. It was great and I'm aware that it will be difficult to find a job like this one with colleagues like you. Thank you very much and good luck to everybody.

Neuchâtel, 20th June, 2002

Appendix 1

ANALYSIS OF LIPOPROTEINS BY CAPILLARY ZONE ELECTROPHORESIS IN MICROFLUIDIC DEVICES: ASSAY DEVELOPMENT AND SURFACE ROUGHNESS MEASUREMENTS

Bruce H. Weiller[a,c] *Laura Ceriotti*[a], *Takayuki Shibata*[a], *Dietrich Rein*[b], *Matthew A. Roberts*[b], *Jan Lichtenberg*[a], *J. Bruce German*[b], *Nico F. de Rooij*[a] *and Elisabeth Verpoorte*[a]

[a]Institute of Microtechnology, University of Neuchâtel, CH-2007 Neuchâtel, Switzerland
[b]Nestlé Research Center, Vers-Chez-les-Blanc, CH-1000 Lausanne 26, Switzerland
[c]Permanent address: The Aerospace Corporation, PO Box 92957 / M2-248, Los Angeles, 90009 CA, USA

ABSTRACT

The development of a new assay for lipoproteins by capillary electrophoresis in fused-silica capillaries and in glass microdevices is described in this paper. The separation of low-density (LDL) and high density (HDL) lipoproteins by capillary zone electrophoresis is demonstrated in fused-silica capillaries with both UV absorption and laser-induced fluorescence (LIF) detection. This separation was accomplished using tricine buffer (pH 9.0) with methylglucamine added as a dynamic coating. With UV detection, LDL eluted as a relatively sharp peak with a migration time of ~11 min and HDL eluted as a

Published in *Anal. Chem.* 2002, Vol 74, Number 7, Pages 1702-1711.

broad peak with a migration time of 12.5 min. Fluorescence detection of lipoproteins stained with NBD-ceramide was used with the same buffer system togive comparable results. Furthermore, fluorescence staining of human serum samples yielded results similar to the fluorescently-stained LDL and HDL fractions showing that this method can be used to quantify lipoproteins in serum samples. The method was also used to detect lipoproteins in glass micro-CE devices. Very similar results were obtained in microdevices although with much faster analysis times, LDL eluted as a sharp peak at ~25 s and HDL as a broad peak at slightly longer time. In addition, higher resolution was obtained on chips. To our knowledge, these results show the first separation and detection of lipoproteins in a microfluidic device using native serum samples. Atomic force microscopy was used to characterize the rms surface roughness (R_q) of microfluidic channels directly. Devices with different surface roughness values were fabricated using two different etchants for Pyrex wafers with a polysilicon masking layer. Using 49% HF the measured roughness is $R_q = 10.9 \pm 1.6$ nm and with buffered HF (NH_4F + HF) the roughness is $R_q = 2.4 \pm 0.7$ nm for. At this level of surface roughness, there is no observable effect on the performance of the devices for this lipoprotein separation.

INTRODUCTION

One of the most important and ubiquitous clinical measurements made today is the quantification of cholesterol in low-density (LDL) and high-density (HDL) lipoproteins from blood. The ratio of cholesterol in LDL ("bad") to that in HDL ("good") is the most commonly accepted indicator of risk for coronary artery disease (1, 2). The currently-used methods for the measurement of LDL and HDL include ultracentifugation (3), selective precipitation, immunoassay (4) and lipoprotein separation by size exclusion chromatography (5). There is interest in developing a microfluidic device for this measurement in order to decrease the measurement time and to reduce the cost and sample volume required (6). In addition, such a device could in principle allow sample preparation and labeling to be performed on chip as well as increased parallel processing of many samples. Both aspects would greatly increase sample throughput in a clinical laboratory (7).

Lipoproteins such as LDL and HDL are complex, nanometer-sized particles consisting of apolipoproteins, cholesterol and a phospholipid monolayer on the surface and an interior consisting of triglycerols, cholesterol and cholesterol-esters (8, 9). The number of apolipoproteins on the surface varies, with one in the case of LDL and as many as eight in the case of HDL. LDL and HDL are defined by their densities in ultracentifugation: 1.006 to 1.063 g/cc for LDL and 1.063 to 1.210 g/cc for HDL (3). This corresponds to particles with size distributions of 20 to 25 nm for LDL and 8 to 12 nm for HDL and apparent molecular weights of 2 to 3 x 10^6 Dalton for LDL and 1.50 to 3.0 x 10^5 Dalton for HDL (10-12). The analysis of lipoproteins is difficult; they are not single molecules but complex particles with distributions of sizes and with a variety of different molecules on their surfaces and interiors. Furthermore the commercial sources of lipoprotein samples are limited and vary in quality. This provides additional challenges in the development of new analytical methods and devices.

An important recent development in the analysis of lipoproteins is the use of capillary electrophoresis (CE) (13-17). The implementation of this powerful analytical technique for this application has been limited by surface adsorption of lipoprotein particles on the walls of fused-silica capillaries. Two approaches for CE of lipoproteins have been used. One approach recently developed by Schmitz et al., uses isotachophoresis in a capillary coated with poly-dimethylsiloxane (PDMS) (14). In this method, serum is stained with a fluorescent dye, either Sudan black or NBD-ceramide, and lipoproteins are separated according to their electrophoretic mobilities at constant velocity. It gives sharp peaks and excellent resolution of all major lipoproteins and subfractions. However, isotachophoresis is a relatively complex technique that requires the use of many spacer compounds (9 in this case) added to the running buffer as well as separate leading and terminating buffers (18-21). A second approach involves the use of a dynamic coating in simple capillary zone electrophoresis (CZE) to reduce the interaction of lipoproteins with the walls. A dynamic coating is of benefit due to the inherent difficulties in applying fixed coatings and their low, long-term reliability. Stocks and Miller showed that, using Tricine buffer with added methylglucamine as a dynamic coating, LDL gives a single sharp peak with UV absorption and that LDL and oxidized LDL can be separated (16). However, they did not analyze for HDL and so the separation of LDL and HDL was not demonstrated with this system. Sodium docecyl sulfate (SDS) has also been used at low concentrations with some success to measure LDL and HDL by CZE; however, lipoprotein particle separation was not demonstrated. Another drawback of this approach is that delipidation and rupture of lipoprotein particles can occur with the use of detergents, which might confuse the interpretation of results (22, 23).

Microfluidic devices for capillary electrophoresis have been very successful for a wide range of bioanalytical measurements (24, 25). The potential of micro-CE devices for clinical applications has been recognized by several groups and some progress in this area has been reported (26). However, there are relatively few reported measurements of samples from human blood using micro-

CE devices. Some notable examples are homogeneous immunoassays for serum theophylline (27, 28) and serum cortisol (29), and the separation of serum proteins in a non-native matrix (7). The analysis of blood samples with microfluidic devices is particularly difficult due to surface adsorption of blood components that causes sample to be lost to the walls and changes the surface properties of the microchannels.

This work describes the development of a CZE separation method for lipoprotein samples from native blood, with subsequent application to a microchip-based assay format. The analytical performance of the method is then compared and contrasted between the two formats. It is shown that LDL and HDL can be separated, using Tricine buffer and methylglucamine as a dynamic coating, and detected by direct UV detection or by fluorescence detection after staining with NBD-ceramide. Similar results were obtained with serum samples showing that the method should work for quantification of lipoproteins in serum samples. Furthermore this method was used to detect and separate LDL and HDL on micro-CE devices using samples from native human blood. To our knowledge, these results represent the first separation and detection of lipoproteins in a microfluidic device. Surface roughness of the microchannels was measured directly by atomic force microscopy for devices produced by two different etching processes. Surface roughness in the range of 2.4 to 10.9 nm has no significant effect on the performance of the devices for this separation.

EXPERIMENTAL SECTION

Lipoprotein fractionation by micro-ultracentrifugation

Fresh blood was collected in tubes without additive and allowed to clot for 20 min at 22°C before separation of serum (1500*g*, 15 min, 4°C). One male borderline-hypercholesterolemic blood donor volunteered throughout the study (total serum cholesterol 5.2-6.2 mmol/L). Five-hundred microliters fresh serum were mixed with 250 µL of Very Low Density Lipoprotein (VLDL) density solution (0.195 M NaCl, d_{20} = 1.006 g/mL). After centrifugation (Sorvall Micro-Ultracentrifuge M150, Sorvall S150AT rotor, Sorvall 2 mL microfuge tubes) at 900 000g and 16°C for 1 h, 250 µL of the VLDL layer was removed using the fine tip of an elongated glass Pasteur pipet. LDL density solution (250 µL, 0.195 M NaCl, 2.44 M NaBr, d_{20} = 1.182 g/mL) was added and mixed. After a second centrifugation (900 000g, 16°C, 2 h), 250 µL of the LDL layer was removed and replaced by 250 µL of the HDL density solution (0.195 M NaCl, 6.37 M NaBr, d_{20} = 1.442 g/mL). After a third centrifugation (900 000g, 16°C, 2.5 h), 250 µL of the HDL layer was removed. Samples were pooled and cholesterol of each fraction was measured on a Cobas Bio (Hoffmann-La Roche, Basel, Switzerland) using a cholesterol reagent according to the manufacturer's specifications (CHOD-PAP, Roche Diagnostics No. 1489232, Rotkreuz, Switzerland).

The lipoprotein fractions were dialyzed as follows to remove excess salt from the ultracentrifugation process: 15 h at 4°C against 1000 volumes of phosphate buffered saline (PBS, Catalog No. 79382, Fluka Chemie GmbH, Switzerland) using dialysis bags with a molecular weight cutoff of 6000-8000 (Spectra/Por, CA, No. 132 665).

Lipoprotein characterization by size exclusion chromatography (SEC)

Lipoprotein characterization was performed using size exclusion HPLC to separate the lipoproteins on the basis of size. The procedure was modified from methods described previously (30, 31). Briefly, 20 µL of diluted serum (1:1 with running buffer) was injected onto a Superose 6HR FPLC column (Pharmacia LKB Biotechnology, Piscataway, NJ). Lipoproteins were eluted with running buffer (Dulbecco's phosphate buffered saline, pH 7.4, 0.02% sodium azide) at a flow rate of 0.6 mL/min (Dionex GP500 HPLC System with an AD20 detector). Lipoprotein cholesterol was determined on-line using a post column reactor. The reactor consisted of a T-connector, through which cholesterol reagent (CHOD-PAP, Roche Diagnostics) was delivered via an HPLC pump (Syknm S2100, Syknm, Gilching, Germany) at a rate of 0.1 mL/min. A mixing coil in a temperature-controlled water bath at 40°C was used to regulate the reaction. The absorbance was recorded at 500 nm and lipoprotein cholesterol ratios were calculated. SCE data was also collected without cholesterol determination using direct UV absorption at 280 nm.

Capillary zone electrophoresis

All experiments were performed on a Beckman MDQ instrument equipped with P/ACE workstation software and a commercial UV absorption or a laser induced fluorescence (LIF) detector. The excitation source was an argon ion laser operating at 488 nm and fluorescence was measured at 520 nm. The detector rise time was set to 1 s and the data rate to 4 Hz. Standard fused-silica capillaries (60 cm, 75 µm internal diameter) were purchased in bulk (Polymicro Technologies, Phoenix, AZ) and cut to size. The instrument was run at 20-28 kV in normal polarity (negative electrode at the detector end). Capillaries were washed with deionized (DI) water, NaOH (0.25 M), DI water and buffer between sample injections. The running buffer was 40 mM Tricine (Sigma) with 40 mM of

methylglucamine (Sigma) and adjusted to pH 9.0 with NaOH. Samples were injected in pressure mode and the capillary temperature was set to 20.0 °C. Sample injection conditions (pressure and temperature) were fixed to keep sample plug lengths to less than 1% of total column length.

Lipoprotein fractions or sera were stained as follows. Lipoprotein solution (25 µL) was diluted with DI water (75 µL, 1:3 v/v) and incubated with a half volume (50 µL) of NBD-ceramide (Molecular Probes, OR) solution (0.5 mg/mL in ethylene glycol: DMSO, 9:1 v/v) for 1.0 min. The solution was then mixed with buffer (250 µL, 3:5 v/v). The final stained solution (400 µL) was used without filtering for both capillary and microchannel electrophoresis.

Microdevices

Two types of microdevices were used, one fabricated in-house and another was purchased commercially (Figure 1). The in-house microdevices (designated IMT-1) were fabricated in 100-mm-diameter borosilicate glass wafers (500 µm thick, Pyrex 7740, Bullen Ultrasonics) using standard photolithographic techniques described previously (32). The structure used had a double tee injector (200 µm long), side channels (10 mm) and an overall separation length of 67.5 mm. Briefly, polysilicon (400 nm thick) was deposited on the wafer by low-pressure chemical vapor deposition at 570 °C in two separate depositions of 200 nm each. This was necessary to prevent pinhole formation in the wet chemical etching procedure. Following silanization with hexamethyldisilazane, positive photoresist (AZ-1518, Clariant) was spun on the wafer, prebaked and exposed using a Cr mask with 10-µm line widths (Delta Mask, Enschede, Netherlands). After development and postbake, reactive ion etching (RIE) was used to transfer the pattern to the polysilicon. The photoresist was stripped in MOS-grade acetone, and the glass was etched in 49% HF (9 µm/min) or buffered HF solution

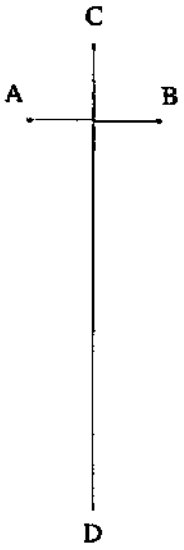

Channel Dimensions	IMT-1	MC-1
AB (mm)	20	10
CD (mm)	67.5	85
Double tee (μm)	200	100
Depth (μm)	20 ± 2	20
Width (μm)	50 ± 4	50

***Figure 1** Diagram of the microfluidic devices. Two types of devices were used in this study, one fabricated in house (IMT-1) and one purchased commercially (MC-1). The dimensions are listed in the table above. The double tee length is the offset between ports A and B. The distance of ports A, B and C to the intersection are the same. Details on the materials and fabrication methods are provided in the Experimental Section.*

(1 part 49% HF/7 parts 40% NH_4F solution, 0.3 μm/min) to give channel depths of 20 ± 2 μm. Channel depths were confirmed by profilometry (Alphastep). The polysilicon was removed in a KOH bath (40% w/w) at 60 °C for ~5 min. A Pyrex coverplate with diamond-drilled holes (Stecher AG, Thun, Switzerland) was bonded to the etched wafer at a temperature of 650 °C for 5 h (33). Cross-sectional SEM measurement of a sealed channel gave a depth of 18 μm and a width at the top of 42 μm, which is within error of the expected channel dimensions of 18 μm × 46 μm. With the sealed channels there may be some deformation of the top of the channel due to the fusion bonding process. Solution reservoirs were formed in different ways: holes (~ 4-mm i.d.) in a thick (~3 mm)

sheet of PDMS (Sylgard 184, Dow Corning) reversibly sealed onto the cover plate, or by pipette tips or short pieces of tubing glued to the wafer.

The commercial microdevices (Part no. MC-BF4-100TT, Micralyne, Alberta, Canada) were also fabricated in borosilicate glass (Schott Borofloat) and are designated MC-1. These devices were very similar to the IMT-1 devices with a channel depth of 20 μm, a 100-μm-long double tee injector, side channels of 5 mm length and an overall separation length of 85 mm. For these devices, solution reservoirs were formed using a Plexiglas plate (5-mm thick) with 6-mm-diameter holes that was aligned and sealed to the cover plate with Viton o-rings. Atomic force microscopy (AFM) measurements were carried out at the bottom of the etched reservoirs in diced pieces of unbonded wafers using a commercial instrument (Nanoscope) operated in tapping mode. The wafers were run through the same thermal cycle used for bonding to control for annealing from this step.

Micro-CE instrumentation

For micro-CE measurements instrumentation was used similar to that described in an earlier report (33). It consisted of two high-voltage power supplies (HCN 7E-12500, F.u.G. Elektronik, Rosenheim, Germany), high-voltage relays (Gunther, Nurnberg, Germany), data acquisition and control cards (AT-MIO-16-XE-50, PC-DIO-24, National Instruments) were used. Data acquisition and instrument control were accomplished using in-house software written in LabView (National Instruments). Electrical contacts with solutions were made using Pt electrodes. Laser-induced fluorescence (LIF) detection used an Ar^+ laser (Ion Technologies, Salt Lake City, UT) at 488 nm coupled to a fiber optic (200-μm i.d.) for excitation at 45° from the bottom of the wafer. The laser beam was collimated and focused to a ~50 μm spot with glass lenses (l = 8 cm). The fluorescence signal was collected and detected using an inverted microscope with objective (NPL FL, 25×, NA 0.35, Leitz), band-pass filter (Melles-Griot

03FIL004, 514 nm, 10 nm FWHM), pinhole (1-mm diam., Melles Griot) and photomultiplier tube, (Hamamatsu, model H5701-50). To remove high-frequency noise, the acquired signal was filtered with a RC low-pass filter (cut off at 33 Hz) and a numerical algorithm (cut-off at 50 Hz). Typical conditions were as follows: sample injection, 1000 V for 30 s; separation, 4000-5000 V applied to the separation channel with 800-1000 V applied to each arm of the double-tee to prevent leakage of sample into the separation channel. This translates into separation field strengths of 593-741 V/cm. (Here and throughout the paper, all voltages are negative).

For mobility measurements, the current monitoring method was used (34). Diluted buffer (90% with DI) was placed in the sample well and buffer was placed is all other wells. Voltage was applied between sample and buffer waste and then switched to the buffer well and buffer waste. The time to clear the channel was measured by monitoring the current. For 40 mM Tricine with 40 mM methylglucamine at pH 9.0, the measured mobility in the IMT-1 device is $\mu_{eof} = 3.9 \times 10^{-4}$ cm^2/Vs.

RESULTS AND DISCUSSION

Lipoprotein fractionation and characterization

The data from size exclusion chromatography of LDL and HDL fractions are shown in Figure 2. The fractions were prepared by ultracentrifugation as described in the Experimental Section and were dialyzed against PBS overnight. The traces show the retention times on a Superose 6HR column with absorbance detection of derivatized cholesterol at 500 nm. Cholesterol was derivatized in a post column reactor with cholesterol reagent as described in the Experimental Section. Panel a shows the data for the HDL fraction and panel b shows the data for the LDL fraction. The large peak at later time in Figure 2a is HDL and the

smaller peak is a small amount of LDL contamination. The fractional peak areas are 5.9 and 94.1 % for LDL and HDL respectively (Table 1). Since the method relies on sequential ultracentrifugation and manual pipetting in microcentrifuge tubes, it is not uncommon to observe a small amount of contamination from the next lighter fraction. It should be noted that, because the detection is based on cholesterol determination, the peak areas represent relative amounts of cholesterol in the particles but not particle concentrations. In fact, since there is more cholesterol in the LDL particles, the method is more sensitive to LDL and the relative particle number of LDL is smaller than apparent. Given typical weight percents of 45 and 17 % cholesterol, and estimated molecular weights of 2.5×10^6 and 2.65×10^5 g/mol of LDL and HDL respectively (9), the fractional concentrations of LDL and HDL particles are 0.3 and 99.7 %, respectively. For the LDL fraction in Figure 2b, the fractional cholesterol peak areas are 99.7 and 0.3 % and the particle concentrations for LDL and HDL are 93 and 7 %. These data show that, when implemented properly, the ultracentrifugation method used here produces good fractionation of lipoproteins with relatively small amounts of cross contamination.

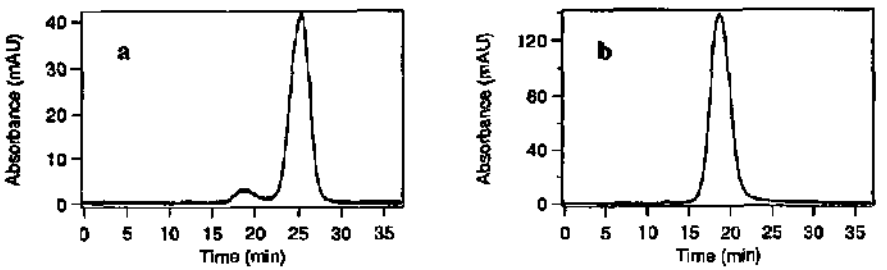

***Figure 2** Size exclusion chromatography of lipoprotein fraction: a) HDL; b) LDL. Fractions were produced by ultracentrifugation of fresh serum samples. The lipoproteins were detected by postcolumn reaction determination of cholesterol by absorbance at 500 nm.*

Table 1 Lipoprotein size exclusion chromatography data.

figure	species	cholesterol peak area	protein peak area	particle concentration
2a	HDL	94.1	-	99.7
	LDL	5.9	-	0.3
2b	HDL	0.3	-	7.0
	LDL	99.7	-	93.0
3a	HDL	4.4	-	53.7
	LDL	93.1	-	45.5
	VLDL	2.5	-	0.8
3b	HDL	51.8	-	96.4
	LDL	46.6	-	3.5
	VLDL	1.6	-	0.1
3c	HDL	-	81.2	95.2
	LDL	-	16.6	4.4
	VLDL	-	1.9	0.3

Similar data from LDL and HDL fractions that are not as well separated are shown in Figure 3. Panel a shows the LDL fraction and panel b shows the HDL fraction; both are cholesterol measurements as in Figure 2. In both traces, three peaks are observed corresponding to VLDL, LDL and HDL cholesterol, respectively. For the LDL fraction, the fractional peak areas are 2.5, 93.1 and 4.4 % for VLDL, LDL and HDL respectively, with corresponding fractional concentrations of 0.8, 45.5 and 53.7 %. The HDL fraction shown in Figure 3b is contaminated with a considerable amount of LDL. There are three peaks corresponding again to VLDL, LDL and HDL cholesterol with fractional peak areas of 1.6, 46.6, and 51.8 % and relative particle concentrations of 0.1, 3.5, and 96.4 %, respectively. Again contamination from the lighter fraction is due to manual pipetting. It should be noted that these data were obtained before the fractionation procedure was optimized. Also shown for comparison is data for the same samples and column without cholesterol derivatization but with direct UV

absorption detection at 280 nm (Figure 3c). There are also three peaks with the same elution times but now the fractional peak areas are 1.9, 16.6 and 81.2 % for VLDL, LDL, and HDL, respectively. Assuming UV absorption at 280 nm is mainly due to aromatic amino acids of the apolipoproteins and assuming 8, 22 and 47% protein in VLDL, LDL, and HDL, we can compare Figures 3b and 3c. Calculating particle distribution starting from cholesterol or protein measurements yields similar particle ratios, 0.1 versus 0.3%, 3.5 vs. 4.4% and 96.4 versus 95.2%, for VLDL, LDL and HDL respectively (Table 1). This is relevant to the CZE measurements with UV detection described below.

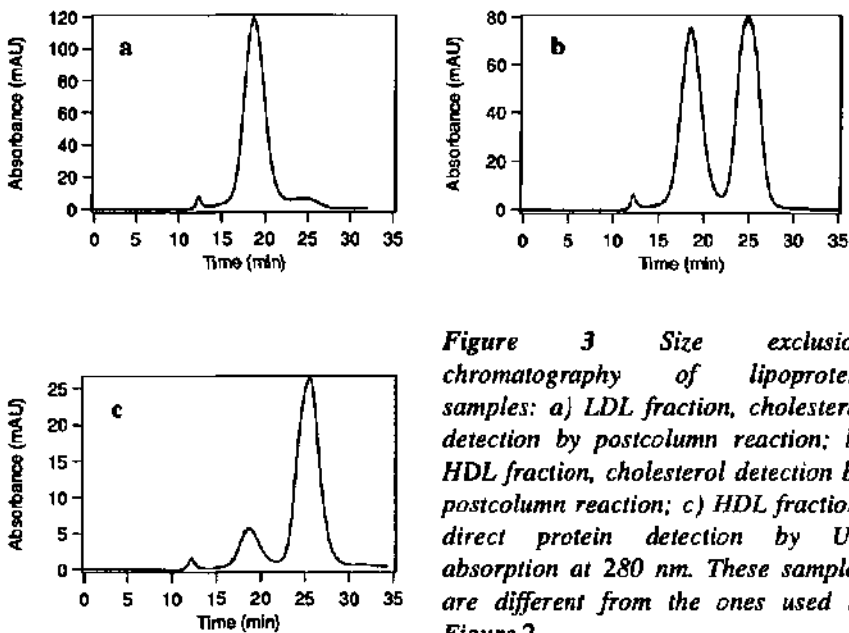

Figure 3 Size exclusion chromatography of lipoprotein samples: a) LDL fraction, cholesterol detection by postcolumn reaction; b) HDL fraction, cholesterol detection by postcolumn reaction; c) HDL fraction, direct protein detection by UV absorption at 280 nm. These samples are different from the ones used in Figure 2.

CZE separation of LDL and HDL

The CZE trace obtained with UV absorption from LDL and HDL fractions and mixtures is shown in Figure 4. The conditions were chosen to be similar to that presented by Stocks and Miller (16); the buffer was 40 mM Tricine (pH 9.0) with methylglucamine at 40 mM with a separation voltage of 20 kV in normal polarity with a 75-μm-diameter capillary. The lipoprotein sample (undialyzed) was diluted with water (1:5 v/v) and then with buffer (3:5 v/v). Figure 4a shows the LDL fraction, Figure 4b shows the HDL fraction, and Figure 4c shows a 1:1 mixture (v/v) of the two. The LDL peak observed is similar in migration time and peak shape as that obtained by Stocks and Miller. In that study, they observed a peak for LDL at 9.2 min with a width of 0.1 min, ($N = 4.7 \times 10^4$, HETP = 11 μm, L_{eff} = 50 cm) while we observe a peak at ~11.5 min with a width of 0.3 min ($N = 8.1 \times 10^3$, HETP = 62 μm, L_{eff} = 50 cm) (35). The fractions used for this experiment are the same ones used for the data in Figure 3. There is a small amount of HDL in the LDL fraction, which corresponds to the small broad peak after the LDL peak. The center trace shows the HDL fraction as a later broad peak with migration time of 12.5 min and a width of 1.4 min ($N = 440$, L_{eff} = 50 cm). Finally, Figure 4c shows a mixture of LDL and HDL (1:1).

The intensities and positions of the peaks in the electropherogram confirm the assignment to LDL and HDL. First, when these fractions are mixed, there are no new peaks; therefore all components elute as these two peaks. This removes any doubt that may arise due to variations in absolute migration times. Second, the intensities of the peaks are in accord with expectations from the volume ratios and the intensities in the separate traces. For example, for the sharp peak, the expected peak height is 0.12 and the measured height is 0.13. For the broad peak the expected height is 0.30 and the measured height is 0.24. While there are other components in the sample, all of the major species that absorb at 214 nm elute as these two peaks.

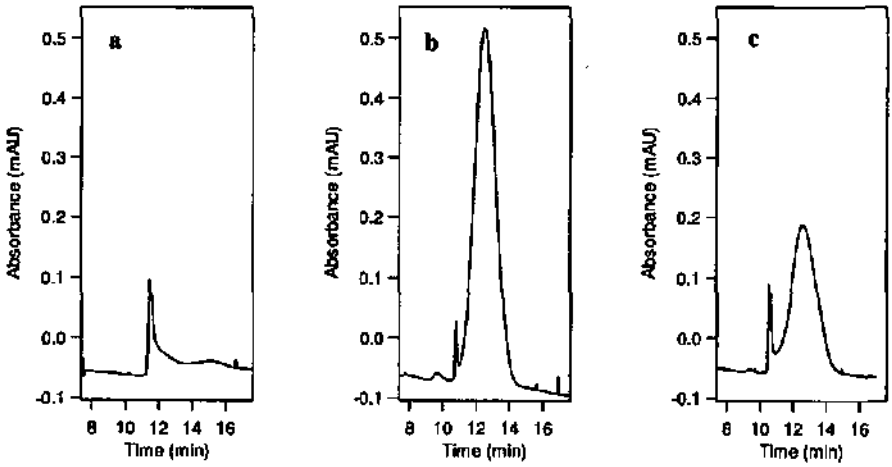

***Figure 4** Separation of LDL and HDL by CZE and detection by UV absorbance. (a) LDL; (b) HDL; (c) 1:1 mixture of HDL and LDL. The detection is at 214 nm, and the separation conditions were as follows: 333 V/cm, L_{eff} = 50 cm, 40 mM Tricine, 40 mM methylglucamine, pH 9, and 75-μm- i.d. fused-silica capillary.*

The relative peak shapes for LDL and HDL are interesting to consider. LDL elutes as a relatively sharp peak whereas HDL elutes as a broad peak. There are two primary factors affecting the peak width of these species, size distribution and particle homogeneity. Both lipoproteins consist of a distribution of particle sizes, 20-25 nm for LDL and 8-12 nm for HDL, as measured by electron microscopy (8). Therefore, the distribution of sizes for HDL is almost twice as broad as for LDL. Data on the capillary electrophoresis of liposome particles, a related chemical system, have been presented (36). For a broad distribution of liposome sizes, 355 ± 210 nm, the observed peak width with UV absorption was quite broad, 0.7 min with a migration time of 5.5 min. Interestingly, the peak width appears to correlate with the size distribution as measured by laser light scattering. For the case of lipoproteins, the size distribution of particles should also affect the peak width and a broader peak for HDL is expected. In addition to the size distribution, the width of the lipoprotein peaks could also be affected by

the number of apolipoproteins on the surface; HDL has many more than LDL. This could lead to greater range of electrophoretic mobilities for HDL compared to LDL, and the combination of these factors should give a much greater peak width for HDL compared to LDL as observed.

The electropherograms for LDL and HDL with fluorescent detection are shown in Figure 5. The LDL and HDL fractions were dialyzed overnight against PBS and were stained with NBD-ceramide as described in the Experimental Section. The voltage was 20 kV and pressure-assisted injection was used. As Figure 5a shows, fluorescently-stained LDL (LDL*) elutes as a sharp peak with migration time of 10.00 min with a width of 0.12 min ($N = 3.9 \times 10^4$, HETP = 13 μm, L_{eff} = 50 cm). (Here we use the superscript* to denote fluorescently stained lipoproteins). Figure 5b shows that fluorescently stained HDL (HDL*) elutes as a broad peak with a migration time of ~10.8 min. The HDL* peak is typically not as symmetric as with the UV absorption detection (Figure 4), and there are typically some features at the trailing edge that could be an indication of a small amount of differentiation in the staining process. It should also be noted that the migration times for labeled lipoproteins detected by LIF are significantly different from the unlabeled ones detected by UV absorption. This is probably due to the NBD-ceramide stain, which causes a chemical modification of the lipoprotein particles.

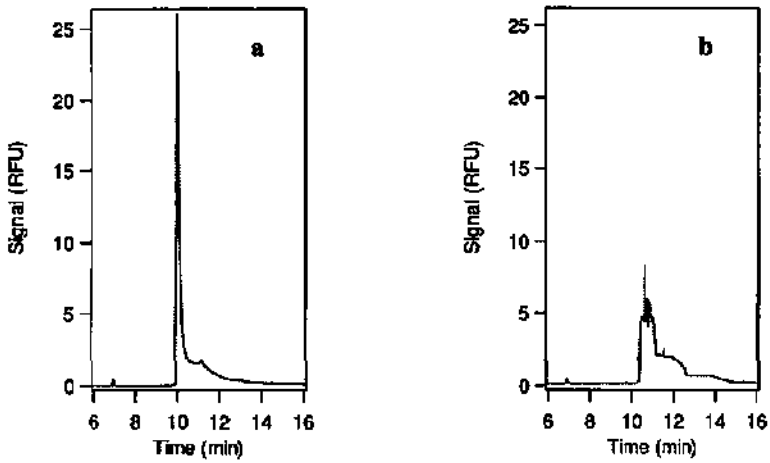

***Figure 5** CE peaks for LDL and HDL with fluorescent detection: a) LDL; b) HDL. Each fraction was prepared as described in the Experimental Section and was stained with NBD-ceramide. Detection was LIF with excitation at 488 nm and detection at 520 nm. The separation conditions were as follows: 333 V/cm, L_{eff} = 50 cm, 40 mM Tricine, 40 mM Methylglucamine, pH 9.0, and 75-μm-i.d. fused-silica capillary.*

Shown in Figure 6 are CZE data for mixtures of LDL and HDL using fluorescent staining for the same samples in Figure 5. Mixtures with HDL:LDL ratios of 2:1, 1:2 and 1:1 (v/v) are shown in Figure 6a-c, respectively. The mixtures were prepared prior to staining. It is worthwhile to compare the ratio of peak areas for the LDL* peak with those expected from the volume ratios. When the LDL* peak areas are normalized with respect to the LDL* peak in the 1:1 mixture, the relative LDL* peak areas for the 2:1 and 1:2 mixtures are 1.50 and 0.72, respectively, in agreement with the expected values of 1.34 and 0.66. Peak areas were integrated using a estimated linear cutoff for the peak separation. This does result in significant error for the peak areas. In any event, the data clearly shows that LDL and HDL can be separated using NBD staining with this buffer system in simple CZE (37).

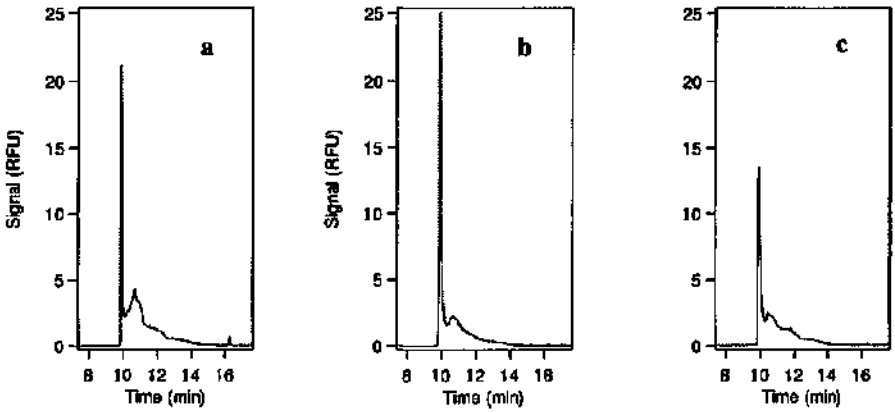

Figure 6 Electropherograms of mixtures of HDL and LDL with fluorescence detection. a) HDL:LDL = 2:1; b) HDL:LDL = 1:2; c) HDL:LDL = 1:1. The mixtures were prepared before staining. The separation conditions were as follows: 333 V/cm, L_{eff} = 50 cm, 40 mM Tricine, 40 mM methylglucamine, pH 9.0, and 75-μm-i.d. fused-silica capillary.

CZE data for a serum sample that was stained with the same procedure as with the lipoprotein fractions is shown in Figure 7. Significantly, a sharp early peak and a broad later peak are observed that are very similar to the peaks observed for LDL and HDL separately. Higher voltage was used for this data (28 kV), which is partly responsible for the shorter migration times and for the increased resolution. However, the migration times do not correlate as expected with field strength. It is possible that other components in the serum could influence the mobility of the lipoprotein particles. While the assignment of these peaks is not conclusive, these data suggest that it is possible to use this simple method to separate and quantify lipoproteins in serum samples. It should be noted that NBD-ceramide is a lipophylic dye and will specifically stain lipoproteins over other components of serum (technical literature, Molecular Probe, Inc.). For example, separate experiments have confirmed that IgG is not detectable with this staining procedure (38).

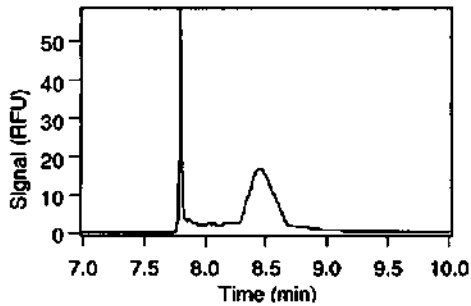

***Figure 7** Electropherogram of fluorescently stained serum. Serum was prepared as described in the Experimental Section and was stained with the same method used for the lipoprotein fractions. The separation conditions were: 467 V/cm, L_{ef} = 50 cm, 40 mM Tricine, 40 mM methylglucamine, pH 9.0, and 75-μm-i.d. fused-silica capillary.*

Integrated capillary zone electrophoresis

To verify that the procedures and instrumentation with the chips give reliable separations and good detection sensitivity, a standard control mixture of amino acids was used. Typically a mixture of FITC-labeled arginine (arg), serine (ser), glycine (gly), and phenylalanine (phe), each at 120 nM concentration was used, and labeling was carried out using the procedure described in the literature (39). The injection and separation conditions were as described in the Experimental Section. The resulting electropherograms are qualititatively similar to those presented in the literature (33, 39). For the unreacted FITC peak, which is at a concentration of 500 nM, the calculated signal-to-noise ratio is SNR = 83 and N = 1.2×10^4 theoretical plates. The effective separation length is 4.2 cm, which gives 3.0×10^5 plates/m or a plate height (HETP) of 3.4 μm. From these data a minimum detectable concentration of 20 nM (SNR = 3) is calculated and was confirmed by dilution experiments. Prior to every run with the microdevices, this mixture was run to confirm chip condition and instrumental performance.

The results for LDL and HDL samples using the IMT-I chips are shown in Figure 8. The lipoprotein samples were prepared and stained using the same

procedure as for the capillary column data. The LDL fraction is shown in Figure 8a, the HDL fraction is shown Figure 8b and a 1:1 mixture in shown in Figure 8c. Comparing the data in Figure 8 to the capillary column data shown in Figure 5 and Figure 6, good agreement is observed. The same qualitative peak shapes for LDL and HDL are observed, with a sharp early peak for LDL and broad later peak for HDL. The respective migration times measured for LDL and HDL are much shorter on chip than in columns with 24.6 and 27.6 s on chip versus 11.5 and 12 min in columns. The calculated theoretical plates for the LDL and HDL peaks are 2.9×10^4 and 1.3×10^3, respectively, in the chips. With the effective column length of 4.2 cm, these convert to plate heights of 1.4 and 33 μm for LDL and HDL, respectively. Recall that for LDL* in capillary column electrophoresis, the plate height was 13 μm at a field strength of 333 V/cm. Assuming a linear relationship between field strength and efficiency, the calculated plate height for the chip at 333 V/cm is 3 μm. Therefore, the efficiency is higher on chip even when the greater separation voltage is accounted for.

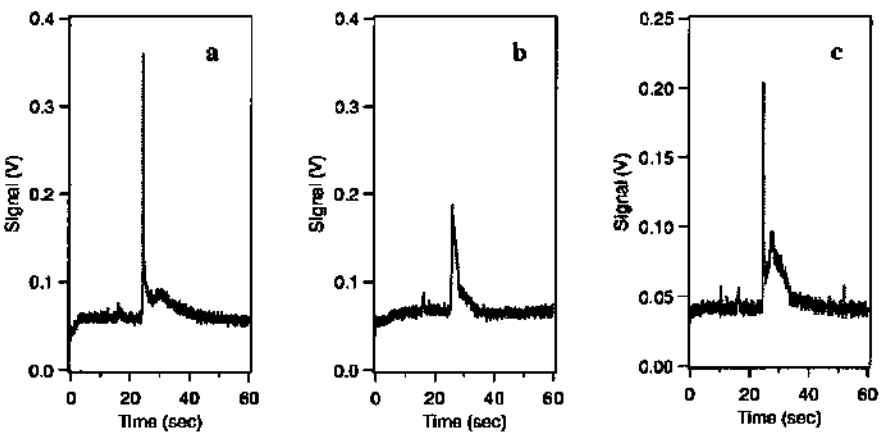

***Figure 8** Electropherograms of lipoproteins on chip. a) LDL; b) HDL; c) HDL:LDL = 1:1. The separation conditions were as follows: 714 V/cm, L_{eff} = 42 mm, 40 mM Tricine, 40 mM methylglucamine, pH 9.0. The chip used was IMT-1.*

The SNR for the data from IMT-1 chips is considerably lower than for the columns. For the LDL peak in Figure 6a, the SNR = 9.2×10^3 (based on peak-to-peak values), whereas for the LDL peak in Figure 8a, the SNR = 22, or ~ 420 times smaller. There are many instrumental factors that will affect the SNR such as relative peak width, detection bandwidth, collection optics, laser power, probe volume, and scattered light. Undoubtedly our instrumentation could be improved with respect to the SNR. However, our primary interest is the performance of the chip with respect to the capillary. A factor that is of concern is the sample recovery on chips relative to capillaries.

Sample recovery in chips could be lower than in fused-silica capillaries if there is increased surface adsorption. It is well known that proteins and other biomolecules readily adsorb to surfaces. Lipoprotein particles are known to adsorb to fused-silica surfaces quite readily. For example, without added methylglucamine, surface adsorption of LDL to fused-silica capillaries is so problematic that no usable peaks in CZE are observed (16). In addition, LDL has been observed to have a greater affinity for untreated fused-silica over silanized fused-silica surfaces (40, 41). The surface-area-to-volume ratio of the microfluidic channels is much greater than for the 75-μm-diameter capillaries. If a surface adsorption process does occur, then it could be enhanced in microfluidic channels.

Enhancement of surface adsorption processes is possible if the chips have rougher surfaces. If surface adsorption does occur, it could greatly affected by an increased number of surface adsorption sites. The surface roughness of fused-silica capillaries has been measured by AFM and in general they are very smooth with root-mean-square (rms) surface roughness values (R_q) of $R_q = 0.42 \pm 0.06$ nm (42). The microfluidic channels are produced by an etching process, which is expected to give a rougher surface. In order to determine if this is a potential problem in the microdevices, the surface roughness of the microfluidic channels was measured directly with AFM.

Surface roughness measurements of microdevices

AFM data for etched Pyrex microchannels is shown in Figure 9a. The data were obtained at the bottom of a channel produced by the process described in the Experimental Section. The measurement was performed in the region of the reservoir in a small piece cut from a processed but unbonded wafer. The wafer was subjected to the same thermal cycle as used for bonding in order to eliminate annealing effects. The data for unetched Pyrex were obtained in the region that was masked by polysilicon. Three separate measurements for unetched and four separate measurements for the etched piece were obtained. The mean rms values ($R_q \pm \sigma$) are for unetched, $R_q = 1.0 \pm 0.2$ nm, and for etched: $R_q = 10.9 \pm 1.6$ nm. Compared with the fused-silica capillaries, the surface roughness of the etched Pyrex channels is ~26 times rougher. Therefore, it is probable that the surface area of these microchannels is significantly greater than the fused silica capillary columns.

To determine whether reduced surface roughness can improve the micro-CZE of lipoproteins, devices were produced with smoother surfaces. As described in the Experimental Section, by simply changing the etchant from 49% HF to buffered HF, we find that smoother surfaces are produced.

All other process steps were kept the same. AFM measurements of the resulting channels etched for 660 min to a depth of 20.3 μm are shown in Figure 9b. The measured surface roughness is $R_q = 2.4 \pm 0.7$ nm for a three-fold reduction in surface roughness.

We have also examined commercially available chips (MC-1) with design and materials similar to that of the IMT-1 chips (Figure 1). They consist of a double-tee injector with length of 100 μm, channel depth of 20 μm, side channels 5 mm long, and overall separation channel length of 85 mm. These devices are also fabricated from a borosilicate glass, Borofloat (43), which is very similar to

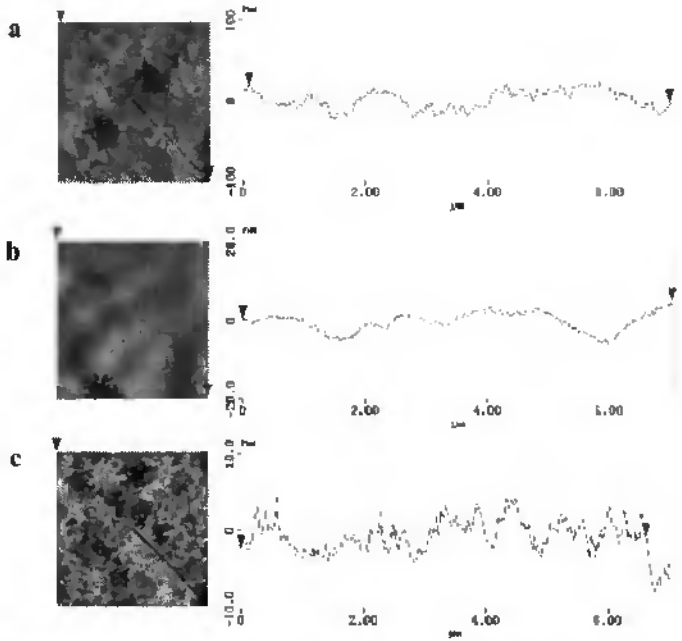

***Figure 9** AFM data for etched microfluidic channels. a) Fabricated from Pyrex 7740 and etched with 49% HF. The y-axis is 200 nm full scale, and the mean rms surface roughness is R_q = 10.9 ± 1.6 nm. b) Fabricated from Pyrex 7740 and etched with buffered HF. The y-axis is 40 nm full scale and R_q = 3.1 ± 0.3 nm. c) Fabricated from Borofloat and etched with HNO/HF/H_2O. The y-axis is 20 nm full scale and R_q = 2.1 ± 0.2 nm. In each case, the data were taken in three places at the bottom of etched channels from unsealed witness plates. For the Pyrex wafers, each was annealed at 650 °C for 5 h to simulate the fusion bonding step.*

Pyrex (44) in chemical composition. A slightly different fabrication process was used (45, 46).

AFM measurements for the etched channels in the MC-1 devices are shown in Figure 9e. The data were taken in the same way as in Figure 9a and 9b for the IMT-1 devices. The unetched data shows a surface roughness of 0.5 ± 0.1 nm, and the etched data shows a surface roughness of 2.1 ± 0.2 nm. The underlying causes for the resulting surface roughness values are related to the

etchant used as well as the other process steps that can affect the surface and bulk properties of the material. We hope to address these issues in a future publication.

Effect of surface roughness on CZE of lipoproteins in microchannels

Using the smooth IMT-1 chips fabricated with buffered HF, we did not observe any significant difference between the two types of chips for this separation. We examined the performance of the chips with respect to sample throughput and efficiency. Both LDL and HDL were examined using fractionated samples from the same batch but stained on different days. The resulting data is very similar to that presented in Figure 8 with minor differences that are within experimental and systematic errors. It should be noted that this does not rule out the effects of surface roughness on CE performance for other systems. We hope to explore this in future studies with a more ideal system than lipoproteins.

The MC-1 chips result in data that are significantly different from that obtained with the IMT-1 chips. Data for the MC-1 chip are shown in Figure 10 for a HDL fraction with a significant LDL contamination. The samples were prepared and stained the same way as for the data in Figure 8 and the detection parameters were also identical. Note the qualitative similarity to the capillary column data in Figure 4 and Figure 6. The difference between this data and that from the IMT-1 devices is also notable with respect to the SNR and peak area for the same detection sensitivity and sample preparation conditions. It should be noted that the injection plug for the MC-1 chips is shorter by a factor of 2. We have already ruled out the effects of surface roughness from the measurements with the IMT-1 chips. Therefore, the differences between the MC-1 and IMT-1 must be attributed to factors other than surface roughness.

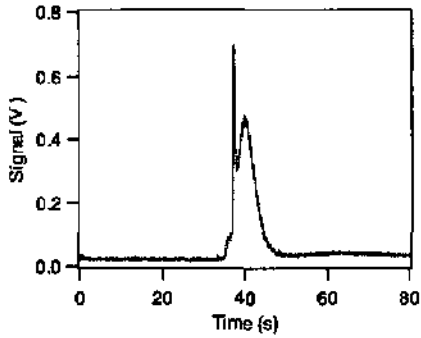

***Figure 10** Electropherograms of an HDL fraction on the MC-1 chip. HDL fraction with a small amount of LDL contamination. The sharp peak is LDL and the broad peak is assigned to HDL. The separation conditions were as follows: 706 V/cm, L_{eff} = 60 mm, 40 mM Tricine, 40 mM methylglucamine, pH 9.0.*

The major difference between the MC-1 chips and the IMT-1 chips is the channel layout as shown in Figure 1. The MC-1 chip has sidearms that are half as long as the IMT-1 chips. It may be that surface adsroption of lipoproteins in the side arms is significant and the longer side arms in the IMT-1 chips enhance this process. However, the short side arms make the MC-1 chips very susceptible to pressure effects due to differences in liquid levels and surface tension developed in the small diameter fluid reservoirs in the cover plates (47). Related issues with these devices have been reported (48). Pressure effects could influence the amount of sample that is injected with these devices. However, control experiments with fluorescein dye do not give similar results but are completely consistent with the volume of sample injected as determined by the double-tee length. Further experiments are required to determine the exact cause of this observation.

CONCLUSIONS

A new assay for lipoproteins has been developed based on the use capillary zone electrophoresis using Tricine buffer, methylglucamine as a dynamic coating, fluorescence staining with NBD-ceramide, and laser induced fluorescence detection. Data from fused-silica capillary columns demonstrate the viability of the method to separate LDL and HDL from native serum samples.

The assay has been shown to function well in the glass microchip format using native serum samples. Analysis times are 26 times shorter on chip than in capillary columns and the resolution is higher as well. Height equivalent theoretical plates for LDL samples have been observed as small as 1.4 μm in chips.

The surface roughness of the microfluidic channels was measured directly and no effect on chip performance was observed in this case. Channels with surface roughness of R_q = 10.9 ± 1.6 nm and R_q = 2.4 ± 0.7 nm were produced with two etchants. Rougher surfaces result from concentrated HF, while the smoother surfaces are produced with buffered HF solution. Over this range of surface roughness, no effect could be observed on the sample recovery or efficiency of the chips for LDL or HDL samples.

Acknowledgements

The very capable assistance of the technical staff at the Institute of Microtechnology is gratefully appreciated. Assistance from Vincent Linder with the design of the high voltage power supply is acknowledged. Financial support was received from the Swiss government under Grant CTI–3969.2. B.H.W. acknowledges support from The Aerospace Corp. during a foreign assignment at the Institute of Microtechnology.

REFERENCES

(1) Kannel, W. B. *J. Atheroscler. Thromb.* 2000, *6*, 60-66.

(2) Williams, S. E.; Matts, J. P. *Atherosclerosis* 2001, *154*, 221-227.

(3) Havel, R. J.; Eder, H. A.; Bragdon, J. H. *J. Clin. Invest.* 1955, *34*, 1345-1353.

(4) Friedewald, W. T.; Levy, R. I.; Fredrickson, D. S. *Clin.Chem.* 1972, *18*, 499-502.

(5) Okazaki, M.; Ohno, Y.; Hara, I. *J. Biochem.* 1981, *89*, 879-887.

(6) Roberts, M. A.; Geiger, W.; German, J. B. *J. Clin. Nutr.* 2000, *71*, 434-437.

(7) Colyer, C. L.; Tang, T.; Chiem, N.; Harrison, D. J. *Electrophoresis* 1997, *18*, 1733-1741.

(8) Lehninger, A. L.; Nelson, D. L.; Cox, M. M. *Principles of Biochemistry*; Worth Publishers: New Your, 1993.

(9) Smith, L. C.; Massey, J. B.; Sparrow, J. T.; Gotto, A. M.; Pownall, H. J. In *Supramolecular structure and function*; Pifat, G., Herak, J.N., Eds.; Plenum Press: New York, 1983, pp 205-244.

(10) Esterbauer, H.; Waeg, G.; Puhl, H.; Dieder-Rotheneder, M.; Tatzber, F. In *Free radicals and Aging*; Emerit, I., Chance, B., Eds.; Birkhaeuser Verlag: Basel, Switzerland, 1992; Vol. 145-157.

(11) Rudel, L. L.; Marzetta, C. A.; Johnson, F. L. *Methods Enzymol.* 1986, *129*, 45-57.

(12) Rye, K. A.; Clay, M. A.; Barter, P. *Atherosclerosis* 1999, *145*, 227-238.

(13) Schmitz, G.; Möllers, C. *Electrophoresis* 1994, *15*, 31-9.

(14) Schmitz, G.; Möllers, C.; Richter, V. *Electrophoresis* 1997, *18*, 1807-13.

(15) Bottcher, A.; Shchlosser, J.; Kronenberg, F.; Dieplinger, H.; Knipping, G.; Lackner, K. J.; Schmitz, G. *J. Lipid Res.* 2000, *41*, 905-915.

(16) Stocks, J.; Miller, N. E. *J Lipid Res.* 1998, *39*, 1305-9.

(17) Stocks, J.; Nanjee, M. N.; Miller, N. E. *J. Lipid Res.* 1998, *39*, 218-227.

(18) Bittolo-Bon, G.; Cazzolato, G. *J Lipid Res.* 1999, *40*, 170-7.

(19) Schlenck, A.; Herbeth, B.; Siest, G.; Visvikis, S. *J Lipid Res.* 1999, *40*, 2125-33.

(20) Zorn, U.; Wolf, C. F.; Wennauer, R.; Bachem, M. G.; a., G. *Electrophoresis* 1999, *20*, 1619-1626.

(21) Inano, K.; Tezuka, S.; Miida, T.; Okada, M. *Ann. Clin. Biochem* 2000, *37*, 708-716.

(22) Macfarlane, R. D.; Bondarenko, P. V.; Cockrill, S. L.; Cruzado, I. D.; Koss, W.; McNeal, C. J.; Spickerman, A. M.; Watkins, L. K. *Electrophoresis* 1997, *18*, 1796-806.

(23) Cruzado, I. D.; Hu, A. Z.; Macfarlane, R. D. *Journal of Capillary Electrophoresis* 1996, *3*, 25-9.

(24) Effenhauser, C. S.; Bruin, G. J. M.; Paulus, A. *Electrophoresis* 1997, *18*, 2203-2213.

(25) Bruin, G. J. M. *Electrophoresis* 2000, *21*, 3931-3951.

(26) von Heeren, F.; Verpoorte, E.; Manz, A.; Thormann, W. *Analytical Chemistry* 1996, *68*, 2044-2053.

(27) Chiem, N. H.; Harrison, D. J. *Clinical Chemistry* 1998, *44*, 591-598.

(28) Chiem, N.; Harrison, D. J. *Analytical Chemistry* 1997, *69*, 373-378.

(29) Koutny, L. B.; Schmalzing, D.; Taylor, T. A.; Fuchs, M. *Analytical Chemistry* 1996, *68*, 18-22.

(30) German, B.; Xu, R.; Walzem, R. L. *Nutr. Res.* 1996, *16*, 1239-49.

(31) Kieft, K. A.; Bocan, T. M.; Krause, B. R. *J. Lipid Res.* 1991, *32*, 859-866.

(32) Dodge, A.; Fluri, K.; Verpoorte, E.; de Rooij, N. F. *Analytical Chemistry* 2001, *73*, 3400-3409.

(33) Lichtenberg, J.; Verpoorte, E.; de Rooij, N. F. *Electrophoresis* 2001, *22*, 258-271.

(34) Huang, X. H.; Gordon, M. J.; Zare, R. N. *Analytical Chemistry* 1988, *60*, 1837-1838.

(35) All the peak widths presented are the measured full width at halp-maximum (fwhm). N denotes the number of theoretical plates as calculated by $N = 5.54\ (t/w)^2$, where t is the migration time and w is the peak width.

(36) Roberts, M. A.; LocascioBrown, L.; MacCrehan, W. A.; Durst, R. A. *Analytical Chemistry* 1996, *68*, 3434-3440.

(37) It should be note that we do observe significant variations in migration times from run to run and from sample to sample. We have not been able to determine the exact cause, but it is most likely due to surface modification from sample adsorption and variations in the samples.

(38) Unpublished data, L. Ceriotti and T. Shibata.

(39) Effenhauser, C. S.; Manz, A.; Widmer, H. M. *Analytical Chemistry* 1993, *65*, 2637-2642.

(40) Ho, C.-H.; Hlady, V. *Protein at Interface II: Fundamentals and Applications*; ACS Symposium Series 602: Amarican Chemical Sociaty: Washington, 1995.

(41) Hlady, V.; Ho, C.-H. *Materialwiss. Werkstofftech* 2001, *32*, 185-192.

(42) Kaupp, S.; Wätzing, H. *Electrophoresis* 1999, *20*, 2566-2574.

(43) The composition of Borofloat is: SiO_2 (81%), B_2O_3 (13%), $Na_2O + K_2O$ (4%), and Al_2O_3 (2%). Borofloat has the same chemical composition as Duran, another Schott product, Schott company literature, www.schottglass.com/Duranb1.htm.

(44) The composition of Pyrex is: SiO_2 (81%), B_2O_3 (13%), Na_2O (4%), and Al_2O_3 (2%), Stockdale, B. *J. Assoc. Lab. Autom.* 1999, 4, 35-39.

(45) The MC-1 chips were etched using the mixture of $HF:HNO_3:H_2O$ = 20:14:66 by volume; Glen Fitzpatrick, Micralyne, Inc., personal communication. This etchant is not compatible with the polysilicon mask we use. See ref. 46 for more details on this etchant.

(46) Vossen, J. L.; Kern, W. *Thin Film Processes*; Academic Press: New York, 1978, pp 437.

(47) Fletcher, P. D. I.; Haswell, S. J.; Paunov, V. N. *Analyst* 1999, *124*, 1273-1282.

(48) Crabtree, H. J.; Cheong, B. C. S.; Tilroe, D. A.; Backhouse, C. J. *Analytical Chemistry* 2001, *73*, 4079-4086.

Appendix 2

LOW-DENSITY LIPOPROTEIN ANALYSIS IN MICROCHIP CAPILLARY ELECTROPHORESIS SYSTEMS

Laura Ceriotti[1], *Takayuki Shibata*[1,†], *Britta Folmer*[2], *Bruce H. Weiller*[1,‡], *Matthew A. Roberts*[1], *Nico F. de Rooij*[1], *Elisabeth Verpoorte*[1,*]

[1] Institute of Microtechnology, University of Neuchâtel, Jaquet-Droz 1, CH-2007 Neuchâtel, Switzerland

[2] Nestlé Research Center, Vers-Chez-les-Blanc, CH-1000 Lausanne 26, Switzerland

[†] Present address: Department of Mechanical Engineering, Faculty of Engineering, Ibaraki, University, 4-12-1 Nakanarusawa, Hitachi, Ibaraki 316-8511, JAPAN

[‡]Permanent address: The Aerospace Corporation, P.O. Box 92957 / M2-248, Los Angeles, 90009 CA, USA

ABSTRACT

Due to the mounting evidence for altered lipoprotein and cholesterol-lipoprotein content in several disease states, there has been an increasing interest in analytical methods for lipoprotein profiling for diagnosis. The separation of low- and high-density lipoproteins (LDL and HDL, respectively) has been recently demonstrated using a microchip capillary electrophoresis (CE) system [1]. In contrast to this previous study, the present report demonstrates that LDL analysis can be performed in an uncoated glass microchannel. Moreover, by adding sodium dodecyl sulfate (SDS) to the sample at a concentration well below the critical micellar concentration prior to injection, the LDL peak undergoes a

Published in *Electrophoresis* **2002**, Vol 23, Pages 3615-3622.

focusing effect and exhibits an apparent efficiency of 2.2×10^7 plates/meter. Laser light scattering experiments demonstrate that the low concentration of SDS used does not significantly alter lipoprotein particle size distribution within the time course that the analysis is performed. It is thus hypothesized that the SDS non-disruptively coats LDL particles. The peak sharpening effect, observed only when SDS is added solely to the sample, is probably due to a mobility gradient created between the sample and the running buffer. The chip-based method demonstrated here has the potential for rapid analysis and sensitive detection of different LDL forms of clinical relevance.

INTRODUCTION

Lipoproteins are macromolecular complexes of lipids and proteins held together by hydrophobic and electrostatic forces. The particle core consists of cholesteryl esters and triglycerides, while the surface is made of proteins (apolipoproteins) and phospholipid headgroups. The three main plasma lipoprotein classes are commonly separated by ultracentrifugation and are therefore described according to their densities as high-, low-, and very-low-density lipoproteins (HDL, LDL and VLDL), respectively [2, 3]. Each class plays a critical role in the whole body transport of cholesterol and triglycerides. Disorders in lipoprotein metabolism facilitate the initiation and progression of atherosclerosis and related diseases [4]. Using gradient gel electrophoresis, subclasses of both LDL and HDL have been identified. In particular, LDL particles can be classified into three groups: large LDL particles (diameter > 25.5 nm), small, dense LDL, and an intermediate pattern [5]. Studies have demonstrated that a high concentration of small, dense LDL is associated with an increased risk of coronary heart disease [5-7] and is also correlated to insulin resistance [8]. Moreover, Avogaro et al. also identified more negatively charged LDL (LDL$^-$), which includes oxidized, glycated and degraded LDL forms [9]. These modified forms have a reduced binding affinity for the LDL scavenger receptors and thus escape capture and removal by phagocytic cells, prolonging their residence in the blood plasma. Higher plasma levels of LDL$^-$ have been found in patients with acute myocardial infarction, unstable angina and thrombogenic carotid atherosclerosis [10, 11], suggesting that this LDL group can be used as a potential biomarker of active atherosclerosis. Another abnormal subfraction, apo-E-rich HDL, is also increased in subjects with cholesterol ester transfer protein (CETP) deficiency, and liver diseases [12, 13]. Therefore, it is important for diagnosis of the different lipoproteinaemias to determine not only the lipoprotein classes but also their subclasses.

Capillary electrophoresis (CE) has been demonstrated to be a powerful tool for separation of biological materials. Hu et al. [14] proposed CE as a convenient alternative to immunoassay [15, 16] and SDS-PAGE methods for lipoprotein characterization. In [14], LDL, lipoprotein a (Lp(a)) and its reduced products, apolipoprotein a (apo(a)) and Lp(a'), were separated within minutes on the basis of their different electrophoretic mobilities, using as background electrolyte 50 mM sodium borate (pH 9) containing 20% acetonitrile and 3.5 mM SDS. LDL and HDL peaks were also detected in borate buffer (pH 9.1) containing 0.5 mM SDS [17]. Under other buffer conditions, lipoprotein peaks were detectable only in the presence of very specific buffer additives used to prevent protein-wall interactions [18]. Application of isotachophoresis (ITP) and capillary ITP (cITP) have also resulted in very promising electrophoretic methods for serum protein analysis [19, 20]. Thanks to the high resolution power of this technique, up to fourteen lipoprotein subclasses were detected and pathological cases could be identified [20, 21].

In general, microdevices have been successfully used for rapid and highly efficient separations of proteins, nucleic acids, and drugs. Moreover, multiple channels in parallel and multiple assay steps can be integrated into one single device, allowing high throughput and complex processes in compact, easy-to-handle devices. Dealing with complex matrices such as blood or other natural fluids is still a challenge in microchannels, but encouraging results are emerging [22-25].

Recently, we demonstrated that a CE method could be used to analyze blood lipoprotein in both capillary and microdevice formats [1]. Purified LDL and HDL fractions were first obtained by ultracentrifugation of serum and subsequent dialysis. They were then labeled with NBD-ceramide (a lipophilic fluorescent dye) and separated in a glass microchannel. Because literature reports indicated that use of a dynamic coating was essential to lipoprotein detection by

CE, this chip-based study utilized a buffer containing 40 mM methylglucamine (MG) to prevent lipoprotein adsorption. The optimized separation conditions allowed LDL/HDL detection in purified fractions (on-chip and in a capillary), as well as directly in serum (in a capillary) [1]. The present report demonstrates, however, that LDL and HDL peaks can also be detected in untreated channels, a result which is contrary to conventional wisdom. Moreover, LDL peak efficiencies can be improved dramatically by simply adding SDS to the sample at a concentration of 0.3 mM. No SDS needs to be added to the running buffer. Laser light scattering (LLS) experiments were performed to support the hypothesis that the low SDS concentration used did not disrupt the lipoprotein particle size distributions within the timeframe of the analysis. This paper therefore represents a significant step forward in the use of microsystems for rapid and sensitive serum protein detection, and specifically as diagnostic tools for atherogenic lipoprotein analysis.

EXPERIMENTAL SECTION

Lipoprotein fractionation by micro-ultracentrifugation

Sample preparation has been described previously [1]. Briefly, fresh blood was collected in tubes without additive and allowed to clot for 20 min at 22°C before separation of serum (1500 *g*, 15 min, 4°C). Fresh serum (500 µL) was mixed with 250 µL of a solution having the same density as VLDL (0.195 M NaCl, d_{20} = 1.006 g/mL) in a 2-mL centrifugation tube. After centrifugation (Sorvall Micro-Ultracentrifuge M150, Sorvall S150AT rotor, Sorvall 2-mL microfuge tubes) at 900 000 g and 16°C for 1 h, 250 µL of the VLDL layer was removed using the fine tip of an elongated glass Pasteur pipette. A 250-µL volume of solution having the same density as LDL (0.195 M NaCl + 2.44 M NaBr, d_{20} = 1.182 g/mL) was then added and mixed. After a second centrifugation

(900 000 g, 16°C, 2 h), 250 µL of the LDL layer was removed and replaced by 250 µL of an HDL-density solution (0.195 M NaCl, 6.37 M NaBr, d_{20} = 1.442 g/mL). After a third centrifugation (900 000 g, 16°C, 2.5 h), 250 µL of the HDL layer was removed.

The lipoprotein fractions were dialyzed to remove excess salt from the ultracentrifugation process. This involved dialysis for 15 h at 4°C against 1000 volumes of phosphate-buffered saline, pH 7.2 (PBS, Fluka Chemie GmbH, Switzerland), using dialysis bags with a molecular-weight cutoff of 6 000-8 000 (Spectra/Por). The fractions were then frozen and stored until use.

Sample preparation for micro-CE run

Lipoprotein fractions were stained with a fluorescent dye, 7-nitrobenz-2-oxa-1,3-diazole-ceramide (NBD-ceramide, Molecular Probes, OR) to be detectable by LIF detection when analyzed in a microchannel. 1 mg of NBD-ceramide was dissolved in 200 µL of dimethylsulfoxide (DMSO) (Merck, Darmstadt, Germany) and diluted with 1800 µL of ethylene glycol (Merck) to a final concentration of 0.5 mg/mL of dye. The staining protocol began with the dilution of the lipoprotein solution (25 µL) with deionized (DI) water (75 µL), following by vortexing in the presence of NBD-ceramide solution (50 µL) for 1 min. Buffer (250 µL of 40 mM Tricine, pH 9.1) was added to the solution. For separations performed in the presence of dynamic coating, both background electrolyte (BGE) and sample buffer contained 40 mM or other molarity of methylglucamine (MG) as specified (Sigma, Buchs, Switzerland). For the preparation of samples containing 0.3 mM and 0.6 mM SDS, different volumes of a stock buffer containing 3 mM SDS were added. Tricine and SDS were purchased from Fluka. The final stained sample solution was loaded into the chip reservoirs without filtering and analyzed by CE in microchannels. Solutions were, however, prepared in 0.2 µm filtered buffer, to prevent clogging of channels.

Chip fabrication and layout

Etched glass channels were fabricated in 100 mm diameter borosilicate glass wafers (500 μm thick, Pyrex 7740, Bullen Ultrasonics, Eaton, OH) using photolithographic techniques described previously [1]. Plastic tubes of 3 mm internal diameter and 9 mm length were glued over each hole in the coverplate to serve as fluidic reservoirs. Volumetric micropipettes (Eppendorf AG, Hamburg, Germany) were employed to load the same volume of solution (typically 50 μL) into each reservoir to prevent hydrostatic pressure differences. Before each set of runs, the channels were rinsed with 0.1 M NaOH (0.2 μm prefiltered, CE-grade, Fluka) for 10 min, with DI water for 4 min, and with buffer for another 4 min.

The structure layout consists of a double-T injector (200 μm long), side channels (10 mm long) and a 67.5 mm long separation channel [1]. Shallow reservoirs (1 mm long × 0.5 mm wide × 0.018 mm deep) were also integrated into the layout to facilitate fluid entry into the channels and simplify the alignment of the etched wafer with the coverplate.

Microchip CE experimental conditions

The set-up for microchip CE experiments has been described in a previous paper [1] and it represents the typical LIF detection system used in our laboratory. The sample was typically injected by first applying -2000 V for 90 s between sample and sample waste reservoirs to fill the intersection. -5000 V was then applied to the separation channel to inject the plug. At the same time, -1500 V was maintained at each side arm of the double-T to push back sample from the intersection, thereby preventing leakage of sample into the separation channel. The equivalent separation field strength, E, was typically -740 V/cm.

The electroosmotic flow mobility, μ_{eo}, was calculated from the migration time of BODIPY (Molecular Probes, obtained from Juro Supply, Lucern, Switzerland), used as neutral fluorescent marker, and the separation length. As

expected, in the presence of 40 mM of the organic additive, MG, the μ_{eo} in the microchannel was reduced from 4.2×10^{-4} cm^2/Vs to 3.5×10^{-4} cm^2/Vs for Tricine buffer, pH 9.1.

Laser light scattering (LLS) instrument

The dynamic light scattering experiments were carried out in a 3D-cross correlation light scattering instrument (LS Instruments, Fribourg, Switzerland) using a laser light source with a wavelength of 835 nm. The instrument has been described in detail by Urban et al. [26]. Inverse Laplace transformations were used to calculate the diffusion coefficients of the particles. The particle sizes were then obtained using the Stokes-Einstein equation ($D = kT/(6\pi\eta r)$), where D is the diffusion coefficient, T is temperature, k is the Boltzmann constant, η is viscosity, and r is the radius of the particle. The measurements were performed at 25°C.

Sample preparation for LLS

Three samples were measured in order to determine the effect of NBD and SDS on the lipoprotein particle size. All three samples consisted of lipoprotein (375 µL) in DI water (50 µL), further diluted in 40 mM Tricine buffer (1000 µL). The first sample was analyzed without any additives. NBD-ceramide (375 µL) was added to the second sample. Both NBD-ceramide (375 µL) and 3 mM SDS (200 µL) were added to the third one. The concentration of SDS in the last sample was thus 0.3 mM. Each sample was freshly prepared and measurements made over a 30 min period, starting 1 minute after sample preparation. Increasingly long time intervals between measurements were used, starting with a 1-min interval and ending with a 10 min long interval over the 30 min period. The final analysis was made using the average of the obtained correlation functions.

RESULTS AND DISCUSSION

Effect of dynamic coating on LDL peak

The development of CE for analysis of lipoprotein from native serum samples in a capillary and, for the first time, in a chip-based system was previously reported [1]. The conditions were chosen to be similar to those described by Stocks and Miller [18], where the CE analysis of LDL was performed in a 75-μm capillary using a solution containing 40 mM Tricine buffer (pH 9.0) and 40 mM MG as background electrolyte (BGE). In that study, the organic base, MG, was used as a dynamic coating to prevent protein adsorption to the capillary wall. In fact, it was reported that inclusion of MG in the BGE was crucial, as no LDL peaks could be detected in untreated fused-silica capillaries without it. On the other hand, increasing MG concentration up to 40 mM in the Tricine buffer led to the observation of a sharp peak [18]. Data about the reproducibility of the peak were not given, but these conditions allowed the detection of oxidized LDL forms [18]. In our case, the use of 40 mM MG in microchannels allowed the detection of LDL as a sharp peak, with what appears to be a broad, low shoulder at a longer migration time (Figure 1). This shoulder could be due to the elution of larger lipoprotein particles. The method of lipoprotein fractionation used often is responsible for the presence of small amounts of HDL contamination in the LDL fractions. This leads to the observation of the type of shoulder seen in Figure 1 [1].

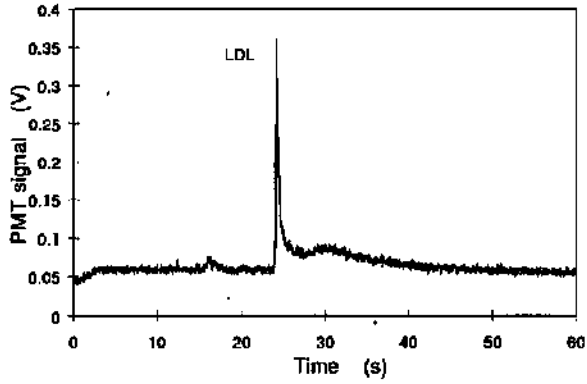

***Figure 1** Electropherogram of LDL(NBD-ceramide) prepared in BGE (40 mM Tricine, 40 mM methylglucamine (MG), pH 9.1). E= 740 V/cm. Channel length: L_{eff} =4.2 cm, L_{tot}= 6.7 cm.*

To see whether peak shape could be improved, the concentration of MG was varied. The broad shoulder became more pronounced with increasing MG up to 50 mM. For concentrations below 40 mM, down to 5 mM MG, peaks became more symmetric, though signal intensity was concomitantly decreased. The plot in Figure 2(a) shows peak areas obtained for one stained LDL sample as a function of MG concentration. (Note that the areas were measured by weighing the paper corresponding to the cut-out peak, tail included.) At 0 mM MG, the signal had decreased by 75 % with respect to the 50 mM MG, indicating that a substantially reduced amount of LDL reached the detector in the 0 mM case. This suggests that by decreasing the concentration of dynamic coating, lipoprotein particles are lost due to wall adsorption, particularly those of the type that elute under the broad shoulder in Figure 1. Figure 2(b) shows that the elution time of the LDL peak also decreases as expected when the additive concentration is reduced, as a result of increasing μ_{eo}. For these experiments, -6000 V were applied along the separation channel. It was interesting to note that the LDL peak was observed without any coating added to the BGE, in contrast to what has been

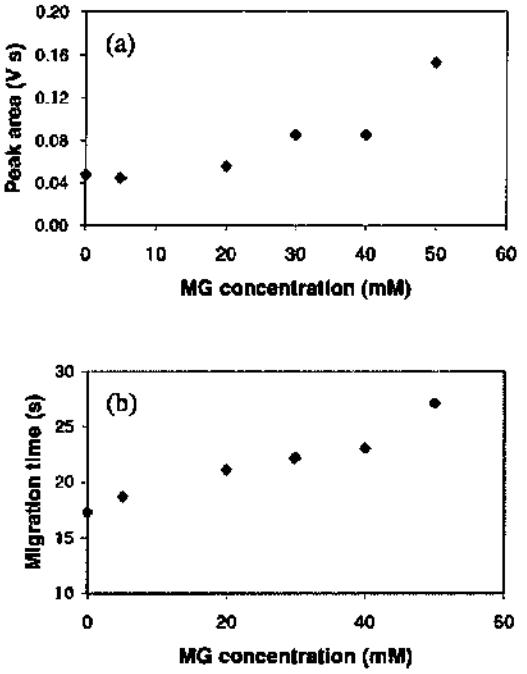

Figure 2 Effect of different concentrations of methylglucamine (MG) on (a) LDL(NBD-ceramide) peak area and (b) migration times. BGE: 40 mM Tricine buffer, pH 9.1. E= 890 V/cm. Channel length: L_{eff} =4.2 cm, L_{tot}= 6.7 cm.

reported for untreated capillaries [18]. The peak achieved in an untreated microchannel is presented in Figure 3. It is generally smaller than LDL peaks like that in Figure 1 achieved in the presence of MG. This is likely due to adsorption, as already alluded to in Figure 2(a). The interesting conclusion that can be drawn from Figure 3, however, is that highly adsorptive compounds can be detected in microsystems, using BGE conditions different from those optimized for a conventional capillary system. The effective length for a microchannel (2-6 cm) is much shorter than that of a fused-silica capillary (30-60 cm), which could allow a higher % recovery at the detection point of protein originally injected into the

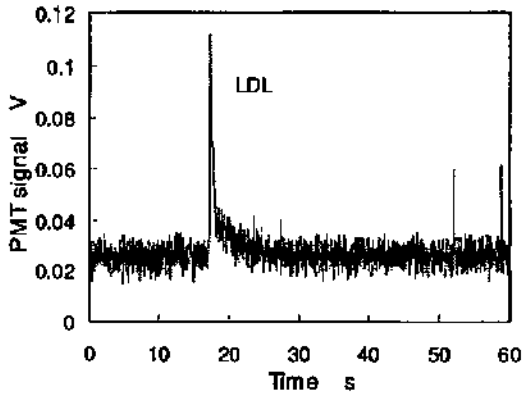

***Figure 3** Electropherogram of LDL(NBD-ceramide) prepared in 40 mM Tricine buffer, pH 9.1. BGE: 40 mM Tricine buffer, pH 9.1. Other separation conditions as in Figure 1.*

channel. Moreover, the higher electric fields that can be applied along a channel (600-1000 V/cm) compared to those applied over capillaries lead to higher flowrates. This could in part limit analyte adsorption to the channel wall by reducing analyte resident times, and hence the time available for LDL diffusion to the wall. Setting the residence time of LDL in an untreated chip equal to the LDL elution time, t_{el}, one can calculate the distance diffused by LDL using the Einstein-Smoluchowski equation [27]:

$$d_{diff} = (2\, D_{LDL}\, t_{el})^{1/2} \qquad [1]$$

The diffusion coefficient of LDL, D_{LDL}, is reported to be 1.8×10^{-7} cm^2s^{-1} [28]. Taking this value for D_{LDL} and the elution time of the LDL peak in an uncoated channel, t_{el}= 17.1 s, an average diffusion distance, d_{diff}, of 25 μm can be calculated. Since this is on the order of the channel cross-section dimensions, the probability of LDL diffusing to the walls of the microchannel before reaching the detection point is reduced if compared to analysis in a 75-μm-diameter capillary.

In the latter case, an average d_{diff} of 150 μm is calculated for the 10 min LDL elution time.

Lipoprotein particles have also been separated in uncoated capillaries by Macfarlane et al. [17]. In their work, 0.5 mM SDS-50 mM sodium borate buffer (pH 9.1) was used both as BGE and for sample preparation, enhancing the negative charge of the particles, and therefore the repulsion of particles from the negatively charged wall. They concluded that this decreased particle-wall interactions, allowing intact lipoprotein particles to be transported through an untreated capillary without loss to the walls. It is known, in fact, that apolipoproteins have a high affinity for SDS, and bind these detergent molecules at concentrations as low as 0.1 mM [29]. In [17], the SDS concentration was intentionally kept low enough to minimize particle delipidation while allowing particle-SDS interaction. It is only at concentrations closer to the critical micelle concentration (8.1 mM in water [30]) that lipoproteins undergo significant delipidation [31].

SDS effect on the LDL peak

To improve LDL solubilization, we added a small amount of SDS to the sample and not to the running buffer, as described in the Experimental Section. As mentioned above, SDS was used at a concentration of 0.5 mM for lipoprotein electrophoresis [17], and at higher concentrations (> 2.7 mM) for apolipoprotein dissociation [31] and lipoprotein delipidation [17]. In our case, SDS was added to the sample at a lower concentration of 0.3 mM in order to minimize particle delipidation, particle adsorption and aggregation [17]. The SDS-containing samples were run under the same conditions used for the other experiments.

The samples in Figure 3 and Figure 4 were taken from the same LDL fraction. With added SDS, a sharp peak was achieved as shown in Figure 4. An apparent efficiency of 928 000 plates (N) was obtained, corresponding to a plate height, H, of 0.05 μm and an N/m of 2.2×10^7 plates/m. The reproducibility of

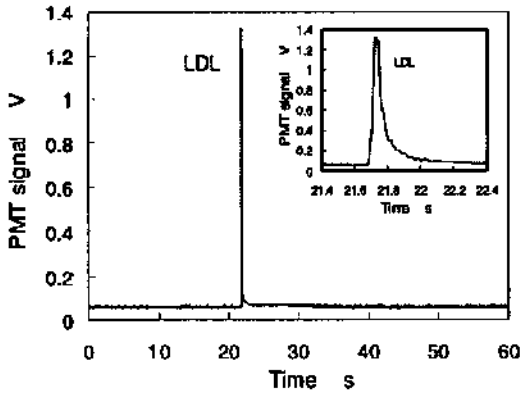

Figure 4 Electropherogram of SDS-LDL(NBD-ceramide) prepared in 40 mM Tricine with 0.3 mM SDS. BGE: 40 mM Tricine buffer, pH 9.1. Separation conditions as described in Figure 1.

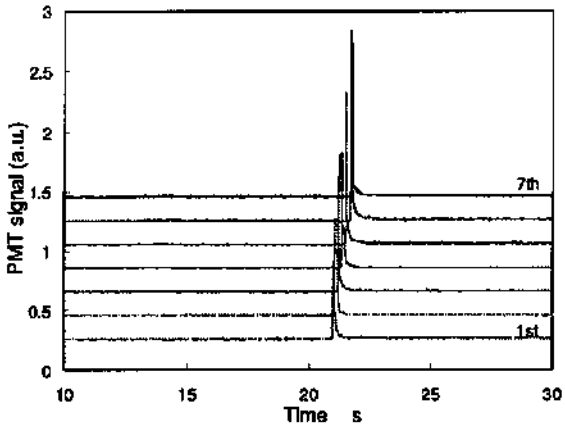

Figure 5 Reproducibility of SDS-LDL(NBD-ceramide) peaks for 7 consecutive injections. The LDL sample was prepared in 40 mM Tricine and contained 0.3 mM SDS. Separation conditions as described in Figure 1.

this peak is also good, as evidenced in Figure 5. Table 1 summarizes the effect of the addition of SDS to the sample on LDL peak migration time, apparent efficiency and area. The values reported in the table are the average values from a series of 7 consecutive injections. As expected, the migration time of LDL in the presence of SDS was shifted from 17 to 21 s, supporting the assumption that SDS has been adsorbed onto the particles, varying particle size and charge and therefore particle mobilities. A narrow peak very similar to the one presented in Figure 4 was reported for lipoprotein a (Lp(a)) samples premixed with 1% (35 mM) SDS-0.5 M Tris buffer [14]. In that study, the running buffer also contained no SDS, and the peak exhibited a plate number higher than 10^7 plates/m. This efficiency was attributed to the formation and co-migration of SDS-Lp(a) micelles. Our sample conditions were quite different from those reported in [14], in that the SDS concentration was more than 2 orders of magnitude smaller. Hence, it is postulated that the sharp peak detected was due to intact, SDS-bound LDL particles stained with NBD-ceramide (SDS-LDL(NBD)), and not SDS micelles or apolipoproteins. A number of observations support this hypothesis: (i) Control experiments showed that SDS micelles can be detected using NBD-ceramide; however, the SDS concentration used here is much lower than the critical micelle concentration (8.1 mM) and no signal was observed in the absence of lipoproteins. (ii) Literature reports state that 0.3 mM SDS is not enough to delipidate LDL particles [17]. (iii) The areas of the peaks in Figure 3

***Table 1** CE performance for LDL analysis in the absence of dynamic coating.*

	Without SDS	*0.3 mM SDS added to the sample*
Migration time (s)	17.1 ± 0.22	21.4 ± 0.28
Plate number, N	7,200 ± 1,400	720,000 ± 180,000
Plate height, H (μm)	6.0 ± 1.1	0.06 ± 0.02
Peak area (Vs)	0.07 ± 0.02	0.08 ± 0.02

and Figure 4 are similar, suggesting that the recovery of the particles is the same with and without SDS present, an indication that particle integrity was preserved.

Light scattering experiments were also carried out to gain more information about possible changes in particle properties upon addition of fluorescent dye and SDS. The results of these experiments confirmed that lipoprotein particles were not destroyed by SDS, as discussed later.

The sharpening effect observed for the peak in Figure 4 is similar to that reported by Kenndler et al. for a CE separation of the two proteins, conalbumin and ovalbumin, with SDS added to the sample only [32]. These researchers found that the presence of SDS in the sample, even at low concentrations (0.05 % w/w, 1.7 mM), and not in the BGE, led to a loss of separation resolution. At the same time, a sharpening of the single peak obtained for a mixture of the two proteins at SDS concentrations of 3.4 mM or more was observed. This focusing effect was not seen when SDS was present at the same level in both the sample and BGE [32]. Similarly, we did not observe peak focusing for LDL when both the sample and BGE contained the same concentration of SDS, which agrees with results of LDL detection by CE described by Macfarlane et al. [17]. Kenndler et al. concluded that the peak focusing was caused by mobility gradients established between the sample and BGE when SDS was added to the sample [32]. The loss of separation resolution reported in [32] upon SDS addition to the protein sample at concentrations higher than 1.7 mM would be an undesirable effect in our lipoprotein analysis, since it is of interest to resolve different lipoprotein forms. However, the concentration of SDS we used was very low (0.3 mM, or 0.009 %), and hence would most likely not be sufficient to cause a complete loss of resolution in the separation of different lipoprotein forms. The observed focusing effect could therefore be quite useful for the preconcentration of lipoproteins present at low concentrations, as is often the case in clinical samples.

SDS effect on the HDL peak

In our previous microchip CE study, the HDL peak eluting after the LDL had a broad shape [1]. This can be explained by the larger variety of apolipoproteins and more variable apolipoprotein content on the HDL particle surface compared to LDL particles. In this study, HDL samples were also tested in an untreated channel without and in the presence of 0.3 or 0.6 mM SDS added to the sample buffer. The results are presented in Figure 6(a) through (c), respectively. Often the HDL fraction contains LDL contamination due to poor zone separation after the ultracentrifugation process. This accounts for the second addition resembles that which occurs for LDL. Hence, it appears that SDS has a similar effect on HDL as on LDL. Integrity of the HDL particles is thus also most likely retained.

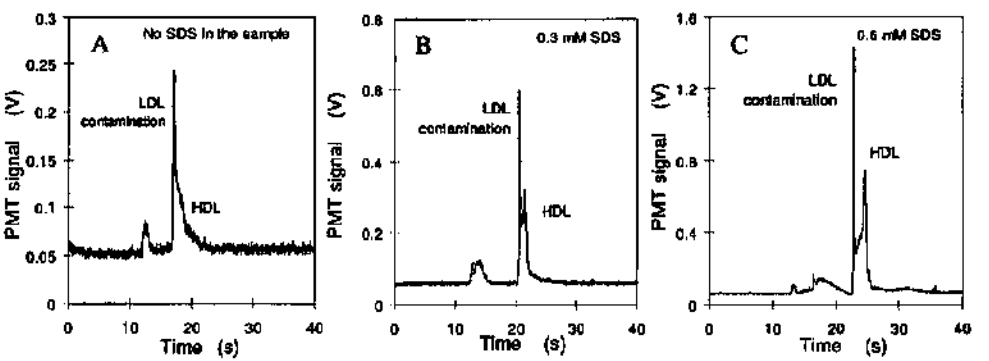

Figure 6 Electropherograms of HDL(NBD-ceramide) prepared in 40 mM Tricine buffer, pH 9.1. The HDL sample contains LDL contamination, which results in the sharp peak just preceding the HDL peak. A) No SDS. B) 0.3 mM SDS and C) 0.6 mM SDS added to the sample. BGE: 40 mM Tricine, pH 9.1. Experimental conditions as in Figure 1.

Laser light scattering (LLS) experiments

In [17], particle density profiles of different lipoprotein fractions after incubation with 0.5 mM SDS were obtained by ultracentrifugation, and compared with control samples containing no SDS. Results from these experiments indicated that changes in particle density and, hence, particle properties occurred. However, this technique does not give a direct insight into particle size. It is therefore only possible to assume that certain particle structural changes have taken place. Thus, laser light scattering (LLS) experiments were performed to further characterize LDL and HDL particles with 0.3 mM SDS added to the sample. Because of the large volume required for the experiments (more than 1000 μL) and the need for high sample concentrations, both the ratios between lipoprotein particles and NBD-ceramide, and lipoprotein and SDS anions, were modified from the protocol used for sample preparation in the microdevice. Thus, the final samples for light scattering experiments contained 0.3 mM SDS with LDL or HDL at concentrations that were three times higher than in the microchip case, and NBD-ceramide at a concentration 1.5 times higher. The sample preparation and the analysis protocol for the scattering experiments were described in the Experimental Section. Analyses were performed separately on three types of LDL and HDL samples: (i) lipoprotein sample with no reagent added, (ii) after the addition of NBD-ceramide and (iii) after the addition of NBD-ceramide and SDS. For each LLS analysis, freshly prepared lipoprotein sample was measured over a period of 30 minutes. In both types of lipoprotein samples, and in particular in the LDL, large aggregates were present, causing some difficulties in the analysis of the data. It was, however, clear in both LDL and HDL samples that the particles were not disrupted after addition of either NBD-ceramide or SDS (data not shown). For HDL, the size of single particles could be determined to be 10 nm in buffer solution, which is in good agreement with values obtained from electron microscopy (31). When NBD-ceramide was

added to the solution, the radius did not change. The addition of SDS, however, increased the particle size to 12 nm, which can be explained by the adsorption of SDS to the hydrophobic parts of the apolipoprotein (28). As mentioned, no disruption of the HDL was observed, so that a similar surface adsorption may be expected for LDL. This was supported by the observation that the electropherograms for LP samples analysed on-chip did not change drastically in the absence and presence of SDS.

CONCLUSIONS

Lipoproteins are delicate and complex samples, but their analysis can be very useful for clinical diagnosis of atherosclerosis and related diseases. A reliable lipoprotein analysis should guarantee good resolution between lipoprotein particles and high reproducibility in a short analysis time. Ideally, it should also consume minimal sample volumes, be compatible with unprocessed biological fluid, i.e. blood, and allow high sample throughput. The integrity of the lipoproteins should also be preserved for further analysis of cholesterol and triglyceride concentrations. Microfluidic devices appear to be a promising platform to perform such rapid and efficient analysis.

We previously proposed a method for lipoprotein analysis, in both conventional and chip-based systems, that required a dynamic coating. However, the microdevice results presented here suggest different requirements from the conventional capillary. This study showed that sample recovery at the point of detection was sufficient for lipoprotein detection without the need for a permanent or dynamic coating. Moreover, the addition of 0.3 mM SDS to the sample prior to analysis modified the sample sufficiently with respect to the BGE to cause a focusing effect that sharpened the eluted LDL peak. This preconcentration effect could be useful in the detection of lipoproteins present at

low concentrations. Moreover, the resolution between lipoprotein particles of different size and charge does not appear to be significantly compromised. The microchip-based CE assay could thus be suited to distinguishing between different LDL types for certain diagnostic applications. In the case where higher resolution is required, the integration of ITP on chip should be considered as a potential approach for future, rapid lipoprotein diagnostics.

Acknowledgements

The authors acknowledge Muriel Fiaux (Nestlé) for the sample preparation in light scattering experiments at the Nestlé Research Center, and Gilles Vuataz (Nestlé) for the refractive index measurements.

REFERENCES

[1] B. H. Weiller, L. Ceriotti, T. Shibata, D. Rein, M. A. Roberts, J. Lichtenberg, J. B. German, N. F. de Rooij, and E. Verpoorte, "Analysis of lipoproteins by capillary zone electrophoresis in microfluidic devices: assay development and surface roughness measurements," *Anal.Chem.*, vol. 74, pp. 1702-1711, 2002.

[2] R. J. Havel, H. A. Eder, and J. H. Bragdon, *J. Clin. Invest.*, vol. 34, pp. 1345-1353, 1955.

[3] J. P. Segrest and J. Albers, "Plasma lipoproteins (Part A: preparation, structure, and molecular biology)," *Methods Enzymol.*, vol. 128, pp. 155-209, 1986.

[4] D. Steinberg, *Atherosclerosis*, vol. 3, pp. 283-301, 1983.

[5] M. A. Austin, J. L. Breslow, C. H. Hennekens, J. E. Buring, W. C. Willette, and R. M. Krauss, "Low density lipoprotein subclass pattern and risk of myocardial infarction," *J. Am. Med. Assoc.*, vol. 260, pp. 97-104, 1988.

[6] N. F. Galeano, H. M. Al, F. Keyserman, S. C. Rumsey, and R. J. Deckelbaum, "Small dense low density lipoprotein has increased affinity for LDL receptor-indipendent cell surface binding sites: a potential mechanism for increased atherogenicity," *J. Lipid Res.*, vol. 39, pp. 1263-1273, 1998.

[7] M. A. Austin, J. E. Hokanson, and J. D. Brunzell, "Characterization of low density lipoprotein subclasses: methodologic approaches and clinical relevance," *Curr. Opin. Lipodol.*, vol. 5, pp. 395-403, 1994.

[8] G. M. Reaven, Y. D. Chem, J. Jeppesen, P. Maheux, and R. M. Krauss, *J. Clin. Invest.*, vol. 92, pp. 141-146, 1993.

[9] P. Avogaro, G. Bittolo-Bon, and G. Cazzolato, "Presence of a modified low-density lipoprotein in humans," *Atheriosclerosis*, vol. 8, pp. 79-87, 1988.

[10] G. Bittolo-Bon, G. Cazzolato, and P. Avogaro, "Does circulating oxidized LDL exist and can it be detected?," in *Free radicals lipoprotein oxidation and atherosclerosis: Biological and clinical aspects*, G. Bellomo, G. Finardi, E. Maggi, and C. Rice-Evans, Eds. London, PA: Ricelieu, 1995, pp. 205-228.

[11] P. Halvoet, G. Perez, Z. Zhao, E. Brouwers, H. Bernar, and D. Collen, "Malondialdehyde-modified low density lipoproteins in patients with atherosclerotic disease," *J. Clin. Invest.*, vol. 95, pp. 2611-2619, 1995.

[12] K. Inano, T. Miida, and M. Okada, "Serum apolipoprotein E-rich HDL-C levels in the subjects with hyperalphalipoproteinemia," *Rinsho Byori*, vol. 45, pp. 903-907, 1997.

[13] F. Tallet, M. P. Vasson, R. Couderc, G. Lefevre, and D. Raichvarg, "Characterization of lipopreteins during human cholestasis," *Clin. Chim. Acta*, vol. 244, pp. 1-15, 1996.

[14] A. Z. Hu, I. D. Cruzado, J. W. Hill, C. J. McNeal, and R. D. Macfarlane, "Characterization of lipoprotein a by capillary zone electrophoresis," *J. Chromatogr. A*, vol. 717, pp. 33-9, 1995.

[15] W. C. Taddei-Peters, B. T. Butman, G. R. Jones, T. M. Venetta, P. F. Macomber, and J. H. Ransom, "Quantification of lipoprotein(a) particles containing various apolipoprotein(a) isoforms by a monoclonal anti-Apo(a) capture antibody and a polyclonal anti-apolipoprotein B detection antibody sandwich enzyme immunoassay," *Clin. Chem.*, vol. 39, pp. 1382-1389, 1993.

[16] J. R. McNamara, T. G. Cole, J. H. Contois, C. A. Ferguson, J. M. Ordovas, and E. J. Schaefer, "Immunoseparation method for measuring low-density lipoprotein cholesterol directly from serum evaluated," *Clin.Chem.*, vol. 41, pp. 232-240, 1995.

[17] R. D. Macfarlane, P. V. Bondarenko, S. L. Cockrill, I. D. Cruzado, W. Koss, C. J. McNeal, A. M. Spiekerman, and L. K. Watkins, "Development of a lipoprotein profile using capillary electrophoresis and mass spectrometry," *Electrophoresis*, vol. 18, pp. 1796-806, 1997.

[18] J. Stocks and N. E. Miller, "Capillary electrophoresis to monitor the oxidative modification of low density lipoproteins," *J. Lipid Res.*, vol. 39, pp. 1305-9, 1998.

[19] G. Schmitz and C. Möllers, "Analysis of lipoproteins with analytical capillary isotachophoresis," *Electrophoresis*, vol. 15, pp. 31-9, 1994.

[20] G. Schmitz, C. Möllers, and V. Richter, "Analytical capillary isotachophoresis of human serum lipoproteins," *Electrophoresis*, vol. 18, pp. 1807-13, 1997.

[21] K. Inano, S. Tezuka, T. Miida, and M. Okada, "Capillary isotachophoretic analysis of serum lipoproteins using a carrier ampholyte as spacer ion," *Ann. Clin. Biochem.*, vol. 37, pp. 708-716, 2000.

[22] B. H. Weigl, R. Bardell, T. Schulte, F. Battrell, and J. Hayenga, "Design and rapid prototyping of thin-film laminate-based microfluidic devices," *Biomedical Microdevices*, vol. 3, pp. 267-274, 2001.

[23] L. B. Koutny, D. Schmalzing, T. A. Taylor, and M. Fuchs, "Microchip electrophoretic immunoassay for serum cortisol," *Anal. Chem.*, vol. 68, pp. 18-22, 1996.

[24] K. Sato, M. Tokeshi, H. Kimura, and T. Kitamori, "Determination of carcinoembryonic antigen in human sera by integrated bead bed immunoasay in a microchip for cancer diagnosis," *Anal. Chem.*, vol. 73, pp. 1213-1218, 2001.

[25] H. Nakamura, Y. Murakami, K. Yokoyama, E. Tamiya, I. Karube, M. Suda, and S. Uchiyama, "A compactly integrated flow cell with a chemiluminescent FIA system for determining lactate concentration in serum," *Anal. Chem.*, vol. 73, pp. 373-378, 2001.

[26] C. Urban and P. Schurtenberger, "Characterization of turbid colloidal suspensions using light scattering techniques combined with cross correlation modes," *J. Colloid Interface Sci.*, vol. 207, pp. 150-158, 1998.

[27] I. N. Levine, *Physical Chemistry*, 2nd Edition ed. New York: McGraw-Hill, 1983.

[28] V. Hlady, J. Rickel, and J. D. Andrade, *Colloids Surf.*, vol. 34, pp. 171-183, 1988/89.

[29] S. Mikano, C. Tanford, and J. A. Reynolds, "The interaction of polypetide components of human high density serum lipoprotein with detergents," *J. Biol. Chem.*, vol. 249, pp. 7379-7382, 1974.

[30] P. C. Hiemenz, *Principles of Colloid and Surface Chemistry*. New York: Marcel Dekker, 1986.

[31] T. Tadey and W. C. Purdy, "Effect of detergents on the electrophoretic behaviour of plasma apolipoproteins in capillary electrophoresis," *J. Chromatogr. A*, vol. 652, pp. 131-138, 1993.

[32] E. Kenndler and K. Schmidt-Beiwl, "Effect of dodecyl sulphate in protein samples on separation with free capillary zone elctrophoresis," *J. Chromatogr.*, vol. 545, pp. 397-402, 1991.

Appendix 3

AN INTEGRATED FRITLESS COLUMN FOR ON-CHIP CAPILLARY ELECTROCHROMATOGRAPHY WITH CONVENTIONAL STATIONARY PHASES

Laura Ceriotti, Nico F. de Rooij and Elisabeth Verpoorte

SAMLAB, Institute of Microtechnology, University of Neuchâtel, Neuchâtel, Switzerland

ABSTRACT

A new polymer device for use with conventional particulate stationary phases for on-chip, fritless, capillary electrochromatography (CEC) has been realized. The structure includes an injector and a tapered column in which the particles of the stationary phase are retained and stabilized. The chips were easily fabricated in poly(dimethylsiloxane) using deep-reactive-ion-etched silicon masters, and tested using a capillary electrophoretic separation of FITC-labeled amino acids. To perform CEC, the separation channel was packed using vacuum with 3-μm, octadecylsilanized silica microspheres. The packing was stabilized in the column by a thermal treatment, and its stability and quality were evaluated using in-column indirect fluorescence detection. The effects of voltage on electro-osmotic flow and on efficiency were investigated, and the separation of two neutral compounds was achieved in less than 15 seconds.

Published in *Anal. Chem.* **2002**, Vol. 74, Number 3, Pages 639-647.

INTRODUCTION

The use of microfabricated fluidic substrates has become increasingly well established for liquid-phase analysis in recent years. This is particularly true for electrokinetically driven separations, where etched microchannels provide an easy route to reduced column diameters, and, hence, increased efficiencies and decreased solvent/sample consumption (1). As with narrow bore (< 75 μm), fused silica capillaries used in conventional capillary electrophoresis (CE) instrumentation, the high surface-to-volume ratios of these chip-based systems enable good dissipation of Joule heat. However, the shortest capillary that can be used in a benchtop instrument is generally no less than 30 cm long, which leads to typical applied electric field strengths on the order of a few hundred volts per cm. With chip CE, working with much shorter separation channels is facilitated, allowing electric fields of 500-1000 V/cm, and decreased analysis times as a result (2-5). The integration of picoliter-volume injection elements into etched CE devices is a further unique feature of the chip format. Microfluidic devices operated using pressure-driven flow (6, 7) and centrifugal pumping (8-11) have also been reported, expanding the range of possible analyses. The microfluidic approach should generally enable high throughput applications (12-14), as well as a high level of automation for real-time testing at the point of care (POC) (15-17).

The many advantages of microfabricated devices for ultrasmall-scale analysis have been demonstrated with a wide variety of examples, including sample preconcentration (18, 19), cell handling (20, 21), PCR amplification (22, 23), fluidic mixing (24, 25), and immunological tests (26, 27). For most of the integrated techniques presented in the literature, solutes and solutions move and react in open tubular structures. They include capillary electrophoresis (2-5, 28, 29), synchronized cyclic capillary electrophoresis (30, 31), and free-flow electrophoresis (32, 33) for the analysis of ions, as well as open-tubular liquid chromatography (OTLC) (34), capillary electrochromatography (35, 36), and

micellar electrokinetic chromatography (MEKC) (37-39) for the analysis of neutral species. In parallel, gel-filled devices have been introduced for DNA analysis (40) and sequencing (41-45). Recently, the growing need to increase the active surface in microfluidic devices has led to the realization of packed micro beds in which reactions, chromatographic partitioning, immunoassays, protein and DNA analysis can be carried out. All of these devices incorporate a physical barrier of some kind to localize particles, which generally results in chips that are somewhat more complex from a fabrication standpoint. An early example involved the integration of a packed, small-bore column, together with a split injector and optical detector cell, onto a silicon chip to partially scale-down high performance liquid chromatography (HPLC) (46). In this case, two arrays of fine V-groove channels 3 μm wide and 2 μm deep retained the 5-μm, stationary-phase particles in the channel serving as separation column. Andersson at al. have described micromachined chambers surrounded by filter-like structures realized for solid phase DNA sequencing (47). Sato et al. incorporated a barrier in a microchannel to block derivatized beads to perform immunoassay on their surface (48). In this paper, we explore a new approach for the preparation of a microcolumn packed with conventional particulate stationary phases for capillary electrochromatography (CEC), that does not necessitate actual blockage of the particles (49).

CEC has emerged in the last few years as a promising, high-performance, separation technique for the analysis of both ionic and neutral species. The plug-like velocity profiles characteristic of electro-osmotic flow (EOF) result in reduced dispersion of the solute band as it passes through the column, increasing column efficiency (50-54). Moreover, the independence of the flow velocity from particle size allows the use of stationary phases having diameters smaller than 3 μm, without having the large pressure drops typical of HPLC (53-55). The most widely used stationary phases in CEC are particulate in nature, based on surface-modified silica particles 5 μm or less in diameter. The performance and stability

of a capillary column packed with these types of particles is very dependent on the integrity of the retaining frits at the ends of the column. There are a number of problems associated with frits, however, including their fabrication, their tendency to act as catalysts for bubble formation, and their unpredictable distortion of EOF, which inevitably introduces band broadening. Numerous studies have therefore focused on developing fritless column technologies. They include tapered outlet geometries (56, 57), new frit design (58), and the preparation of monolithic beds using gels (59-68) or whole-column sintering methods (69, 70).

As with other separation techniques, CEC would benefit from integration onto microchips, especially in terms of reduced separation/analysis times; however, packing microchannels with commercially available stationary phases is not trivial. Frit fabrication techniques prove to be as inconvenient on chips as in fused silica capillaries, if not more so. There are reported examples of microfabricated CEC devices employing "fritless" technologies, such as *in situ* polymerization of the stationary phase, based on techniques developed for conventional systems (71, 72), or even open tubular methods (34-36). However, these methods may also be difficult to implement. For instance, restricting stationary phase polymerization to specific channels on a wafer requires accurate control of fluids in all branches of the microchannel network. The limited channel diameters (< 2 μm) desired for rapid mobile phase transfer in open channel separations may also pose difficulties, such as rapid clogging. In addition, in-channel optical detection in such shallow channels is problematic because of the extremely short path length available. Regnier et al. introduced an alternative fritless approach by which the stationary phase support structures, small columns termed "collocated monolith support structures" (COMOSS), were formed photolithographically inside the separation channel simultaneously with the channel structures themselves (73, 74). This is a fascinating example of the power

of microfabrication, although the mecbanisms involved in the chromatographic process need further investigation.

Although methods employing approaches to circumvent the need to pack microchannels with particulate phases for CEC are certainly worth pursuing, conventional silica-based phases remain attractive due to their easy availablity and well-characterized properties. Only recently, Oleschuk et al. realized a 200-µm-long, bead-packed cavity, surrounded by a wall on a glass chip, for solid phase extraction and chromatographic separation (75). In our work, conventional particulate stationary phases are packed and stabilized in a separation microcolumn 4 cm long and incorporating an injector. Unlike other devices published to date, all that is required to achieve packing is a simple, tapered geometry to induce particles to aggregate. The microstructures are replicated in an elastomer, poly(dimethylsiloxane) (PDMS), on account of the excellent optical properties of this material, as well as the ease with which structures may be made and the accompanying flexibility in cross-sectional profile. This type of replication in plastic represents an interesting approach for realizing disposable microfluidic analysis systems (76).

EXPERIMENTAL SECTION

Chemicals and Materials

Tris(hydroxymethyl)aminomethane (Tris), boric acid, 1 M NaOH (0.2 μm filtered) and benzaldehyde were purchased from Fluka (Buchs, Switzerland). Acetonitrile, acetone, 2-propanol, methanol, dichloromethane, hexane, potassium dihydrogen phosphate and potassium hydrogen phosphate were purchased from Merck (Darmstadt, Germany), while dry toluene and dimethyloctadecylchlorosilane were obtained from Aldrich (Buchs, Switzerland). All compounds and solvents were reagent grade. 5 mM potassium phosphate (pH 7), 100 mM Tris-20 mM boric acid (pH 9), and 19 and 20 mM sodium borate (pH 8) buffers were prepared in deionized water. A 20:80 (v/v) mixture of acetonitrile and phosphate buffer was also prepared for CEC studies. Fluorescein sodium (Sigma, Buchs, Switzerland) was added to this solution at a concentration of 1 mM to allow indirect fluorescence detection. 1 mM stock solutions of four amino acids (arginine, phenylalanine, serine and glycine (Sigma)) were prepared in 100 mM Tris-20 mM boric acid (pH 9) and used for CE studies. The amino acids were labeled by adding 100 μL of a 1 mM solution of fluorescein isothiocyanate isomer I (FITC) (Sigma) in acetone to 1 mL of 1 mM amino acid solution, as previously described (3). After reaction overnight, the FITC-labeled amino acid solutions were diluted in Tris buffer to a concentration of 10 μM with respect to FITC. All aqueous solutions (buffers and samples), with the exception of the 1 M NaOH, were filtered through 0.2 μm filters (Semadeni, Ostermunding, Switzerland) before use.

The stationary phase used to pack the microcolumn was Nucleosil ODS1 (Stacroma, Reinach, Switzerland), consisting of porous, C-18-modified, 3-μm particles. 16 mg of these dry, reverse phase particles were ultrasonicated for about 50 min. A slurry was then prepared by adding 800 μL of acetone to the particles,

and this suspension (2% w/v) was ultrasonicated for at least another 10 min. This slurry was used to pack the separation microcolumn as described below. Thiourea (Sigma) was used as a neutral marker to measure electro-osmotic flow for CEC experiments, as it is not retained on C-18 phases.

The microstructures were realized in poly(dimethylsiloxane) (PDMS) (Sylgard 184, Dow Corning, Midland, MI, USA; obtained from Distrelec AG, Nanikon, Switzerland) and sealed on a 1.5-mm-thick glass wafer (Guinchard, Yverdon-les-Bains, Switzerland).

Instrumentation

Fluorescent sample detection was effected by laser-induced fluorescence (LIF) using an Ar ion laser (Model 5400-220-00, Ion Laser Technology, Salt Lake City, UT, USA) emitting at 488 nm. A portion of the channel was illuminated through collimating and focusing lenses at an angle of about 45°. The point of detection was around 2 cm below the injection cross, and the fluorescence light was collected perpendicularly to the surface of the chip by means of a microscope objective (25 X; N.A.= 0.35; Leica, Glattbrugg, Switzerland) mounted on a homemade microscope body. After being transmitted through a bandpass filter at 514 nm (Melles Griot 03FIL004, 10 nm FWHM; Irvine, California, USA) and a 1-mm pinhole, fluorescence was detected with a Hamamatsu R1477 photomultiplier tube (PMT) (Hamamatsu Photonics K.K., Schüpfen, Switzerland). Two high-voltage power supplies (Models HCN 2000 (0-2kV) and HCN 12500 (0-12.5 kV), FUG Elektronik GmbH, Rosenheim, Germany), six relays (Günther GmbH, Nürnberg, Germany) and a control system (PC with LabVIEW™, National Instruments, Austin, TX, USA) were assembled to automate injection and separation, and allow data acquisition and analysis. A chip holder was mounted on an *x-y* translational stage in order to allow variation of the effective separation length by changing the position of the chip with respect to the detector.

Chip design and fabrication

The layout of the structures used in this work is presented in Figure 1. The injection element consists of two 16-µm-wide channels entering into the main straight channel to form two offset, slanted T-junctions. The length of the double-T intersection is 150 µm. The separation channel was designed for fritless CEC, and it includes a gradual tapering at the top of the separation column just below the intersection. The channel width in this region decreases from 70 µm to 16 µm over distances of 0.5, 0.8 or 1 mm, depending on the layout. The program CleWin (Delta Mask, Enschede, The Netherlands) was used for the design of the layout.

We have chosen to work with polymeric microdevices based on the elastomer, poly(dimethylsiloxane) (PDMS), because they are easy to handle, rapidly fabricated by replica molding, and inexpensive. Fabrication involves casting a solution of the PDMS prepolymer onto a master whose surface has been dry-etched to yield a topography whose structure is not restricted with respect to channel layout or aspect ratio (76). When cured, PDMS faithfully replicates, with nm resolution, the surfaces with which it has been in contact. Microchannels are thus easily formed in PDMS if the corresponding master has a raised network of ridges to serve as microfluidic network mold. Use of photolithographic processes to form the master allows features of micrometer dimensions. In our case, 10-cm-diameter, (100)-oriented silicon wafers (Siltronix, Vernier-Geneve, Switzerland) with a positive surface relief were used as masters for casting microchannel devices. These were manufactured in-house using standard photolithography and deep reactive-ion etching (DRIE), done in a Surface Technologies Systems machine (STS, Newport, UK).

Wafers were first subjected to dehydration for 30 min at 200 °C, followed by a 10-min surface passivation in hexamethyldisilazane vapor to improve adhesion of the photoresist. Positive photoresist AZ 1518 (Shipley, Coventry, England) was then spin-coated onto the wafers at 4000 rpm for 40 s, to yield a 1.8-µm-thick layer. After a 30-min prebake at 85°C, the channel pattern was

photolithographically transferred to the resist using a mask aligner (Electronic Vision AL 6, Schaerding, Austria). After 90 s of development in a 1:1 mixture (v/v) of AZ 351 developing solution and deionized water, the resist was postbaked at 120 °C for 20 min. Negative MAN 420 photoresist (Micrn Resist Technology, Berlin, Germany) can be also used. In this case, a 2.1-μm-thick resist layer was obtained at 3000 rpm, and a 1:1 mixture (v/v) of MA-D 336 developer and deionized water was required for the development. After postbake, the patterned wafers were ready for DRIE.

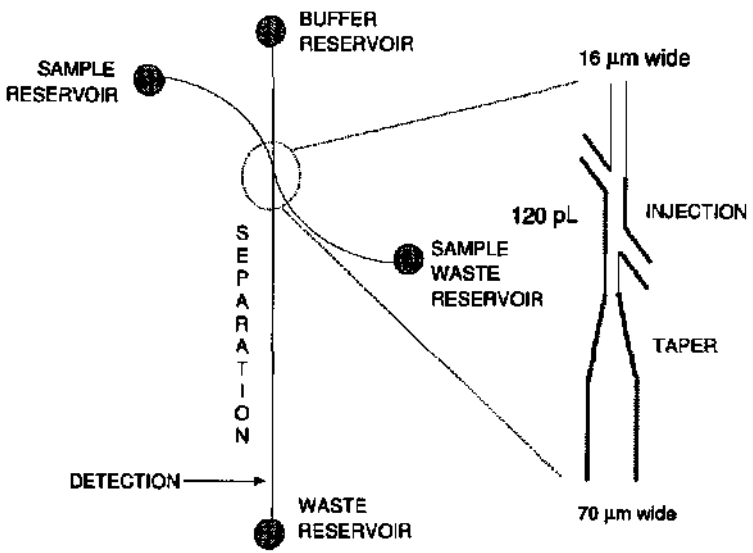

***Figure 1** Chip layout for fritless CEC in poly(dimethylsiloxane) (PDMS). The channel structure consists of two side channels entering into the main channel to form slanted T intersections. This so-called "double-T" injection scheme (3) allows pinched injection of small, well-defined volumes of sample into the straight column. As shown in the close-up, the separation column includes a gradual tapering just below the intersection, which is used to stop stationary phase particles, leaving the injector particle-free.*

During DRIE, the ions present in the chamber are directed perpendicularly at the wafer surface, so that etching is also a primarily unidirectional process into the wafer bulk. All the areas surrounding the patterned photoresist lines are anisotropically etched, leaving the structures that will be replicated in PDMS to form the channels. Thus, rectangular, smooth-walled profiles are achieved, and by increasing the etching time, high-aspect-ratio structures can be realized. In this work, the relief patterns had heights of either 30 or 50 μm, which corresponds to height-to-width ratios for the 16-μm-wide features of 2-3, respectively. Rectangular profiles like this can be achieved by anisotropic wet etching of (100)-oriented silicon wafers (77, 78); however, the orientation of features with respect to the crystal planes of silicon is restricted with this type of etching. This makes curved relief patterns with vertical walls like that of the injection element of this chip impossible to achieve. Anisotropic wet etching of <100> silicon has also been used to produce masters for plastic channel replication (79-81), but the resulting channels had trapezoidal cross-sections with aspect ratios < 1. Again, there is little freedom in channel layout design, since possible structure geometries are dictated by crystalline orientation. Alternatively, resist reliefs on silicon wafers can be used as masters, as reported by Duffy et al. (82) and Hong et al. (83). They employed the negative photoresist EPON SU-8, which appears to be an attractive choice in terms of fabrication time and layout freedom (76). Moreover, features 5 to 1200 μm high are possible with aspect ratios approaching 20 (84-86). To date, 1:1 aspect ratio structures (channels with equal height and depth) were used for PDMS molding and they can be used indefinitely (76); however, experience in our lab has revealed that a number of problems are associated with the use of SU-8. These include lack of adhesion of the resist to the silicon wafer, thermally induced stress in the resist, and difficulty with development, all of which could compromise structure integrity and profile. Masters realized by silicon etching, on the other hand, are monolithic, and the profile and surface quality can be well controlled during the fabrication process.

Two kinds of mask were tested for the realization of the silicon master: a chromium mask (from Delta Mask, Enschede, Holland) and a transparency (from DIP SA, Lausanne, Switzerland). Photolithography done with the chromium mask yielded structures with smooth vertical walls, as shown in the scanning electron micrograph (SEM) for a detail of the injector in Figure 2a (SEM obtained using an XL 30, ESEM-FEG instrument from Philips). The transparency mask, produced by a commercial laser printer with a resolution of 7 µm, gives reasonable results for straight channels, but side walls are scalloped for curves or tapered geometries (Figure 2b). This effect is similar to that reported in (82). As discussed later, the application presented in this paper required smooth wall profiles for the taper, so that chromium masks were preferred. On the other hand, the use of transparencies eliminates the 1-2-week waiting period for delivery of chromium masks made externally, so that prototyping can be done more rapidly. In our lab, the realization of a silicon master by DRIE using a transparency mask takes about 3 days.

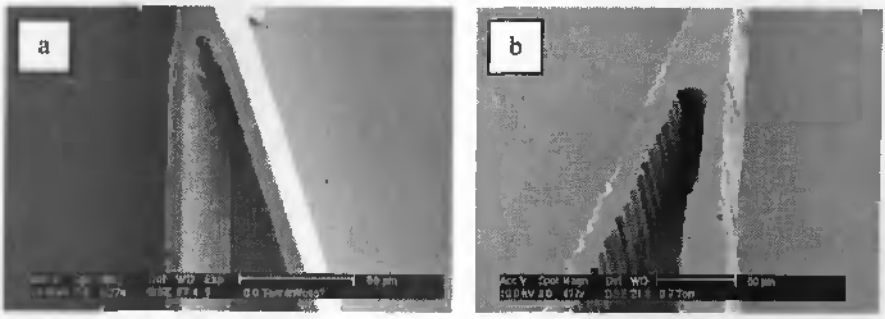

***Figure 2** SEM images of the injector element on silicon masters fabricated by deep reactive-ion etching (DRIE), using (a) a chromium mask and (b) a transparency mask during the photolithography process.*

Before use, the silicon masters were silanized in 3% (v/v) dimethyloctadecylchlorosilane (ODS) in dry toluene for 2 h to facilitate peeling of the cured replica from the master. The masters were cleaned with hexane, 2-propanol, dichloromethane and water, 3 min each, before every casting. A 10:1 mixture of PDMS prepolymer and curing agent was vigorously stirred and poured onto the silicon master. The PDMS was then allowed to stand at room temperature for 30 min to allow the dissipation of air bubbles introduced during the mixing process. After curing for 4 h at 65 °C, the PDMS replica was peeled from the master. Reservoirs (3 mm in diameter) were punched through the 5-mm-thick silicone rubber at the ends of the channels. The PDMS slab was then cleaned with 2-propanol and water in an ultrasonic bath (Soltec srl, Milan, Italy), 5 min each, dried with filtered nitrogen, and sealed onto a glass support by mere adhesion. This sealing is reversible, so that if a device clogged, it was simply peeled off the support, rinsed with water and used again. Thus, the same plastic chip could be used several times for preliminary studies. It was also possible to seal the PDMS replica and glass wafer irreversibly by oxidizing both the glass and the PDMS for 0.8 min in an oxygen plasma-based cleaner (Tegal Asher no. 6, Tegal Corp., Novato, CA) and bringing them immediately into contact. Clean, flat surfaces are absolutely necessary for both types of sealing.

Chip operation

Before CE experiments, the channels were conditioned with 1 M NaOH for 5 min to activate the surface, then rinsed with water and filled with buffer solution by applying vacuum to one reservoir.

The so-called "double-T" injection scheme (close-up in Figure 1) is integrated into the structure to allow pinched injection of small, well-defined sample volumes (~120 pL). The sample is loaded into the double-T intersection by inducing a flow traveling from the sample reservoir to the sample waste reservoir for 30 s (for samples containing fluorescein and fluorescently labeled

amino acids). The sample plug was confined to the intersection by electro-osmotically pumping a counter flow of buffer from the waste reservoir toward the sample waste reservoir. Ideally, the sample plug should be pinched at the other end as well by using a flow of buffer from the buffer reservoir to the sample waste. However, this would mean that the buffer would have to pass through the plug, which would result in substantial sample dilution (19, 87, 88). Hence, the buffer reservoir was left floating during sample loading. In any case, microscope images of plug formation indicate that very little sample spills out of the injector into the upper buffer channel. The slanted geometry of the double-T intersection was partially responsible for this, since inertial flow dictates that the solution will prefer to continue traveling in a downward direction, rather than make a 135° turn. A Venturi-like effect, which sees the moving sample stream drawing stagnant buffer out of the field-free buffer channel, also helped prevent diffusion of the sample towards the buffer reservoir (88). In fact, the plug showed a greater tendency to enter the separation channel, due most likely to the lower flow resistance of the taper geometry.

To switch to the separation mode, the applied potentials were reconfigured so that the principal flow path was from the buffer reservoir to the waste reservoir. Negative potentials of 450-4000 V were applied at the buffer reservoir. This corresponds to electric field strengths of 90-800 V/cm for 5-cm-long channels. To inject a small analyte plug into the separation column, the sample and sample waste reservoirs were maintained at 60% of the potential applied to the waste. In this way, the excess analyte was pulled away from the cross intersection, and sample leakage could be avoided. This method of loading and injecting the sample is very reproducible in the double-T geometry presented here, as demonstrated by injecting fluorescein plugs in a native PDMS chip (data not shown). This is in accordance with the behaviour for the more traditional double-T geometries having perpendicular sample delivery channels (3, 88).

As mentioned above, the separation channel was designed for fritless CEC; it includes a gradual tapering used to stop stationary phase particles just

below the injector. To prepare the chromatographic bed, oxidized PDMS structures were preferred for their enhanced wettability. Irreversible sealing of oxidized PDMS to glass or to itself made it possible to construct devices that resisted the pressure applied during packing. After oxidation, a suspension of octadecylsilanized (ODS) particles (3-μm size, 2% in acetone) was loaded into the column by applying vacuum and pressure (by means of a 10-mL syringe) at the sample waste reservoir and at the waste reservoir, respectively. New suspension was added to the waste reservoir every few minutes. Once packed, the column was flushed with deionized water for 2 h by applying vacuum at the sample waste reservoir, and intermittent manual pressure at the waste reservoir. The packing was then heated overnight at 115° C. Finally, the column was flushed with methanol and deionized water, and conditioned directly with the mobile phase, 5 mM phosphate:ACN (pH 7) (80:20), containing 1 mM sodium fluorescein for indirect fluorescence detection.

RESULTS AND DISCUSSION

Capillary electrophoresis (CE) test

The layout depicted in Figure 1 was employed to perform a CE separation of amino acids using oxidized PDMS structures and fluorescence detection. Amino acids (arginine, phenylalanine, serine, glycine) labeled with FITC were used at concentrations of 10 μM each in the running buffer (100 mM Tris-20 mM boric acid, pH 9). The CE test was performed in 30-μm-deep structures. As shown in Figure 3, the separation of the four labeled amino acids was achieved in less than 50 s, for an effective length of 2 cm and an electric field strength, E, of 260 V/cm. This compared well with the reported separation of amino acids in oxidized PDMS channels (82). However, it is well-known that the oxidative treatment of PDMS surfaces is not stable (82, 89), so that the reproducibility between runs is poor compared to that reported for untreated devices (90). This observation has led to interest in different types of coatings for plastic microfluidic devices to control polymer surface chemistry. Polyelectrolyte multilayers, for instance, have been employed to coat plastic devices and to define flow direction and electro-osmotic mobility in polystyrene and acrylic microfluidic devices (91, 92), in copolyester (93) and in PDMS (94, 95).

Keystone effect

As mentioned above, the taper is integrated in the structure to block and confine the stationary phase in the separation channel. The suspension of ODS-modified particles is introduced into the column from the buffer waste reservoir and drawn towards the intersection. At the taper, the density of the particles increases and they aggregate without requiring a physical barrier or filter. These first particles act as the "keystones", blocking the others and allowing the packed section to grow longer in the opposite direction towards the waste (56, 57). The

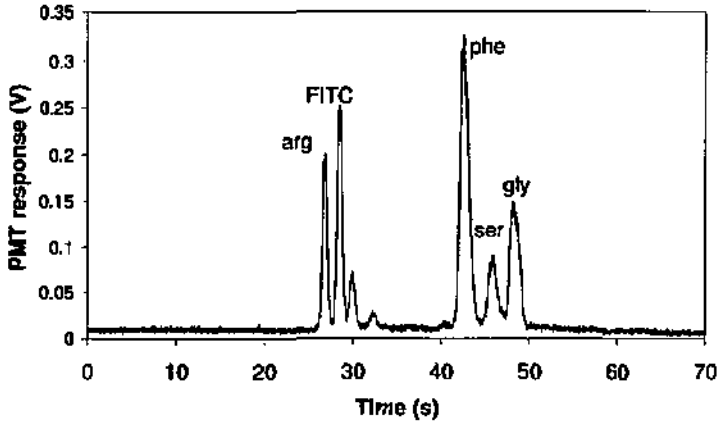

***Figure 3** Electropherogram of a mixture of 10 μM FITC-labeled amino acids, achieved in an oxidized PDMS/glass device. L_{tot}= 6 cm; L_{eff}= 2.5 cm; E= 580 V/cm; buffer, 100 mM Tris-20 mM boric acid (pH 9); detection system, Ar^+ laser (488 nm) and band-pass filter at 520 nm; control system, PC with LabVIEW™.*

"keystone effect" is depicted in Figure 4. It is important to note that the intersection remains particle-free. This packing method was applied to tapered straight and spiral microcolumns, 30 and 50 μm deep, realized in hybrid PDMS/glass devices, as shown in Figure 5. Also shown in Figure 5c is a SEM of a cross-section of a packed microcolumn realized in a wholly PDMS device before thermal treatment. The good aspect ratio and smooth edges of this channel reflect the excellent quality of the original DRIE master.

Critical packing conditions

The "keystone effect" (56, 57) can be a very simple way to confine particles in an on-chip microcolumn. In our case, a 2% suspension of 3-μm-size particles could be retained in a reproducible way in a taper 16 μm wide at its narrow end. On the other hand, the effect is sensitive to many parameters. Not

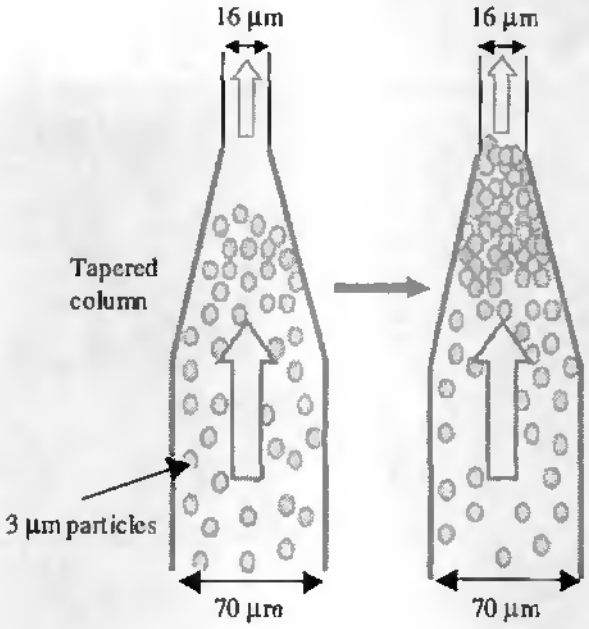

Figure 4 *Diagram of the "keystone effect". A suspension of ODS-modified particles is drawn from the waste reservoir towards the taper by vacuum. At the taper, the density of the particles increases, and they aggregate without requiring a physical barrier or frit. These first particles act as the "keystones", blocking the others and allowing the packed segment to grow longer in the opposite direction.*

unexpectedly, it was observed that the concentration of particles in the suspension is critical. At higher concentrations, the particles tended to aggregate somewhere in the separation column before reaching the taper, while at lower concentrations the particle density at the taper was insufficient, and particles filled the injection channels. This means that for new ratios of column width-to-injection channel width, preliminary tests with different particle concentrations would probably be required. In the case described here, this ratio was about 5:1, a value taken from a report describing the use of tapered fused silica capillaries for fritless CEC (57).

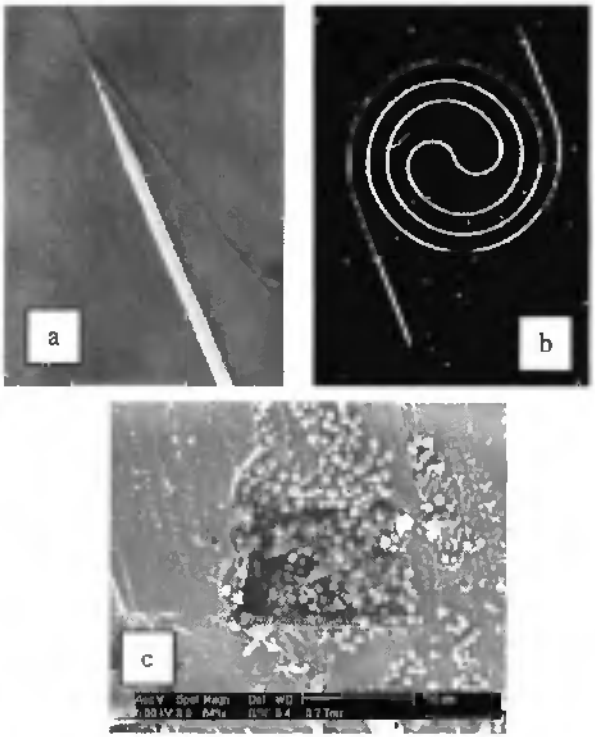

Figure 5 *Photographs of tapered (a) straight and (b) spiral PDMS channels, packed with ODS-derivatized particles according to the packing method described in this paper. (c) A scanning electron micrograph (SEM) of a packed plastic channel cross-section before thermal treatment. Particles are 3 μm in diameter.*

The sonication of the dry particles and of the slurry is also critical, and needs to be optimized. The taper length itself, however, does not seem to be very important for the "keystone effect". Tapers of 0.5, 0.8 and 1 mm length were tested without any significant difference in the packing process being observed. However, difficulties were often encountered when attempting to pack the tapered channel realized using a transparency mask, indicating that unevenness in the channel walls must be kept to a minimum.

In the packing method presented here, the particles stop at the taper, but the simple use of vacuum to aggregate them is not enough to make them stable. In fact, if an electric field is applied directly after packing, the particles are set in motion and will travel to the reservoirs at both the ends of the separation column.

Stabilization of the packing can be achieved by placing the chip in an oven overnight at 115 °C, after rinsing the packing for 2 hours with doubly distilled water. The channels are still filled with water when heating is commenced. This thermal treatment is indispensable for fixation of the particulate stationary phase within the tapered microchannel. Several possible mechanisms for this low temperature stabilization were considered. The occurrence of silica particle sintering was ruled out, since this process, used for making frits, is carried out at temperatures above 260 °C (70). It was thought that shrinkage of the PDMS upon heating for a prolonged period of time could be responsible for a more compressed, and, hence, more stable packing. However, this possibility was rejected, after microscope measurements of channel dimensions before and after heating showed no appreciable difference. The most likely mechanism for packing stabilization, then, involves interparticle bonding, as proposed by Adam et al. (96). These researchers published a method for stabilization of microparticulate silica columns using a hydrothermal treatment. The fused silica capillary (i.d. 25–100 μm) was positioned in the core of a heating coil, which could be moved along the length of the capillary to heat the packing locally. The coil temperature was adjusted to maintain an internal capillary temperature between 300 and 400 °C. The coil was moved along the capillary at velocities between 0.5 and 5 mm/s (97). It was postulated that upon heating, silica at the outer surface of the particles dissolved in water to form a saturated solution of polysilic acids, which redeposited as silica between the particles upon cooling. SEMs taken of the packing confirmed that the particles were fused together chemically during the heating process. Our thermal treatment, although at a lower temperature, was much longer (ca. 10 h, as compared with a few seconds for the

localized heating approach), and so could lead to a similar particle-bonding effect. The stabilization process is probably also aided by particle-wall interactions. It was observed that a stable monolayer of ODS-modified beads was formed upon thermal treatment of a few drops of particle-containing slurry deposited on a microscope slide. Without heating, no particles remained attached to the slide after evaporation upon application of a stream of nitrogen gas. It should also be mentioned that chip substrate material does not appear to influence the stabilization process. Packing in glass and quartz channels was equally well stabilized upon an overnight treatment at 115°C.

Effect of voltage oo electro-osmotic flow (EOF) velocity and efficiency

The packed column was prepared as described above. Thiourea (1 mg/mL), prepared in the mobile phase, was employed as unretained neutral marker to test column performance. The sample loading step was 40 s long, and the run voltage along the straight channel (4 cm long) was varied from 1.7 kV to 5.6 kV. To detect the non-fluorescent compound, 1 mM fluorescein was added to the mobile phase. Thus, a negative peak was recorded by indirect fluorescence detection when the compound passed the detection point at 1.5 cm below the injector. The laser beam was focused into the packed portion of the channel. In-column detection lends flexibility in the choice of effective separation length. It also avoids the band-broadening introduced when a separated sample zone enters the empty column below the packing, where on-column detection would normally take place. However, detection sensitivity is compromised when detecting directly in the packing itself, since both incident and emitted light do not follow straight paths in this system.

As shown in Figure 6a, a linear relationship between field strength, E, and linear velocity was determined as expected (50, 98, 99). A minimum plate height of ~ 5 μm was achieved, in agreement with the values reported for CEC in 3-μm-

particle packed capillaries (50, 53), which are lower than for HPLC in similar columns. This performance was not compromised at linear mobile phase velocities up to at least 3 mm/s (Figure 6b). In our case, no peak was observed at mobile phase velocities < 0.5 mm/s, because of the significant axial diffusion at this velocity rendering sample zones too diffuse to detect. Relatively flat H-velocity curves such as the one presented in Figure 6b for flow rates > 1 mm/s have also been reported in the literature for conventional, electrically-driven, packed capillaries. This is in contrast to pressure-driven, 3-μm-particle-packed columns, for which the plate height increases rather steeply with increasing linear velocity (54, 98). At low velocities, dispersion by axial molecular diffusion (the B-term in the van Deemter plate height equation) dominates in both electro- and pressure-driven techniques. At higher values, however, eddy diffusion (the A term in the same equation) contributes more to final band broadening in the pressure-driven than in the electro-driven case, as predicted by theory (53). This

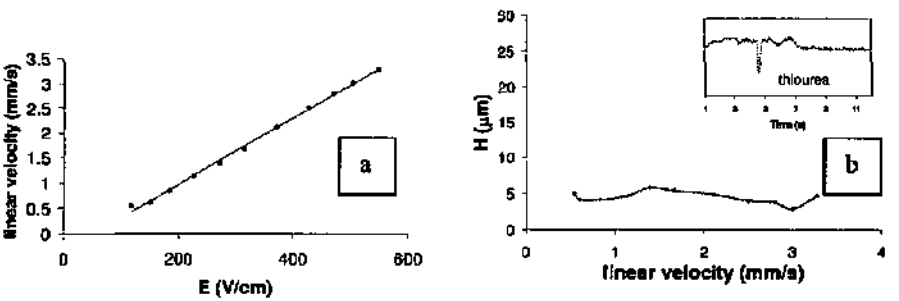

***Figure 6** a) Plot of mobile-phase linear velocity versus applied electric field strength, E. Linear velocity was determined by injecting sample plugs containing the unretained marker, thiourea. b) Plot of height equivalent to a theoretical plate (H) versus mobile phase linear velocity. L_{tot} 4 cm; L_{eff} 1.5 cm; stationary phase, 3 μm, Nucleosil, ODS-modified particles; mobile phase, 5 mM phosphate: acetonitrile (80:20, pH 7) and 1 mM fluorescein; sample, thiourea (1 mg/mL).*

is because the flat, plug-like profile of the mobile phase in CEC ensures a smaller variation in flow velocities in the individual flow paths across the bed compared to the parabolic flow profile of HPLC (50, 52-54, 99). A flat H-linear velocity curve for flow rates above 0.5 mm/s and a plate height of 5 μm have also been reported by Ericson at al. (71) for a continuous separation bed polymerized *in situ* in a microchannel, confirming the analogies between packed capillaries and channels. The thiourea peak in Figure 6b exhibits a plate height of 4 μm (N= 3200 plates or 210 000 plates/m) and elutes in 5 s on 1.5 cm of chromatographic bed at 600 V/cm. These results are in the range reported for 3-μm, ODS-packed capillaries (3-5-μm plate height) (54, 100). EOF mobility, μ_{EOF}, was measured with the current monitoring method (101) using 20 and 19 mM Na-borate buffers at pH 8. For the 7 columns tested, the EOF in packed channels was reduced by 30-50% of the value in empty columns because of the presence of the particles (54, 99). The average value found for μ_{EOF} in packed columns was $1.2 \times 10^{-4} \pm 0.26$ cm^2/Vs. For oxidized, empty columns, the average value was $2.6 \times 10^{-4} \pm 0.3$ cm^2/Vs (n= 5), measured just a couple of hours after oxidation.

Capillary electrochromatography (CEC) test

The separation of neutral compounds was performed to test the chromatographic properties of the packed channel. Baseline separation (Rs = 5) of methanol, used as unretained compound, and benzaldehyde was achieved in less than 15 s for an effective length of 1.7 cm and an E of 500 V/cm. The separation is presented in Figure 7. The drift in the baseline is due to fluorescein being bleached in the detector volume between runs. Once the separation is started, fresh mobile phase replaces bleached solution at the point of detection, leading to an increasing PMT response. Methanol and benzaldehyde peaks yield an efficiency of 290 000 and 120 000 plates/meter, respectively. It was observed that the EOF remained stable within a given packed column, with a run-to-run retention time reproducibility of < 0.3 s for the analyte benzaldehyde. However,

intercolumn variability remained significant, due to the instability of oxidized PDMS surfaces (82, 89) and differences in packing length. Other samples containing neutral compounds were tested, but this often resulted in clogging of the structure, particularly at the intersection, because of analyte sorption by PDMS. This polymer, in fact, is well-known for its sorptive properties, which makes it a good substrate for solid-phase extraction (102). Most chips were, therefore, used for one day only. Continuous polymer beds derivatized with isopropyl groups (C_3^-, used for weak reverse-phase separation) and sulfonic acid groups (SO_3^-, used for the generation of EOF at low pHs as well as higher pHs) yield efficiencies equivalent to 350 000 plates/meter for uracil (71), while 500 000 plates/meter were reported for fluorescein on an ODS-coated bead bed (75). These results compare favourably with those presented here, proving the feasibility of the tapered microchannel approach for chip-based CEC using standard particulate phase.

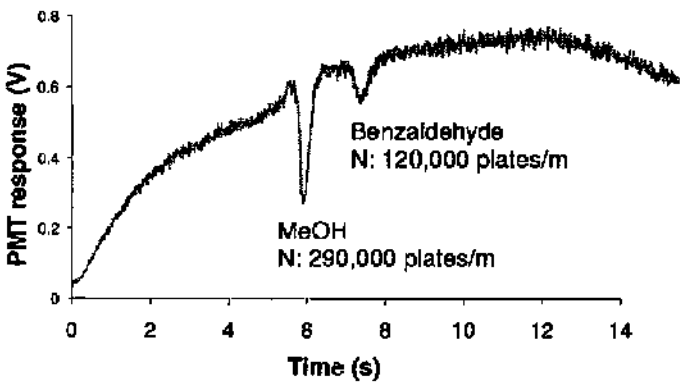

***Figure 7** CEC separation of methanol and benzaldehyde in the plastic packed microcolumn. L_{tot} 5 cm; L_{eff} 1.7 cm; E, 4.5 kV; stationary phase, 3 μm, Nucleosil, ODS-modified particles; mobile phase, 5 mM phosphate:acetonitrile (80:20, pH 7) and 1 mM fluorescein.*

CONCLUSIONS

The successful preparation of a stable particulate chromatographic bed in a microchip using the "keystone effect" has been presented. By integration of a tapered geometry at the beginning of a microchannel acting as column, particles can be spatially retained and packed without the need of frit structures of any kind. This can simplify fabrication of packed bed devices, since features can all have the same depth (or height, as the case may be). DRIE has proven to be a good process for fabrication of silicon masters with rectangular and high-aspect-ratio profiles. This process provides complete freedom when designing channel layouts, and allows easy incorporation of taper geometries and the like. It is thus much easier to experiment with different channel geometries using this type of micromachining technology combined with replication in plastic than it would be using standard, fused silica capillaries. Devices made this way could thus be a useful tool to systematically investigate how geometry influences column performance by obtaining a better understanding of dispersion and diffusion effects in coiled and bent packed channels and capillaries. The high-aspect-ratio rectangular channels, which can be achieved are also attractive for performing on-chip UV detection, since a narrow, deep channel ensures both a small detection volume and a usable optical path length.

Although PDMS is a useful material for fast replication purposes, it is not compatible with many analytes and organic solvents (76). This will necessitate the modification of channel walls to prevent clogging and loss of the sample to the substrate, an issue being considered by a number of research groups. Alternatively, other plastic substrates could be patterned by hot embossing or polymer casting using DRIE-fabricated masters, to offer greater analyte compatibility.

The possibility to trap and pack beads in microstructures is an important development for microfluidics, because it will expand the sample handling

capabilities of these devices enormously and bring researchers closer to achieving a true μTAS.

Acknowledgements

The SAMLAB technical staff is acknowledged for their help, in particular for the deep reactive-ion etching process. Dr. M. Dadras and Ms. M. Leboeuf are thanked for the SEM images. We also appreciate the helpful discussions with N. Djordjevic, F. Fitzpatrick and G. J. M. Bruin (Novartis Pharma AG, Basel, Switzerland), especially in the initial phase of this work. This work was financially supported by the Swiss Commission for Technology and Innovation Program *MedTech*, Project No. 523.

REFERENCES

(1) Bruin, G. J. M. *Electrophoresis* 2000, *21*, 3931-3951.

(2) Harrison, D. J.; Fluri, K.; Seiler, K.; Fan, Z. H.; Effenhauser, C. S.; Manz, A. *Science* 1993, *261*, 895-897.

(3) Effenhauser, C. S.; Manz, A.; Widmer, H. M. *Analytical Chemistry* 1993, *65*, 2637-2642.

(4) Jacobson, S. C.; Hergenröder, R.; Koutny, L. B.; Ramsey, J. M. *Analytical Chemistry* 1994, *66*, 1114-1118.

(5) Jacobson, S. C.; Culbertson, C. T.; Daler, J. E.; Ramsey, J. M. *Analytical Chemistry* 1998, *70*, 3476-3480.

(6) Verpoorte, E. M. J.; van der Schoot, B. H.; Jeanneret, S.; Manz, A.; Widmer, H. M.; de Rooij, N. F. *Journal of Micromechanics and Microengineering* 1994, *4*, 246-256.

(7) Daridon, A.; Sequeira, M.; Pennarun-Thomas, G.; Dirac, H.; Krog, J. P.; Gravesen, P.; Lichtenberg, J.; Diamond, D.; Verpoorte, E.; de Rooij, N. F. *Sensors and Actuators B* 2001, *76*, 235-243.

(8) Duffy, D. C.; Gillis, H. L.; Lin, J.; Sheppard, N. F., Jr.; Kellogg, G. J. *Analytical Chemistry* 1999, *71*, 4669-4678.

(9) Ekstrand, G.; Holmquist, C.; Örlefors, A. E.; Hellman, B.; Larsson, A.; Andersson, P. *Micro Total Analysis Systems 2000: Proceedings of the μTAS 2000 Symposium*, Enschede, The Netherlands, May 14-18, 2000; Kluwer Academic Publishers; Dordrecht 2000; 311-314.

(10) Thomas, N.; Ocklind, A.; Blikstad, I.; Griffiths, S.; Kenrick, M.; Derand, H.; Ekstrand, G.; Ellström, C.; Larsson, A.; Andersson, P. *Proceedings of the μTAS 2000 Symposium*. Enschede, The Netherlands, May 14-18 2000; Kluwer Academic Publishers; Dordrecht 2000; 249-252.

(11) Eckersted, A.; Örlefors, A. E.; Ellström, C.; Erickson, K.; Löfman, E.; Eriksson, A.; Eriksson, S.; Jorsback, A.; Tooke, N.; Derand, H.; Ekstrand, G.; Engström, J.; Honerud, A.-K.; Aksberg, A.; Hedsten, H.; Rosengren, L.; Stjernström, M.; Hultman, T.; Andersson, P. *Proceedings of the μTAS 2000 Symposium*, Enschede, The Netherlands, May 14-18, 2000; Kluwer Academic Publishers; Dordrecht 2000; 521-524.

(12) Lagally, E. T.; Simpson, P. C.; Mathies, R. A. *Sensors and Actuators B-Chemical* 2000, *63*, 138-146.

(13) Simpson, P. C.; Roach, D.; Woolley, A. T.; Thorsen, T.; Johnston, R.; Sensabaugh, G. F.; Mathies, R. A. *Proceedings of the National Academy of Sciences of the United States of America* 1998, *95*, 2256-2261.

(14) Cheng, S. B.; Skinner, C. D.; Taylor, J.; Attiya, S.; Lee, W. E.; Picelli, G.; Harrison, D. J. *Analytical Chemistry* 2001, *73*, 1472-1479.

(15) Petersen, K. E.; McMillan, W. A.; Kovacs, G. T. A.; Northrup, M. A.; Christel, L. A.; Pourahmadi, F. *Biomedical Microdevices* 1998, *1*, 71-79.

(16) Northrup, M. A.; Benett, B.; Hadley, D.; Landre, P.; Lehew, S.; Richards, J.; Stratton, P. *Analytical Chemistry* 1998, *70*, 918-922.

(17) Weigl, B. H.; Kriebel, J.; Mayes, K. J.; Bui, T.; Yager, P. *Mikrochimica Acta* 1999, *131*, 75-83.

(18) Khandurina, J.; Jacobson, S. C.; Waters, L. C.; Foote, R. S.; Ramsey, J. M. *Analytical Chemistry* 1999, *71*, 1815-1819.

(19) Lichtenberg, J.; Verpoorte, E.; de Rooij, N. F. *Electrophoresis* 2001, *22*, 258-271.

(20) Li, P. C. H.; Harrison, D. J. *Analytical Chemistry* 1997, *69*, 1564-1568.

(21) Waters, L. C.; Jacobson, S. C.; Kroutchinina, N.; Khandurina, J.; Foote, R. S.; Ramsey, J. M. *Analytical Chemistry* 1998, *70*, 158-162.

(22) Kopp, M. U.; de Mello, A. J.; Manz, A. *Science* 1998, *280*, 1046-1048.

(23) Woolley, A. T.; Hadley, D.; Landre, P.; Demello, A. J.; Mathies, R. A.; Northrup, M. A. *Analytical Chemistry* 1996, *68*, 4081-4086.

(24) Erbacher, C.; Bessoth, F. G.; Busch, M.; Verpoorte, E.; Manz, A. *Mikrochimica Acta* 1999, *131*, 19-24.

(25) Jacobson, S. C.; McKnight, T. E.; Ramsey, J. M. *Analytical Chemistry* 1999, *71*, 4455-4459.

(26) Dodge, A.; Fluri, K.; Verpoorte, E.; de Rooij, N. F. *Analytical Chemistry* 2001, *73*, 3400-3409.

(27) Sato, K.; Tokeshi, M.; Kimura, H.; Kitamori, T. *Analytical Chemistry* 2001, *73*, 1213-1218.

(28) Harrison, D. J.; Manz, A.; Fan, Z. H.; Ludi, H.; Widmer, H. M. *Analytical Chemistry* 1992, *64*, 1926-1932.

(29) Manz, A.; Harrison, D. J.; Verpoorte, B. M. J.; Fettinger, J. C.; Paulus, A.; Ludi, H.; Widmer, H. M. *Journal of Chromatography* 1992, *593*, 253-258.

(30) Burggraf, N.; Manz, A.; Effenhauser, C. S.; Verpoorte, E.; de Rooij, N. F.; Widmer, H. M. *Journal of High Resolution Chromatography* 1993, *16*, 594-596.

(31) Burggraf, N.; Manz, A.; Verpoorte, E.; Effenhauser, C. S.; Widmer, H. M.; de Rooij, N. F. *Sensors and Actuators B* 1994, *20*, 103-110.

(32) Raymond, D. E.; Manz, A.; Widmer, H. M. *Analytical Chemistry* 1994, *66*, 2858-2865.

(33) Raymond, D. E.; Manz, A.; Widmer, H. M. *Analytical Chemistry* 1996, *68*, 2515-2522.

(34) Manz, A.; Miyahara, Y.; Miura, J.; Watanabe, Y.; Miyagi, H.; Sato, K. *Sensors and Actuators B* 1990, *1*, 249-255.

(35) Jacobson, S. C.; Hergenröder, R.; Koutny, L. B.; Ramsey, J. M. *Analytical Chemistry* 1994, *66*, 2369-2373.

(36) Kutter, J. P.; Jacobson, S. C.; Matsubara, N.; Ramsey, J. M. *Analytical Chemistry* 1998, *70*, 3291-3297.

(37) Moore, A. W.; Jacobson, S. C.; Ramsey, J. M. *Analytical Chemistry* 1995, *67*, 4184-4189.

(38) von Heeren, F.; Verpoorte, E.; Manz, A.; Thormann, W. *Analytical Chemistry* 1996, *68*, 2044-2053.

(39) Kutter, J. P.; Jacobson, S. C.; Ramsey, J. M. *Analytical Chemistry* 1997, *69*, 5165-5171.

(40) Effenhauser, C. S.; Paulus, A.; Manz, A.; Widmer, H. M. *Analytical Chemistry* 1994, *66*, 2949-2953.

(41) Woolley, A. T.; Mathies, R. A. *Analytical Chemistry* 1995, *67*, 3676-3680.

(42) Schmalzing, D.; Adourian, A.; Koutny, L.; Ziaugra, L.; Matsudaira, P.; Ehrlich, D. *Analytical Chemistry* 1998, *70*, 2303-2310.

(43) Schmalzing, D.; Tsao, N.; Koutny, L.; Chisholm, D.; Srivastava, A.; Adourian, A.; Linton, L.; McEwan, P.; Matsudaira, P.; Ehrlich, D. *Genome Research* 1999, *9*, 853-858.

(44) Salas-Solano, O.; Schmalzing, D.; Koutny, L.; Buonocore, S.; Adourian, A.; Matsudaira, P.; Ehrlich, D. *Analytical Chemistry* 2000, *72*, 3129-3137.

(45) Koutny, L.; Schmalzing, D.; Salas-Solano, O.; El-Difrawy, S.; Adourian, A.; Buonocore, S.; Abbey, K.; McEwan, P.; Matsudaira, P.; Ehrlich, D. *Analytical Chemistry* 2000, *72*, 3388-3391.

(46) Ocvirk, G.; Verpoorte, E.; Manz, A.; Grasserbauer, M.; Widmer, H. M. *Analytical Methods and Instrumentation* 1995, *2*, 74-82.

(47) Andersson, H.; van der Wijngaart, W.; Enoksson, P.; Stemme, G. *Sensors and Actuators B* 2000, *67*, 203-208.

(48) Sato, K.; Tokeshi, M.; Odake, T.; Kimura, H.; Ooi, T.; Nakao, M.; Kitamori, T. *Analytical Chemistry* 2000, *72*, 1144-1147.

(49) Ceriotti, L.; Verpoorte, E.; de Rooij, N. F., *Proceedings of the μTAS 2000 Symposium*, Enschede, The Netherlands, May 14-18 2000; Kluwer Academic Publishers; Dordrecht 2000; 225-228.

(50) Knox, J. H.; Grant, I. H. *Chromatographia* 1991, *32*, 317-328.

(51) Knox, J. H.; Grant, I. H. *Chromatographia* 1987, *24*, 135-143.

(52) Yan, C.; Schanfelberger, D.; Erni, F. *Journal of Chromatography A* 1994, *670*, 15-23.

(53) Dittmann, M. M.; Wienand, K.; Bek, F.; Rozing, G. P. *LC-GC* 1995, *13*, 800-808.

(54) Colón, A.; Reynolds, K. J.; Alicea-Maldonado, R.; Fermier, A. M. *Electrophoresis* 1997, *18*, 2162-2174.

(55) Seifar, R. M.; Kraak, J. C.; Kok, W. T.; Poppe, H. *Journal of Chromatography a* 1998, *808*, 71-77.

(56) Lord, G. A.; Gordon, D. B.; Myers, P.; King, B. W. *Journal of Chromatography A* 1997, *768*, 9-16.

(57) Mayer, M.; Rapp, E.; Marek, C.; Bruin, G. J. M. *Electrophoresis* 1999, *20*, 43-49.

(58) Chen, J. R.; Dulay, M. T.; Zare, R. N.; Svec, P.; Peters, E. *Analytical Chemistry* 2000, *72*, 1224-1227.

(59) Dulay, M. T.; Kulkarni, R. P.; Zare, R. N. *Analytical Chemistry* 1998, *70*, 5103-5107.

(60) Chirica, G.; Rencho, V. T. *Electrophoresis* 1999, *20*, 50-56.

(61) Tang, Q. L.; Xin, B. M.; Lee, M. L. *Journal of Chromatography a* 1999, *837*, 35-50.

(62) Chirica, G.; Rencho, V. T. *Analytical Chemistry* 2000, *72*, 3605-3610.

(63) Peters, E. C.; Petro, M.; Svec, F.; Frechet, J. M. J. *Analytical Chemistry* 1997, *69*, 3646-3649.

(64) Peters, E. C.; Petro, M.; Svec, F.; Frechet, J. M. J. *Analytical Chemistry* 1998, *70*, 2288-2295.

(65) Peters, E. C.; Petro, M.; Svec, F.; Frechet, J. M. J. *Analytical Chemistry* 1998, *70*, 2296-2302.

(66) Ericson, C.; Hjerten, S. *Analytical Chemistry* 1999, *71*, 1621-1627.

(67) Hayes, J. D.; Malik, A. *Analytical Chemistry* 2000, *72*, 4090-4099.

(68) Ishizuka, N.; Minakuchi, H.; Nakanishi, K.; Soga, N.; Nagayama, H.; Hosoya, K.; Tanaka, N. *Analytical Chemistry* 2000, *72*, 1275-1280.

(69) Dittmann, M. M.; Rozing, G. P. *Journal of Chromatography a* 1996, *744*, 63-74.

(70) Asiaie, R.; Huang, X.; Farnan, D.; Horváth, C. *Journal of Chromatography A* 1998, *806*, 251-263.

(71) Ericson, C.; Holm, J.; Ericson, T.; Hjerten, S. *Analytical Chemistry* 2000, *72*, 81-87.

(72) Ngola, S. M.; Fintschenko, Y.; Choi, W. Y.; Shepodd, T. J. *Analytical Chemistry* 2001, *73*, 849-856.

(73) He, B.; Regnier, F. E. Journal of Pharmaceutical and Biomedical Analysis 1998, *17*, 925-932.

(74) He, B.; Tait, N.; Regnier, F. E. *Analytical Chemistry* 1998, *70*, 3790-3797.

(75) Oleschuk, R. D.; Shultz-Lockyear, L. L.; Ning, Y.; Harrison, D. J. *Analytical Chemistry* 2000, *72*, 585-590.

(76) McDonald, J. C.; Duffy, D. C.; Anderson, J. R.; Chiu, D. T.; Wu, H.; Schueller, O. J. A.; Whitesides, G. M. *Electrophoresis* 2000, *21*, 27-40.

(77) Drott, J.; Lindström, K.; Rosengren, L.; Laurell, T. *Journal of Micromechanics and Microengineering* 1997, *7*, 14-23.

(78) Madou, M. *Fundamentals of microfabrication*, first ed.; CRC Press: Boca Raton, Florida, 1997.

(79) McCormick, R. M.; Nelson, R. J.; Alonso-Amigo, M. G.; Benvegnu, D. J.; Hooper, H. H. *Analytical Chemistry* 1997, *69*, 2626-2630.

(80) Martynova, L.; Locascio, L. E.; Gaitan, M.; Kramer, G. W.; Christensen, R. G.; MacCrehan, W. A. *Analytical Chemistry* 1997, *69*, 4783-4789.

(81) Effenhauser, C. S.; Bruin, G. J. M.; Paulus, A.; Ehrat, M. *Analytical Chemistry* 1997, *69*, 3451-3457.

(82) Duffy, D. C.; McDonald, J. C.; Schueller, O. J. A.; Whitesides, G. M. *Analytical Chemistry* 1998, *70*, 4974-4984.

(83) Hong, J. W.; Fujii, T.; Seki, M.; Yamamoto, T.; Endo, I. *Electrophoresis* 2001, *22*, 328-333.

(84) Shaw, J. M.; Gelorme, J. D.; LaBianca, N. C.; Conley, W. E.; Holmes, S. J. *IBM Journal of Research and Development* 1997, *41*, 81-94.

(85) Lorenz, H.; Despont, M.; Fahrni, N.; LaBianca, N.; Renaud, P.; Vettiger, P. *Journal of Micromechanics and Microengineering* 1997, *7*, 121-124.

(86) Lorenz, H.; Despont, M.; Fahrni, N.; Brugger, J.; Vettiger, P.; Renaud, P. *Sensors and Actuators A* 1998, *64*, 33-39.

(87) Manz, A.; Effenhauser, C. S.; Burggraf, N.; Harrison, D. J.; Seiler, K.; Fluri, K. *J. Micromech. Microeng.* 1994, *4*, 257-265.

(88) Shultz-Lockyear, L. L.; Colyer, C. L.; Fan, Z. H.; Roy, K. I.; Harrison, D. J. *Electrophoresis* 1999, *20*, 529-538.

(89) Morra, M.; Occhiello, E.; Marola, R.; Garbassi, F.; Humphrey, P.; Johnson, D. *Journal of Colloid and Interface Science* 1990, *137*, 11-24.

(90) Ocvirk, G.; Munroe, M.; Tang, T.; Oleschuk, R.; Westra, K.; Harrison, D. J. *Electrophoresis* 2000, *21*, 107-115.

(91) Barker, S. L. R.; Tarlov, M. J.; Canavan, H.; Hickman, J. J.; Locascio, L. E. *Analytical Chemistry* 2000, *72*, 4899-4903.

(92) Barker, S. L. R.; Ross, D.; Tarlov, M. J.; Gaitan, M.; Locascio, L. E. *Analytical Chemistry* 2000, *72*, 5925-5929.

(93) Wang, S. C.; Perso, C. E.; Morris, M. D. *Analytical Chemistry* 2000, *72*, 1704-1706.

(94) Liu, Y.; Fanguy, J. C.; Bledsoe, J. M.; Henry, C. S. *Analytical Chemistry* 2000, *72*, 5939-5944.

(95) Yang, T.; Jung, S.-y.; Mao, H.; Cremer, P. S. *Analytical Chemistry 2001*, *73*, 165-169.

(96) Adam, T.; Unger, K. K.; Dittmann, M. M.; Rozing, G. P. *Journal of Chromatography A* 2000, *887*, 327-337.

(97) Dittmann, M.; Rozing, G. P.; Unger, K. K.; Adam, T. *US PATENT: 5,858,241*, 1999 (column for capillary chromatographyc separations and method of manufacturing same).

(98) van den Bosch, S. E.; Heemstra, S.; Kraak, J. C.; Poppe, H. *Journal of Chromatography A* 1996, *755*, 165-177.

(99) Choudhary, G.; Horvath, C. *Journal of Chromatography A* 1997, *781*, 161-183.

(100) Yamamoto, H.; Baumann, J.; Erni, F. *Journal of Chromatography* 1992, *593*, 313.

(101) Huang, X. H.; Gordon, M. J.; Zare, R. N. *Analytical Chemistry* 1988, *60*, 1837-1838.

(102) Mayer, P.; Vaes, W. H. J.; Hermens, J. L. M. *Analytical Chemistry* 2000, *72*, 459-464.